Prediction of acid rock drainage (ARD) from sulphidic slates using GIS analysis of mineralogical, geochemical, magnetic and geological parameters: a test case in southern Nova Scotia.

by

Donald L. Fox, B.Sc. (Honours), M.Sc., M.A.Sc., Adv. Dip. (GIS)

Submitted in partial fulfillment of the requirements
for the degree of Doctor of Philosophy

at

Dalhousie University
Halifax, Nova Scotia
April 1, 1999

Dedicated to the late
Mrs. Patricia K. Wadden

Table of Contents

List of Figures

List of Tables

Abstract

The physical disruption of sulphide-bearing rocks in humid environments leads to the oxidation of the two most common iron-sulphide minerals, pyrite (FeS_2) and pyrrhotite ($Fe_{1-x}S$), and the generation of acid rock drainage (ARD). ARD, also called acid mine drainage (AMD), is typically associated with mining operations that create waste rock piles and tailings impoundments. However, it also occurs in any area that causes physical disruption of the bedrock, such as highway construction, quarry operations, and urban development or expansion. The resulting drainage from these areas generally has acidic pH values in the range of 2 to 4, and high contents of potentially harmful elements that are toxic to local ecosystems.

ARD chemistry, and the overall intensity and duration of the drainage, very much depends on local conditions and the mineralogical components of the bedrock. Acidic drainage from bedrock dominated by pyrite may be very different from bedrock dominated by pyrrhotite, since pyrrhotite reacts much more quickly than pyrite. In pyrrhotite-rich areas, this difference in reactivity rate could lead to toxic "pulses" of low pH waters released into surrounding waterways.

The area selected to test these hypotheses is southern Nova Scotia, which includes the site of one of the most serious cases of ARD in Eastern Canada, the Halifax International Airport. In this study, sulphide mineral textures, compositions, and associations were analysed in detail throughout an area of several hundred square kilometres. Monoclinic pyrrhotite, with varying proportions of pyrite, are the predominant sulphide minerals. The location of pyrrhotite can be detected by magnetic susceptibility measurements made with a hand-held meter, field-scale magnetometer surveys, and regional-scale, airborne magnetic surveys.

Regional-scale stratigraphic, structural, and geophysical data that are presently available in digital form, were incorporated into a geographical information system (GIS), and used as evidence to predict areas that have a high potential of generating ARD. The potential or "favourability" maps generated through expert-driven Boolean logic and fuzzy logic, as well as data-driven, weights of evidence modelling proved very useful for outlining areas that may produce ARD in the future, if the bedrock is disrupted and exposed to surface oxidizing conditions. Due to the high cost of ARD treatment, and the limited success of presently available treatment technology, prediction and avoidance is the best option. In areas where avoidance is impossible, detailed mineralogical studies are necessary in order to plan for, and establish, the best approach to treatment and amelioration.

The conclusions of this study should be applicable in other areas of the world underlain by sulphidic-rich black slate, including the carbonaceous and sulphidic slate of the Anakeesta Formation in North Carolina and Tenessee (southern Appalachians), and the black shale formations of the Karelia Supergroup in eastern Finland.

Acknowledgements

This study would not have been possible without the understanding, patience, and close friendship of my wife Debbie. We survived the ordeal with plenty of room to spare.

I wish to thank my thesis supervisor, Dr. Marcos Zentilli whose enthusiastic guidance, support, and encouragement made this thesis possible. He leads the way in bringing new scientific ideas and concepts into the "traditional" earth sciences, and inspires all his student to do their best. I thank Dr. Ian MacInnis for guidance and discussions about the problem of acid rock drainage in the Meguma Supergroup. Ian's initial work on sulphide oxidation rates set the foundation for many aspects of the present study. Milton Graves has always been a constant source of input into the ARD study group at Dalhousie University, and has never failed to help when needed.

I sincerely thank past Dalhousie students, Joanna Brown, Rachel Jones, Kerry Knee, and Clare Robinson whose enthusiastic work on acid rock drainage in Nova Scotia has helped formulate my own ideas and direction of this thesis.

Tim Webster (COGS) helped substantially in the computer aspects and instructed me on the modelling techniques. He has also allowed open access to his collection of digital data from the province of Nova Scotia. I thank Dr. Ken Howells for allowing the use of geophysical data, as well as co-authorship on a paper submitted to Atlantic Geology (Chapter 6).

Sandy Grist has donated his time and expertise in lab procedures to help in this research. Gordon Brown prepared all thin sections, and Robert MacKay assisted with all microprobe analyses. Keith Taylor and Lexie Arnott introduced me to the use of X-ray Diffraction. Lynne Maillet-Frotten helped using the SEM. Cyril Cole (DalTech) performed many of the chemical analyses and openly discussed analytical techniques. Dr. Bob Ryan at Nova Scotia Department of Natural Resources donated some of the samples used in Chapter 5. Debra Grantham (Dalhousie Scientific Imaging) helped with printouts of the GIS maps for Chapter 7.

Funding was provided through Dalhousie Graduate Scholarships (1996-1998), the major component of which came from the Fission Track Research Laboratory and a Dalhousie grant in lieu of salary from Dr. Marcos Zentilli.

Chapter 1

Introduction

1.1 General Statement

Acid rock drainage (ARD), also called acid mine drainage (AMD), results from the oxidation of sulphide minerals such as pyrite (FeS_2) and pyrrhotite ($Fe_{1-x}S$). ARD is typically associated with mining operations that create waste rock piles, expose bedrock in open pits and create tailings impoundments. However, ARD occurs wherever sulphide minerals are exposed to oxidizing conditions. In the Meguma Supergroup of Nova Scotia, the disruption of sulphide-bearing rocks is mainly by construction activities. The exposed sulphide minerals create low pH drainage water with high metal content resulting in extensive and costly environmental problems. Probably the best known case of ARD in Nova Scotia occurs at the Halifax International Airport (HIA) where the construction of runways and taxiways has resulted in acid runoff containing high levels of heavy metals (King, 1987; Lund, 1987; Worgan, 1987). In addition to a general deterioration in surface water quality, ARD throughout the Meguma Supergroup has caused fish kills, fish hatchery closures, disruption of public water supplies, contamination of private wells, and damage to engineering works (Hennigar & Gibb, 1987). Once started, ARD may last tens to hundreds of years depending on the local conditions, and is difficult to stop and expensive to treat.

The preferred solution to the ARD problem would be to avoid the disruption of sulphide-bearing rocks in the first place. The focus of this thesis is on factors that

influence the development of ARD in the Meguma Supergroup, and methods that can be used to detect and predict where ARD will occur. Once these parameters are understood, avoidance or treatment will be much more effective than has been in the past. This thesis demonstrates that GIS is an effective tool in analysing geological, mineralogical, and geophysical data to predict where ARD is likely to occur.

1.2 Background Of Meguma Supergroup And Acid Rock Drainage

1.2.1 Meguma Supergroup

The Meguma Supergroup of southern mainland Nova Scotia consists of a 12-14 km thick suite of Cambro-Ordovician metasedimentary rocks (Fig. 1.1). The Supergroup is comprised of the lower Goldenville Group (mainly thickly bedded greywackes with lesser slate interbeds) and the upper Halifax Group (mainly slate and siltstone) (Schenk, 1983; Schenk, 1995). The Goldenville and Halifax Groups have been further subdivided into formations in the southwestern area (Mahone Bay area, Fig 1.1) and in the northwestern area of Nova Scotia (Schenk, 1995). In the Mt. Uniacke area of central mainland Nova Scotia (Fig. 1.1), recent mapping has outlined geological units that have been correlated with those in the Mahone Bay area, but because of the preliminary nature of this work, these geological units have not been formally subdivided into formations at this time (Ryan et al., 1996). Figure 1.2 shows the stratigraphic terminology of the geological formations (and preliminary units) that comprise the western and central Meguma Supergroup. According to Schenk (1995), the general model for deposition of the Meguma Supergroup is one of overall shoaling

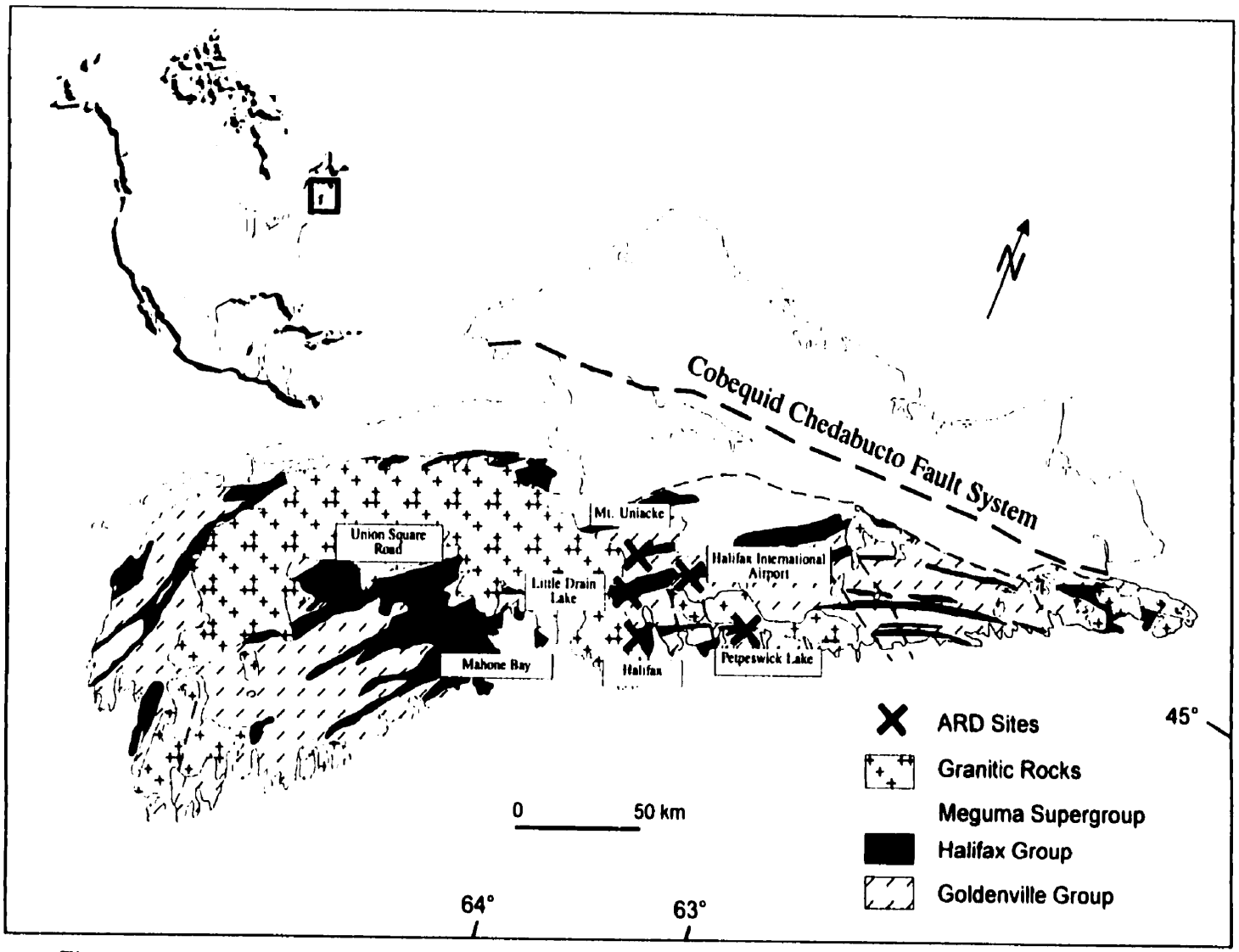

Figure 1.1 Simplified geological map of Nova Scotia showing the distribution of the Meguma Supergroup and the location of some of the past and present acid rock drainage sites (geology modified after Keppie, 1979a).

Geological Time			Units (Western Nova Scotia)	Thickness (m)	Units (Central Nova Scotia)	Thickness (m)
Ordovician			Basal Annapolis Supergroup			
	Meguma Supergroup	Halifax Group	Rockville Notch	32		
			Delanceys	1850		
			Feltzen	2000	Glen Brook Unit	1900
			Cunard	8000	Rawdon Unit	1100
			Mosher's Island	500	Beaverbank Unit	300
			West Dublin	1000	Steve's Road Unit	700
		Goldenville Group	Risser's Beach	1000		
Cambrian			New Harbour	+ 7000	Lewis Lake Unit	1700
					Long Lake Unit	1100
					Mt. Uniacke Unit	1200

Figure 1.2 Summary of stratigraphic terminology for the Meguma Supergroup. Western Nova Scotia after Schenk (1995), and central Nova Scotia after Ryan et al. (1996).

upwards towards the base of the overlying Annapolis Supergroup. The Meguma Supergroup developed from submarine fans, through a channel-levee complex, to a prograding wedge, ending with shelf and nearshore lithologies. Each of the formations retain overall characteristics that were developed in this changing depositional environment.

In the Goldenville Group, the New Harbour Formation consists of thickly bedded, fine grained metawacke interbedded with thin green to grey, sandy slate. These rocks formed by deposition of voluminous sandy turbidite sequences. The Risser's Beach Formation consists of black slate at its base, followed by thinly stratified, very fine grained sandstones. The West Dublin Formation consists of thickly bedded, fine grained sandstone. Both the Risser's Beach and West Dublin Formations define a sedimentary transitional zone towards the overlying Mosher's Island Formation.

In the Halifax Group, the Mosher's Island Formation contains one of the best marker horizons within the Meguma Supergroup. It is a relatively thin, laminated, grey slate that is enriched in manganese and other metals including lead, copper, zinc, and barium (Zentilli et al., 1986). The formation is locally calcareous, and contains coticules that are composed mainly of spessartine garnet and quartz. The Mosher's Island Formation also contains carbon and sulphide minerals and generally is the equivalent of the Goldenville Halifax Transition zone (GHT) referred to by Zentilli et al. (1986). However, it should be noted that the GHT is defined as a "geochemical transition zone" between typical Goldenville and Halifax Groups and therefore may also include parts of the Risser's Beach and West Dublin Formations, as well as parts

of the Cunard Formation.

The Cunard Formation is a thick slate sequence interbedded with fine grained siltstone and sandstone. The slates are generally black and rich in carbon, and sulphide minerals are common in all lithologies of this formation. The Feltzen Formation is comprised of light grey to dark grey slate interbedded with thinly bedded, grey sandstone. This formation is generally poorer in sulphide minerals than the underlying Cunard Formation (O'Brien, 1986). The Delanceys and Rockville Notch Formations consist of slate to silty slate, pelitic laminite, and mudstone (diamictite). In general, the Feltzen, Delanceys, and Rockville Notch Formations were deposited in well-oxygenated, shallower water environments than the underlying Cunard and Mosher's Island Formations which were deposited in an anoxic environment. The abundance and distribution of sulphide mineralization reflects this changing depositional environment with the Mosher's Island and Cunard Formations containing the most abundant sulphide mineralization.

It is important to note here that in the eastern part of mainland Nova Scotia (Fig. 1.1), the Meguma Supergroup has been formally subdivided into only the Halifax Group and Goldenville Group (using recent terminology of Schenk, 1995). Individual formations or units have not been mapped out in detail. However, equivalents of the Mosher's Island and Cunard Formations are relatively easy to identify based on their distinctive character. It is unknown if equivalents to the upper formations of the Halifax Group (Feltzen, Delanceys, and Rockville Notch Formations) exist in the eastern part of the Meguma Supergroup. Also, in the eastern area, the Goldenville Group remains

undivided. For this thesis, which concentrates almost exclusively in the eastern part of the Meguma Supergroup, it is the undivided Goldenville Group and the Mosher's Island and Cunard Formations (or their metamorphosed equivalents) of the Halifax Group that have been sampled.

1.2.2 Acid Rock Drainage in the Meguma Supergroup

In southern mainland Nova Scotia, the best known ARD problems occur mainly within the lower Halifax Group because these well-cleaved rocks commonly contain up to 10% pyrrhotite and/or pyrite. The sulphide minerals are subjected to surficial oxidizing conditions where bedrock is exposed as a result of urban development, quarry operations, or highway and runway construction. Figure 1.1 shows some of the locations where serious ARD has occurred, or is still occurring, in the Meguma Supergroup. These sites have experienced fish kills or presently are served by active ARD treatment facilities. Figure 1.3 shows examples of roadside quarries and exposed roadside outcrop where ARD potential is high and/or is actively occurring at the present time.

Fish kills resulting from construction at the HIA, have been traced back as far as the late 1950s (Table 1.1 showing events from 1957-1976), however, most of the previous work relating to ARD did not start until the middle to late 1970s. Table 1.2 shows a list of some of the better-known studies on ARD in the Meguma Supergroup. Table 1.3 is a list of ARD student research projects. Much of the work performed prior to the inception of this thesis, was related either to ARD treatment, or to investigations

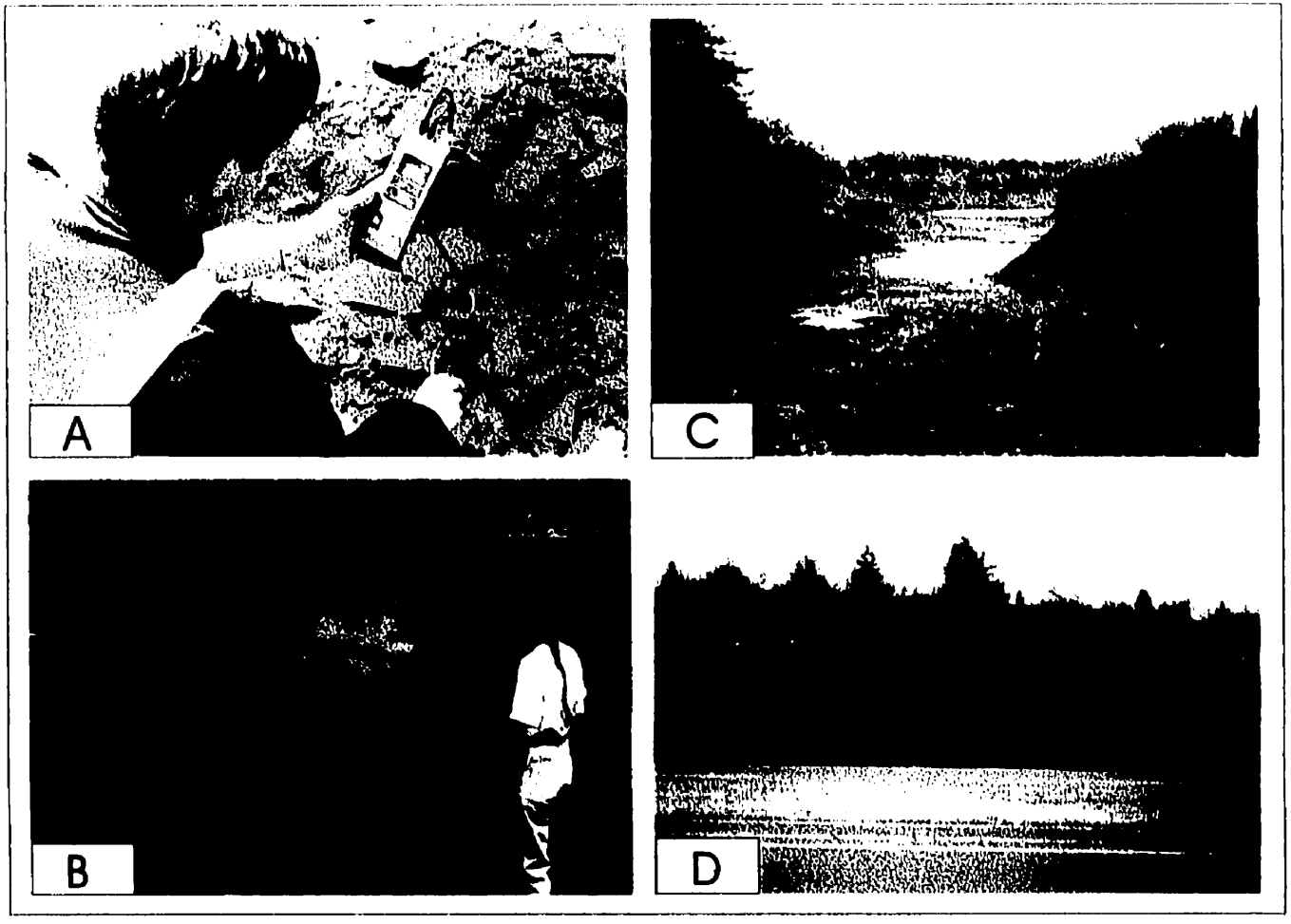

Figure 1.3 Photographs of ARD sites and roadside outcrops showing examples of waste rock piles and ARD ponds. A) pH 2.69 in quarry at Mt. Uniacke, B) pond in a quarry in the Mahone Bay area showing that the size of ARD ponds from quarry operations can be significant, C) quarry in the Mahone Bay area showing the typical nature of waste rock piles left open to oxidizing conditions, D) roadside outcrop near the city of Halifax where bedrock left "in-situ" is exposed to oxidizing conditions.

Table 1.1 History of fish kills and slate disturbances at the Halifax International Airport for the period 1957 to 1976 (Environmental Protection Service, 1976).

Slate Disturbances	Date	Major Fish Kills
Terminal and runways	1957-1960	September, 1960
Imperial Oil	1959-1960	
IMP Hangar (large)	1959	
IMP Hangar (small)	1961	
Air Canada Hangar	1961	
Air Halifax Hangar	1961	October, 1961
Highway slate needs	1965	October, 1965
Avis Service Station	1966	September, 1966
Highway slate needs	1968	November, 1968
Halifax Flying Club	1970	
Mobil Oil Hangar	1972	
Highway Overpass	1974	August, 1974
Aircon Tank Farm	1975	October, 1975
EPA Hangar	1976	September, 1976

Table 1.2 Summary of some of the previous publications on ARD in the Meguma Supergroup. Most publications are cited in the text of this thesis. See the reference list for full citation.

Environmental Protection Service	A report on the causes of fish kills in the Shubenacadie River at Enfield, Nova Scotia.	1976
Thompson, B.D.	An investigation of Meguma bedrock leaching in the Shubenacadie - Stewiacke river basin.	1978
Pettipas, B.	Union Square, Lunenburg County: a statistical evaluation of the effect of acid leachate on water quality.	1979
Kerekes et al.	Comparison of the characteristics of an acidic eutrophic, and an acidic oligotrophic lake near Halifax, Nova Scotia.	1984
Ogden, J.G. & Machell, J.	Ionic and mass balances in a dilute acidified brown water lake.	1985
King, M.	Acid drainage and the acidification of Nova Scotia waters.	1985
Nova Scotia Research Foundation Corporation.	Test geophysical methods to detect shallow sulphide mineralization in Cambro-Ordovician slates near Halifax International Airport.	1985a
Nova Scotia Research Foundation Corporation.	The evaluation of some geophysical methods for the detection of shallow sulphide mineralization (Final Report).	1985b
Lutwick, G.D.	Mineral composition and acid consuming potential of Nova Scotia shales.	1986
Manchester, K.	A survey of quarry pits in Halifax Formation rocks of Southwestern Nova Scotia.	1986
King, M. & Hart, W.	Contribution of acidity and heavy metals to surface and groundwater by pyritiferous slates in the vicinity of the Halifax Airport.	1987
Lund et al.	Impact of acid drainage pollution from mineralized slate at Halifax Airport.	1987
Albright, R.	Prediction of Acid Drainage in Meguma Slates.	1987
Guilcher, M.	Acid mine drainage in reactive slates: "The Halifax Airport Case".	1987
Hennigar T.W. & Gibb, J.E.	Surface and groundwater impacts of acid mine drainage from the Meguma slates of Nova Scotia.	1987
Lund, O.P.	Acid drainage from mineralized slate at Halifax Airport.	1987
McCready, R.G.L.	A review of the physical, chemical and biological measures to prevent acid mine drainage: An application to the pyritic Halifax shales.	1987
Worgan, J.	Acid mine drainage in reactive slates: "The Hailfax International Airport Case" Transport Canada perspective.	1987
Murray et al.	Laboratory and field testing of a salt-supplemented clay cap as an impermeable seal over pyritic slates.	1988
Silver, M.	Construction of a wetland vegetated system designed to decrease acid and toxic metal loadings from quarry effluents.	1988
King, M. & Hart, W.	Groundwater contribution to acid drainage from the Halifax Formation in Nova Scotia.	1990
Bechard et al.	Microbial treatment of acid mine drainage at Halifax International Airport.	1995

Table 1.3 List of ARD-related theses dealing with the Meguma Supergroup.

Student	Degree	General Topic
Roberts, J.D. - 1986	Master of Environmental Studies (MES) - Dalhousie University	Use of peat for ARD treatment
King, M. W. G. - 1987	Master of Applied Science - Technical University of Nova Scotia	Acidity and heavy metals to surface and groundwater near HIA
Bechard, G.M. - 1993	PhD - Carleton University	ARD treatment using microbiological processes
Samostie, A. - 1994	Master of Environmental Studies (MES) - Dalhousie University	GIS for predicting ARD risk
Bottaro, C.S. - 1994	BSc - St. Mary's University	Inhibiting sulphide oxidation
Knee, K. - 1995	BSc - Dalhousie University	Mineralogy and magnetic susceptibility
Robinson, C. - 1996	BSc - Dalhousie University	Mineralogy and acid base accounting
Brown, J.C.S. - 1997	Master of Environmental Studies (MES) - Dalhousie University	Precautionary principle as applied to acid rock drainage regulations
Jones, R.A. - 1997	BSc - Dalhousie University	Relative sulphide oxidation rates

on the extent of the problem and outlining the level of contamination and influence on the local ecosystems. Little work had been done on the mineralogically-related causes or controls, or on the problem of ARD prediction techniques. The current view of many practitioners who work on the treatment of ARD is that ARD cannot be properly treated without a thorough understanding of the causes and controls. Also, avoidance and planning will not be effective without a proper understanding of ARD prediction techniques. It is in this context that the present research project was undertaken.

It is important to note here that ARD problems not specifically related to the mining industry also occur in other areas of the world. For example, trout streams in the Great Smoky Mountains (North Carolina and Tennessee in southeastern United States) have been contaminated by ARD resulting from highway construction through the Anakeesta Formation (Bacon and Maas, 1979). The Anakeesta Formation consists of carbonaceous and sulphidic slate and mica schists with varying amounts of pyrite. In addition, Schaeffer and Clawson (1996) performed work on the identification and treatment of potential acid-producing rocks along a transmission line through the Anakeesta, Nantahala, and Ammons Formations in the Blue Ridge Province of southwestern North Carolina.

In eastern Finland, black shale formations of the Karelia Supergroup have been suggested as the probable source of contamination of mercury in pike in Lake Kolmisoppi (Loukola-Ruskeeniemi, 1990). The black shales are rich in carbon, sulphur, and other metals (e.g., copper, zinc, nickel) as well as mercury, and generally contain between 1% to 3% pyrite. Natural weathering and sulphide oxidation were

suggested as the cause of the mercury contamination (Loukola-Ruskeeniemi, 1992).

These examples discussed above indicate that the potential for ARD exists wherever sulphide-bearing rocks are exposed to oxidizing conditions. This includes both mining and non-mining related areas where sulphide-bearing bedrock is disrupted. The results of this thesis should be applicable to other areas throughout the world were similar bedrock occurs, and the ARD problem is not restricted to the Meguma Supergroup of Nova Scotia.

1.3 Purpose And Objectives

During the initial stages of this research it was recognized that, even though ARD problems in Nova Scotia have been known to occur for many years, there has been little or no work done on the basic mineralogical causes and controls of ARD in the Meguma Supergroup. For example, the presence and abundance of pyrrhotite in the Halifax Group has been known for many years (e.g., McGrath, 1970), but until recently, its relationship to ARD had not been studied in detail (Knee, 1995; Robinson, 1996; Fox et al., 1997; Jones, 1997). This thesis attempts to answer the following questions. Firstly, what is the mineralogy (primary and secondary) of rocks of the Meguma Supergroup and how does this affect the development of ARD? Secondly, how can the mineralogy and geology be used to predict more accurately where ARD will occur? Thirdly, can one effectively integrate field and laboratory data and analyse these using the tools of geographic information systems (GIS)?

1.4 Methodology

Sulphide minerals were studied in detail at Dalhousie University using polished thin sections and reflected light microscopy, electron microprobe microanalysis (Bob McKay, technologist), and X-ray diffraction (Keith Taylor, technologist). The data are used for basic mineral identification, and for determining the major- and trace-element mineral chemistry.

Relative sulphide reactivity rates were determined at Dalhousie University by an experimental design using two sets of polished thin sections treated with: 1) a natural water sample of ARD containing bacteria, and 2) a sterile sample of ARD. Reactivity was monitored using photomicrographs and scanning electron microscopy (see Chapter 3).

The chemical prediction of ARD was studied by acid-base accounting techniques using sulphur and carbon analyses, and acid-base titrations (Chapter 5). Chemical analyses were performed by the author at Dalhousie University or at the Materials Engineering Centre, DalTech Campus, Dalhousie University (Cyril Cole analyst).

Geophysical surveys including terrain conductivity, magnetometer, VLF electromagnetic, spontaneous potential, and induced polarization, for locating shallow sulphide mineralization were used based on surveys carried out in 1985 by Ken Howells (then of the Nova Scotia Research Foundation Corporation) (see Chapter 6). Magnetic susceptibility of rock samples was measured using a hand-held, model K-2 meter (Scintrex Limited) (see Chapter 5).

A GIS-based study consisting of boolean logic, fuzzy logic, and weights of

evidence modelling for ARD prediction was carried out at the College of Geographic Sciences (COGS) (see Chapter 7). The digital data used in the GIS study were provided by the Nova Scotia Department of Natural Resources (Brian Fisher). Data-driven and knowledge-driven map modelling techniques were performed using the SPANS GIS package (TYDAC, Inc.) on Pentium-based systems in the NT/OS environment.

The author proposed, designed, and co-supervised the Honours Theses of Knee (1995), Robinson (1996), and Jones (1997), and their data have been revised, expanded, and incorporated in this thesis.

1.5 Organization

After the general introduction in this chapter, the outline and organization of the remaining thesis is as follows. Chapter 2 is entitled "Pyrrhotite and associated sulphides and their relationship to acid rock drainage in the Halifax Group, Meguma Supergroup, Nova Scotia". This chapter presents details on sulphide mineral chemistry, textures, and pyrrhotite compositions. The chapter was published in *Atlantic Geology*, Volume 33, Number 2, in September, 1997, and is one of six papers of a *Special Issue* on "Environmental Geology of the Meguma Supergroup". Chapter 2 has been co-authored with Clare Robinson and Marcos Zentilli (Fox et al., 1997) and has not been re-written from the original publication.

Chapter 3 is entitled " Relative rates of sulphide mineral reactivity, and the role of mineralogy and texture in the development of acid rock drainage from the Meguma Supergroup, Nova Scotia". This chapter presents the results of a laboratory experiment

designed to determine the relative rates of reactivity of common sulphide minerals in rocks of the Meguma Supergroup (Fox and Jones, in prep).

Chapter 4 is entitled "Secondary minerals and their relationship to acid rock drainage in the Meguma Supergroup, Nova Scotia". This chapter focuses on the importance of secondary minerals and their role in the overall ARD process. The secondary iron minerals, rozenite and schwertmannite have been positively identified.

Chapter 5 is entitled "Static tests and acid base accounting for the prediction of acid rock drainage in the Meguma Supergroup, Nova Scotia". Static tests have become important for ARD prediction and their use is required, in some form or another, as part of environmental regulations in many areas of the world. In Nova Scotia, static testing is required before disposal of sulphide-bearing materials. This chapter compares several methods of determining neutralization potential of rock samples and presents an account of how to measure the acid potential. A new technique is introduced for determining the acid potential using a magnetic susceptibility meter.

Chapter 6 is entitled "Geophysical methods for detecting shallow sulphide mineralization in metasedimentary rocks of the Meguma Supergroup, Nova Scotia". This chapter is co-authored with Dr. Ken Howells (Howells and Fox, in press) and has been submitted for publication in *Atlantic Geology* in a *Special Issue* on "Current Environmental Geology Research in Atlantic Canada" edited by Dr. Ian Spooner and Dr. Sandra Barr of Acadia University. All the original data collection was preformed under the direction of Ken Howells, then of the Nova Scotia Research Foundation Corporation. My contribution has been the re-interpretation of the geophysical data in

terms of mineralogy and ARD, and in the drafting of all figures from original paper copies.

Chapter 7 is entitled "GIS-based knowledge-driven and data-driven modelling for the prediction of acid rock drainage in the Meguma Supergroup, Nova Scotia". This chapter deals with the use of existing digital geological data, combined with various computer-assisted map modelling techniques to produce "ARD predictive maps" that show areas in Nova Scotia where there is a likelihood of ARD development if the bedrock is disrupted and exposed to oxidizing and weathering conditions. Modelling procedures that are covered include boolean logic, fuzzy logic, and weights of evidence methods of combining map layers. Input data layers were regional geology, regional metamorphism, contact metamorphism, vertical gradient airborne magnetics, regional scale anticline axial traces, and location of the Goldenville-Halifax transition zone (GHT).

1.6 General Thesis Conclusions

1) Sulphide type, mineral associations, texture, grain size and trace element content are all important aspects of the causes and severity of ARD. Monoclinic pyrrhotite is the dominant sulphide mineral in the samples collected for this thesis. In general, pyrrhotite has been found to be one of the fastest sulphide minerals to oxidize. On the other hand, the most common form of pyrite found in the Meguma Supergroup, is relatively non-reactive in the short term.

2) Secondary iron minerals such as rozenite are relatively soluble and provide either a sink or source for iron and sulphate ions, depending on the prevailing local conditions at the time. Schwertmannite originates from precipitation of iron-rich solutions and its presence can be used as an indicator for the conditions of ARD. Both these minerals have been identified in ARD areas in the Meguma Supergroup.

3) Static tests, including acid base accounting, are useful for pre-screening rocks for ARD potential. The use of carbonate content to calculate the neutralization potential can be misleading for rocks in the Meguma Supergroup because of the presence of iron and manganese carbonate minerals. Magnetic susceptibility is an important and easily measured parameter of rock samples. As a first approximation, a linear equation derived from susceptibility vs wt% total sulphur content can be effectively used to predict total acid potential (TAP). Error deviation is caused by the contribution of sulphur from the presence of non-magnetic sulphide minerals including pyrite. This simple method can be indexed by routine mineralogical observations.

4) Geophysical surveys including terrain conductivity, magnetometer, and VLF electromagnetic can be used to locate shallow sulphide mineralization. In particular, magnetic surveys can be used to locate pyrrhotite which is a major cause of short term ARD in the Halifax Group. Again, these techniques must be accompanied by routine mineralogical observations to be useful.

5) Digital geological data can be used with various map modelling techniques to produce ARD prediction maps. The ARD prediction maps produced in this thesis cover most of the Meguma Supergroup in eastern mainland Nova Scotia. The maps are of regional-scale, and show areas of high, medium, and low potential of the bedrock to produce ARD if the rocks are exposed to oxidizing conditions. Boolean logic, fuzzy logic, and weights of evidence modelling all indicate that most of the high risk areas are located within the lower Halifax Group and Goldenville Halifax Transition zone (GHT).

Chapter 2

Pyrrhotite and associated sulphides and their relationship to acid rock drainage in the Halifax Group, Meguma Supergroup, Nova Scotia

2.1 Introduction

The physical disruption of sulphide-bearing metasedimentary rocks of the Halifax Group leads to oxidation of iron-sulphide minerals and the generation of acid rock drainage (ARD). Although pyrrhotite occurs in many places throughout the Halifax Group, previous ARD studies have not considered in detail the mineral chemistry, texture, and distribution of this mineral nor how these factors may potentially influence the development of ARD. For this study, pyrrhotite-bearing samples of the Halifax Group were collected in the field and from drill core at four locations in southwestern Nova Scotia. Samples were taken from different geological settings, such as proximal and distal to granitic intrusions and from different stratigraphic positions, to obtain a variety of mineral assemblages. Petrographic, microprobe and X-ray diffraction work indicate that the pyrrhotite in all samples is mainly monoclinic Fe_7S_8, and its composition is relatively homogeneous regardless of geological environment. Inclusions of chalcopyrite and detectable quantities of As, Co and Ni are common. In regionally metamorphosed, greenschist facies areas, pyrrhotite is preferentially aligned along cleavage planes and thus is easily accessible to oxidizing air and fluids. Because pyrrhotite is regionally developed, contains potentially toxic trace elements, and occurs along cleavage planes, it is considered to play a significant

role in ARD development in the Halifax Group. Also, pyrrhotite oxidizes substantially faster than many other sulphide minerals and may be especially significant in the early stages of ARD.

2.2 Background

Acid rock drainage (ARD) results mainly from the oxidation of iron-sulphide minerals. Pyrite (FeS_2) and pyrrhotite ($Fe_{1-x}S$) are two of the most commonly encountered iron-sulphide minerals in areas where ARD is prevalent. However, other sulphide minerals such as sphalerite (Zn(Fe)S), galena (PbS), arsenopyrite (FeAsS) and chalcopyrite ($CuFeS_2$) are also important, especially for the possible release of trace elements into the environment. It is now well established that different sulphide minerals have different relative rates of reactivity and it is widely accepted that pyrrhotite oxidizes substantially faster than pyrite, under both chemically and biologically controlled oxidizing conditions (e.g., Bhatti et al., 1993; Jambor, 1994; Nicholson, 1994; Nicholson and Scharer, 1994; MacInnis et al., 1994). For example, under controlled laboratory conditions (22°C and atmospheric concentrations of O_2), the abiotic oxidation rate of pyrrhotite was found to be on the order of 100 times faster than the oxidation rate of pyrite (Nicholson and Scharer, 1994). Therefore, an abundance of pyrrhotite has the potential to oxidize and create ARD in the surrounding environment at much faster rates than pyrite. This situation could have a detrimental affect on the surrounding ecosystem by creating toxic pulses of metal-rich ARD in shorter periods of time compared to pyrite.

According to Nicholson and Scharer (1994), the oxidation of pyrrhotite is not a well understood process compared to that of pyrite, and the rate controls on the reactions and the oxidation products are poorly known. Recently however, pyrrhotite has become the focus of much research (e.g., Jones et al., 1992; Bhatti et al., 1993; Nicholson, 1994; Mycroft et al., 1995; Pratt et al., 1996). In its simplest form, the overall oxidation of pyrrhotite by oxygen is illustrated by the general equation (Nicholson, 1994):

$$Fe_{(1-x)}S + (2 - \frac{x}{2})O_2 + (x)H_2O \rightarrow (1-x)Fe^{2+} + SO_4^{2-} + (2x)H^+$$

In this equation, x represents the iron-deficiency in pyrrhotite and can vary from 0.0 to 0.125. At the end member where x = 0 (troilite - FeS) no H^+ ions are produced. However, the end-member where x = 0.125 (monoclinic pyrrhotite - Fe_7S_8) leads to the maximum amount of H^+ ions produced. In this case, one mole of Fe_7S_8 leads to 1/4 moles of H^+ ions being produced. Therefore, for pyrrhotite, the number of H^+ ions released into solution depends on its composition (and therefore structural type). In theoretical terms based on simple balanced chemical reactions, of all the possible types of pyrrhotite minerals, monoclinic pyrrhotite (Fe_7S_8) will result in the highest amount of acidity released into the surrounding environment. However, it should be noted that with a typical value of x = 0.1 in pyrrhotite, oxidation still only produces about one-tenth as much acid as pyrite (Nicholson, 1994). Pyrrhotite oxidation may be especially

important in the early stages of ARD development.

It has been speculated that the iron-deficiency in the pyrrhotite crystal structure may have an affect on pyrrhotite oxidation kinetics and that monoclinic pyrrhotite oxidizes faster than hexagonal pyrrhotite although no estimation of the actual rates was given (Nicholson, 1994). More recently, it has been shown that specific surface area of pyrrhotite crystals appears to be a dominant control on reaction kinetics under conditions of oxidation by ferric iron, oxidation by dissolved oxygen and non-oxidative dissolution (Janzen et al., 1997). The rate of pyrrhotite oxidation, and perhaps more importantly the oxidation of sulphide minerals in association with pyrrhotite, may also be affected through galvanic processes (Natarajan, 1990; Kwong and Lawrence, 1994). Under galvanic conditions, the rate of oxidation may depend on such factors as the type and size of sulphide minerals in contact with pyrrhotite, as well as the nature and duration of the contact (Natarajan, 1990). It has also been suggested that trace metal content in sulphide minerals can affect oxidation rates (Kwong and Lawrence, 1994). Regardless, an understanding of the trace metal content is also important due to their possible release into the surrounding environment.

These factors that may affect pyrrhotite oxidation and ARD development are further complicated by the fact that, in nature, pure pyrrhotite phases are relatively rare and most crystals consist of intergrowths of monoclinic and hexagonal phases (e.g., Arnold, 1967). The type and abundance of intergrowths depends on many factors but prevailing thermal conditions, availability of hydrothermal solutions and degree of anisotropic stress (i.e., metamorphic and structural history) are important (Lianxing and

Vokes, 1996).

Pyrrhotite is known to be regionally distributed throughout much of the Halifax Group in Nova Scotia. Although a quantitative estimate of pyrrhotite abundance for the entire Halifax Group is impossible, mainly because of lack of detailed mapping and attention to sulphide minerals in general, previous workers have generally estimated up to 10 wt.% in specific areas (e.g., Schwarz and McGrath, 1974; Binney et al., 1986; Haysom et al., 1997). The purpose of this paper is to present the results of a study of the pyrrhotite mineralogy in a suite of samples selected from a diverse range of geologic environments within the Halifax Group. The focus is on the determination of texture, structural type, and major and trace element content of pyrrhotite and other sulphide minerals associated with pyrrhotite. The actual development of ARD under natural conditions depends on a number of factors including prevailing environmental conditions (e.g., temperature, amount of rainfall), availability of oxidants such as O_2 and Fe^{3+}, and the presence or absence of bacteria. Therefore we view this study as a first step that will lead to a better understanding of the acid generating process in the Halifax Group, and may also aid in the prediction, prevention and eventual remediation of ARD sites.

2.3 Regional Geology

The Cambro-Ordovician Meguma Supergroup crops out throughout much of southern Nova Scotia (Fig. 2.1) and consists of an interstratified assemblage of clastic metasedimentary rocks approximately 12 to 14 km thick (Schenk, 1970). The Meguma

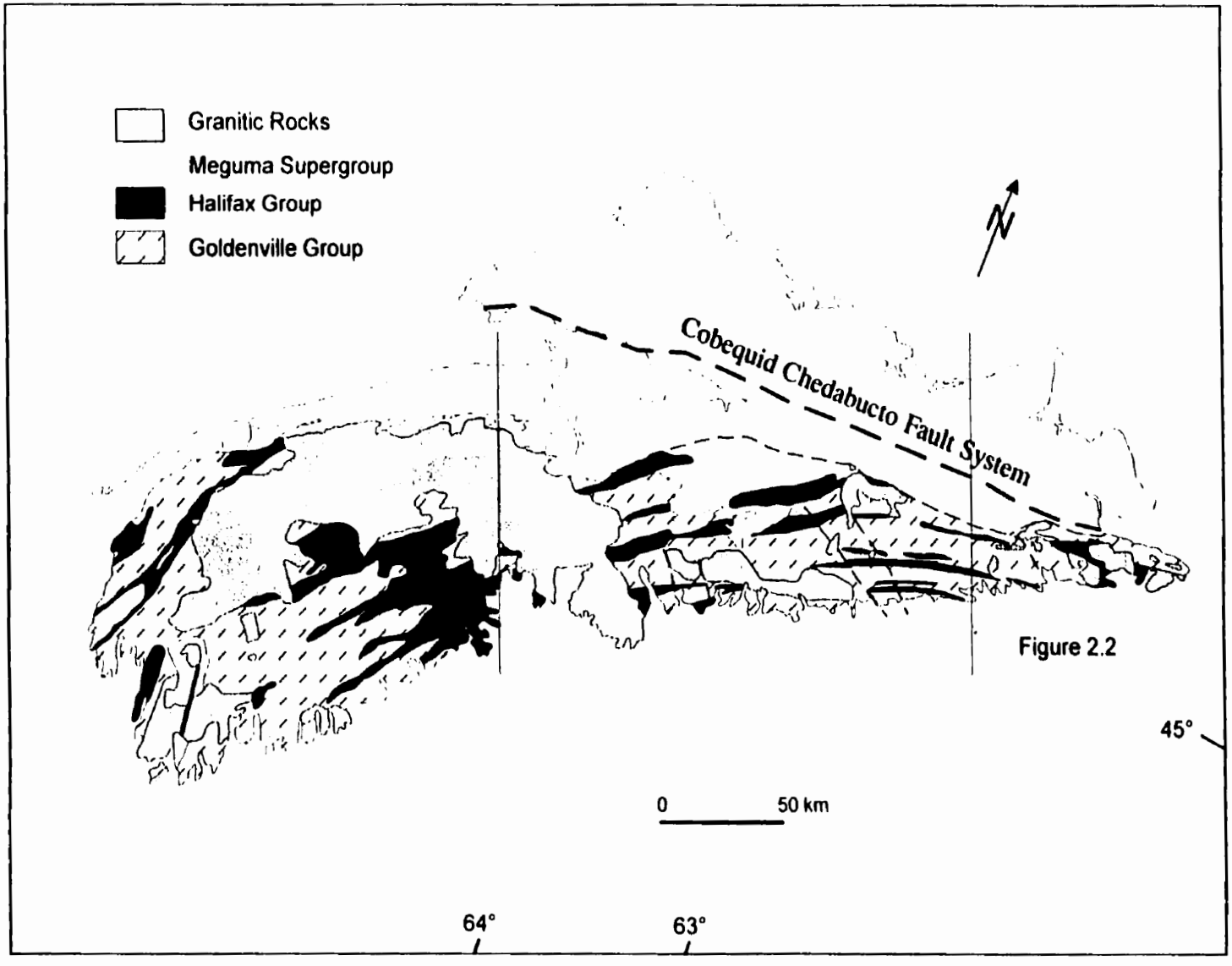

Figure 2.1. Simplified geological map of Nova Scotia showing the distribution of the Meguma Supergroup and granitic rocks (modified from Keppie, 1979a).

Supergroup consists of a lower unit of thickly bedded metasandstone with thin slate interbeds (Goldenville Group) and an upper unit of slate with thin metasiltstone interbeds (Halifax Group). The transition between the two formations is informally referred to as the Goldenville-Halifax Transition zone (GHT) (Zentilli et al., 1986). The GHT contains a distinctive marker unit consisting of finely laminated, manganiferous argillite that contains calcareous or calc-silicate nodules and spessartine coticules (Graves and Zentilli, 1988). Thickness of the GHT varies from less than 50 m at Eastville (Binney et al., 1986) to 2 km in the Mahone Bay area (O'Brien, 1986).

During the Devonian Acadian Orogeny, the Meguma Supergroup was intruded by granitoid rocks, the largest body of which is the South Mountain Batholith (e.g., Fairbairn et al., 1960). Regional metamorphism from greenschist to amphibolite facies, as well as contact metamorphism related to the granitoid intrusions, has affected the Meguma Supergroup (Taylor and Schiller, 1966). Major, kilometer-scale, upright folds trending east-west are developed throughout the Meguma Supergroup, with axial traces approximately parallel to the coastline of southwestern Nova Scotia (Keppie, 1979b). Spaced cleavage is well developed in metasandstone of the Goldenville Group and slaty cleavage is well developed throughout the Halifax Group (Henderson et al., 1986).

2.4 Acid Rock Drainage From The Halifax Group

Disruption of the sulphide-bearing metasedimentary rocks of the Halifax Group results in the development of ARD that has caused serious and costly environmental problems in Nova Scotia (e.g., King, 1985; Manchester, 1986; Hennigar and Gibb,

1987; Worgan, 1987). For example, ARD resulting from construction activities is a serious problem at the Halifax International Airport (HIA). Acidic drainage at the airport site has probably occurred since construction began in the mid 1950s although the first recorded fish kill in the Shubenacadie River, approximately 6 km north of the HIA, occurred late summer of 1960 (Worgan, 1987). Eight fish kills correlating to construction activity at the HIA were recorded in the Shubenacadie River between 1960 and 1976 (Worgan, 1987). It has also been demonstrated that ARD from the HIA has resulted in severely degraded water quality and aquatic habitat in receiving streams in the headwater region of the 50 km^2 Salmon River watershed to the south (Porter Dillon Limited, 1985). In this area, ARD is treated through a lime treatment facility before discharging into McDowell Brook; however, only about 50% of ARD actually gets treated (Lund et al., 1987). Untreated ARD by-passes the treatment facility through a stormwater interceptor drain and through groundwater leakage. Lund et al. (1987) estimated approximately 16,000 kg/year Al and 250,000 kg/year acidity by-pass the treatment facility and discharge directly into McDowell Brook. Total expenditures for remediation efforts at the HIA are unknown but millions of dollars have been spent. Examples include the capping of a waste rock pile at a cost of $800,000, construction of a treatment facility ($500,000), and operation and maintenance of the treatment facility that has cost $240,000 annually since 1982 (Worgan, 1987).

Additional problem areas in Nova Scotia relating to ARD from the Halifax Group have also been documented. ARD has resulted from construction of Highway 107 near Petpeswick Lake (approximately 20 km east of the city of Halifax), where a

trench approximately 0.5 km in length exposed continuous outcrops of the Halifax Group up to 5 m high (Jacques, Whitford and Associates Limited, 1990). Remedial efforts included capping of the exposed slate with shotcrete and the construction and operation of a small treatment facility. In 1977, fish kills in the Mahone Bay area of southwestern Nova Scotia resulted when crushed slate was used to re-surface a secondary road (Thompson, 1978; Pettipas, 1979). Manchester (1986) found an average pH of 3.78 in standing water bodies in 50 slate quarries in the Mahone Bay area. Kerekes et al. (1984) documented the acidification (mean pH of 3.6 and 4.0) of two lakes located approximately 15 km north of the city of Halifax and attributed this to sulphide oxidation from exposed slate in the drainage basin. Also, a wetland vegetated system has been installed at a quarry near the HIA (Silver, 1988). These examples of ARD areas in the Halifax Group suggest that some ARD problem areas are still undocumented, and that the true magnitude of the problem has yet to be addressed.

The seriousness of these accidents and the high cost of abatement and ameliorative procedures have led to the "Sulphide Bearing Material Disposal Regulations" by the Nova Scotia Department of the Environment which require lithological sampling and predictive test procedures before allowing physical disruption of sulphide-bearing rocks (Environment Act. 1994-95, c.1, s.1).

2.5 Abundance And Regional Distribution Of Sulphide Minerals In The Halifax Group

Although ARD from the Halifax Group has been well known for many years,

there is a lack of information concerning the detailed mineralogical aspects of this problem. In particular, the abundance, type, texture, size, trace element content and regional distribution of sulphide minerals, as well as their relationship to carbonate and silicate minerals has not been well documented. For example, it is only recently that the mineralogy of drill core samples from the HIA have been studied in detail (Knee, 1995; Pasava et al., 1995). Both studies have concluded that monoclinic pyrrhotite is the predominant sulphide mineral but pyrite, marcasite, arsenopyrite and chalcopyrite are also present.

Regional-scale magnetic anomalies over the Halifax Group in Nova Scotia are caused by the presence of pyrrhotite (McGrath, 1970; Schwarz and Broome, 1994; King, 1997). Average concentrations of 6 to 12 wt.% (determined by geophysical modelling techniques) and 2 wt.% (determined in a small number of surface samples) have been suggested (Schwarz and Broome, 1994). The discrepancy in estimated pyrrhotite concentrations is discussed in detail by Schwarz and Broome (1994) and may be due to weathering of surface samples or by limitations of the geophysical modelling technique used.

Schwarz and Broome (1994) citing P. McGrath (personal communication) considered that magnetic anomalies in the Halifax Group near granitic intrusions likely result from local concentrations of magnetite but no mention was made of the occurrence of sulphide minerals in such areas. However, O'Brien (1986) reported that pyrite and pyrrhotite are the common sulphide minerals in contact metamorphic aureoles, although the relative abundance of each was not estimated. Samostie (1994)

reported that pyrite is virtually absent from the Halifax Group within 2 km of granitic intrusions, and concluded that risk of ARD in these areas is greatly reduced. However, no mention of pyrrhotite or other sulphide minerals was given, although an adequate assessment of ARD risk can only be done after all mineralogical details are known. Hence, the need for more mineralogical observations in contact metamorphosed rocks of the Halifax Group is vital for the assessment of ARD in such areas.

Lithologies within the GHT also have the potential to cause ARD problems. Based on a regional sampling program, the GHT was found to be a significant control for metals (Graves and Zentilli, 1988). Some calcareous argillite and black slate units are preferentially enriched in Mn, total C, Ba, Pb, Zn, Cu, Mo, W, and Au over average crustal values and other GHT lithologies (Graves and Zentilli, 1988). In general, the highest concentration of metals was found to be associated with iron-sulphide minerals but the average abundances of the sulphide minerals were not determined. Within the GHT at Eastville, a bed of black slate 5 to 15 m thick contains 5 to 10% pyrrhotite (Binney et al., 1986).

2.6 Methods

A total of 15 rock samples from exposed outcrops and drill core were collected from four areas of the Halifax Group (Fig. 2.2). Two of the areas (Halifax and Mount Uniacke sites) are within 0.5 km of the South Mountain Batholith and were chosen to represent areas affected by contact metamorphism. Samples from the Beaverbank Highway site are representative of Halifax Group rocks affected by regional greenschist

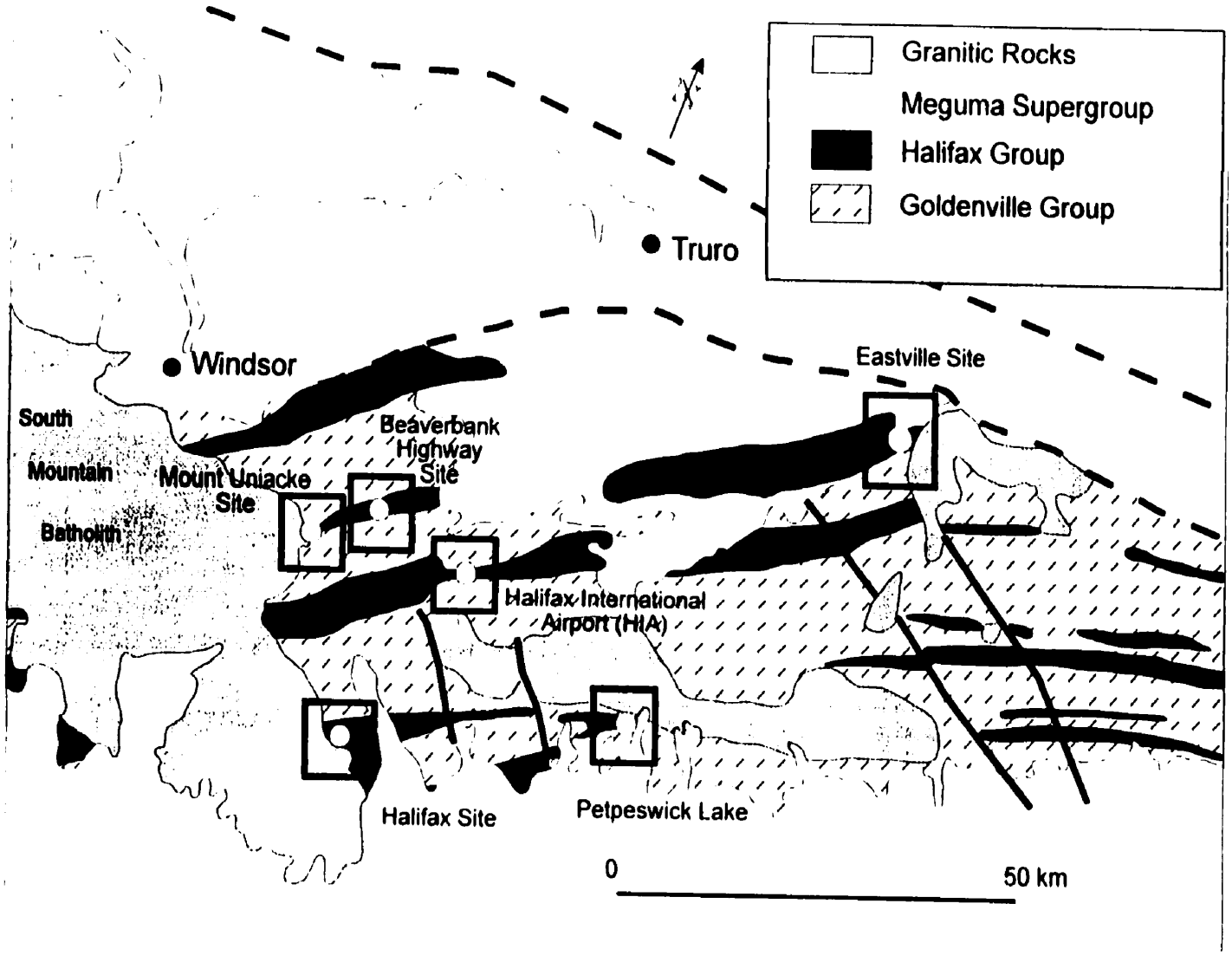

Figure 2.2. Geological map showing location of sample sites. Also shown is the location of the Halifax International Airport (HIA) and Petpeswick Lake, two sites of ongoing mitigation efforts for the abatement of ARD (geology modified from Keppie, 1979a).

facies metamorphism. Drill core from the Eastville site was sampled mainly within the GHT as interpreted by MacInnis (1986).

Samples were chosen on the basis that they contained visible sulphide mineralization and pyrrhotite was specifically targeted using a K-2 magnetic susceptibility meter. The pyrrhotite structural types of interest in this study give at least some susceptibility response because of their iron-deficiency. Polished thin sections were made from all samples and minerals were studied using petrographic and ore microscopic techniques.

A JEOL 733 electron microprobe at Dalhousie University was used to determine the composition of selected grains. The microprobe is equipped with four wavelength dispersive spectrometers and an Oxford Link eXL energy dispersive system which was used for all elements. Resolution of the energy dispersive detector was 137 eV at 5.9 KeV. Each spectrum was acquired for 40 seconds with an accelerating voltage of 15 kV and a beam current of 15 nA. Probe spot size was approximately 1 micron. The raw data were corrected using Link's ZAF matrix correction program. Instrument calibration was performed on cobalt metal. Instrument precision on cobalt metal ($n=10$) was $\pm$ 0.5% at one standard deviation. Relative accuracy for major elements was $\pm$ 1.5 to 2.0%. Geological standards, including arsenopyrite, chalcopyrite, pyrrhotite, and sphalerite, were used as controls. Approximate detection limits in weight % are as follows: Fe (0.15), S (0.30), As (0.20), Zn (0.50), Ni (0.25), Co (0.30), Cr (0.15), Cu (0.30) and Ti (0.10).

X-Ray diffractograms were collected on selected pyrrhotite mineral separates

using a Philips PW1050/37 instrument with Co-K$\propto$ radiation. Most pyrrhotite was separated magnetically, with the exception of pyrrhotite in sample CR-95-003. Pyrrhotite in that sample was very coarse grained and a pyrrhotite "chip" was easily obtainable. The XRD instrument is equipped with a diffracted-beam monochromator and fully automated through the X'PERT hardware - software system (Philips, 1993). Each sample was counted in steps of 0.02° 2θ for 1 second per step. Operating conditions of 40 kV and 45 mA were used for generator tension and generator current, respectively.

2.7 Geology Of The Sample Sites

2.7.1 Halifax site

Three samples (CR-95-001 to CR-95-003) were collected near the Bayers Lake Business Park, near the city of Halifax. Samples were collected within 0.5 km of the contact with the South Mountain Batholith (Fig. 2.2). In general, the outcrops consist of medium to dark grey, massive hornfels. Bedding is still discernable in spite of well developed hornfelsic texture. Any pre-existing cleavage has been destroyed by contact metamorphism. Large (up to 1.5 cm in length) andalusite porphyroblasts are easily distinguishable in outcrop, and cordierite is also present. Sulphide minerals are difficult to detect due to very fine grain size. Detailed mapping has not been done in this area but the samples may be from metamorphosed contact equivalents of the Cunard or Moshers Island members of the Halifax Group, as mapped by O'Brien (1986) in the southwestern part of Nova Scotia.

2.7.2 Mount Uniacke site

At the Mount Uniacke site (Fig. 2.2), two samples (CR-95-004 and CR-95-005) were collected from a slate quarry and one sample (CR-95-006) from a road-side outcrop. All samples were collected within 0.5 km of the contact with the South Mountain Batholith. Thick bedding (1 metre scale) is visible in outcrop and some individual beds are dominated by andalusite and cordierite porphyroblasts. Thin bedding (mm and cm scale) is visible in some hand samples. The appearance of these samples varies from fine to medium grained, from medium to dark grey, and from massive to spotted hornfels that reflects original bedding. Cleavage is present in the spotted hornfels but not in the massive hornfels. Recent detailed mapping suggests these rocks are contact metamorphosed equivalents of the Cunard unit of the Halifax Group (Ryan, 1994; Ryan et al., 1996; Haysom et al., 1997).

2.7.3 Beaverbank Highway site

Four samples (CR-95-007 to CR-95-010) were taken from the Beaverbank Highway site (Fig. 2.2), located about 15 km from the mapped contact with the South Mountain Batholith. Sample locations lie within the Uniacke syncline (Haysom et al., 1997) and the samples were chosen to represent typical Halifax Group rocks affected by regional greenschist facies metamorphism (Keppie and Muecke, 1979). This area of the Meguma Supergroup has been the focus of recent detailed geological mapping and the stratigraphy is presented elsewhere (Ryan, 1994; Ryan et al., 1996; Feetham et al., 1997; Haysom et al., 1997). Samples CR-95-007, CR-95-008 and CR-95-010 are from

the Cunard unit and sample CR-95-009 is located in the lower Beaverbank unit (see Haysom et al., 1997). Samples CR-95-007 and CR-95-008 are medium to light grey, fine grained metasiltstones. Sample CR-95-010 is black slate with well developed cleavage. Sample CR-95-009 is Mn-rich, dark to medium grey metasiltstone. In this sample, spessartine garnet is abundant and thin beds are tightly folded on a centimetre scale. The sample is typical of the calcareous coticule layers described at various other localities in the Meguma Supergroup (e.g., MacInnis, 1986; Graves and Zentilli, 1988; O'Brien, 1988).

2.7.4 Eastville site

At Eastville, stratabound base metals occur in the basal portion (GHT) of the Halifax Group (Binney et al., 1986; MacInnis, 1986; Sangster, 1990). Five samples (CR-95-011, CR-95-012, CR-95-014, CR-95-016 and CR-95-017) were taken of drill core from the Eastville site (Fig. 2.2). The samples are from drill holes 224-12, 224-13, 224-8 and 224-24, which are located more than 3 km from the closest known contact with granitoid intrusions. The samples are of quartz metawacke or calcareous quartz metawacke and contain variable amounts (up to 35%) of spessartine garnet. Samples are from either within or very close to the manganiferous unit of the GHT, as interpreted by MacInnis (1986).

2.8 Sulphide Mineralogy And Textures

Table 2.1 is a summary of sulphide mineral abundances in the samples examined

Table 2.1. Abundance of sulphide minerals.

Sample Site	Sample Number	Po	Py	Cpy	Aspy	Spl	Ma
Halifax	CR-95-001	A		M			
Halifax	CR-95-002	A	M	M			
Halifax	CR-95-003	A		M			
Mount Uniacke	CR-95-004	A	C	M			
Mount Uniacke	CR-95-005	M	C	M			
Mount Uniacke	CR-95-006	A		M	M		
Beaverbank Highway	CR-95-007	A	C	M	M		
Beaverbank Highway	CR-95-008	A	C	M		M	M
Beaverbank Highway	CR-95-009	A		M			
Beaverbank Highway	CR-95-010	A	C	M			M
Eastville	CR-95-011	A	M	M			
Eastville	CR-95-012	A	M	M			
Eastville	CR-95-014	A	M	M			
Eastville	CR-95-016	A	M	M	M		
Eastville	CR-95-017	A	C				

Po = pyrrhotite; Py = pyrite; Cpy = chalcopyrite; Aspy = arsenopyrite; Spl = sphalerite; Ma = marcasite.

A = abundant (> 5%); C = common (1 - 5%); M = minor (< 1%).

in this study. Pyrrhotite is by far the most abundant sulphide mineral and varies from approximately 1 to 15%. In samples not affected by contact metamorphism, pyrrhotite is typically elongate in the plane of cleavage, forming a well defined mineral lineation, and ranges in length from less than 1 mm up to 1 cm (Fig. 2.3 A,B). In contact metamorphosed samples, pyrrhotite is typically much smaller (less than 2 mm in length) and is more commonly disseminated throughout the matrix. A pyrrhotite mineral lineation is evident in some places (Fig. 2.3C,D). In the samples from Eastville examined in this study, pyrrhotite occurs in two textures. One occurrence is mainly massive but confined to individual beds and fills spaces between garnet grains (Fig. 2.3E). The other occurrence consists of tiny (< 0.5 mm) pyrrhotite grains in the center of individual garnet porphyroblasts, or larger pyrrhotite aggregates surrounded by aggregates of garnet. The latter texture is common in the Mn-rich layers of the GHT in the Meguma Supergroup and was also observed in sample CR-95-009 in the Beaverbank Highway site (Fig. 2.3F; see also Feetham et al., 1997). More detailed studies of pyrrhotite mineralogy and texture at Eastville were presented by Jenner (1982) and Binney et al. (1986).

Alteration of pyrrhotite to marcasite (and/or pyrite?) occurs in several of the samples from the Beaverbank Highway site (Fig. 2.3G) and appears to be confined to rocks with well developed cleavage (see also Haysom et al., 1997). This type of replacement texture has been described in mine tailings (Jambor, 1994) and is common in the formation of "birds eye" textures (Ramdohr, 1969). The new mineral formed in the replacement texture is commonly called marcasite but according to Ramdohr

Figure 2.3. Photomicrographs of various sulphide mineral assemblages.

(A) Sample CR-95-008, Beaverbank Highway site, reflected light. Pyrrhotite (po) with long axis parallel to cleavage plane. Scale bar represents 0.62 mm.

(B) Same as A but plane polarized light, crossed nicols.

(C) Sample CR-95-003, Halifax site, reflected light. Fine-grained pyrrhotite (po) in contact metamorphic aureole of the South Mountain Batholith. Scale bar represents 0.62 mm.

(D) Same as C but plane polarized light, crossed nicols. Andalusite (AND) and cordierite (CRD) porphyroblasts are common.

(E) Sample CR-05-011, Eastville site, reflected light. Pyrrhotite (po) fills space between garnet (gnt) porphyroblasts. Scale bar represents 0.62 mm.

(F) Sample CR-95-009, Beaverbank Highway site, reflected light. Aggregate of pyrrhotite (po) rimmed by aggregates of spessartine garnets (gnt). This is a common feature of the coticules in the GHT throughout the Meguma Supergroup. Scale bar represents 0.155 mm.

(G) Sample CR-95-010, Beaverbank Highway site, reflected light. Pyrrhotite (po) rimmed by marcasite (ma) and/or pyrite?. Scale bar represents 0.62 mm.

(H) CR-95-007, Beaverbank Highway site, reflected light. Euhedral pyrite (py) associated with anhedral pyrrhotite (po). Scale bar represents 0.62 mm.

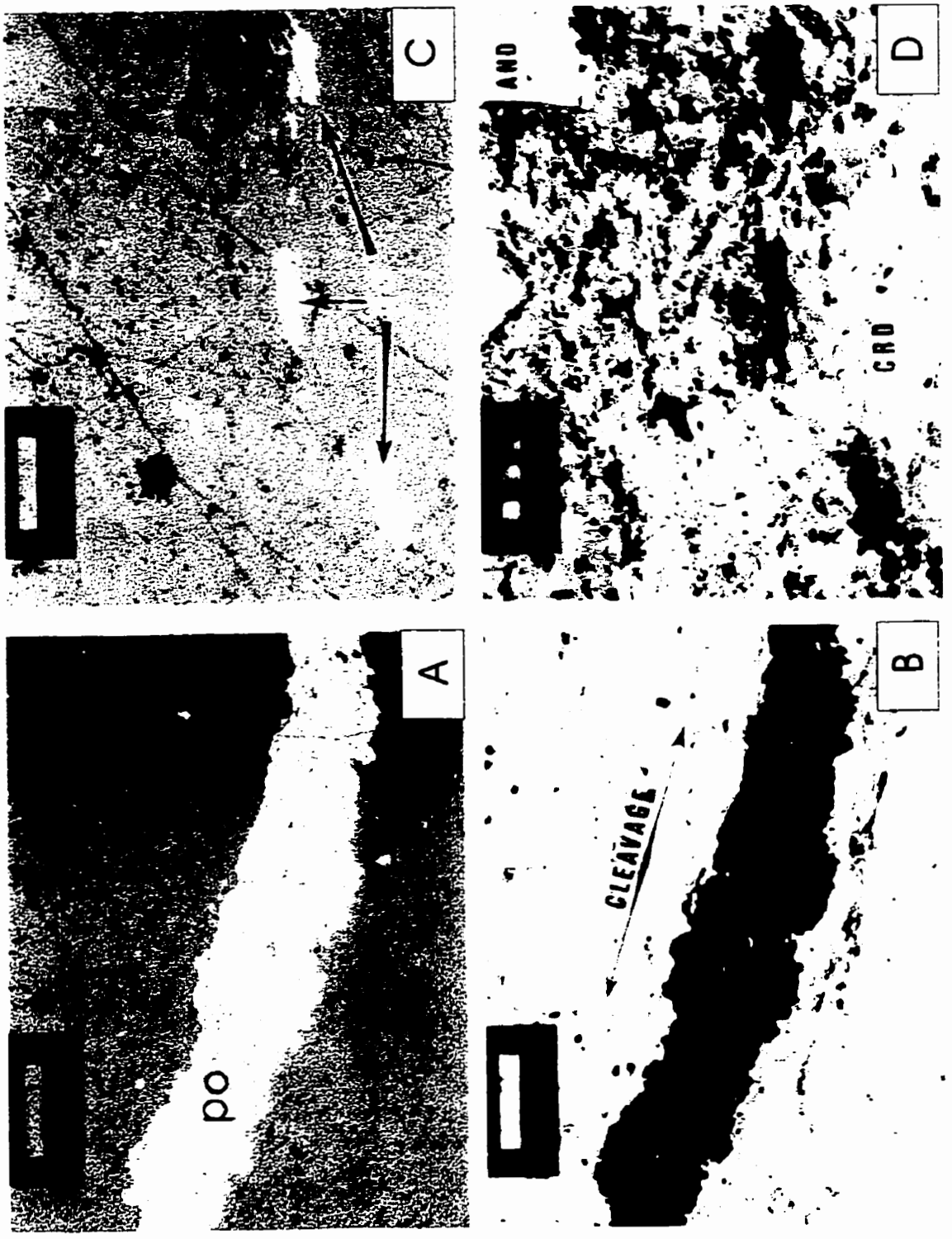

Figure 2.3 (Continued)

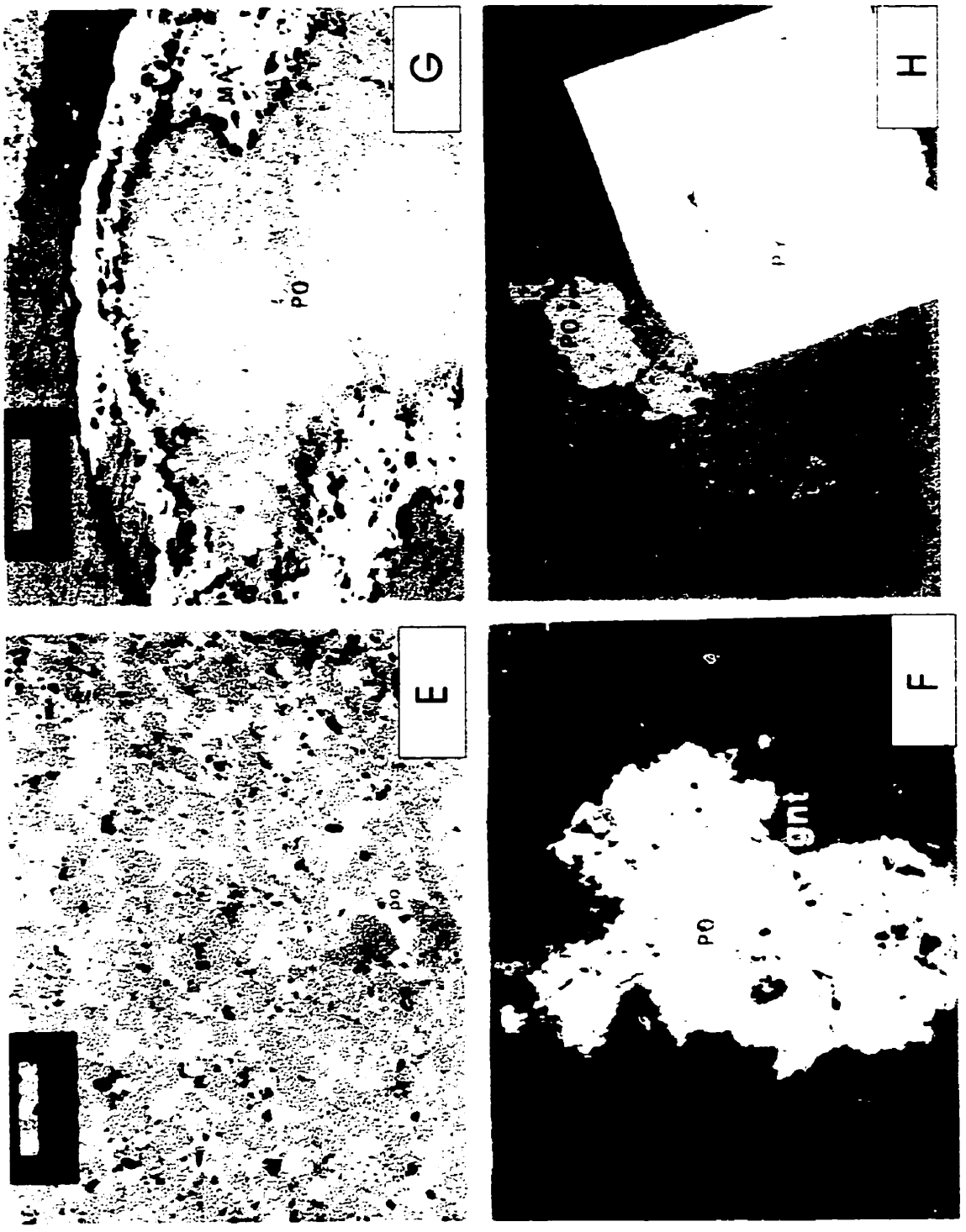

Figure 2.3 (Continued)

(1969), pyrite either coexists or is the only secondary mineral present. Replacement rims of ilmenite and/or rutile (anatase?) are common around pyrrhotite and occur in nearly all samples. Also in virtually all samples, pyrrhotite crystals contain abundant inclusions of silicate, oxide and other sulphide minerals. In several cases, inclusion trails are aligned and curved parallel to the cleavage direction; in other samples the inclusions are entirely random. The curved inclusion trails appear to be confined to low grade, regionally metamorphosed rocks such as at the Beaverbank Highway site and have been observed in samples taken at the HIA (unpublished data).

Pyrite is the next most abundant sulphide mineral, comprising less than 5% of all samples. It commonly occurs as large (0.5 cm or more across) euhedral grains with sharp crystal edges (Fig. 2.3H). Inclusions in these crystals are much less abundant than in pyrrhotite. Marcasite (and/or pyrite?) is a minor component and was observed only in samples CR-95-008 and CR-95-010. Marcasite rims pyrrhotite in both cases forming a replacement texture (see above). The secondary marcasite in this texture contains abundant inclusions and is anhedral, with embayed or corroded crystal edges. Other sulphide minerals that are common but occur in only minor amounts (less than 1%) include chalcopyrite, sphalerite and arsenopyrite. In addition, sample CR-95-006 contains the arsenic mineral, löllingite ($FeAs_2$). Typically, these minerals occur as inclusions in pyrrhotite.

2.9 Sulphide Mineral Chemistry

Average analyses of pyrrhotite crystals are presented in Table 2.2. The majority

Table 2.2. Pyrrhotite compositions (wt.%)*.

Sample Site	Sample Number	Fe	S	As	Ni	Co	Total	Fe**	S**
Halifax	CR-95-001 (2)	59.49	38.70	0.24	0.03	0.24	98.97	7.062	8.000
Halifax	CR-95-002 (1)	59.76	38.01	0.32	0.35	0.40	98.89	7.224	8.000
Halifax	CR-95-003 (2)	59.14	38.60	0.21	0.13	0.29	98.53	7.038	8.000
Mount Uniacke	CR-95-004 (5)	60.00	39.83	0.19	0.07	0.20	100.43	6.920	8.000
Mount Uniacke	CR-95-006 (2)	59.75	38.66	0.22	0.05	0.22	99.01	7.100	8.000
Beaverbank Highway	CR-95-007 (3)	60.37	39.24	0.25	0.05	0.30	100.34	7.067	8.000
Beaverbank Highway	CR-95-008 (2)	61.08	39.20	0.40	0.02	0.05	100.89	7.157	8.000
Beaverbank Highway	CR-95-009 (2)	59.03	38.74	0.23	0.38	0.24	98.96	7.000	8.000
Beaverbank Highway	CR-95-010 (7)	60.05	39.70	0.24	0.05	0.19	100.42	6.949	8.000
Eastville	CR-95-011 (6)	60.11	39.94	0.20	0.18	0.32	100.91	6.912	8.000
Eastville	CR-95-012 (5)	60.00	39.88	0.22	0.06	0.27	100.51	6.912	8.000
Eastville	CR-95-014 (5)	59.54	39.94	0.28	0.19	0.20	100.29	6.848	8.000

* Values are averages. Number of analyses given in parentheses.

** The two last columns for Fe and S represent atomic proportions in the formula of pyrrhotite.

of analyses cluster around the monoclinic pyrrhotite end-member (Fe_7S_8), the most magnetic and iron-deficient phase (Fig. 2.4). The similarity in compositions indicate that, for the crystals analyzed in this study, pyrrhotite composition is relatively uniform (monoclinic type) regardless of the specific geological environment. The average composition of most pyrrhotite is near 46.5 atomic % Fe, in the ideal monoclinic pyrrhotite range (Fig. 2.4b). The average stoichiometric proportions of Fe and S range from $Fe_{6.912}S_{8.000}$ to $Fe_{7.224}S_{8.000}$ (Table 2.2). These values are similar to analyses of pyrrhotite from samples from drill core taken at the HIA, which cluster around 46.5 atomic % Fe (Fig. 2.5). The average stoichiometry of pyrrhotite from the HIA site was calculated to be $Fe_{7.058}S_{8.000}$, indicative of monoclinic pyrrhotite (Pasava et al., 1995).

Trace element contents in pyrrhotite (Table 2.2) are mostly below or very close to detection limits; however some pyrrhotite contains significant concentrations of arsenic, nickel and cobalt. Although only in trace amounts, these elements may have environmental implications considering the relatively high rate of reactivity of pyrrhotite compared to some of the other sulphide minerals such as pyrite, arsenopyrite and sphalerite (e.g., Jambor, 1994; Nicholson, 1994). Trace element contents are also given for pyrite, arsenopyrite, chalcopyrite and sphalerite (Table 2.3) and indicate that arsenic and cobalt are significant in pyrite and cobalt is significant in arsenopyrite.

2.10 X-ray Diffraction Analyses

Stoichiometric pyrrhotite (troilite) contains equal proportions of iron and sulphur and is represented by the formula FeS (or Fe_8S_8). However, most pyrrhotite in

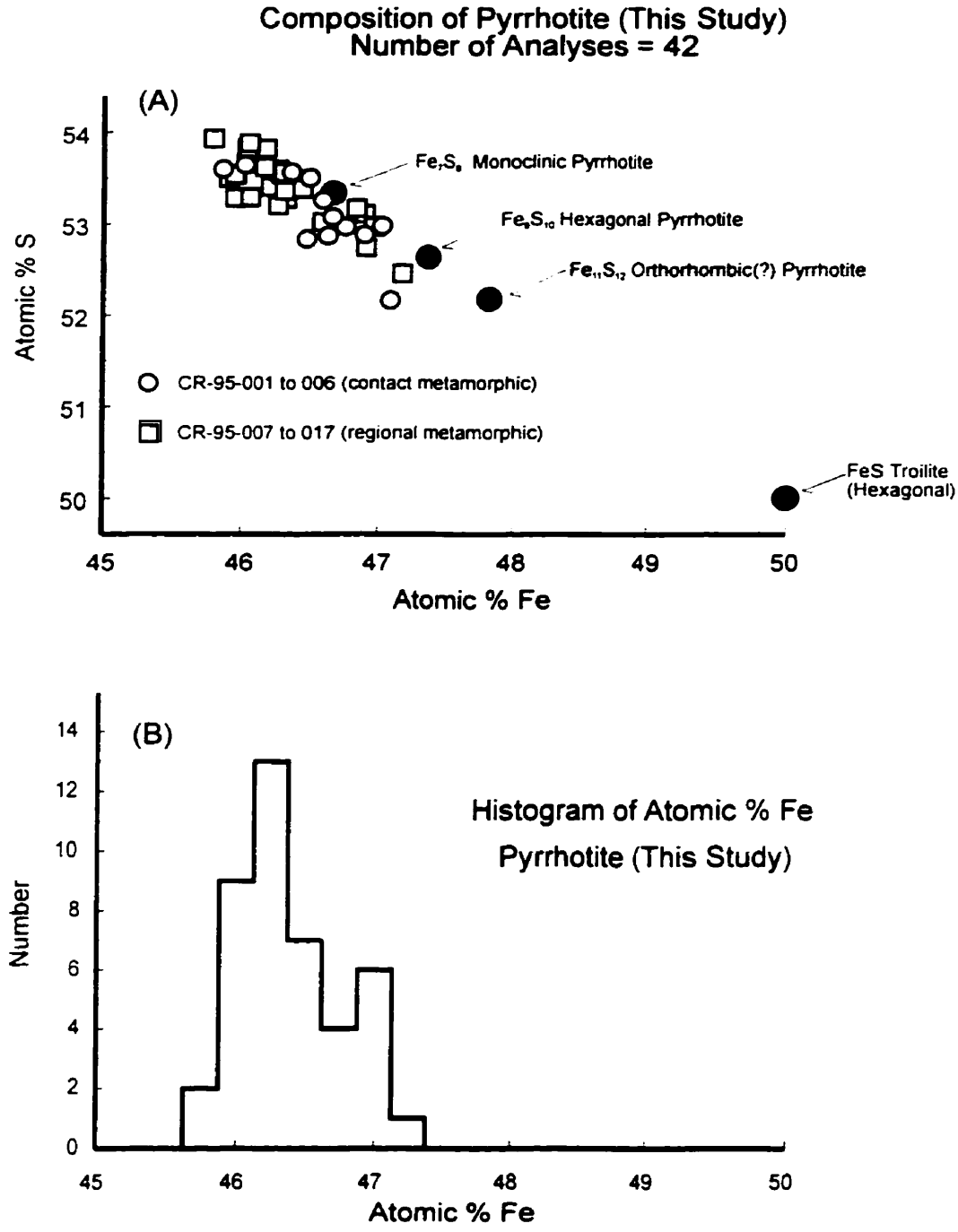

Figure 2.4. (A) Plot of atomic % S against atomic % Fe for pyrrhotite analyzed in this study. Several ideal pyrrhotite compositions are plotted for reference (structural types from Craig and Scott, 1974). Most pyrrhotite clusters around monoclinic Fe_7S_8. (B) A histogram showing that the majority of crystals contain between 46 and 47 atomic % Fe.

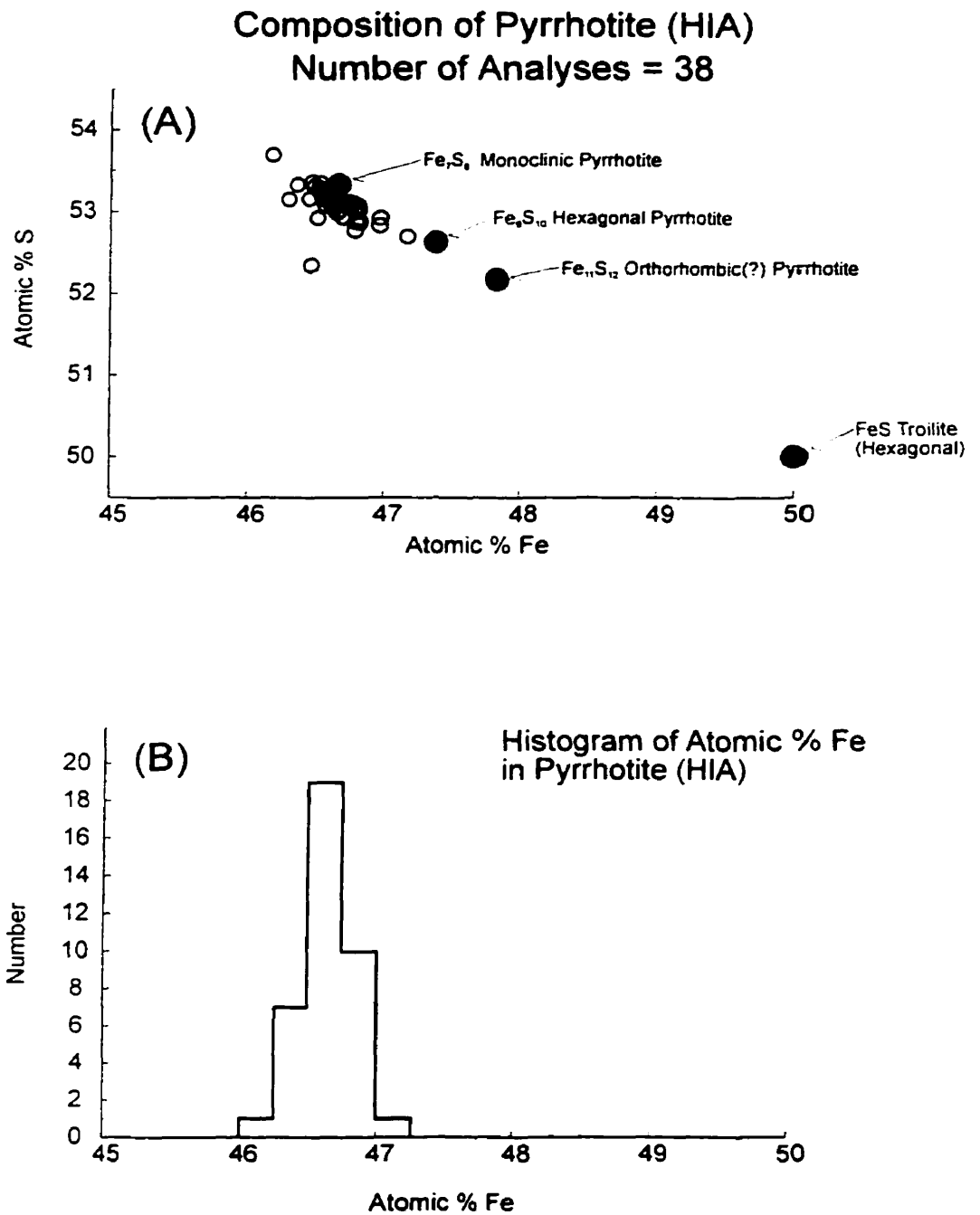

Figure 2.5. (A) Plot of atomic % S against atomic % Fe for pyrrhotite crystals from drill core taken at the Halifax International Airport (data from Knee, 1995). The majority of pyrrhotite is monoclinic Fe_7S_8. (B) Histogram showing that the majority of crystals contain between 46 and 47 atomic % Fe.

Table 2.3. Pyrite, arsenopyrite, chalcopyrite, and sphalerite compositions (wt.%)*.

Mineral	Sample Site	Sample Number	Fe	S	As	Zn	Cu	Ni	Co	Ti	Total
pyrite	Mount Uniacke	CR-95-004 (3)	46.53	52.21	0.26	0.07	0.04	0.23	0.26	0.00	99.61
pyrite	Mount Uniacke	CR-95-005 (1)	46.53	53.28	0.24	0.19	0.01	0.17	0.19	0.08	100.72
pyrite	Beaverbank Highway	CR-95-007 (5)	46.68	52.75	0.48	0.09	0.01	0.09	0.17	0.00	100.28
pyrite	Beaverbank Highway	CR-95-008 (2)	47.21	53.52	0.66	0.19	0.06	0.00	0.14	0.00	101.81
pyrite	Beaverbank Highway	CR-95-010 (6)	46.54	53.31	0.26	0.10	0.02	0.05	0.15	0.00	100.44
pyrite	Eastville	CR-95-014 (1)	46.18	52.76	0.33	0.21	0.00	0.10	0.22	0.00	99.79
arsenopyrite	Mount Uniacke	CR-95-006 (2)	31.89	16.86	48.22	0.00	0.07	0.10	1.57	0.01	98.73
arsenopyrite	Beaverbank Highway	CR-95-007 (1)	34.79	20.34	44.34	0.05	0.00	0.00	0.27	0.00	99.79
chalcopyrite	Mount Uniacke	CR-95-006 (1)	30.06	33.92	0.07	0.01	36.28	0.00	0.00	0.01	100.34
chalcopyrite	Beaverbank Highway	CR-95-008 (3)	30.81	34.44	0.07	0.03	36.66	0.00	0.07	0.03	102.11
chalcopyrite	Beaverbank Highway	CR-95-009 (1)	30.51	34.14	0.10	0.27	36.34	0.03	0.21	0.01	101.63
chalcopyrite	Beaverbank Highway	CR-95-010 (2)	30.72	34.69	0.10	0.14	35.66	0.00	0.01	0.00	101.34
sphalerite	Beaverbank Highway	CR-95-008 (3)	5.65	29.30	0.00	57.18	0.49	0.03	0.07	4.43	97.14

* Values are averages. Number of analyses given in parentheses.

nature is iron-deficient and can be expressed by the simplified formula $Fe_{1-x}S$ where x ranges from 0.0 to 0.125 (i.e., compositions from Fe_8S_8 to Fe_7S_8). Troilite is non-magnetic and is relatively rare, occurring mostly in meteorites, but it has been described in some sulphide ores from various localities throughout the world (e.g., Carpenter and Desborough, 1964; Lianxing and Vokes, 1996). The structure of troilite is hexagonal and is a derivative structure of the NiAs mineral nickeline (Wuensch, 1974). All pyrrhotite minerals are considered to be derivatives of the NiAs structure through suppression of the symmetry operation translation (Wuensch, 1974). This situation leads to larger-than-normal unit cells called superstructures. Because of the range of Fe-deficiency (non-stoichiometry) for most pyrrhotite minerals, a variety of superstructures are possible, such as 4C monoclinic, 1C hexagonal, 5C hexagonal and 11C orthorhombic (e.g., Carpenter and Desborough, 1964; Fleet, 1971; Craig and Scott, 1974; Morimoto et al., 1975). For the purposes of this study, the traditional classification of hexagonal and monoclinic structural types (Arnold, 1967; Vaughan and Craig, 1978) is used.

X-ray diffraction powder peaks in the 50° to 52° 2θ range (Co Kα) can be used to determine the pyrrhotite structural state (Arnold, 1966, 1969). Two closely spaced reflections of approximately equal intensity are indicative of monoclinic pyrrhotite, whereas a single peak indicates hexagonal pyrrhotite (Vaughan and Craig, 1978). Arnold (1966) showed that for double-peak profiles, increasing intensity of the lower 2θ peak corresponds to an increase in the abundance of hexagonal pyrrhotite in monoclinic-hexagonal mixtures.

Five samples of pyrrhotite from this study were analysed by the X-ray diffraction powder method (Fig. 2.6). All five samples show near-equal intensity double peaks, indicating that the majority of the pyrrhotite has monoclinic structure. However, double-peak intensities in the same sample vary slightly. Samples CR-95-003 and CR-95-006 show a more intense lower (left side) 2θ peak, possibly reflecting a minor component of hexagonal pyrrhotite. The other samples (CR-95-001, CR-95-007 and CR-95-011) show more intense higher (right side) 2θ peaks. This is consistent with so-called "anomalous" pyrrhotite described by Clark (1966). Little is known about "anomalous" pyrrhotite in terms of its stability field but it is apparently common in low-temperature, sedimentary environments. Like hexagonal pyrrhotite, it is considered to be antiferromagnetic but may have a triclinic(?) structure (Clark, 1966). Taylor (1971) has shown that one possible way in which anomalous pyrrhotite forms is by oxidation of hexagonal pyrrhotite, although he also indicated that it has been described as forming borders or rims on monoclinic pyrrhotite.

The XRD analyses presented here suggest that the main pyrrhotite type is monoclinic Fe_7S_8. This is consistent with results from microprobe analyses presented above although some variation in Fe and S proportions occur. Hexagonal pyrrhotite may be present in minor amounts and anomalous pyrrhotite may occur, but more detailed work needs to be done to further validate this little-known pyrrhotite type. In terms of chemical behaviour and ARD development, the distinction between monoclinic and anomalous pyrrhotite types may not be significant, as the proportions of Fe and S are very similar.

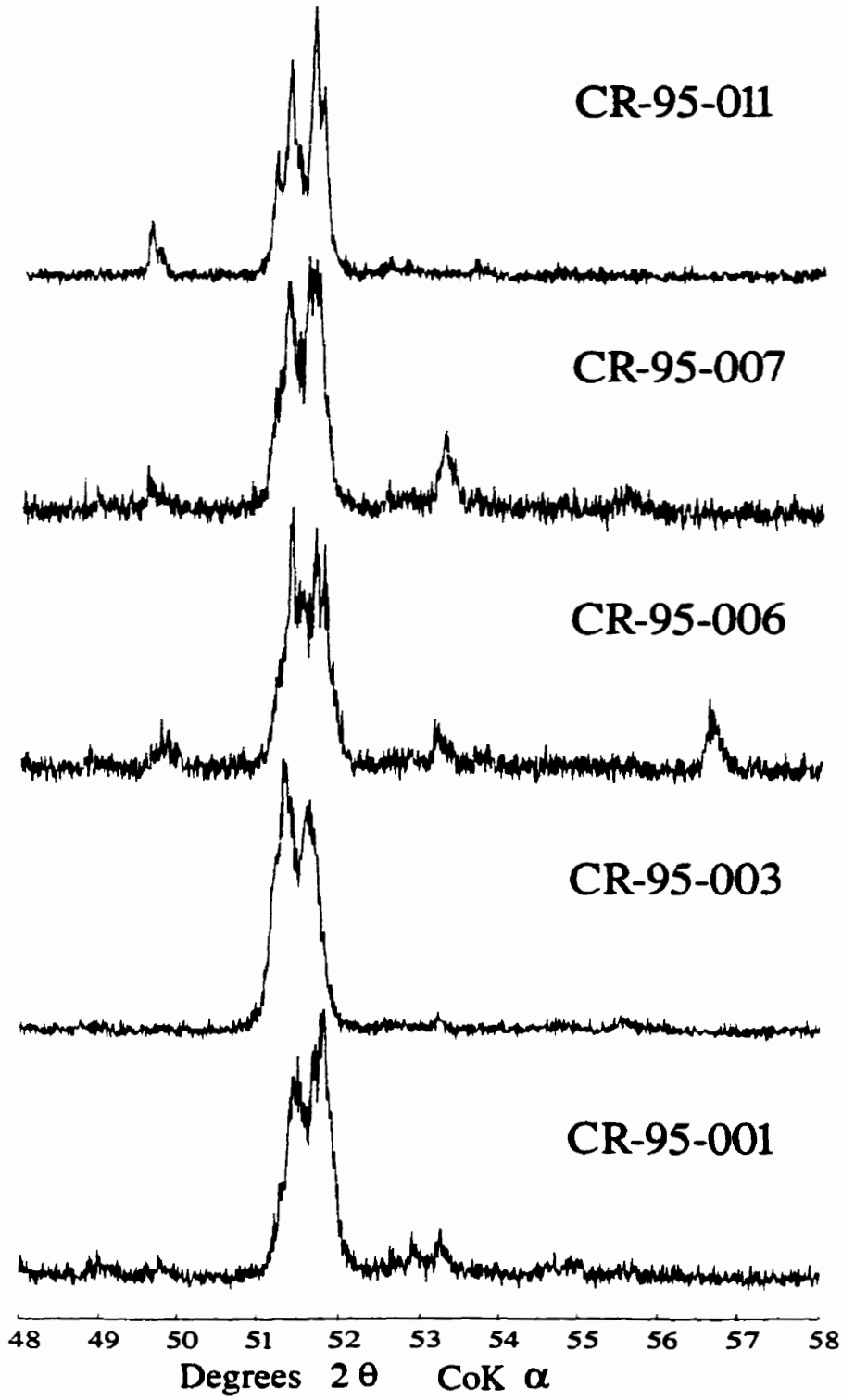

Figure 2.6. Powder XRD diffractograms for five representative samples from this study. All patterns show typical double peaks indicative of monoclinic Fe_7S_8. See text for further discussion.

2.11 Discussion

The data and observations presented above have important implications for understanding the processes involved in the production of ARD from Halifax Group rocks. Firstly, identification of the major sulphide minerals in the Halifax Group, including the abundance and regional distribution of monoclinic pyrrhotite (Fe_7S_8) is of fundamental importance. The higher reactivity of pyrrhotite compared to pyrite (and most other sulphide minerals) makes its proper identification essential. In simple terms, high reactivity and an abundance of pyrrhotite lead to high production of ARD under the right oxidizing conditions. This is especially true in the initial stages of ARD development. The pyrrhotite examined in this study appears to be almost purely monoclinic, with only minor amounts of hexagonal and possibly anomalous pyrrhotite types. The monoclinic variety may be the fastest to oxidize and will theoretically contribute the maximum amount of acidity compared to other pyrrhotite forms. Oxidation tests are currently in progress to test these hypotheses and it should be emphasised that actual oxidation kinetics under field conditions can be assessed only on a site-specific basis.

Secondly, mineral texture is an important factor. In regionally metamorphosed (greenschist facies) areas of the Halifax Group, pyrrhotite is commonly coarse grained and occurs along cleavage planes. When these rocks are disrupted by activities such as construction or quarrying, they tend to break naturally along the cleavage planes, exposing an increased amount of pyrrhotite to oxidation processes. Such activities may also result in grain size reduction of pyrrhotite. Grain size reduction may also lead to

increased oxidation rates by exposing higher surface areas of the pyrrhotite crystals. Natural weathering processes may also lead to increased pyrrhotite oxidation because of the easy access of fluids to pyrrhotite surfaces by fluid migration along cleavage planes.

In contact metamorphosed rocks, pyrrhotite texture is quite different. Pyrrhotite is finer grained and evenly disseminated throughout the matrix. The smaller grain size means higher surface area but fluid access to crystal surfaces is limited because cleavage is not well developed. Consequently, ARD development in these areas may be less significant than in regionally metamorphosed areas but this has to be assessed on a site specific basis. For example, this may be the case under natural weathering conditions as in a roadside outcrop. However, these textural observations may be less important in a tailings environment where all grains are reduced to silt size particles.

The pyrite observed in this study is typically euhedral with sharp crystal edges and does not form along cleavage planes. Jones and Fox (1997) and Jones (1997) have determined that euhedral pyrite is considerably resistant to oxidative dissolution under acidic conditions (over a six week period). Under natural field conditions, given its relative resistance to oxidation and its textural features, pyrite may not pose as significant a risk as pyrrhotite, especially in the short term. Secondary marcasite (and/or pyrite?) replaces pyrrhotite and has only been observed in the low grade, greenschist facies rocks. The marcasite is anhedral with highly corroded crystal edges, occurs along cleavage planes, and would therefore be easily accessible to fluids. The other sulphide minerals (chalcopyrite, arsenopyrite, and sphalerite) typically occur as inclusions in pyrrhotite crystals and it is possible they are galvanically protected from

oxidation.

Thirdly, in addition to sulphide mineral identification and texture, trace element abundances are also important. Arsenic, for example, will not be released from arsenopyrite if that mineral is not reactive. Trace amounts of arsenic in pyrrhotite, however, may easily be released into the surrounding environment considering that pyrrhotite is highly reactive. As presented above, pyrrhotite can also contain detectable concentrations of Ni and Co. These elements have been found in very high concentrations, for example, in pore water (Ni: 181-188 mg/L; Co: 93-105 mg/L) and seepage (Ni: 23-43 mg/L; Co: 4.5-9.8 mg/L) from the waste rock pile at the HIA (Lund et al., 1987). These observations suggest that pyrrhotite is a contributor to the ARD problem at the HIA and an understanding of that mineral should be a part of any remediation effort, as well as future planning processes.

ARD from the Halifax Group has been, and continues to be, a very expensive environmental problem in Nova Scotia. Sulphide-rich rocks are widespread throughout the province and avoidance is difficult, especially for large scale construction projects such as highway development, municipal expansion, or any other projects that require disruption of the bedrock. For example, the entire city of Halifax is underlain by the Halifax Group and avoidance is impossible. Mineralogical and geological research such as this study is fundamental to the understanding of ARD development, and through this type of approach successful remediation efforts may be applied. ARD problems are unlikely to be fixed if it is not understood how they develop in the first place. Predicting which rocks and areas are susceptible to ARD can only be accomplished

through a thorough understanding of the mineralogy.

2.12 Conclusions

The predominant sulphide mineral in the samples from the Halifax Group examined in this study is pyrrhotite. Also present, in lesser amounts, are pyrite, marcasite, chalcopyrite, arsenopyrite and sphalerite. Microprobe data indicate that the pyrrhotite is the monoclinic variety (Fe_7S_8). The compositions of all pyrrhotite crystals probed are between 45.5 and 47.5 atomic % Fe, in the ideal monoclinic pyrrhotite range. Data from pyrrhotite in drill core samples from the Halifax International Airport overlap with the data from this study.

XRD analyses of pyrrhotite from five samples show typical, almost equal intensity double peaks, indicative of monoclinic pyrrhotite. These data confirm the results of the microprobe work. Comparisons of pyrrhotite compositions among samples taken from different geological settings (i.e., within and outside the contact metamorphic aureoles of granitic intrusions) suggest there is little to no regional variation in pyrrhotite composition.

This study confirms a risk of ARD is present throughout the lower Halifax Group (including the GHT) in central Nova Scotia. Whether or not ARD actually occurs depends on numerous factors and can only be assessed on a site-specific basis. Thorough sampling and accurate testing to predict ARD potential, including detailed mineralogical studies, are an essential step in land use planning throughout the Halifax Group.

Chapter 3

Relative Rates Of Sulphide Mineral Reactivity, And The Role Of Mineralogy And Texture In The Development Of Acid Rock Drainage From The Meguma Supergroup, Nova Scotia

3.1 Introduction

The intensity and duration, and hence, the environmental impact of acid rock drainage (ARD) can be attributed, to a large degree, to the relative rate of reactivity of the sulphide minerals present. Simply, if pyrite is non-reactive, and is the only sulphide mineral present, no ARD will develop. On the other hand, the release of Cu from chalcopyrite will only be possible when that mineral begins to react, and can only be released until all the chalcopyrite is consumed. Clearly the relative rate of reactivity is important for the prediction of ARD chemistry as well as for ARD remediation.

Unfortunately, there is no single, unique reactivity sequence for sulphide minerals. Perhaps the only generality that appears to hold under natural settings, and in tailings impoundments, is that pyrrhotite is more susceptible to reaction than pyrite (Jambor, 1994). Table 3.1 shows the differences in relative reactivities of some common sulphide minerals and it is clear that the differences are substantial. As presented by Jambor (1994), marcasite can be highly reactive or relatively unreactive; pyrrhotite however, is nearly always one of the first sulphide minerals to react. In a study of sulphide oxidation in samples from three mines owned by Placer Dome Inc., Kwong and Lawrence (1994) demonstrated the mineralogy-related factors that influence the rate and extent of sulphide oxidation. They ranked the factors as follows: formation

Table 3.1 - Relative reactivity of some common sulphide minerals (from Jambor, 1994)

Increasing order of resistance	Condition
sphalerite > galena > chalcopyrite > pyrite	abiotic, calculated
marcasite > pyrrhotite > chalcopyrite > pyrite = arsenopyrite	waste rock
pyrrhotite > chalcopyrite > fine pyrite > sphalerite > galena > coarse pyrite	gossan
pyrrhotite > arsenopyrite > pyrite > chalcopyrite > sphalerite > galena	laboratory, pH 2-6
pyrrhotite > pyrrhotite-pyrite > pyrrhotite-arsenopyrite > arsenopyrite > pyrite > chalocpyrite > sphalerite > galena > chalcocite	——
pyrrhotite > chalcocite > tetrahedrite > galena > arsenopyrite > sphalerite > pyrite > marcasite > chalcopyrite	——
sphalerite > tetrahedrite group > chalcopyrite > Bi-Sb sulfosalts > galena > arsenopyrite > pyrite	gossan
pyrite > chalcopyrite > galena > sphalerite	air oxidation

of a galvanic couple > defects density > grain size > bacterial coverage > trace and minor element content > crystallographic orientation > abundance of acid-neutralizing neighbour. However, these factors depend on the local circumstances, and it therefore becomes a matter of studying the details of mineralogy, mineral chemistry, textures, and mineral associations for each local area in order to determine the relative rates of sulphide reactivity.

The purpose of this part of the study was to determine the relative order of reactivity (both chemical and microbially assisted) of the following representative sulphide minerals from the Meguma Supergroup: monoclinic pyrrhotite (Fe_7S_8), hexagonal pyrrhotite (Fe_9S_{10}), pyrite (FeS_2), arsenopyrite (FeAsS), chalcopyrite ($CuFeS_2$), galena (PbS) and sphalerite (ZnS). These minerals were identified using a petrographic microscope, along with microprobe analyses, and x-ray diffraction data . This study is significant because there were no previous studies of sulphide oxidation in rocks of the Meguma Supergroup in Nova Scotia. Therefore, there was a limited knowledge-base about the factors that control the development of ARD in these rocks.

In general, sulphide minerals exposed to unfiltered, biologically active ARD dissolve faster than in filtered ARD. In the microbial treatment, the relative degree of reactivity among sulphide minerals was galena > hexagonal pyrrhotite > monoclinic pyrrhotite > marcasite > > arsenopyrite, sphalerite > pyrite > chalcopyrite. In the sterile treatment, the relative degree of reactivity was galena > marcasite > monoclinic pyrrhotite > > hexagonal pyrrhotite, arsenopyrite, sphalerite > pyrite > chalcopyrite.

Based on the overall abundance (up to 10% by volume), and the relative reaction rates, monoclinic pyrrhotite is one of the most important sulphide minerals contributing to acidity in the short term, and initial stages of ARD development. Marcasite reacted very quickly, but was a minor component, found in only one sample of this study. Hexagonal pyrrhotite also was quick to react but its abundance and distribution within the Meguma Supergroup has not been well defined. In general, more field studies including sulphide mineralogy are needed within the Meguma Supergroup to better understand the distribution and abundance of these minerals.

A temporal pattern of possible trace metal release into the surrounding environment is implicated with Pb > > As, Zn > Cu. although this does not indicate in any way the mobility or solubilities of these elements under various environmental conditions in the field (see Section 3.5 for further discussion).

3.2 The Role of Sulphur- And Iron-Oxidizing Bacteria In Sulphide Oxidation

The general field of "geomicrobiology" has received much attention lately as evidenced by recent short courses by the Mineralogical Society of America (Banfield and Nealson, 1997) and the Mineralogical Association of Canada (McIntosh and Groat, 1997). Specific to sulphide mineralogy, reviews are presented within the short course volumes on the geomicrobiology of sulphide mineral oxidation (Nordstrom and Southam, 1997) and the role of bacteria in the breakdown of sulphide minerals (McIntosh et al., 1997). The intent here is to present a brief overview of bacteria, and the main role played in the development of ARD.

The metabolism (abbreviated as the suffix "-trophy") of sulphur- and iron-oxidizing bacteria involves a chemical energy source (abbreviated as the prefix "chemo-") instead of light energy ("photo-"), they use inorganic electron donors ("litho-") instead of organic ("organo-") and they reduce their own carbon from CO_2 (auto-") instead of assimilating carbon from other organisms ("hetero-"). Therefore, sulphur- and iron-oxidizing bacteria are said to be "chemolithoautotrophic". Specifically, these bacteria can oxidize (remove electrons from) reduced sulphur compounds or ferrous iron, and reduce (add electrons to) molecular oxygen. Also, the bacteria *Thiobacillus ferrooxidans* (Nordstrom, 1982), *T. thiooxidans* and *Sulfolobus acidocaldarius* (Brock and Gustafson, 1976, cited in Nordstrom, 1982) can use ferric iron as an electron acceptor in the absence of oxygen. Table 3.2 lists some of the bacteria found associated with ARD. According to Nordstrom and Southam (1997), one of the most widely studied bacteria linked to pyrite oxidation is *T. ferrooxidans*. Figure 3.1 shows a schematic diagram for pyrite oxidation and the role of bacteria. The diagram gives an indication of the overall sequence of reactions, and the interaction between oxidizing agents, catalysts, and mineral products (Nordstrom, 1982).

An overall, but highly simplified reaction showing the oxidation of pyrite can be described by the following equation (Nordstrom, 1982):

(3.1) $$FeS_2 + 15/4\ O_2 + 7/2\ H_2O \text{ ----> } Fe(OH)_3 + 2\ H_2SO_4$$

For every mole of pyrite oxidized, one mole of ferric hydroxide and two moles of sulfuric acid are produced. The rate of oxidation of ferrous to ferric iron by the following reaction:

Table 3.2 - Some members of the Bacteria genera *Thiobacillus*, *Leptospirillum*, and *Sulfobacillus*. Acidophilic species are underlined. Also shown are the inorganic substances the Bacteria utilize, and four Archaea spp. that are known to be associated pyrite oxidation and acid rock drainage (compilation taken from Nordstrom and Southam, 1997; original sources: Egorova and Deryugina. 1963; Kelly and Harrison, 1984; Wood and Kelly, 1991; Barrett et al., 1993).

Thiobacillus albertis	H_2S, $S_2O_3^{2-}$
Thiobacillus acidophilus[1]	S^o, $S_2O_3^{2-}$, $S_3O_6^{2-}$, $S_4O_6^{2-}$
Thiobacillus denitrificans	H_2S, S^o, $S_2O_3^{2-}$, $S_4O_6^{2-}$
Thiobacillus delicatus	S^o, $S_2O_3^{2-}$, $S_4O_6^{2-}$
Thiobacillus ferrooxidans	H_2S, sulfide minerals, S^o, $S_2O_3^{2-}$, $S_4O_6^{2-}$, Fe^{2+}
Thiobacillus halophilus[2]	S^o
Thiobacillus intermedius	S^o, $S_2O_3^{2-}$, $S_4O_6^{2-}$
Thiobacillus neapolitanus	H_2S, sulfide minerals, S^o, $S_2O_3^{2-}$, $S_3O_6^{2-}$, $S_4O_6^{2-}$
Thiobacillus novellus	$S_2O_3^{2-}$, $S_4O_6^{2-}$
Thiobacillus perometabolis	S^o, $S_2O_3^{2-}$, $S_4O_6^{2-}$
Thiobacillus tepidarius	H_2S, S^o, $S_2O_3^{2-}$, $S_3O_6^{2-}$, $S_4O_6^{2-}$
Thiobacillus thermophilica[3]	H_2S, sulfide minerals, S^o
Thiobacillus thiooxidans	S^o, $S_2O_3^{2-}$, $S_4O_6^{2-}$
Thiobacillus thioparus[4]	H_2S, sulfide minerals, S^o, $S_2O_3^{2-}$, $S_3O_6^{2-}$, $S_4O_6^{2-}$
Thiobacillus versutus	H_2S, $S_2O_3^{2-}$
Leptospirillum ferrooxidans	Fe^{2+}, sulfide minerals
Leptospirillum thermoferrooxidans	Fe^{2+}, sulfide minerals
Sulfobacillus thermosulfidooxidans	Fe^{2+}, S^o, sulfide minerals
Archaea spp.	
Acidianus brierleyi	Fe^{2+}, S^o, sulfide minerals
Sulfolobus solfataricus	S^o
Sulfolobus ambivalens	S^o
Sulfolobus acidocaldarius	Fe^{2+}, S^o

[1] Also known as *T. organoparus*
[2] Wood and Kelly, 1991
[3] Egorova and Deryugina, 1963 (not a *Thiobacillus* sp.)
[4] Range of pH = 3 to 10

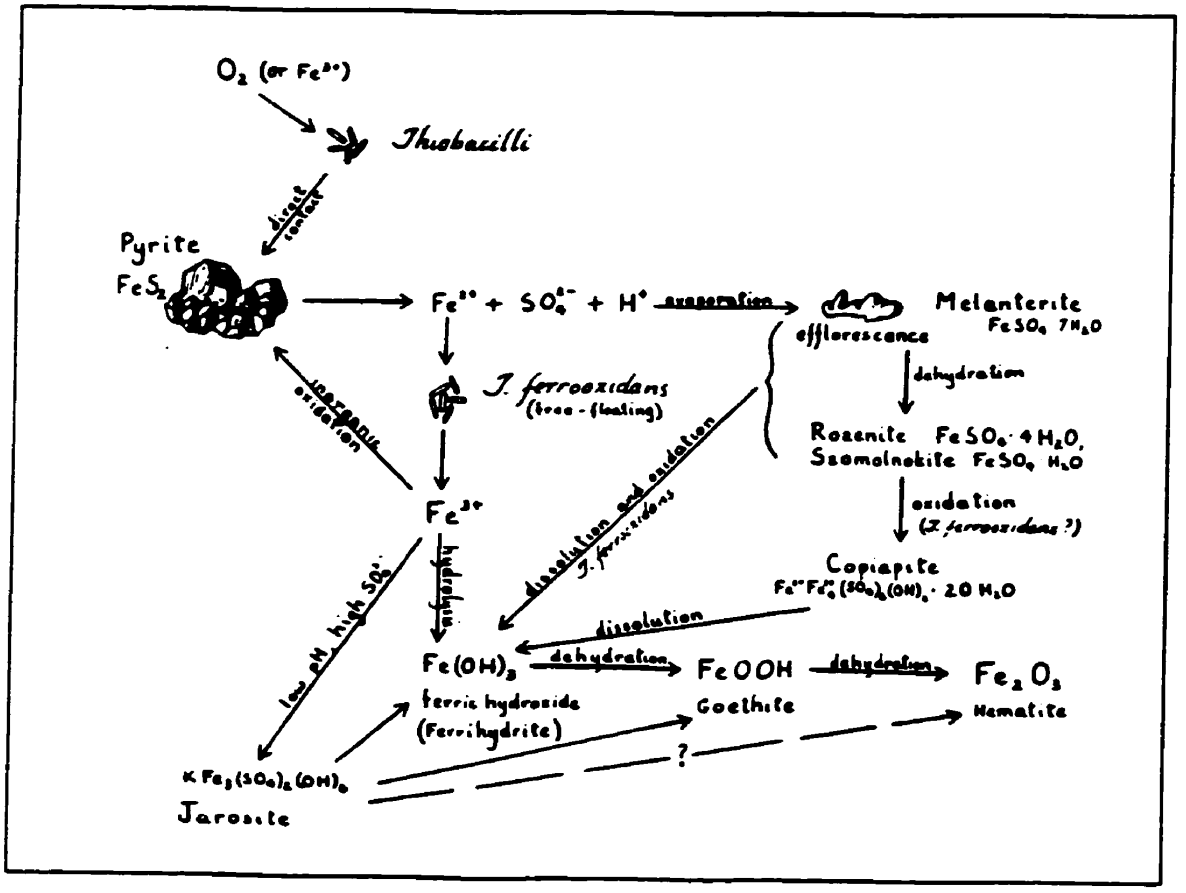

Figure 3.1. Schematic model for pyrite oxidation, and the relationships between oxidizing agents, secondary minerals and catalysts (from Nordstrom, 1982).

(3.2) $Fe^{2+} + 1/4\ O_2 + H^+ \text{---} > Fe^{3+} + ½\ H_2O$

was shown to be a function of pH in abiotic systems (Singer and Stumm, 1970). At pH > about 4.5, the rate is increasingly faster while at pH < about 3.5, the reaction rate is nearly independent of pH. At pH < 3.5, the oxidation rate is catalyzed by *T. ferrooxidans* and is increased by at least several orders of magnitude. The oxidation of ferrous to ferric iron was suggested to be a major rate-determining step in the overall sequence of ARD formation (Singer and Stumm, 1970).

Pyrite can also be oxidized by ferric iron according to the reaction:

(3.3) $FeS_2 + 14\ Fe^{3+} + 8H_2O \text{---} > 15\ Fe^{2+} + 2\ SO_4^{2-} + 16\ H^+$

This reaction requires acidic conditions since ferric iron is insoluble at circumneutral pH (Nordstrom and Southam, 1997).

This overall summary of pyrite oxidation is quite simplified and some of the more complicated details that occur in natural environments are presented in Nordstrom and Southam, (1997). Two factors that are noteworthy here are that:

1) elemental sulphur is an intermediate between reduced sulphides and sulphuric acid, and may form during either nonoxidative dissolution, or partial oxidation of a sulphide (Ahonen and Tuovinen, 1992).

2) the oxidation products are not necessarily pure ferric hydroxide, but can include other phases, or mixtures of phases, including goethite, jarosite, ferrihydrite, and schwertmannite. Secondary mineralogy is discussed further in Chapter 4 of this thesis.

As shown in Figure 3.1, bacteria can play either a direct or indirect (or both) role in the oxidation of pyrite. The direct mechanism means that the bacterium is acting

directly on the mineral surface (attached), whereas the indirect mechanism involves the oxidation of ferrous to ferric iron (equation 3.2) and subsequent oxidation of pyrite by ferric iron (equation 3.3). The relative importance of these two mechanisms is difficult to establish because they depend on factors such as the type of bacteria, degree of attachment, supply of nutrients and oxygen, pH, Eh, and temperature (McIntosh et al., 1997). Nordstrom and Southam (1997) suggest that the main role of iron- and sulphur-oxidizing bacteria is in the oxidation of ferrous iron. The ferric iron that is produced can then rapidly oxidize pyrite. The rate of oxidation of ferrous iron to ferric iron and the rate of oxidation of pyrite by ferric iron is similar.

3.3 Sample Locations And Descriptions

Six representative samples were selected from locations throughout the Meguma Supergroup (Fig. 3.2) to represent the major sulphide minerals that occur. Samples were chosen from both the Goldenville and Halifax Groups and contain a variety of textures and mineral associations.

Sample RJ-96-001 was collected from a dark grey to black, thinly bedded slate and siltstone unit within the Halifax Group, on Tancook Island, in the Mahone Bay area of southwestern Nova Scotia. The sample contains large (2mm) euhedral pyrite (up to 15%), with sparse fractures, and with thin rims of pyrite of the same composition. The sample also contains rare (less than 1%) marcasite with abundant, very fine grained inclusions, associated with chalcopyrite and thin rims of Fe-Ti oxide minerals.

Sample RJ-96-002 is from a rock dump of the Montreal Slate Belt within the

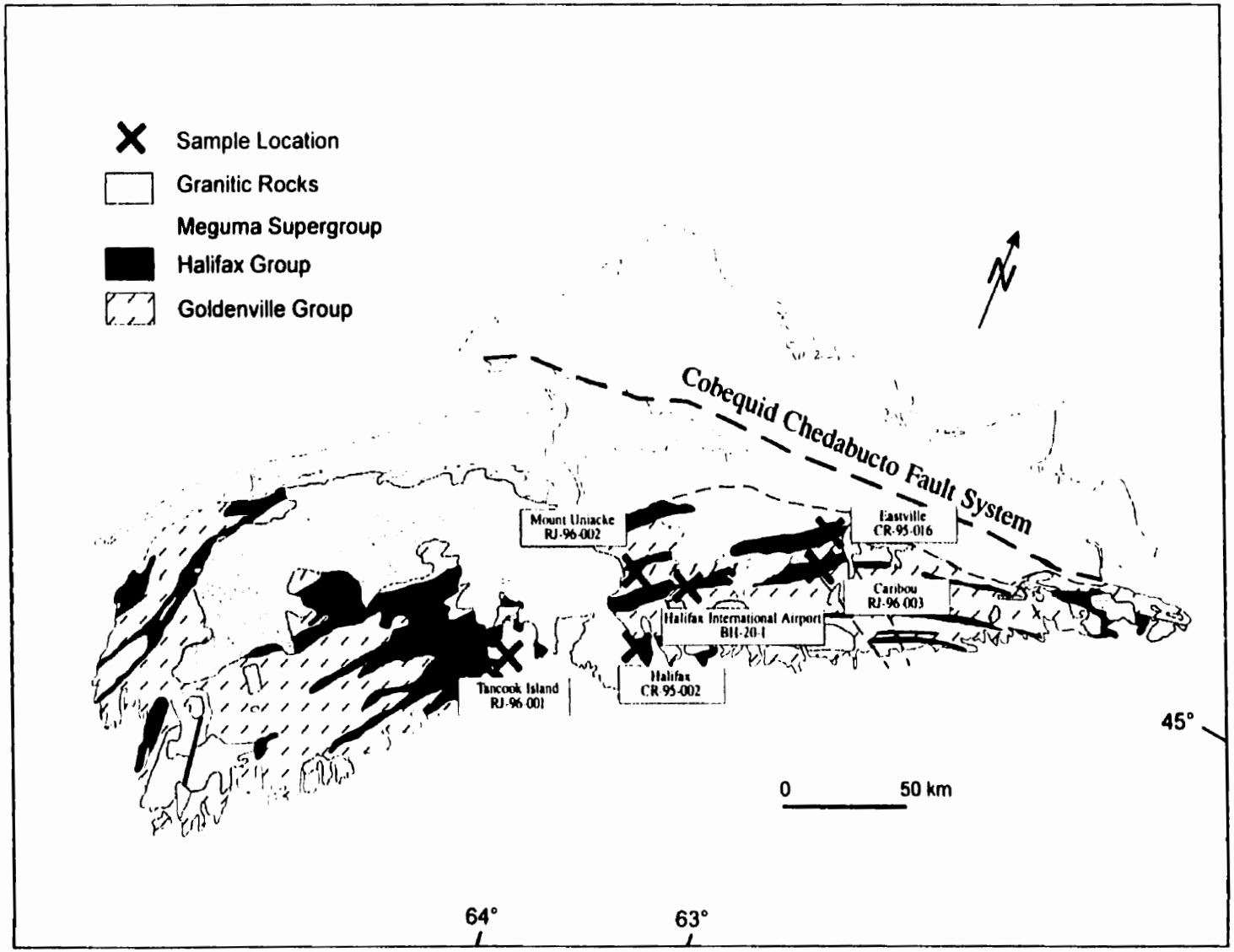

Figure 3.2. Simplified geological map of Nova Scotia showing the distribution of the Meguma Supergroup and granitic rocks (modified from Keppie, 1979a).

Mt. Uniacke Gold District. The Mt. Uniacke area lies within the Goldenville Group which is known to contain slate units at many of the gold districts. The main sulphide mineral is large (1-5mm) elongate arsenopyrite, slightly fractured, with pressure shadows of quartz. A minor amount of subhedral pyrite is also present.

Sample RJ-96-003 was collected from drill core obtained at the Caribou Gold District, and is stratigraphically located near the top of the Goldenville Group. The sample is a vein of massive sulphide, mostly hexagonal pyrrhotite (distinguished from monoclinic pyrrhotite by XRD analysis), with chalcopyrite rims, and inclusions of galena, chalcopyrite, arsenopyrite and oxides. Subgrains of hexagonal pyrrhotite are visible under crossed polars and vary from large and equant to small and elongate. Rare fractures cut across subgrains.

Sample BH-20-I is from drill core taken of the Halifax Group at the Halifax International Airport. The sample contains large, elongate (approximately 1x5 mm), monoclinic pyrrhotite oriented parallel to cleavage and cross-cutting bedding. Short sides of grains are irregular and commonly rimmed with rutile. Long sides are smoother. Minor sulphide inclusions in pyrrhotite include chalcopyrite, sphalerite, and trace galena. Small (0.1 - 0.3 mm) euhedral pyrite grains are scattered throughout the matrix. Elongate, irregular subgrains of monoclinic pyrrhotite are visible under crossed polars.

Sample CR-95-002 is a contact metamorphic hornfels collected within 0.5 km of the contact with the South Mountain Batholith. Large andalusite porphyroblasts (up to 1.5 cm in length) comprise up to 30% of the sample. The sulphides consist of small

(0.1-0.4 mm) monoclinic pyrrhotite associated with ilmenite and rutile, and rare inclusions of (Co,Ni)AsS (solid solution between gersdorffite and cobaltite).

Sample CR-95-016 is dark grey slate from the transition zone between the Goldenville and Halifax Groups. The sample was collected from drill core of the Eastville zinc-lead deposit (Binney et al., 1986). The sulphides are pyrite, monoclinic pyrrhotite, and minor chalcopyrite. The rock is thinly bedded with the following sulphide textures: pyrite and pyrrhotite form fine beds of large elongate grains (up to 0.4 x 1.0 mm) that are interfingered in places, pyrrhotite forms globular grains rimmed by garnet (0.1 to 0.4 mm in diameter), pyrrhotite forms small elongate grains parallel to bedding.

3.4 Experimental Design And Procedure

At every stage of the experiment, aseptic techniques were used in order to avoid contamination of the samples. Two polished thin sections from each of the six samples were made from adjacent slices of rock so that the pair would be as similar as possible. The slices were cut extra thickly (approximately 1 mm instead of the standard 30μm) to allow for volume loss during oxidation and repolishing. Initially, the thin sections were photographed in reflected light to document the surface appearance. All thin sections were sterilized by soaking in methanol which leaches water out of cells and denatures proteins, effectively killing bacteria (Dr. M. Silver, pers. comm., 1996). Success of the sterilization process was confirmed by using a control sample.

The medium used for the oxidation experiment was ARD (pH 3.0-3.5) collected

from a pond in a slate quarry near the Halifax International Airport. Although the specific, possible types of bacteria in the ARD were not determined, the presence of at least an iron-oxidizing type was confirmed within several hours after starting the experiment (Fig. 3.3). Since the ARD medium was collected from a natural setting, it is likely that there was a mixture of bacteria types present. ARD for the sterile treatment was double filtered using a pre-sterilized, Nalgene filterpack with a 0.2 micron filter to physically remove bacteria. ARD for the bacterial treatment was not filtered.

The apparatus was designed to contain 13 thin sections (6 in the bacterial treatment, 6 in the sterile treatment, and 1 control of the overall sterilization procedure) covered with ARD, and with a constant supply of air. The temperature was held constant at 25°C to encourage microbial growth. Thirteen, 500 mL mason jars individually held each thin section, and a sterile air supply continuously aerated the 300 mL of ARD in each jar. The air was sterilized with an in-line polytetrafluoroethylene (PTFE) 50 mm membrane filter with an average pore size of 0.2 microns. The bubbles entering the water caused gentle turbulence, so all the water was uniformly oxygenated. After soaking in methanol, thin sections were rinsed in sterile ARD to remove the residue, and transferred to the sterile jars.

To observe the thin sections under a microscope, they were transferred to plastic petri dishes with 25 mL filtered ARD (just enough to cover the thin section surface). Observations and photographs were taken through the cover of the dish. To photograph the sulphide surfaces in the bacterial treatment, the organisms had to be removed with a fine brush. The experiment was allowed to run for 42 days (six weeks).

Figure 3.3. (a) Rust-coloured precipitate in the microbial treatment. (b) No precipitate in the sterile treatment, indicating that filtering has removed bacteria.

Photomicrographs were taken before the experiment began, 2 days into the experiment, and at 42 days. At the end of the experiment, sulphide mineral surfaces were also documented using a scanning electron microscope (SEM).

In each thin section, the relative amount of reactivity was judged by surface appearance. In reflected light, colour changes and etched scratches, fractures or pits were interpreted as oxidation or corrosion. In general, stronger or darker colours and darker polishing scratches indicated a greater degree of corrosion. The use of colour to observe oxidation is supported by the work of Steger (1982), who found that pyrrhotite followed a sequence of colour changes with increasing oxidation: steel-grey to orange-brown to blue-purple to blue-green to orange-brown. Steger further suggests that the blue-purple is due to an insoluble secondary product of Fe^{2+} oxidation, such as $Fe(OH)(SO_4) * xH_2O$, the orange-brown is due to ferric oxide, and the other colours are mixtures of the two precipitates. Blue, purple, orange, yellow or brown tarnish have also been noted on chalcopyrite (Chen *et al.*, 1980; Kwong and Lawrence, 1994), pyrite, and sphalerite (Kwong and Lawrence, 1994). SEM images confirm that tarnish is associated with corrosion, because more strongly coloured and etched sulphide grains had lower and more irregular topography, consistent with loss of material.

3.5 Results

3.5.1 Sample BH-20-I

Figure 3.4 shows monoclinic pyrrhotite (cream), pyrite (white), chalcopyrite (yellow) and sphalerite (grey) at 0, 2, and 42 days in the microbial treatment. It is clear

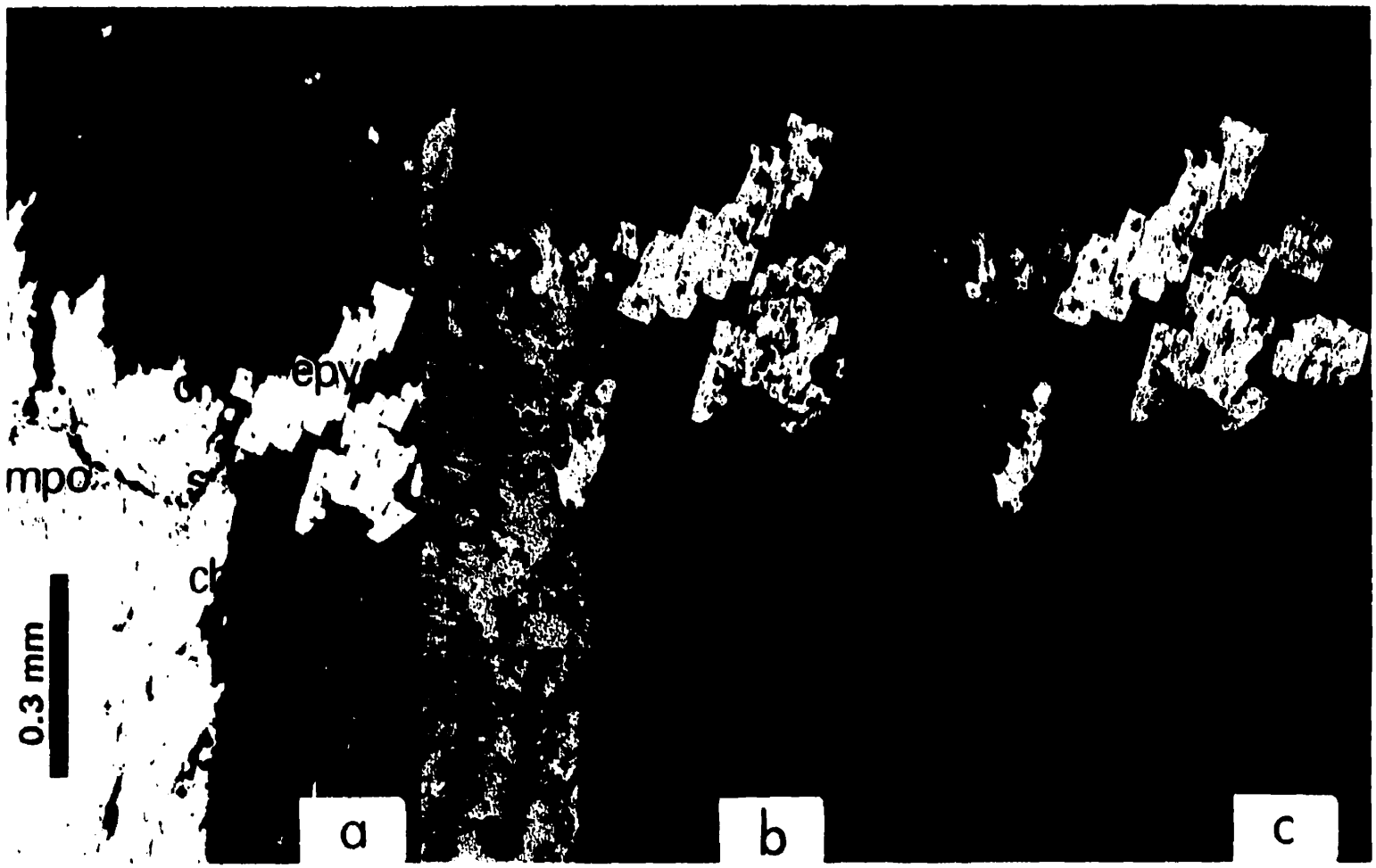

Figure 3.4. Photomicrographs of sample BH-20-I from the microbial treatment, taken in reflected, plane polarized light with a blue filter, showing surface characteristics at (a) 0 days (b) 2 days and (c) 42 days of oxidation. Monoclinic pyrrhotite (mpo), which developed etched polishing scratches and colour changes, clearly oxidized much more than euhedral pyrite (epy), sphalerite (s), or chalcopyrite (ch). Sphalerite and pyrite developed slight signs of oxidation (discolouration and scratches), but chalcopyrite remained unchanged.

by the colour changes (from cream to multicolours to black) and appearance of etched polishing scratches that monoclinic pyrrhotite has changed much more than pyrite, chalcopyrite or sphalerite. Sphalerite has a little discolouration, in pyrite the polishing scratches became visible after 42 days but is otherwise unchanged, and chalcopyrite is still perfectly clean. SEM images clearly illustrate the topographical differences among monoclinic pyrrhotite, chalcopyrite and sphalerite (Fig. 3.5). The monoclinic pyrrhotite exhibits crystallographically oriented lamellar intergrowths that terminate abruptly at sub-grain boundaries. This intergrowth texture may have developed by exsolution of monoclinic pyrrhotite from hexagonal pyrrhotite upon cooling (e.g., Lianxing and Vokes, 1996). Figure 3.6 is a simplified temperature-composition diagram showing the stability fields for the main sulphide minerals in the FeS - FeS_2 system. The arrow shows a possible example of a compositional path upon cooling. Hexagonal pyrrhotite can exsolve pyrite during cooling at temperatures above approximately 254°C. Upon further cooling, monoclinic pyrrhotite can be exsolved as the temperature drops rapidly across the upper boundary of the two-phase field for monoclinic + hexagonal pyrrhotite. In the example from this study (Fig. 3.5), the phases have not been determined. However, note the preferential loss of material along the darker phase. Further work is needed on this type of texture to clearly define the phases and oxidation rates.

In the sterile treatment, monoclinic pyrrhotite is the most darkly coloured in comparison to chalcopyrite, sphalerite and pyrite, but it is not as strongly oxidized as the monoclinic pyrrhotite in the microbial treatment. Also, pyrite and sphalerite have

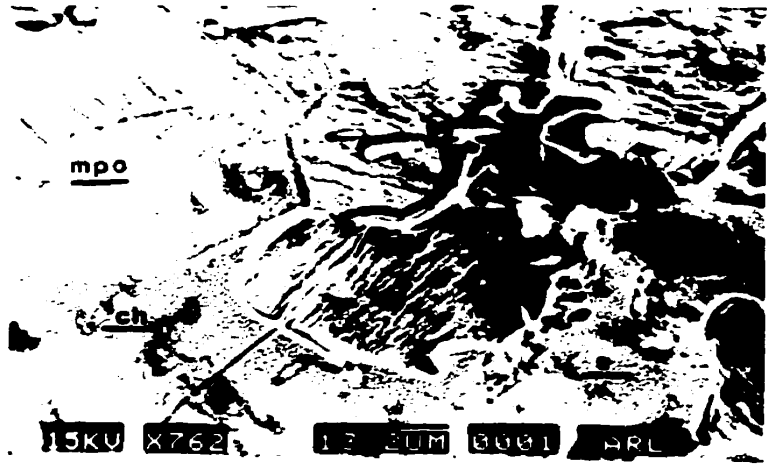

Figure 3.5. SEM image of sample BH-20-I from the microbial treatment showing surface features after 42 days of oxidation. Monoclinic pyrrhotite (mpo) has a much lower topography than that of chalcopyrite (ch) or sphalerite (s), indicating greater loss of material. Subgrains of mpo are clearly defined showing surface roughness and advanced oxidation around subgrain boundaries. Note the presence of lamellar intergrowth texture in the monoclinic pyrrhotite.

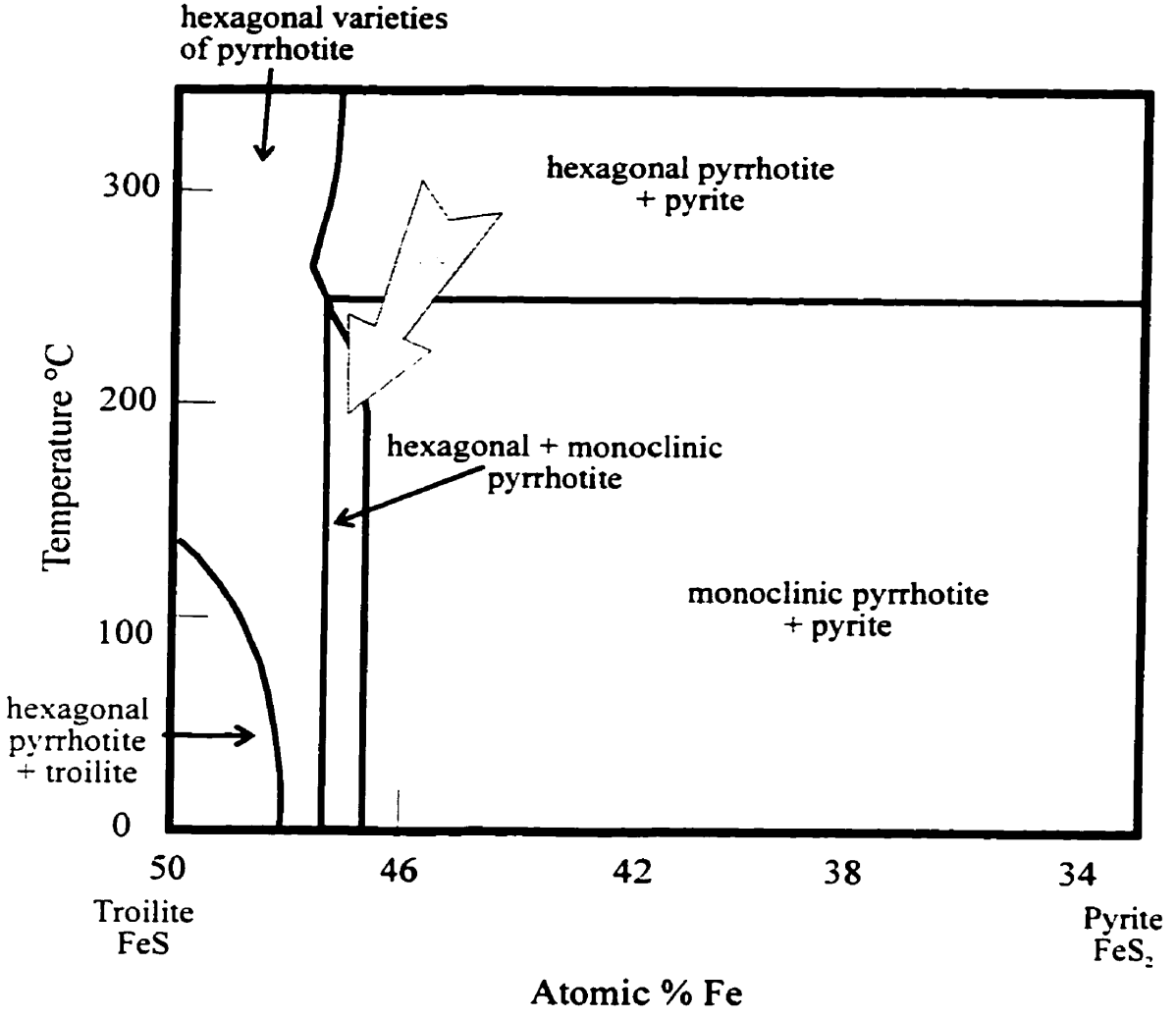

Figure 3.6 Simplified composition - temperature diagram showing a possible cooling path for hexagonal pyrrhotite. Upon cooling below 254 °C, hexagonal pyrrhotite eventually can exsolve monoclinic pyrrhotite. (modified from Klein and Hurlbut, 1985).

less visible effects in the sterile treatment. Chalcopyrite is very similar in the two treatments, however, in the sterile treatment it appears to have a very small amount of tarnish. Pyrite is smooth compared to the etched scratches in the microbial treatment.

3.5.2 Sample RJ-96-003

Figure 3.7 A and B shows hexagonal pyrrhotite (cream), chalcopyrite (yellow), and galena (light grey) in crossed polars (to show subgrains) and plain polarized light (to show initial colours) respectively. Figure 3.7 C and D shows the same minerals at two days (C) and at six weeks (D) of oxidation in the microbial treatment. The hexagonal pyrrhotite turned dark brown, and then almost black indicating very strong oxidation. The chalcopyrite remained clean bright yellow. Galena oxidized faster than the hexagonal pyrrhotite. At only two days, it is recognizable only by its dark outline within the hexagonal pyrrhotite. SEM images indicate differences in surface texture among chalcopyrite, hexagonal pyrrhotite and galena. Chalcopyrite is as smooth as the matrix, and the other two are covered with tiny crystals of possible secondary minerals. Galena has corroded much more than pyrrhotite. This sample also contains a small amount of arsenopyrite that did not alter at all, even after six weeks.

In the sterile treatment, the relative order of oxidation among the minerals is the same, but hexagonal pyrrhotite has oxidized much less than in the microbial treatment. At two days, galena has turned black, but the hexagonal pyrrhotite is only slightly discoloured in patches. At six weeks, a secondary mineral coating covered the hexagonal pyrrhotite, but not the galena, and clean unoxidized hexagonal pyrrhotite can

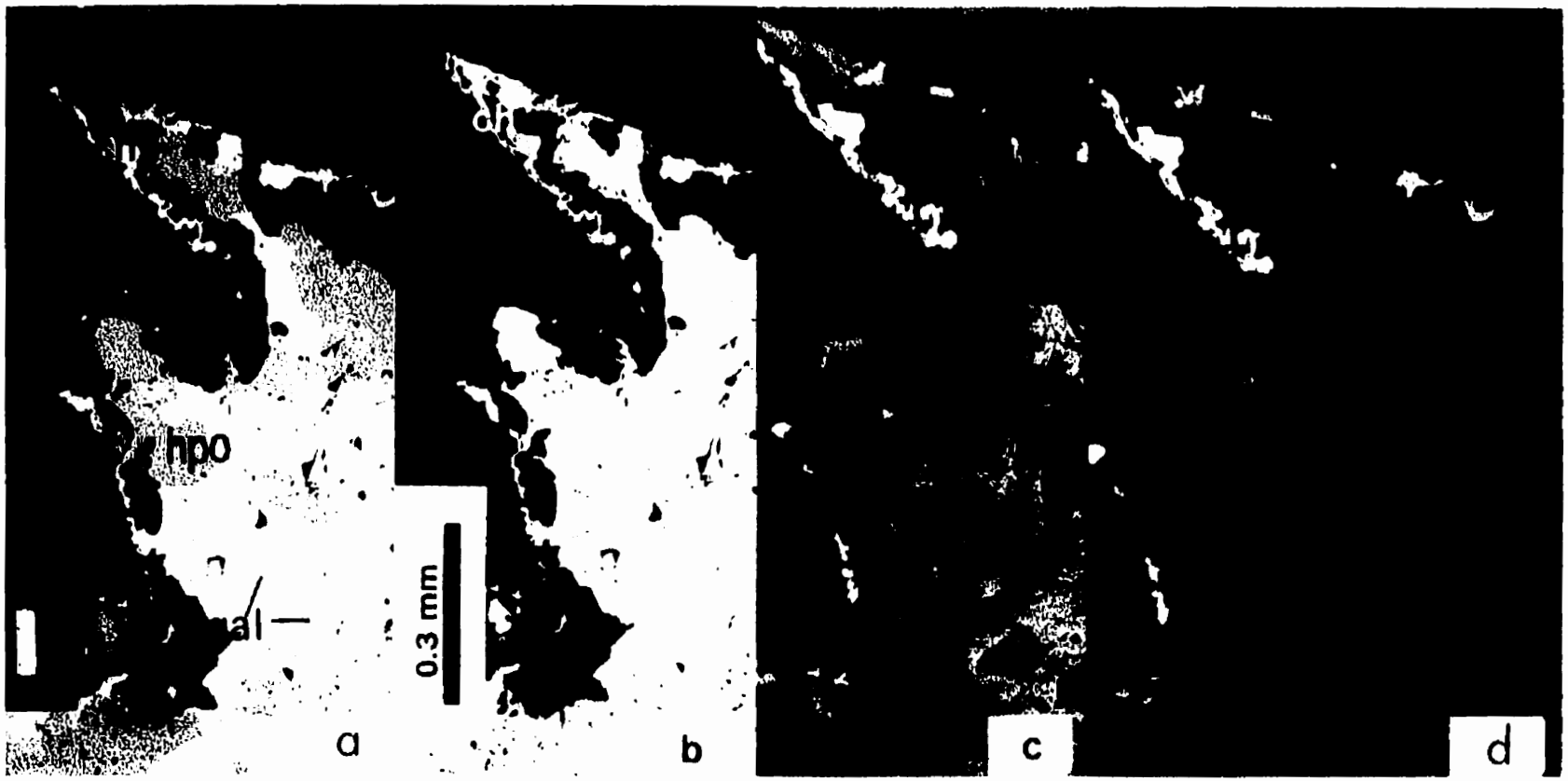

Figure 3.7. Photomicrographs of sample RJ-96-003 from the microbial treatment, taken in reflected light with a blue filter, showing surface characteristics at (a) 0 days (under crossed polars) (b) 0 days (under ppl) (c) 2 days (under ppl) and (d) 42 days (under ppl) of oxidation. Chalcopyrite remained unaltered, hexagonal pyrrhotite (hpo) corroded strongly (dark, with scratches), and galena (gal) corroded the most.

be seen surrounding the galena where the coating was thin. This could be an example of a galvanic effect discussed further in Section 3.6.2. SEM images indicate that the galena has been substantially more corroded than pyrrhotite, and both have different surface textures than in the microbial treatment.

3.5.3 Sample RJ-96-001

This sample contains marcasite and euhedral pyrite. The pyrite changed very little over six weeks. In the microbial treatment some polishing scratches became visible (Fig. 3.8), but not in the sterile treatment. The marcasite produced extremely different results. At two days there was little change, but by six weeks the marcasite had turned black (Fig. 3.9), and its location was visible only by contrast with the adjacent unchanged chalcopyrite. In reflected light, the marcasite looked indistinguishable between the sterile and microbial treatments in reflected light. However, SEM images suggest that the microbial treatment sample has been corroded a little more than the sterile treatment. The surfaces are both very irregular. Figure 3.10 shows an SEM image of the marcasite surface from the microbial treatment indicating the topography of the mineral is lower than that of the matrix or inclusions. Note the texture is similar to the lamellar intergrowth texture of pyrrhotite shown in Figure 3.5. If this texture results from exsolution, the exsolved phase and host phase have not been determined. Several microprobe analyses from this grain indicate a composition of FeS_2, however possible exsolution lamellae may be too fine to distinguish using the microprobe with a spot size of approximately 1 micron.

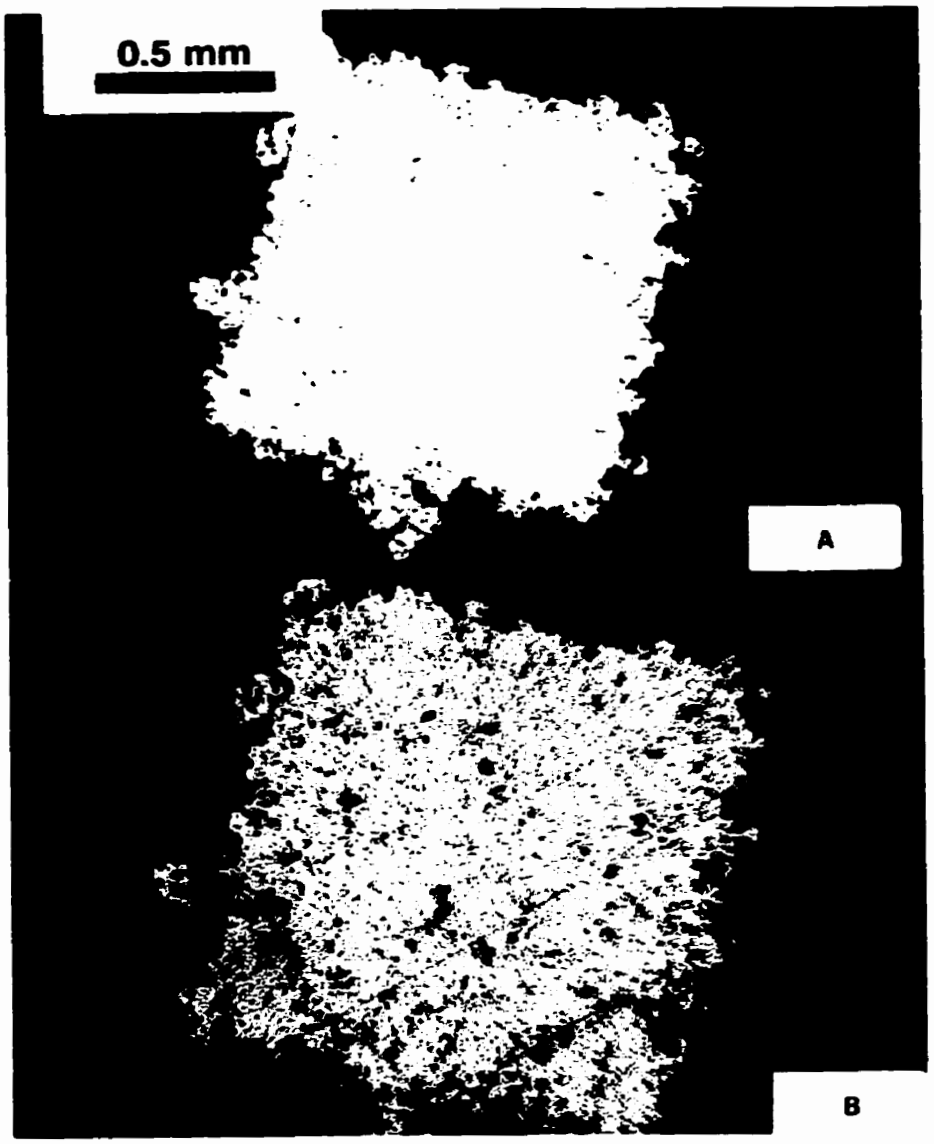

Figure 3.8. Photomicrographs of euhedral pyrite in sample RJ-96-001 from the microbial treatment, taken in reflected, plane polarized light with a blue filter, showing surface characteristics at (a) 0 days and (b) 42 days of oxidation. Note the appearance of polishing scratches.

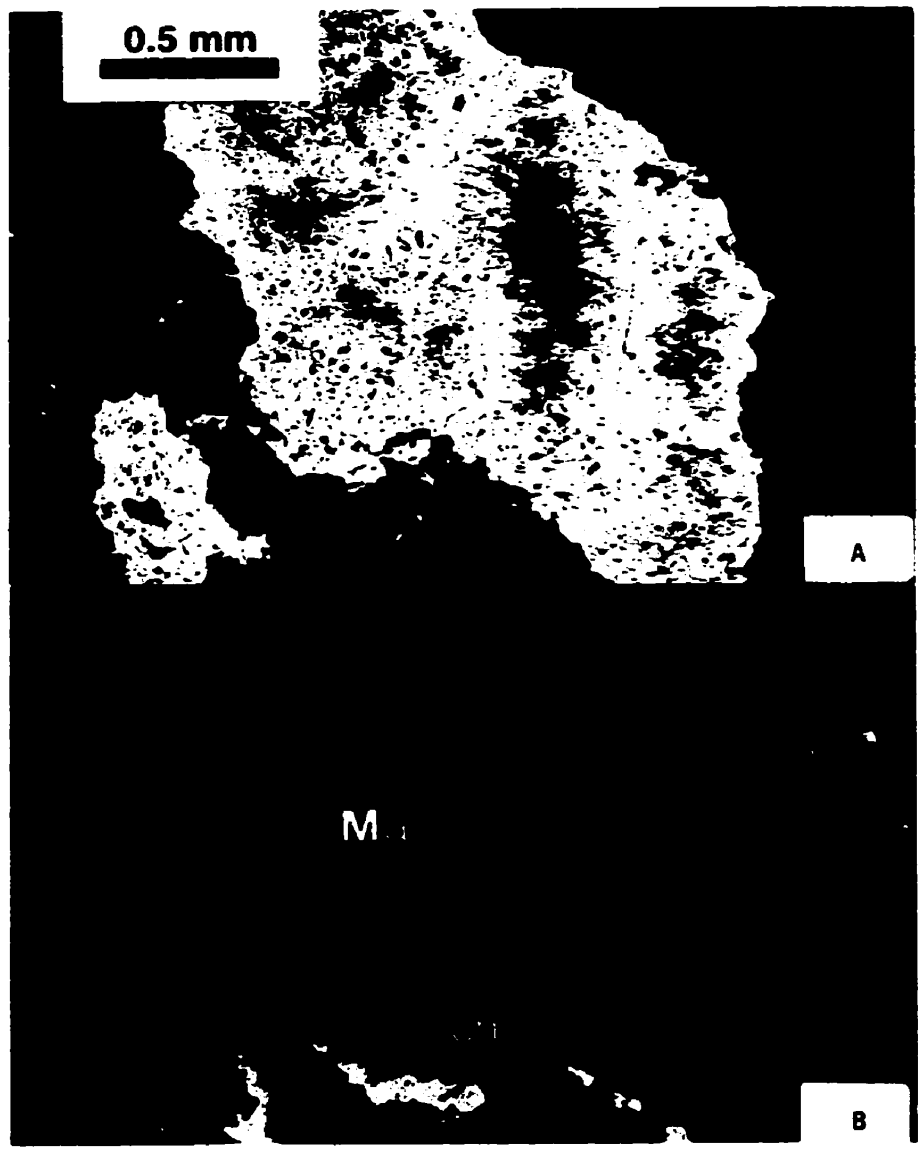

Figure 3.9. Photomicrographs of marcasite and chalcopyrite (ch) in sample RJ-96-001 from the sterile treatment, taken in reflected, plane polarized light with a blue filter, showing surface characteristics at (a) 0 days and (b) 42 days of oxidation. The marcasite turned black, indicating very strong corrosion, in sharp contrast to chalcopyrite which remained unchanged.

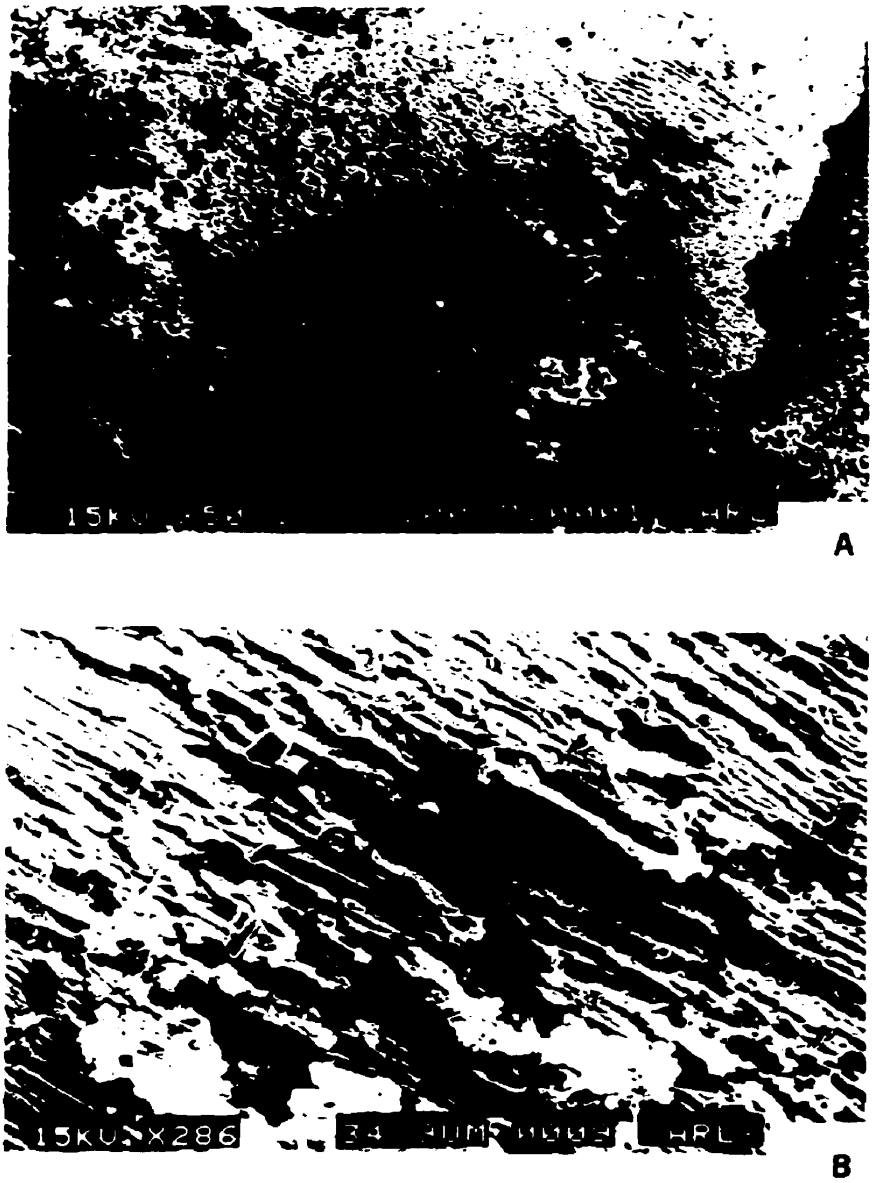

Figure 3.10. SEM images of marcasite in sample RJ-96-001 from the microbial treatment showing the surface after 42 days of oxidation. (a) An overview of possible lamellar intergrowth(?) texture. (b) Detailed image showing surface roughness, rounded oxide (ox) inclusions provide a baseline for topographic comparison, assuming the oxides have not changed and represent the level of the original polished surface.

3.5.4 Sample RJ-96-002

Arsenopyrite was oxidized visibly, but not as much as the pyrrhotite in samples BH-20-I or RJ-96-003. Brown discolouration and corrosion occurred to a greater degree in the microbial treatment than in the sterile treatment. In the microbial treatment, there was evidence for differential corrosion across sub-grain boundaries within a larger grain, indicating that grains of different orientations oxidize at different rates (Fig. 3.11).

3.5.5 Sample CR-95-016

The sulphides present in this sample are pyrite, monoclinic pyrrhotite, and chalcopyrite. Chalcopyrite did not oxidize in either treatment, as in the other samples. Pyrite remained fairly white at two days, although some grains developed a secondary coating after six weeks. Monoclinic pyrrhotite appeared to oxidize differentially. Many grains turned a uniform light brown, however sub-grains from the microbial treatment turned very different colours, ranging from cream to dark purple or blue (Fig 3.12). Separate pyrrhotite grains also oxidized at very different rates, again with a range of colour from deep blue-purple to light orange (Fig. 3.13). Polishing scratches were more visible on the deep blue grains indicating stronger oxidation.

3.5.6 Sample CR-95-002

The sulphides in this sample are monoclinic pyrrhotite with rare tiny inclusions of a sulphide compositionally intermediate between cobaltite and gersdorffite. Both

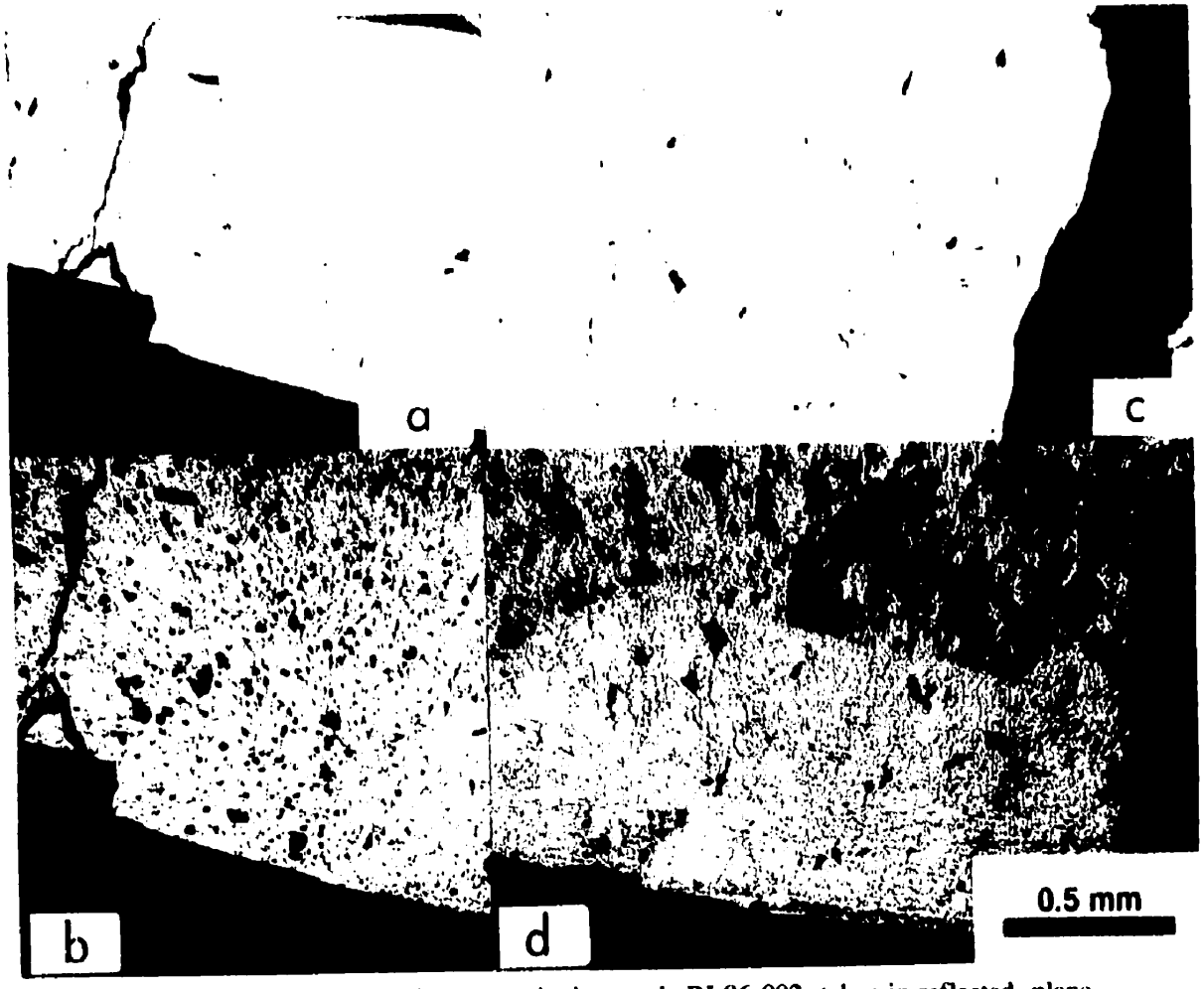

Figure 3.11. Photomicrographs of arsenopyrite in sample RJ-96-002, taken in reflected, plane polarized light with a blue filter, showing surface characteristics at (a) 0 days, sterile treatment (b) 42 days, sterile treatment, (c) 0 days, microbial treatment, and (d) 42 days, microbial treatment. It is clear by the discolouration that arsenopyrite in the microbial treatment oxidized faster than in the sterile treatment. Also microbial treatment shows evidence of differential oxidation across subgrain boundaries (d).

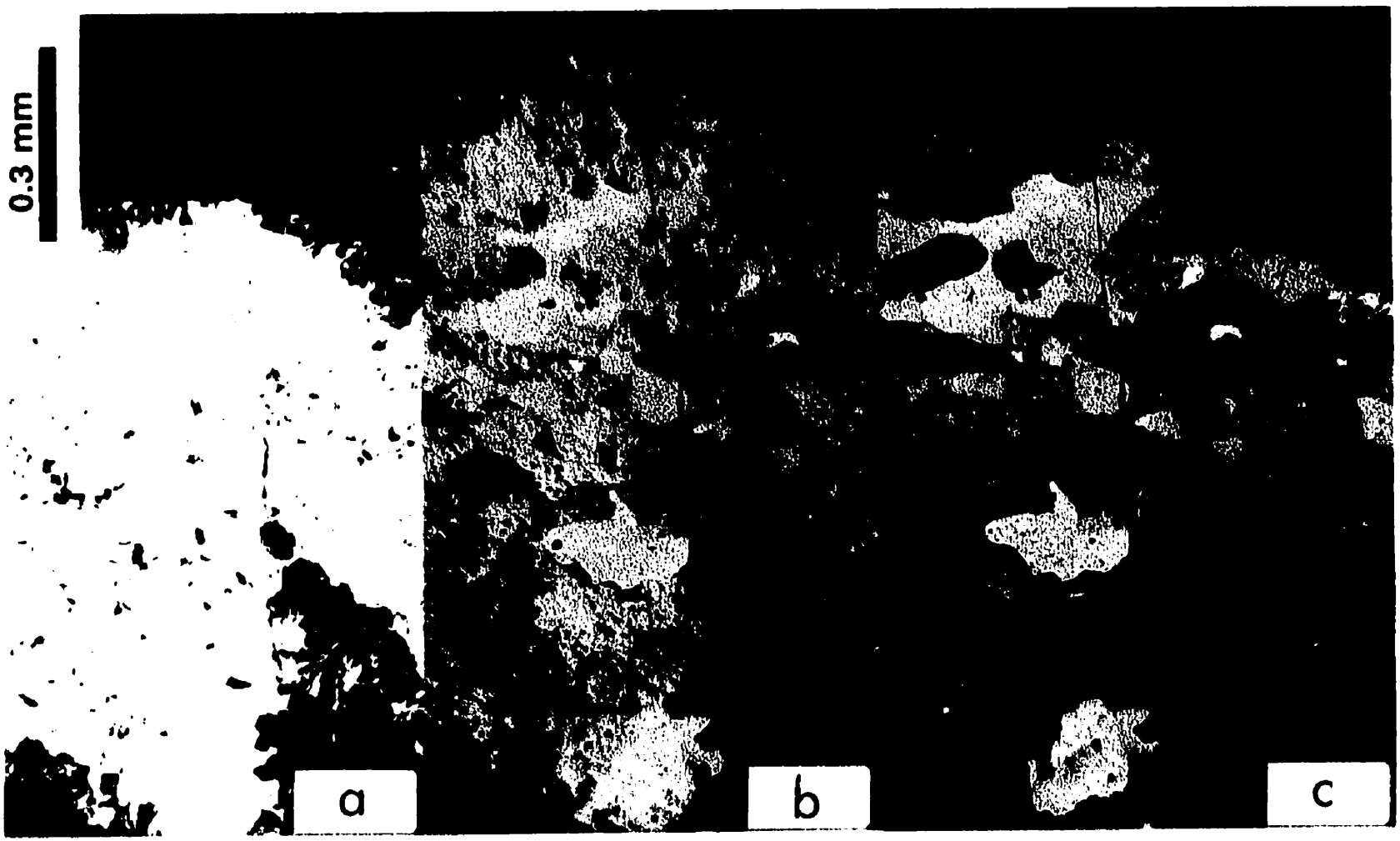

Figure 3.12. Photomicrographs of a pyrrhotite grain in sample CR-95-016 taken in reflected, plane polarized light with a blue filter, showing surface characteristics at (a) 0 days (b) 2 days and (c) 42 days of oxidation. Subgrains have oxidized at different rates. Some subgrains are still cream coloured (unaltered), and some are deep blue-purple (oxidized).

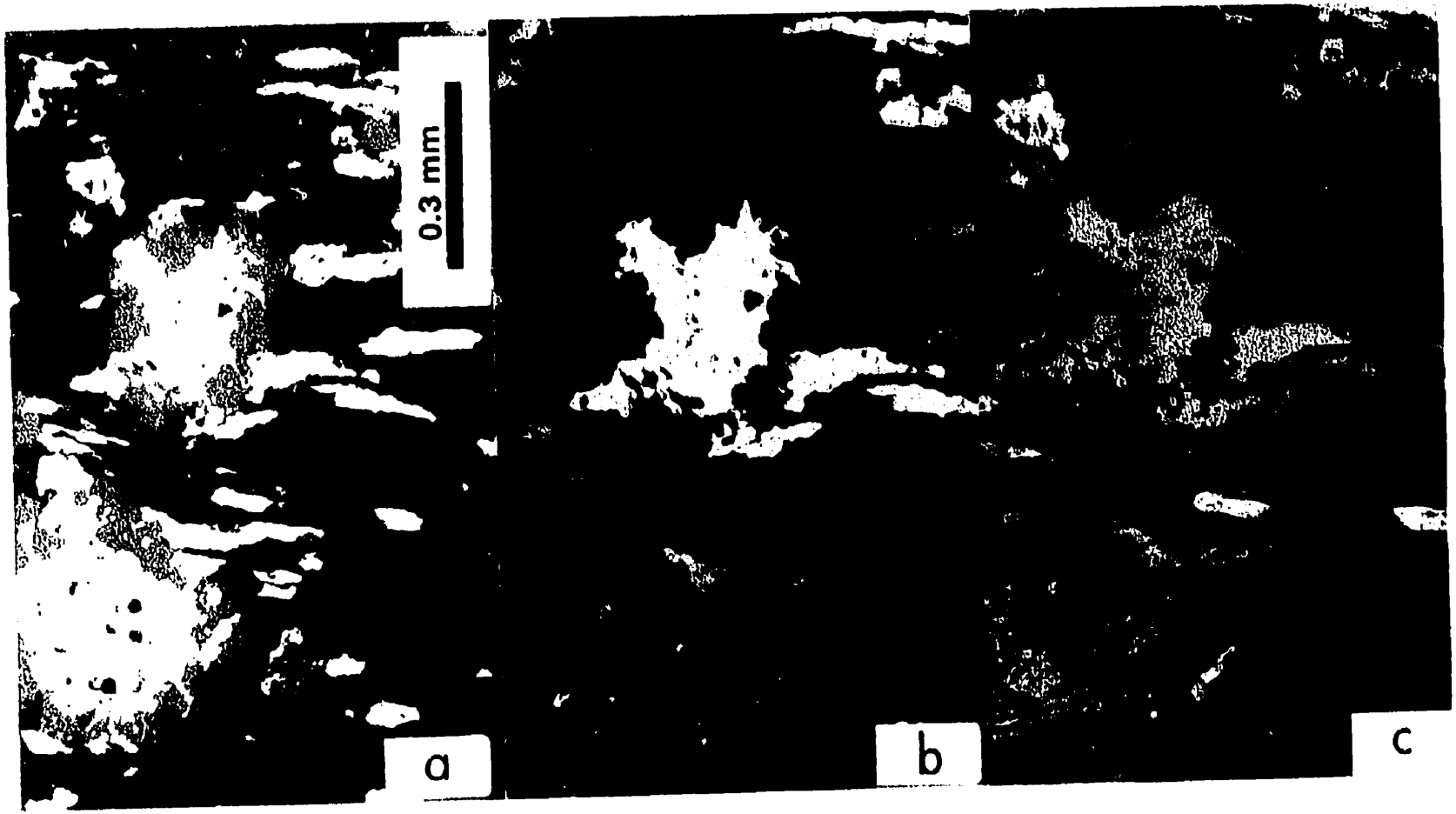

Figure 3.13. Photomicrographs of two pyrrhotite grains in sample CR-95-016 taken in reflected, plane polarized light with a blue filter, showing surface characteristics at (a) 0 days (b) 2 days and (c) 42 days of oxidation. These two grains and their smaller neighbours have oxidized at very different rates (cream or light orange verses dark blue-purple).

treatments of this sample behaved similarly, with slightly stronger oxidation in the microbial treatment. The tiny inclusions remained white and unoxidized. At two days pyrrhotite oxidized strongly and a well-developed, lamellar intergrowth texture became visible. At six weeks, the lamellae turned black, while the surrounding host phase was still brown. SEM images (Fig. 3.14) give further evidence that this colour difference was due to differential oxidation rates, because the lamellae are significantly lower than their host.

3.5.7 Summary of reactivity rates

Table 3.3 describes the relative order of oxidation among sulphide minerals in each sample. Overall, the relative order of oxidation of sulphide minerals in the microbial treatment was galena > hexagonal pyrrhotite > monoclinic pyrrhotite > marcasite > > arsenopyrite, sphalerite > pyrite > chalcopyrite. In the sterile treatment, the relative order was galena > marcasite > monoclinic pyrrhotite > > hexagonal pyrrhotite, sphalerite, arsenopyrite > pyrite > chalcopyrite. The apparent rate of oxidation between hexagonal pyrrhotite and monoclinic pyrrhotite was substantial enough between the microbial and sterile treatments to cause the order in the overall sequence to change. However, this conclusion should be treated with caution because the two pyrrhotite type were from different thin sections. Further work is necessary to confirm the results of this experiment.

Based on the overall reactivity sequence, toxic elements could be released from sulphide minerals in the following order: Pb (galena) > > Zn, As (sphalerite and

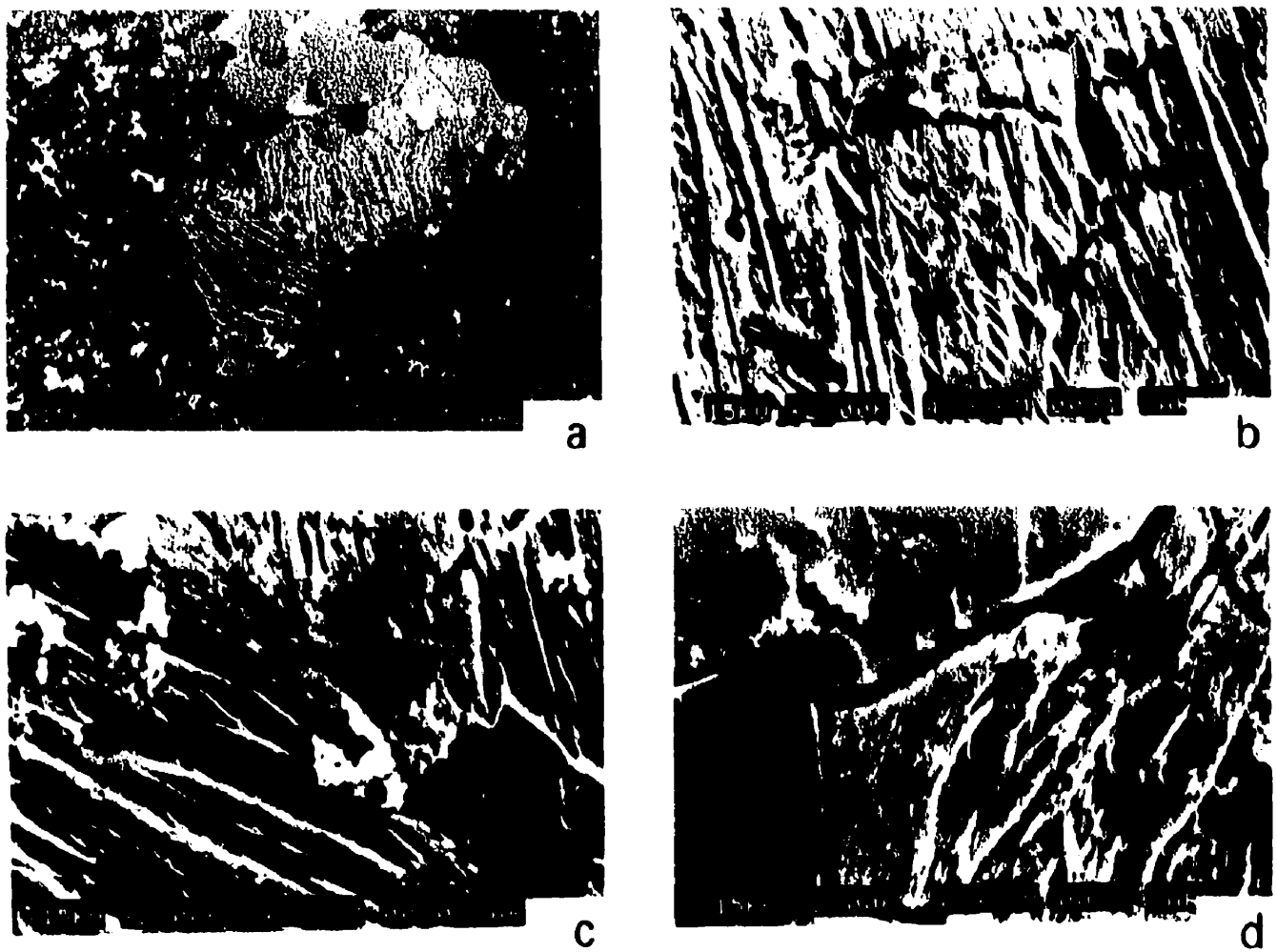

Figure 3.14. SEM images of lamellar intergrowth texture in pyrrhotite in sample CR-95-002 from the sterile treatment showing the surface after 42 days of oxidation. (a) Overview of the grain. (b) Lamellar have two predominant orientations. (c) Lamellar end at subgrain boundaries. (d) Subgrains have different depths of etching.

Table 3.3. Relative rate of reactivity among sulphide minerals for each sample.

Sample	Treatment	Order of oxidation
BH-20-I	microbial	galena > monoclinic pyrrhotite > > sphalerite > euhedral pyrite > chalcopyrite
	sterile	monoclinic pyrrhotite > > euhedral pyrite, chalcopyrite
RJ-96-001	microbial	marcasite > > euhedral pyrite
	sterile	marcasite > > euhedral pyrite
RJ-96-002	microbial	arsenopyrite
	sterile	arsenopyrite
RJ-96-003	microbial	galena > hexagonal pyrrhotite > > arsenopyrite, chalcopyrite
	sterile	galena > > hexagonal pyrrhotite > arsenopyrite, chalcopyrite
CR-95-002	microbial	monoclinic pyrrhotite
	sterile	monoclinic pyrrhotite
CR-95-016	microbial	monoclinic pyrrhotite > pyrite > chalcopyrite
	sterile	monoclinic pyrrhotite > pyrite > chalcopyrite

arsenopyrite) > Cu (chalcopyrite). Note this does not consider the mobility or relative solubilities of various secondary Pb, Zn, As, or Cu minerals that may develop under the changing environmental conditions possible in the field. This is based on only the reactivity sequence of the sulphide minerals observed in this study. For example, although galena appears to be one of the first minerals to react, the common secondary Pb mineral anglesite ($PbSO_4$) is considered to be insoluble and can cause attenuation of Pb close to the source of sulphide oxidation (Alpers et al., 1994a). Therefore the precipitation of anglesite can prevent significant Pb from entering into the surrounding environment. Also this ignores possible trace abundances of Pb, Zn, As, and Cu in other sulphide minerals, as well as other processes such as non-oxidative dissolution that could play a role in the release of these elements. Further work is necessary to determine the possible paths of these elements through the local environment.

Most sulphides (monoclinic pyrrhotite, galena, sphalerite, arsenopyrite, and pyrite) oxidized significantly more in the microbial than in the sterile treatment. Exceptions were hexagonal pyrrhotite, which displayed an extreme difference, marcasite, which was very strongly oxidized in both treatments, and chalcopyrite, which was unoxidized throughout.

3.6 Discussion

Controls on the reactivity rate of sulphide minerals are varied and can be difficult to measure because many controls can be acting on a single sample. This study is further complicated in that the acidic medium used for the leach experiments is a

natural sample of ARD and possibly contains a variety of bacteria types. Also, the rock samples contain a variety of sulphide types as well as different mineral textures, resulting in complex systems. However, many of the observations presented above, give strong evidence for galvanic interaction, crystal lattice effects (including surface area, grain boundaries, and crystallographic orientation), and the presence or absence of bacteria as factors that strongly affect the rate of reactivity of the samples studied.

3.6.1 Eh and pH as environmental controls

The breakdown of many of the common sulphide minerals is predominantly controlled by oxidation - reduction reactions involving the iron and sulphur systems. Not surprisingly, the two most important controls on the stability of sulphide minerals are Eh (oxidation potential) and pH (hydrogen activity). Eh - pH diagrams, based on chemical equilibrium thermodynamics, exist for many sulphide minerals and in general, can be used to predict the conditions under which the minerals are expected to breakdown (e.g., Garrels and Christ, 1965). For example, Figure 3.15 shows an Eh - pH diagram for the iron oxide and iron sulphide system (Fig. 3.15 a), along with a similar diagram showing stability limits for natural aqueous environments (Fig. 3.15 b). ARD (mine water) is highly oxidizing with low pH, and sulphide minerals are thermodynamically unstable in such environments. In order for efficient mineral oxidation to proceed, there must be a large difference between the oxidation potential of the medium compared to that of the sulphide mineral.

In microbial systems, there are also optimal Eh - pH conditions for which

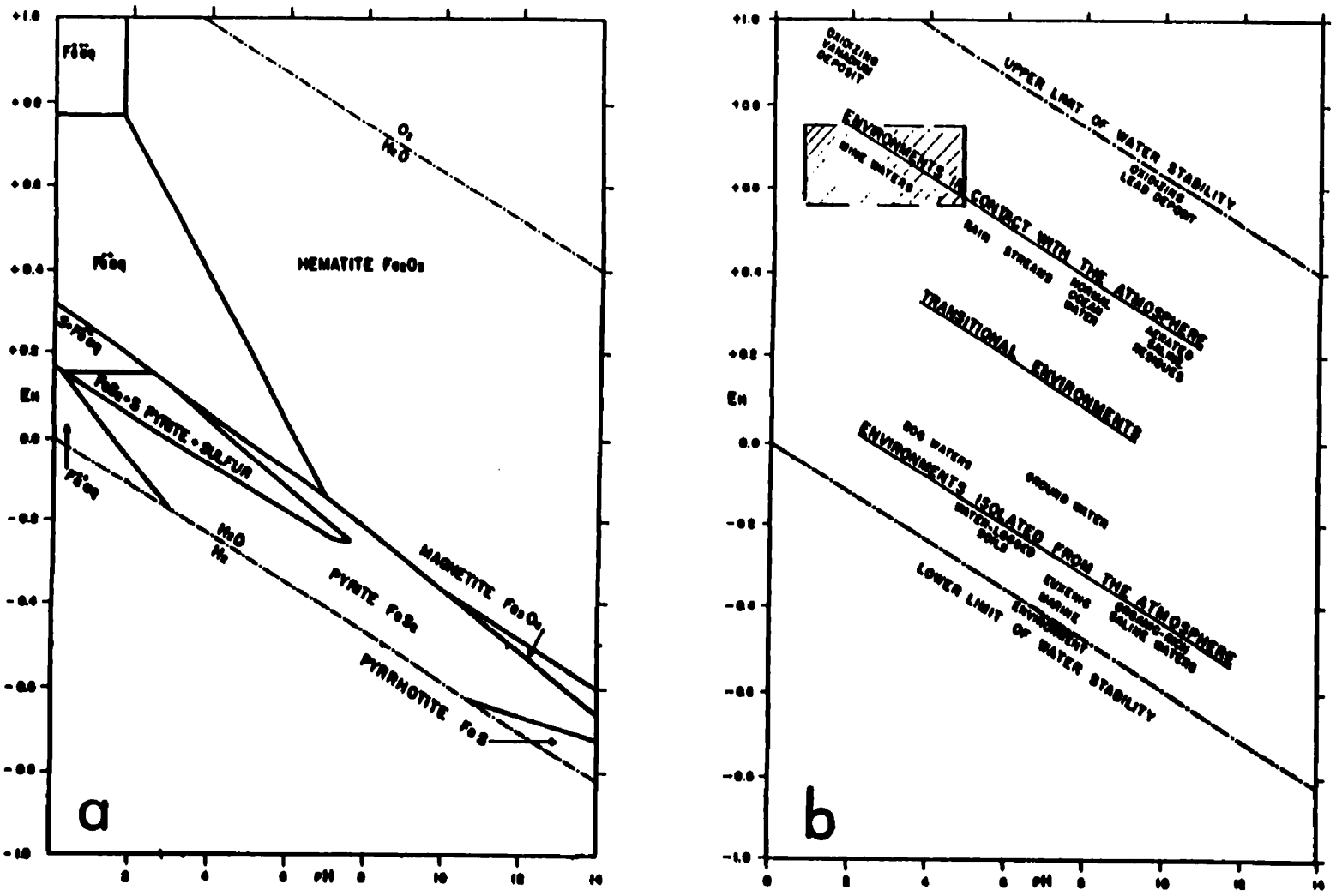

Figure 3.15. Eh - pH diagrams showing (a) stability fields of iron oxides and iron sulphides in water at 25°C, 1 atmosphere total pressure, with an activity of dissolved sulphur of 10^{-1}, and (b) stability fields for various aqueous environments (modified after Garrels, 1960). Mine waters (box shown in b) and acid rock drainage (ARD) occur at high Eh (oxidizing conditions) and low pH.

certain bacteria are metabolically active, since they derive their energy from electrons. Figure 3.16 shows the environmental Eh - pH conditions of the sulphur- and iron-oxidizing bacteria (Fig. 3.16 a), and an Eh - pH diagram for the chalcopyrite-water system (Fig. 3.16 b). Figure 3.16a shows that *T. ferrooxidans* are stable in highly oxidizing, low pH conditions. Figure 3.16b shows the measured stability limits for *T. ferrooxidans* in the leaching of chalcopyrite. The presence of bacteria drives the Eh of the solution upwards, likely through a process that involves the oxidation of ferrous iron. In general, this figure indicates that the electrochemical conditions for efficient bacterial leaching need to include an optimal Eh that considers both the bacteria as well as the sulphide mineral.

Although Eh - pH diagrams are useful for a generalized prediction of environmental conditions under which sulphide minerals oxidize, they do not include kinetic factors that influence the rate of reactions. Sulphide minerals can exist metastably in their environment and although the theoretical data may suggest instability, breakdown may not occur because reaction rates are too slow. Other factors are needed to explain why some sulphide minerals react differently than others.

3.6.2 Galvanic interaction

As explained by Natarajan (1990) and Kwong (1995), two contacting sulphide minerals in an oxygenated aqueous medium can form a galvanic cell, with one sulphide behaving like the cathode and the other like the anode. Preferential oxidation will occur at the anode (the sulphide with lower rest potential, i.e., the equilibrium electrode

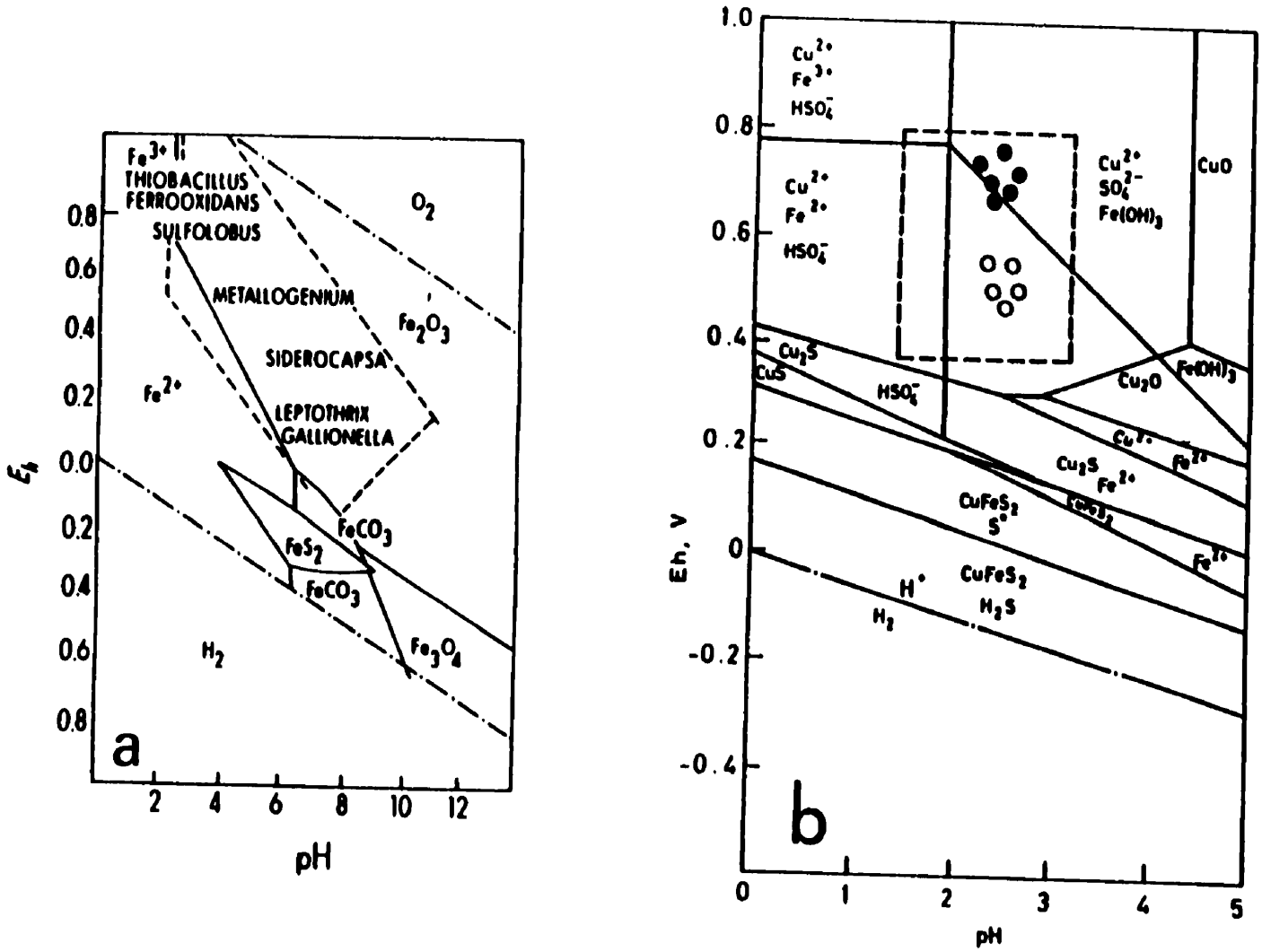

Figure 3.16. (a) Eh - pH diagram showing the preferred environments of some iron-oxidizing bacteria (from Lundgren and Dean, 1979). (b) Eh - pH diagram showing stability fields for the chalcopyrite - water system. Also shown are the stability and activity limits for *T. ferrooxidans*. Filled circles are measured Eh values during chalcopyrite leaching in the presence of bacteria, open circles in the absence of bacteria (from Natarajan, 1990).

potential when the net anode or cathode current is zero), protecting the cathode from oxidation. Rest potentials for some common sulphide minerals are presented in Table 3.4. As an example, in a system containing pyrite and pyrrhotite in contact with other, the oxidation of pyrrhotite (lowest rest potential) will be galvanically enhanced. The following reaction, using a bivalent metal sulphide (MS) as an example, would occur at the anode (Kwong, 1995):

(3.4) $MS \text{ ----> } M^{2+} + S^0 + 2e^-$

and the cathodic reaction is:

(3.5) $\frac{1}{2} O_2 + 2H^+ + 2e^- \text{ ----> } H_2O$

Natarajan (1990) notes that systems containing more than two sulphide minerals in contact are more complex. However, two principles can be applied:

1) a sulphide with the most negative potential will always be the anode, while the mineral with the most positive potential will always be the cathode, and;

2) intermediate sulphides nearer the anode will tend to be more cathodic and those nearer the cathode will tend to become more anodic.

The most compelling example of galvanic interactions in this study is the common occurrence of chalcopyrite within pyrrhotite, where the chalcopyrite is consistently resistant to reaction (e.g., Figs. 3.4 and 3.7). It is well known that chalcopyrite in contact with pyrite is more prone to oxidation than chalcopyrite by itself (e.g., Ahonen and Tuovinen, 1992). Figure 3.17 shows schematic diagrams for the galvanic mechanisms involved in the breakdown of chalcopyrite in contact with pyrite (a), and the galvanic protection of chalcopyrite in the presence of pyrrhotite (b). The

Table 3.4. List of rest potentials of some common sulphide minerals (from Kwong, 1995). Note that rest potentials can change depending on the solution chemistry and the specific mineral chemistry.

Mineral	Formula	Rest Potential (Volts vs. Standard Hydrogen Electrode)	Solution	Temperature
Pyrite	FeS_2	0.63	1.0 M H_2SO_4	25°C
Chalcopyrite	$CuFeS_2$	0.52	1.0 M H_2SO_4	20°C
Chalcocite	Cu2S	0.44	1.0 M H_2SO_4	20°C
Covellite	CuS	0.42	1.0 M H_2SO_4	25°C
Galena	PbS	0.28	1.0 M H_2SO_4	20°C
Sphalerite	ZnS	-0.24	1.0 M H_2SO_4	20°C
Pyrrhotite	FeS	-0.28	1.0 M H_2SO_4	20°C

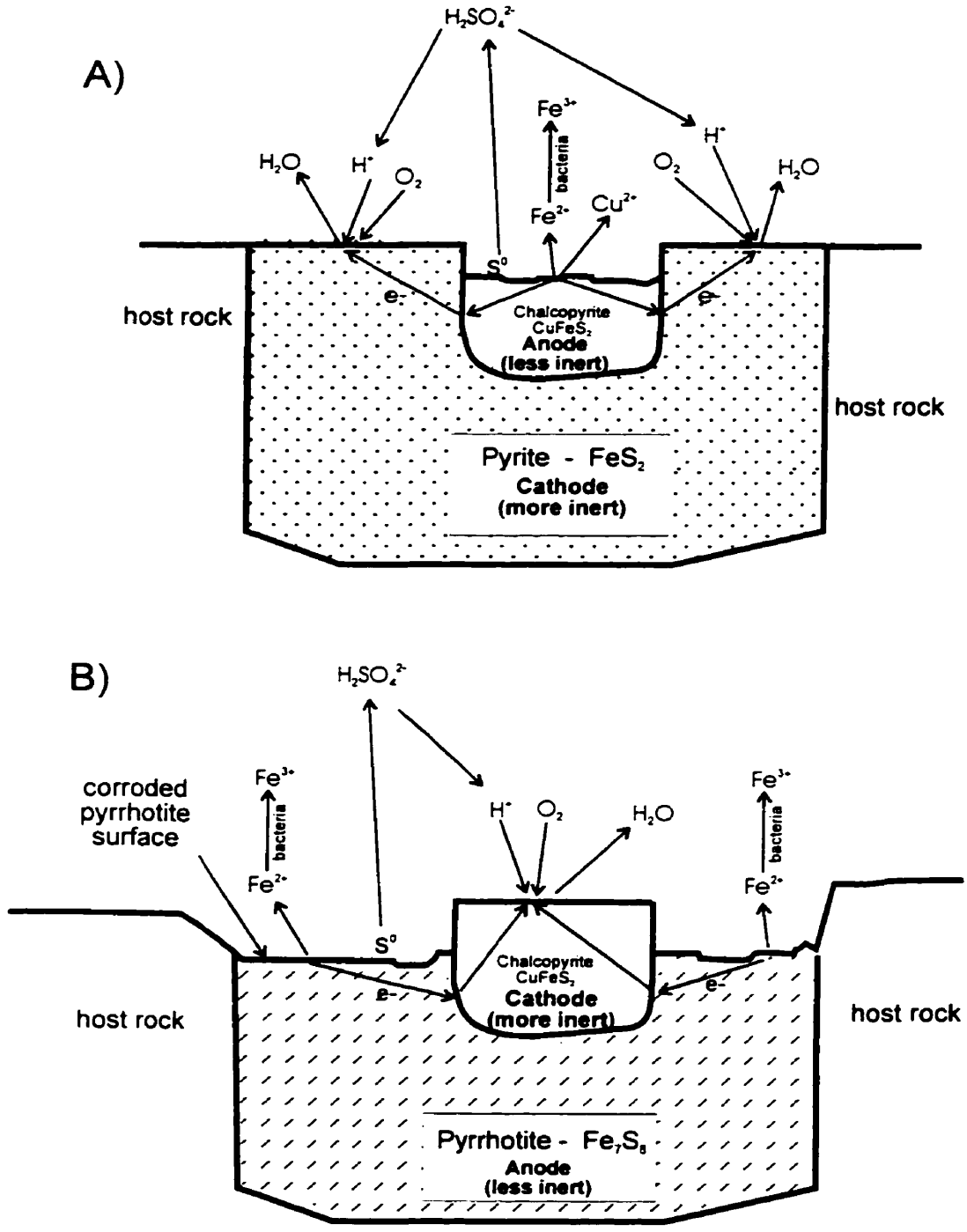

Figure 3.17. Galvanic reactions that take place when chalcopyrite occurs within pyrite (A), and when chalcopyrite occurs within pyrrhotite (B). (Diagrams modified from McIntosh et al., 1997; Natarajan, 1990).

representation in Figure 3.17b is the important model for the samples from the Meguma Supergroup observed in this study. Other possible examples of galvanic interactions observed in this study are pyrite in contact with pyrrhotite (pyrrhotite preferentially oxidized), and small arsenopyrite grains within pyrrhotite (pyrrhotite preferentially oxidized).

3.6.3 Crystal Lattice Effects

Crystal lattice structure can be interrupted by impurities, vacancies, dislocations, fractures, or grain boundaries, all of which affect the stability of the mineral (Callister, 1993). For example, grain boundaries are less stable than the interior because the grain boundary atoms do not bond beyond the boundary limit. Therefore all bond locations are not satisfied. Figure 3.5 shows an SEM image of monoclinic pyrrhotite with highly corroded subgrain boundaries where preferential oxidation has occurred. This is strong evidence that the existence of subgrain boundaries has an affect on the reactivity of the pyrrhotite in this study.

Experimental evidence from this study also indicates differential reactivity of various crystal lattice orientations within pyrrhotite. Figure 3.12 shows that different pyrrhotite subgrains have oxidized at different rates (indicated by colour differences). In their study of sulphide samples from three different mine sites owned by Placer Dome Inc., Kwong and Lawrence (1994) argued that the apparent control on sulphide oxidation by crystallographic orientation is an artifact of the thin sectioning process. In other words, few of the orientations in the thin section would occur in natural grab

samples. However, in the pyrrhotite from the Meguma Supergroup, the different crystallographic orientations occur in various subgrains in larger, metamorphically recrystallized grains. The different subgrain orientations are not thin section artifacts and they occur in the natural samples. Therefore the orientation affect is applicable to pyrrhotite samples examined in this study.

Several more examples of the possible influence of crystal lattice effects in minerals from this study are shown in Figures 3.5, 3.10 and 3.14. In these examples, pyrrhotite and marcasite reacted quickly compared to most of the other sulphide minerals. The common link between these two minerals is the surface texture that may be related to lamellar intergrowths. The pyrrhotite texture shown in Figure 3.14A is remarkably similar to the intergrowth texture described by Lianxing and Vokes (1996) that developed by exsolution of monoclinic pyrrhotite from hexagonal pyrrhotite upon cooling. The orientation of the intergrowth texture is crystallographically controlled and changes direction abruptly at subgrain boundaries (Fig. 3.5). Clearly there has been differential oxidation between lamellae and host (Fig. 3.14B), however in this case the phases have not been determined. Although the orientations of the lamellae appear to be crystallographically controlled, ultimately the chemistry and type of lamellae is determined by temperature and composition of the host. An important consideration in oxidation rates is the possibility of galvanic effects due to different mineral compositions in contact with other (Section 3.6.2).

For the marcasite (Fig. 3.10), the texture appears similar to that of the pyrrhotite (Figs. 3.5 and 3.14). However, it is not clear that this texture is definitely

due to lamellar intergrowths. Again, possible phases have not been determined in this study. One of the recommendations in Chapter 8 of this thesis is that more detailed work be carried out on sulphide mineral compositions and textures. Clearly this type of texture is important in that the minerals that oxidized the fastest overall appear to contain similar textures.

It should be noted here that an alternative explanation of the marcasite texture is that it is caused by fractures, which have the overall affect of increasing the surface area. Janzen et al. (1997), found similar textures on 12 pyrrhotite samples collected from a variety of locations throughout North America. They concluded the texture was due to fractures along cleavage planes and that surface area and preferential oxidation at areas of high strain appears to be the most influential factor affecting the oxidation rate of the pyrrhotite. The possibility of exsolution and lamellar intergrowths was not discussed.

3.6.4 Influence of bacteria

The overall affect of bacteria on sulphide reactivity in this study was that bacterial presence enhanced the rate of reactivity. For the most part, the order of reactivity did not change with the exception of monoclinic and hexagonal pyrrhotite. Kwong et al. (1994) also found that microbial mediation enhances sulphide oxidation rates, but the order of reactivity did not change. An important factor to consider here is that the presence of bacteria such as *T. ferrooxidans* shifts the Eh for all sulphide minerals in a positive direction, likely by enhancing the efficiency of ferric iron

oxidation (Natarajan, 1990). Therefore, the principles of galvanic interactions for example, remain the same in the presence or absence of bacteria but, as noted by Kwong and Lawrence (1994), in the presence of bacteria, the efficiency of galvanic reactions may be enhanced.

Regarding the large difference between the treatments for the monoclinic and hexagonal pyrrhotite, one possible reason is that catalysis by microorganisms was facilitated by a higher concentration of iron, favouring the oxidation of hexagonal pyrrhotite over monoclinic. Another complexity of pyrrhotite is that the mineral contains both Fe^{2+} and Fe^{3+}. In order to maintain an electrically neutral crystal structure, an ideal formula for pyrrhotite can be written as $(Fe^{2+}_{1-3x}Fe^{3+}_{2x})V_xS$, where V represents vacancies in the cation position (Klein and Hurlbut, 1993). The presence of Fe^{3+} has been confirmed spectroscopically by Pratt et al. (1994), who found 32% Fe^{3+} and 68% Fe^{2+} in research grade, monoclinic pyrrhotite from Mexico. The ratios of ferrous to ferric iron in the monoclinic and hexagonal pyrrhotite from this study are unknown, but presumably different ratios could affect the behaviour of iron-oxidizing bacteria.

3.7 Conclusions

Detailed image analyses of pyrite, monoclinic and hexagonal pyrrhotite, arsenopyrite, galena, and sphalerite, at various stages of oxidation over a six week period, has led to important information about the controls of reactivity rates. Galvanic interactions play a significant role, especially in the galvanic protection of chalcopyrite

within pyrrhotite. Pyrite and arsenopyrite, when in contact with pyrrhotite, may also be galvanically protected, although these occurrences are much rarer than that of chalcopyrite within pyrrhotite.

Crystal lattice affects (fractures, crystal orientations, subgrain boundaries) are also significant. Subgrain formation is well developed in all pyrrhotite, and in some arsenopyrite observed in this study. Different subgrains oxidize at different rates, and subgrain boundaries appear to be more highly oxidized than the subgrain centers.

The presence of bacteria has the overall affect of increasing the reaction rates for most sulphide minerals studied. In general, the order of reactivity between sterile and microbial treatments did not change with the exception of monoclinic and hexagonal pyrrhotite. Hexagonal pyrrhotite, containing more iron than the monoclinic type, oxidized faster in the presence of bacteria, possibly reflecting an enhanced oxidation of ferrous to ferric iron.

The overall affect that the lamellar intergrowth texture has on the bulk mineral oxidation rate for pyrrhotite and marcasite is not clear. There is a definite difference in the rate of oxidation between host and lamellae and it is noteworthy that the minerals that have this texture oxidized relatively quickly overall. The significance of this requires further study.

It is clear that an accurate prediction of the intensity and duration of acid rock drainage must involve a detailed study of the minerals involved, because many of the controls are mineralogically related and site-specific.

Chapter 4

Secondary Minerals And Their Relationship To Acid Rock Drainage In The Meguma Supergroup, Nova Scotia

4.1 Introduction

The formation of secondary minerals from the oxidation of sulphide minerals is a necessary stage in the generation of acid rock drainage (ARD). As presented in Chapter 3, the overall reaction for the oxidation of pyrite can be described by the following equation (Nordstrom, 1982);

(4.1) $$FeS_2 + 15/4\ O_2 + 7/2\ H_2O \text{ ----> } Fe(OH)_3 + 2\ H_2SO_4$$

For every mole of pyrite oxidized, one mole of "ferric hydroxide" and two moles of sulfuric acid are produced. The secondary "ferric hydroxide" forms as a solid phase and precipitates out of solution. However, in nature, the reactions involved are more complex than as shown in equation 4.1 and the solid phase that actually forms depends on factors such as the type of sulphide reacting, host lithology, pH, presence or absence of bacteria, and time. Considering all the possible sulphide minerals, there are a multitude of possible secondary minerals that can form. This chapter focuses on secondary "iron" minerals resulting from oxidation of pyrite and/or pyrrhotite since these are the primary sulphide minerals present in the Meguma Supergroup (see Chapter 2). Secondary minerals from the oxidation of Pb, Zn, and Cu sulphides are not discussed here, but may be locally important in the Meguma Supergroup, especially in areas such as the Eastville lead-zinc deposit (Binney et al., 1986).

The identification and characterization of secondary iron minerals is important

for several reasons. Firstly, they are known to control, at least partially, the pH of the resulting ARD. For example, Alpers and Nordstrom (1991) found that the pH at Iron Mountain in California could be driven below zero by precipitation of melanterite ($FeSO_4 * 7H_2O$). Secondly, secondary minerals are known to control the activity of trace elements such as Cu and Zn. Alpers et al. (1994b) show that the seasonal concentrations and variations of Zn and Cu from portal effluent at Iron Mountain are partially controlled by precipitation and dissolution of Zn-Cu-bearing melanterite. In general, geochemical models for the development of ARD, as well as remediation techniques must include an understanding of the secondary mineralogy.

In this part of the study, several secondary minerals have been identified, including schwertmannite, that has not previously been described from ARD areas in the Meguma Supergroup.

4.2 Background of Secondary Iron Mineralogy

Figure 3.1 (Chapter 3) presents a generalized model for the oxidation of pyrite, and shows some of the secondary iron minerals, as well as the processes in which they form. In general, the minerals can be divided into two groups "hydrated ferrous/ferric sulphates" and "ferric oxide/hydroxides". Table 4.1 shows the mineral names and ideal chemical formulas for these two groups.

According to Nordstrom (1982), the hydrated sulphate minerals typically form yellow to white, efflorescent crusts, on or near sulphide minerals. They form by evaporation during dry periods, when dissolved ferrous and sulphate ions reach

Table 4.1. Some of the common, secondary iron sulphate and oxide/hydroxide minerals that can develop from the oxidation of iron sulphides (data modified from Alpers et al., 1994a; Bigham, 1994).

Ferrous/Ferric Sulphates		**Ferric Oxide/Hydroxides**	
szomolnokite	$FeSO_4 * H_20$	goethite	α FeOOH
rozenite	$FeSO_4 * 4H_20$	lepidocrocite	γ FeOOH
siderotil	$FeSO_4 * 5H_20$	feroxyhyte	δ FeOOH
ferrohexahydrite	$FeSO_4 * 6H_20$	ferrihydrite	$Fe_5OH_8 * 4H_2O$
melanterite	$FeSO_4 * 7H_20$	schwertmannite	$Fe_8O_8(OH)_6SO_4$
rhomboclase	$(H_3O)Fe^{3+}(SO_4)_2 * 3H_2O$	jarosite	$KFe_3(OH)_6(SO_4)_2$
coquimbite	$Fe_2^{3+}(SO_4)_3 * 9H_2O$		
copiapite	$Fe^{2+}Fe^{3+}(SO_4)_6(OH)_2 * 20H_2O$		

saturation with respect to melanterite. Upon further drying, melanterite dehydrates to rozenite or szomolnokite. Oxidation of these minerals can result in the formation of copiapite and coquimbite (oxidation of Fe^{2+} to Fe^{3+}). The crusts that are associated with oxidizing sulphide minerals may contain various combinations of all these sulphate minerals. All the hydrated sulphate minerals discussed here are highly soluble. During rainstorm events, the minerals easily dissolve and may add to the increased acidity and dissolved solids loading in receiving streams (Nordstrom, 1982). When all the Fe^{2+} in solution is oxidized to Fe^{3+}, the ferric oxide/hydroxide minerals begin to precipitate. In the past, the secondary oxide/hydroxide minerals have been referred to as "amorphous ferric hydroxide" and were grouped under the general term "ochre" deposits (e.g., Bigham, 1994; Murad et al., 1994). Their very fine grain size and poor crystallinity has made identification difficult, however, various techniques can be used for identification purposes including colour, crystal shape, and X-ray diffraction (Bigham, 1994; Murad et al., 1994). Table 4.2 shows the main minerals that make up many ochre deposits and lists their characteristics. Typical X-ray diffraction profiles for ferrihydrite, schwertmannite, goethite, and jarosite are shown in Figure 4.1.

Schwertmannite, an iron oxyhydroxysulphate, was approved as a new mineral in 1992 (Bigham et al., 1994). The mineral has an ideal chemical formula of $Fe_8O_8(OH)_6(SO_4)$ (Bigham et al., 1994; Schwertmann et al., 1995). The mineral is believed to have a tunnel structure similar to that of akaganeite [FeO(OH,Cl)]. However, sulphate (SO_4^{2-}) occurs as the stabilizing element instead of chloride. Depending on the degree of saturation with SO_4^{2-}, the chemical formula may range to

Table 4.2. Characteristics of some common secondary iron oxide/hydroxide minerals associated with acid rock drainage (taken from Bigham, 1994).

Mineral Name:	Goethite	Lepidocrocite	Ferrihydrite	Schwertmannite	Jarosite‡
Ideal Formula:	α-FeOOH	γ-FeOOH	~$Fe_5OH_8 \cdot 4H_2O$	$Fe_8O_8(OH)_6SO_4$	$KFe_3(OH)_6(SO_4)_2$
Crystal system	Orthorhombic	Orthorhombic	Trigonal	Tetragonal	Hexagonal
Cell dimensions (Å)	a = 4.608 b = 9.956 c = 3.022	a = 3.88 b = 12.54 c = 3.07	a = 5.08 c = 9.4	a = 10.66 c = 6.04	a = 7.29 c = 17.16
Color	Yellowish brown (7.5YR-10YR)	Orange (5YR-7.5YR)	Reddish brown (5YR-7.5YR)	Yellow (10YR-2.5Y)	Straw yellow (2.5Y-5Y)
Crystal shape	Short rods	Laths	Spherical	Pin-cushion	Pseudocubic
Crystallinity	Moderate	Moderate	Poor	Poor	Good
Most intense XRD spacings (Å)	4.18, 2.45 2.69	6.26, 3.29, 2.47, 1.937	2.54, 2.24, 1.97, 1.73, 1.47	4.86, 3.39, 2.55, 2.28, 1.66, 1.51	5.09, 3.11, 3.08
Major IR bands (cm^{-1})	890, 797	1161, 1026, 753	Nil	1175, 1125, 1055 975, 680, 615	1181, 1080, 1003 628, 493, 472
Néel temp. (K)	400	77	28-115§	75	55-60
Magnetic hyperfine field (T) at:					
295K	38.2	—	—	—	—
77K	50.0	—	≤ 45.1	—	—
4.2K	50.6	46.0	46.5-50.0	45.4	47.0

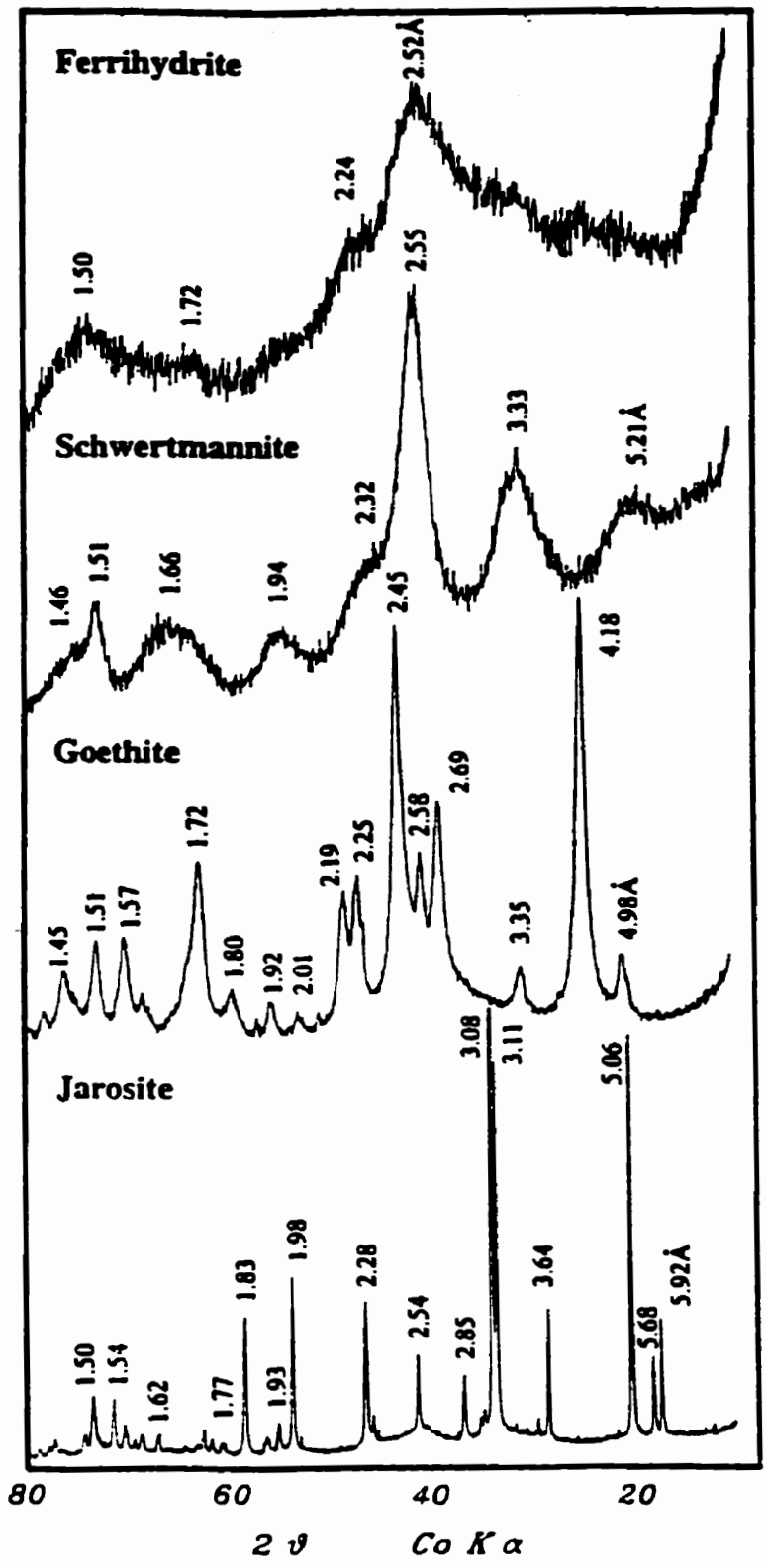

Figure 4.1. Representative X-ray diffractograms for some common, secondary ferric iron minerals (taken from Bigham, 1994).

$Fe_8O_8(OH)_{4.5}(SO_4)_{1.75}$ (Bigham et al., 1996). It also has a unique "pin-cushion" morphology in which needle-like structures radiate from large spherical to ellipsoidal aggregates (Bigham et al., 1994).

Bigham (1994) has outlined a generalized, biogeochemical model for the formation of the common ferric oxide/hydroxide minerals (Fig. 4.2). Schwertmannite is typically associated with ARD that has a pH in the range of 3.0 to 4.0. Jarosite forms in a pH range of 1.5 to 3.0 and ferrihydrite forms from solutions with a pH over 5.0. All minerals except ferrihydrite are considered to result, at least partially, through oxidation of ferrous to ferric iron by bacteria (*Thiobacillus ferrooxidans*). In general, the most stable mineral is goethite, and all others are metastable, but overall these minerals are more stable than the iron sulphates described above. Nordstrom (1982) notes that ferrihydrite and jarosite are not stable longer than a season.

4.3 Sample Descriptions and Methods

Two common types of secondary mineral precipitates occur in all areas of ARD investigated in this study. One type is a red to orange crust that can be observed at the bottom of standing water bodies in quarries, and on the surfaces of shotcrete and ditches at the Petpeswick Lake ARD site. The other type is a thin, white coating that occurs on, or near, sulphide mineral surfaces and along outcrop fractures and bedding planes. Figure 4.3 shows examples of both types. King (1985) also found that both types of secondary minerals occurred in many of the 27 quarries he studied in the Halifax Group of southwestern Nova Scotia.

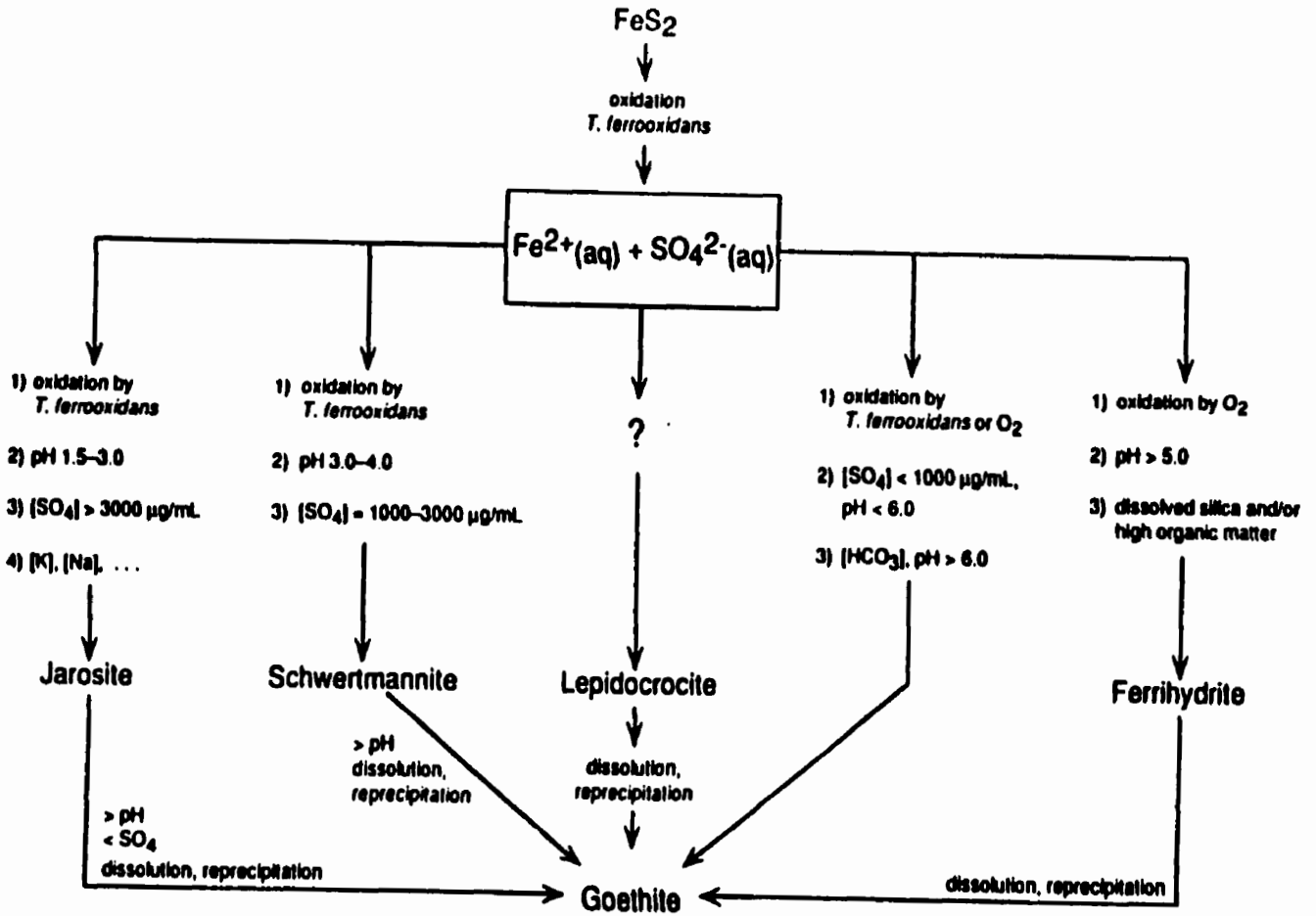

Figure 4.2. Biogeochemical model for the formation of secondary ferric iron minerals associated with ARD (taken from Bigham, 1994).

Figure 4.3 Photographs of secondary iron precipitates, schwertmannite and rozenite. A) and B) precipitate at Petpeswick Lake ARD site, C) schwertmannite sample in quarry at Mt. Uniacke, D) rozenite formed on pyrite surfaces.

Figure 4.3 Continued

A sample of the red precipitate was taken from a slate quarry near Mt. Uniacke in June, 1995 (Fig. 4.4). The abundance of the precipitate on rock surfaces permitted the collection of relatively large pieces without further laboratory refinement. The sample was allowed to dry completely at room temperature. The mineral was hand picked with the aid of a binocular microscope in order to avoid other mineral particles or rock chips which were inevitably present. The very fine grain size and delicate nature of the mineral separate allowed for light hand-crushing in a mortar and pestal. Samples of the white, sulphide mineral coatings were taken from the surfaces of rock samples collected from quarries near the Halifax International Airport and in the Mahone Bay area of southwestern Nova Scotia (see Fig. 1.1).

XRD was performed on a Philips PW1050/37 instrument using Cu-K$\propto$ radiation. The instrument was equipped with a diffracted-beam monochromator and fully automated through the X'PERT hardware - software system (Philips, 1993). The sample was counted in steps of 0.02° 2θ with count times of 1 second per step. Operating conditions of 40 kV and 45 mA were used for generator voltage and generator current respectively. Back-scattered electron images were collected using the SEM facilities in the Faculty of Science at Dalhouise University.

The pH measurements were taken with a Fisher Scientific, Accumet 1003 handheld meter calibrated with standard buffers 1.68 pH and 4.00 pH. Measurements were taken by placing the electrode directly into the pond in the quarry.

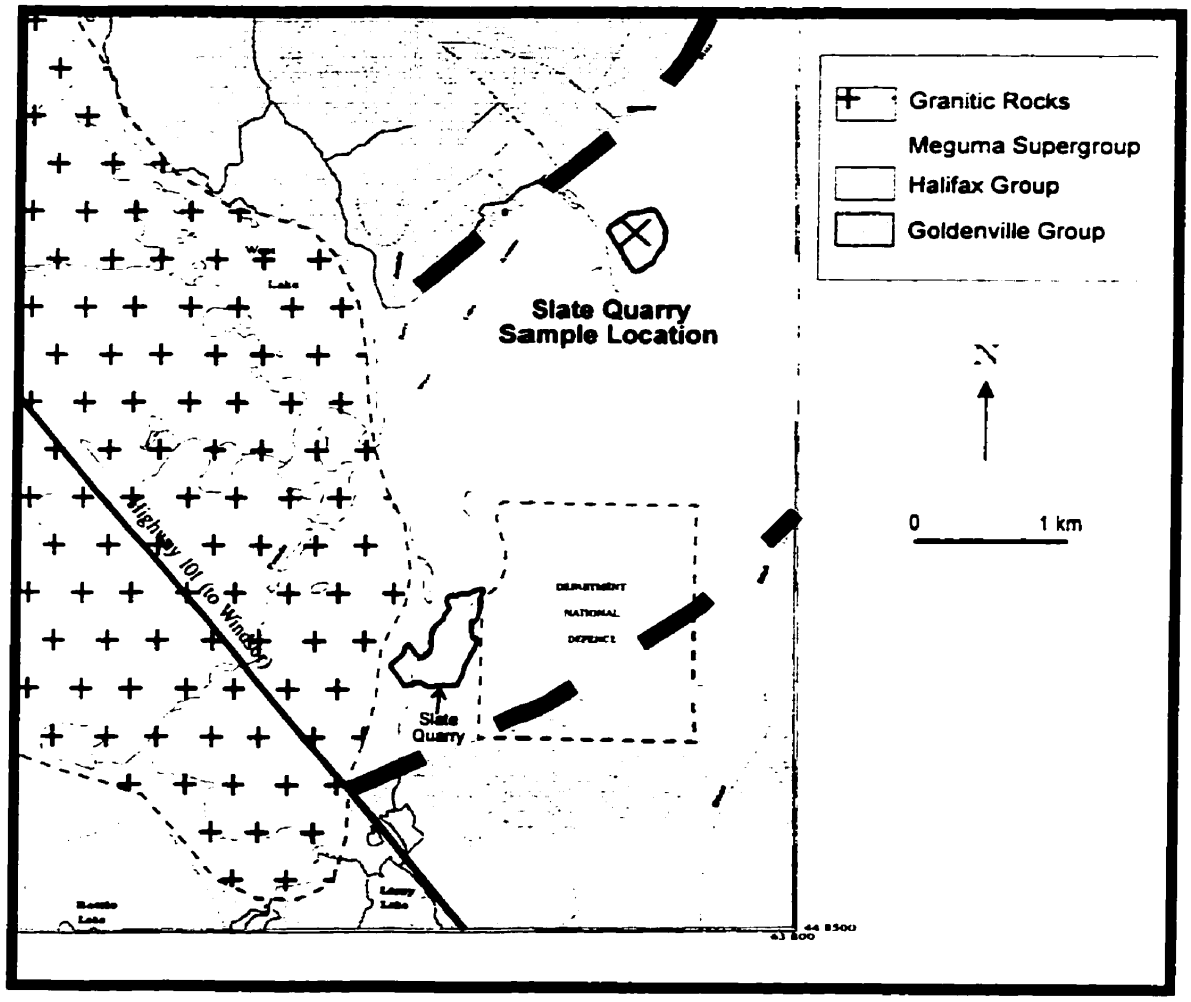

Figure 4.4: Generalized geological map of the Mount Uniacke area showing the location of the Schwertmannite sample site (Geology adapted from M.C. Corey, 1987).

4.4 Results

A pH of 2.72 was measured in the field where the red mineral precipitate was collected. A back-scattered SEM image of the precipitate is shown in Figure 4.5 and shows a fibrous or "pin-cushion" morphology that is typical of schwertmannite samples from around the world (Bigham, 1994). Figure 4.6 shows the XRD profile obtained for this mineral. Overall. the profile consists of seven, broad peaks with the main, identifiable peaks near d-spacings 3.33, 2.55 and 1.51. The general shape of the profile matches that of schwertmannite as shown in Figure 4.1. The broadness of the XRD peaks suggest poor crystallinity and reflects the very fine grain size of the mineral.

The white precipitate has been identified as rozenite (Fig. 4.7). This particular sample is from a quarry in Mahone Bay and the sulphide mineral that the precipitate coats has been identified as pyrite (Fig. 4.7).

4.5 Discussion And Conclusions

Although the number of samples collected for this part of the study is limited, the importance of secondary minerals cannot be overstated. The identification of rozenite (and the hydrated iron sulphate minerals in general) is important in that it identifies one of the processes of ARD formation, and is an intermediate step towards the formation of the more stable ferric oxide/hydroxide minerals. The iron sulphate minerals are hydrous compounds and their stability range is defined by temperature and water activity (Alpers et al., 1994a). Evaporation is an important mechanism in their formation, and in Nova Scotia they will form mainly during dry periods, in the summer

Figure 4.5. SEM image showing the fibrous or "pin-cushion" morphology of the schwertmannite collected from the Mt. Uniacke quarry.

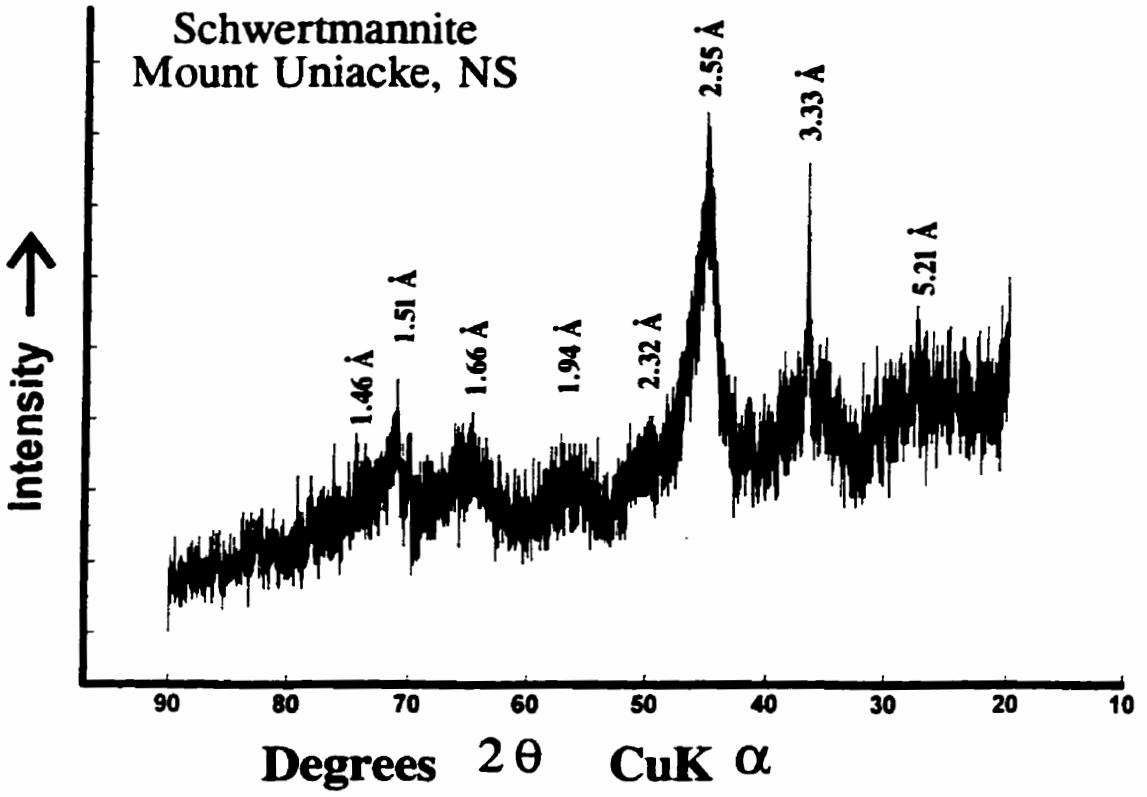

Figure 4.6 X-ray diffractogram of schwertmannite collected at Mt. Uniacke

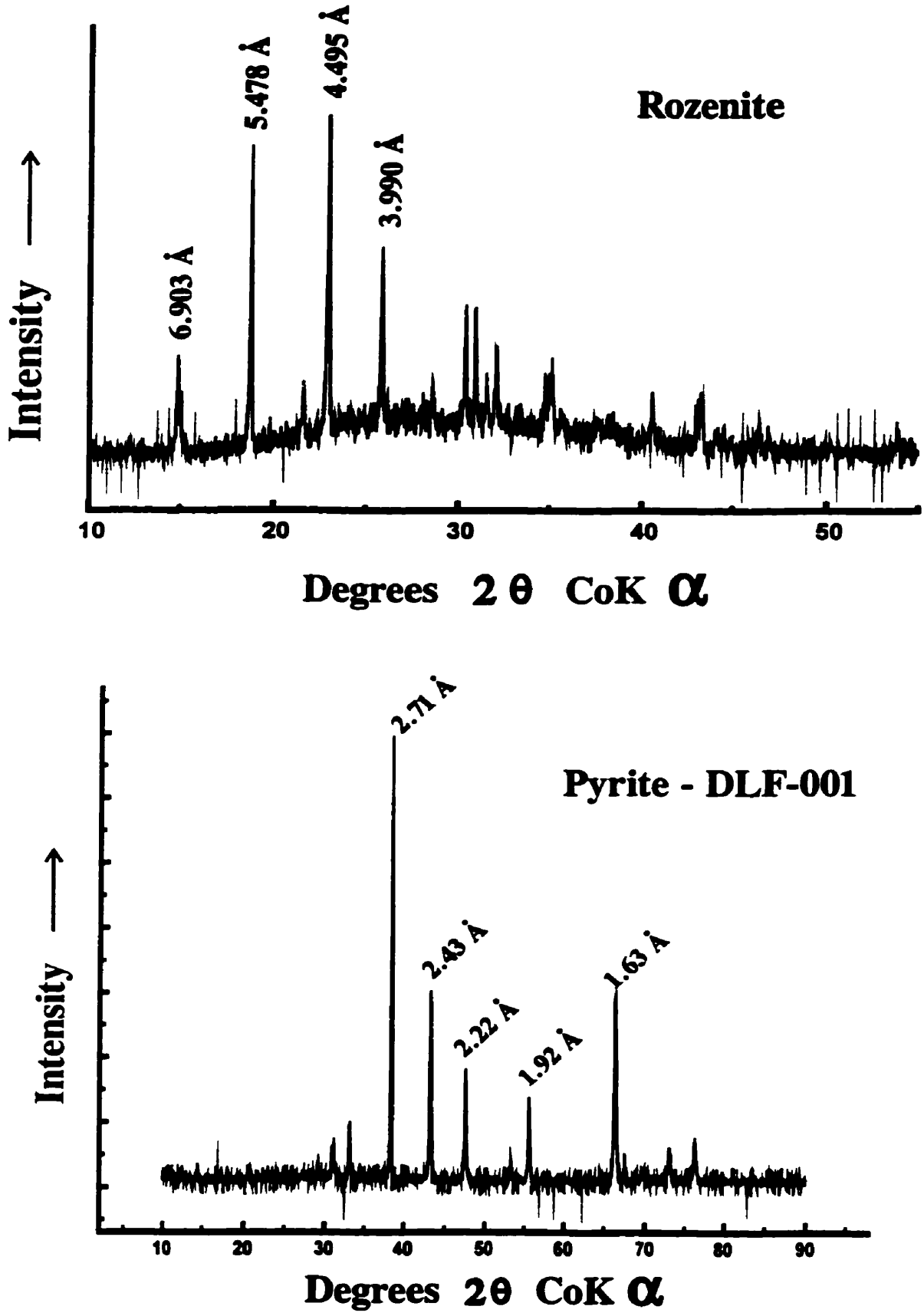

Figure 4.7 X-ray diffractograms for rozenite and pyrite

and early fall months. Generally, the hydrous iron sulphate minerals form close to their source and the rozenite observed in this study formed either on, or close to, sulphide mineral surfaces, and along fractures, cleavage and bedding planes. Therefore, during dry periods, the formation of rozenite acts as a sink for iron and sulphate close to the original source of oxidizing sulphide minerals.

Although easily precipitated, the hydrated iron sulphate minerals also are readily soluble during wetting events. They are a sink for iron and sulphate only on a temporary basis. According to Nordstrom (1982), the high dissolution of these minerals may add to the acidity and total dissolved solids loading into nearby streams, especially after rainstorm events. Rozenite formation and dissolution, during drying and wetting events respectively, is a mechanism for an increase in iron and sulphate loading in streams. This has important implications for predicting the intensity and duration of ARD in that seasonal variations must also be taken into consideration. For example, during dry periods it may be expected that iron and sulphate concentrations would be relatively low in streams affected by ARD. However, this should not be taken as conclusive evidence for a lack of sulphide oxidation. It may be reasonable that these elements are temporarily stored in the secondary hydrous iron sulphate minerals.

With respect to the formation of the ferric oxide/hydroxide minerals, one of the important considerations is the overall effect on the amount of hydrogen ions (and hence pH) produced. The following three reactions have been reported to occur from the experimental oxidation of pyrrhotite (Bhatti et al, 1993):

(4.2) $Fe^{3+} + 2H_2O \text{ ---> } FeOOH + 3H^+$ (oxyhydroxide formation)

(4.3) $K^+ + 3Fe^{3+} + 2SO_4^{2-} + 6H_2O \text{ ---> } KFe_3(SO_4)_2(OH)_6 + 6H^+$ (jarosite formation)

(4.4) $8Fe^{3+} + SO_4^{2-} + 14H_2O \text{ ---> } Fe_8O_8(OH)_6SO_4 + 22H^+$ (schwertmannite formation)

By the dissolution of hydrous iron sulphate minerals such as rozenite during wetting events, ferrous iron is eventually released into streams where it can be oxidized to ferric iron. Clearly, the precipitation of various ferric oxide/hydroxide minerals has the ability to lower the pH, especially in the precipitation of schwertmannite (equation 4.4). In general, the ferric oxide/hydroxide minerals form farther from the original source of sulphide oxidation, and are less soluble than the hydrous iron sulphates. Therefore, they are less likely to adversely affect water quality after their initial development (Alper et al., 1994). Also, note that for the dissolution of schwertmannite for example (reverse of equation 4.4), a considerable amount of H^+ ions are consumed and under the right conditions, an increase in overall stream pH could result. This may or may not be beneficial because a release of trace elements from the ferric oxide/hydroxides is also possible (see below).

Another important consideration in the formation of secondary minerals is their ability to retain metals such as Cu and Zn, either through solid solution or by sorption. As an example of solid solution, Alpers et al. (1994b) determined that Zn/Cu ratios in acid water from Iron Mountain, California, were controlled by the precipitation and dissolution of Cu-Zn-bearing melanterite [$(Fe^{2+},Zn,Cu)SO_4 * 7H_2O$)]. Seasonal variations in the Zn/Cu ratios were related to seasonal cycles of precipitation and

dissolution of melanterite that, in this particular case, was found to have incorporated Cu in preference to Zn.

In addition to solid solution, the concentrations of trace elements also are affected by sorption and coprecipitation with the ferric oxide/hydroxide minerals. This is a result of their very fine grain size and high specific surface area. In general, these minerals are more stable than the hydrous iron sulphates, however, they are still soluble and under the right conditions may release trace elements in the environment over longer periods of time.

In conclusion, the secondary minerals resulting from sulphide oxidation can be properly identified, and due to their different solubilities, an effort should always be made in this direction. The seasonal variations in iron, sulphate, and pH in any given system will depend on the abundance and type of secondary minerals. Any attempt at geochemical modelling of ARD must include the formation of these relatively unstable secondary minerals. Trace element distributions can also be affected by secondary mineral precipitation, oxidation, and dissolution.

It is clear that a proper understanding of secondary minerals is necessary to understand the overall processes involved in the formation of ARD in the Meguma Supergroup of Nova Scotia. Precipitation and dissolution reactions can have both a beneficial and detrimental effect in the local ecosystem and one of the key elements controlling these reactions is seasonal variation. Future considerations that involve the study of secondary iron minerals in the Meguma Supergroup should include a much larger sample set taken over various time periods, and in different hydrological

regimes, in order to determine what mineral transformations may occur, and under what conditions.

Chapter 5

Static Tests And Acid-Base Accounting For The Prediction Of Acid Rock Drainage In The Meguma Supergroup, Nova Scotia

5.1 Introduction

Sulphide-bearing rocks of the Meguma Supergroup typically contain various proportions of pyrrhotite and pyrite and therefore have the potential to produce acid rock drainage (ARD). However, this does not necessarily mean the rocks are overall, net acid producers. Other minerals, including carbonates, some silicates, and phosphates (primarily apatite) have the ability to consume or neutralize, at least partially, the acid produced by the oxidation of sulphide minerals (e.g., Sherlock et al., 1995).

One method of assessing whether rocks are net acid producers, and to better quantify the nature of ARD in general, is by static testing. Static tests measure the quality and quantity of different constituents in a sample, at one point in time, and include parameters such as major and trace element content, paste pH, mineralogy, and acid-base accounting (ABA) (Price, 1997). ABA is a standard procedure developed to analytically estimate the amount of acid potential (AP) and neutralization potential (NP) in a sample. The net neutralization potential (NNP) is the difference between acid potential and neutralization potential (NNP = AP - NP).

This chapter presents the results of static testing performed on a suite of samples collected from various locations in the Meguma Supergroup. The samples include the

Caribou drill core (stratigraphic section from Halifax Group through the GHT into the top of the Goldenville Group), Beaverbank Highway samples (GHT samples), Eastville drill core (random samples), and a collection of samples mainly from contact metamorphic rocks near the South Mountain Batholith (Fig. 5.1). In addition, a method for rapidly estimating the total acid potential (TAP) is introduced that uses magnetic susceptibility of a rock sample measured with a handheld meter (Section 5.5). Although not highly accurate, this method is very rapid and can provide useful information on a "first pass" basis.

This part of the study shows that in general, rocks in the Meguma Supergroup have very low neutralization potential. Some rocks do contain carbonate minerals and appear to have high neutralization potential. However, this should be interpreted with care because some of the carbonate minerals may be Fe and Mn-bearing, which are not good ARD neutralizers due to slow reaction rates. Also, hydrolysis of the Fe and Mn creates acidity that can effectively consume any alkalinity that may be generated by the presence of carbonate.

5.2 Background On Static Tests And Acid-Base Accounting (ABA)

The most complete and up-to-date procedures for static testing in ARD studies are given in draft form in "Guidelines and recommended methods for the prediction of metal leaching and acid rock drainage at minesites in British Columbia" (Price, 1997). In that document, a detailed analysis is given for the uses and interpretation of many static test procedures for ARD prediction. In terms of ABA, the recommended method

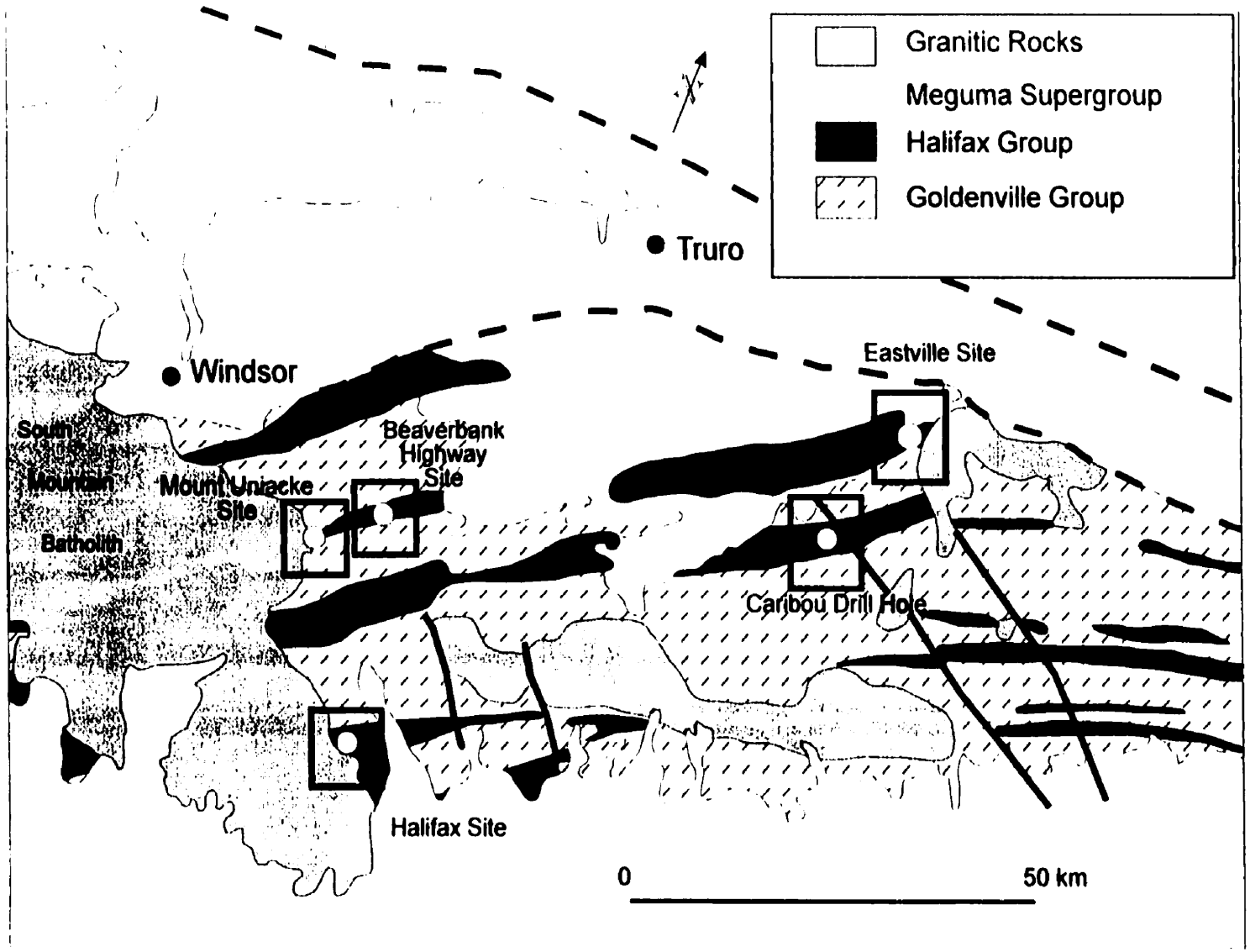

Figure 5.1 Geological map showing location of sample sites. Halifax Site (CR1-3), Mount Uniacke Site (CR4-6), Beaverbank Highway Site (CR7-10 and all MF samples), Eastville Site (CR11-17), Caribou Drill Hole (all CB samples). (Geology modified from Keppie, 1979a).

is the U.S. Environmental Protection Agency's Acid-Base Accounting procedure (also called Sobek method or EPA-600 method) (Sobek et al., 1978). However, there are many ABA procedures available, and there is no one clear method that works the best.

Probably the two most widely accepted ABA procedures are the B.C. Research Initial Test (BCRIT, also referred to as the Duncan test) (Bruynesteyn & Duncan, 1979) and the Sobek method. The major difference between these two methods lie in their determination of the neutralization potential (NP). The BCRIT has been used in the past in Nova Scotia (Albright, 1987; Lund, 1987), and is still used today (C. Cole, personal communication, 1998); however, the Sobek procedure appears to be the most favored elsewhere (Price, 1997). Controversy exists over which of these two tests provides the best results for predicting ARD (e.g., Calow et al., 1995). Figure 5.2 shows a plot of the neutralization potential for eight samples of tailings from an abandoned gold mine and shows significant differences between the two NP methods. The Sobek method consistently gave the highest NP values. In another study, Lawrence and Wang (1997) found that the standard Sobek method consistently overestimated the NP values of 120 samples (mostly waste rock and tailings) from mines around the world. However, the BCRIT method was not included in their study. One of the main factors cited for the overestimate, is the extreme conditions of the Sobek method (i.e., strong acid and boiling procedure - see below for further discussion on methodology).

In addition to the two ABA procedures presented above, Lawrence and Wang (1997) propose another method of determining the NP value of a sample that is based on the CO_2 content. The NP is called Carbonate NP, and is discussed further below.

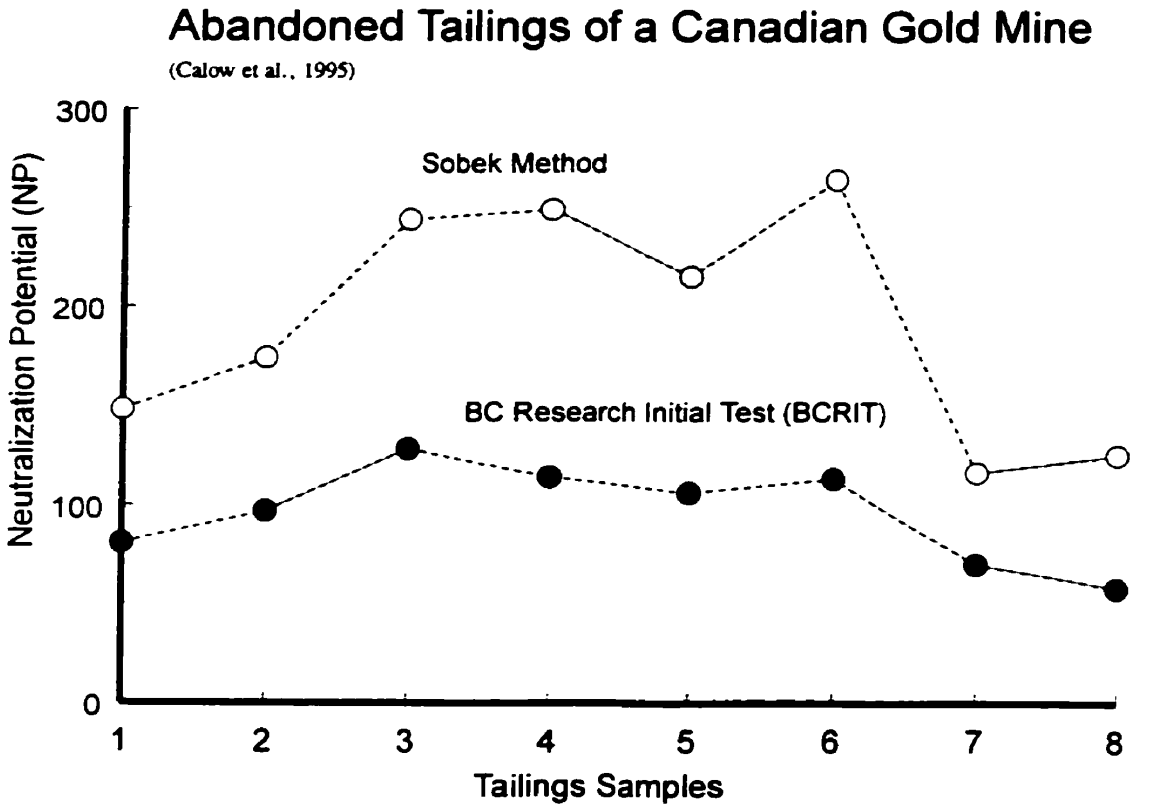

Figure 5.2 Comparison of Neutralization Potential (NP) for the BCRIT and Sobek methods. Samples are from abandoned tailings of a Canadian gold mine (modified from Calow et al., 1995). Units for the BCRIT and Sobek methods are kg H_2SO_4/tonne and tonnes $CaCO_3$ equivalents/1000 tonnes respectively.

The overall objective in ABA is to calculate the net neutralization potential (NNP) which can give insights into the potential of a rock to produce acidity. Whether a site actually produces acidity in the field is based on a number of factors including reaction rates and oxidizing conditions. However, ABA is useful for an initial assessment and is especially effective when combined with kinetic data obtained through long-term kinetic testing.

5.2.1 BCRIT Method

The complete methodology for the BCRIT method is given in Appendix A. The acid potential (AP) is a theoretical value calculated from a total sulphur analysis and is based on the following equation (Duncan, 1972; Bruynesteyn & Duncan, 1979):

(5.1) $4FeS_2 + 15O_2 + 14H_2O \text{ ---> } 4Fe(OH)_3 + 8H_2SO_4$

The method relies on the assumption that all sulphur in a sample occurs as pyrite and a one-to-one conversion factor is assumed. In this reaction, two moles of sulphuric acid are produced per mole of pyrite oxidized. Alternatively, one mole of sulphuric acid is produced per mole of sulphur (i.e., a one-to-one conversion factor). The ratio of H_2SO_4 (MW = 98) to sulphur (MW = 32) is 3.06. Therefore, 1 g of sulphur is equivalent to 3.06 g of H_2SO_4. Using units of kg/tonne:

(5.2) S/100 * 3.06 * 1000 = wt% sulphur * 30.60 = AP (kg H_2SO_4 / tonne)

The neutralization potential (NP) is obtained by a titration method. A sample is prepared by grinding to 100% passing through -100 mesh. A 10 gram portion of slurried sample is titrated directly with room temperature, sulphuric acid to an endpoint of pH 3.5 for four hours. The amount of sulphuric acid used in the titration is converted to units of kg H_2SO_4 per tonne of sample and compared to the acid potential (AP) values.

5.2.2 Sobek Method

The detailed methodology for the Sobek method is presented in Appendix A. This acid-base accounting procedure was developed at West Virginia University (Sobek et al., 1978) and is based on the following reaction:

(5.3) $FeS_2 + 2CaCO_3 + 3.75O_2 + 1.5H_2O \text{ ---> } Fe(OH)_3 + 2SO_4^{2-} + 2Ca^{2+} + 2CO_2$

This reaction shows that one mole of pyrite (1 FeS_2 = 64g of sulphur) is neutralized by 2 moles of calcite (2 $CaCO_3$ = 200g). This corresponds to a ratio of 1g sulphur to 3.125g of $CaCO_3$. Using units of "tonnes per 1000 tonnes" means that 31.25 tonnes of $CaCO_3$ equivalent is needed to neutralize 1000 tonnes of rock containing 1.0 wt.% pyritic sulphur. Therefore, the total wt % sulphur value is multiplied by 31.25 to get the acid potential (AP) value in units of tonnes $CaCO_3$ equivalent / 1000 tonnes).

As in the BCRIT method, the NP value is obtained by titration, however there are several notable differences. The Sobek method uses HCl as opposed to H_2SO_4, a

back titration using sodium hydroxide is used, and the sample is boiled. Also the amount of acid added is determined by a fizz test (Appendix A). There are clearly major differences between the two methodologies.

An additional parameter that is commonly collected along with the Sobek method is paste (crushed) pH. Paste pH is a pH measurement of a paste created from a crushed sample (usually 2 g of < 250 μm grain size) mixed with distilled water. The amount of water added is just enough to wet the entire sample to form a paste without allowing excess water to pool on the sample (Sobek et al., 1978).

5.2.3 Carbonate NP

Another method that can be used to determine the NP of a sample is based on a measurement of the inorganic carbon content (Lawrence and Wang, 1997). The calculation of Carbonate NP is a measure of the maximum theoretical neutralization capacity if all carbonates in a sample react like calcite (Price, 1997). The calculation is as follows:

(5.4) Carbonate NP = $\%CO_2$ * (100.09 / 44.01) * 10
(units in tonnes $CaCO_3$ equivalent / 1000 tonnes).

Total carbon can be used if there is no significant organic carbon in the samples. As presented in Chapter 1, many of the rocks examined in this study are from the Cunard or Mosher's Island Formations and are black slates rich in organic carbon. Therefore Carbonate NP values have limited use for these rocks (see Section 5.4.4 for further

discussion).

5.3 Sample Locations And Descriptions

A total of 78 samples were used for this study and were chosen based on stratigraphic position within the Meguma Supergroup, as well as availability of additional information including thin section descriptions, major and trace element chemistry, and microprobe data. General sample locations are shown in Figure 5.1. Detailed locations and descriptions of all CR samples are presented in Chapter 2. All MF samples are from the Beaverbank Highway section and detailed geochemistry and petrography are given by Feetham (1996). These samples are from a section of the GHT and were collected as part of a geochemical study to characterize the GHT in that area. All CB samples are from the Caribou drill core (Fig. 5.1) and have been described in detail by Burns (1997). The Caribou drill hole is the most complete section through the lower Halifax Group stratigraphy and represents a major portion of the Halifax Group, the GHT, and the upper part of the Goldenville Group. General descriptions of all MF and CB samples are presented in Appendix B.

5.4 Results And Discussion

The measured and calculated parameters are presented in Appendix C. The data are in a spreadsheet format that has been set up as a Meguma Supergroup ARD database, and at this stage, not all parameters have been measured.

5.4.1 Acid Potential

In the calculation of the AP value, it is important to know the sulphur species present in the sample, and to differentiate between wt% total sulphur and wt% sulphide sulphur. Specifically, the AP value should be calculated only from the sulphur content contained in sulphide minerals. Barite ($BaSO_4$) and gypsum ($CaSO_4$) for example, contain significant amounts of sulphur but do not contribute to ARD. In the Meguma Supergroup, it is reasonable to use wt% total sulphur because neither barite or gypsum are common phases. Note that caution must be used when sampling because, as presented in Chapter 4, various types of secondary iron sulphate minerals are known to occur, and could contribute to the overall sulphur content. This is of concern, only if sampling highly weathered rock. Figure 5.3 shows a plot of wt% sulphide sulphur vs wt% total sulphur from a set of samples collected by Jacques, Whitford and Associates Limited (1990), at an ARD site in the Meguma Supergroup. Sulphide sulphur content is identical to total sulphur content and there are no other sulphur species present. For the present study, it is assumed that all sulphur is contained in sulphide minerals. Since wt% total sulphur is used to calculate the AP values, they are termed total acid potential (TAP).

Wt% total sulphur has been analysed for all 78 samples in this study. Overall, the values range from 0.01 to 6.12 wt% with a mean value of 1.07. However the samples are from various locations and stratigraphy, and a more useful analysis is shown in Figure 5.4 where wt% total sulphur is plotted against depth for the Caribou and Beaverbank Highway samples. For the Caribou samples, the highest sulphur

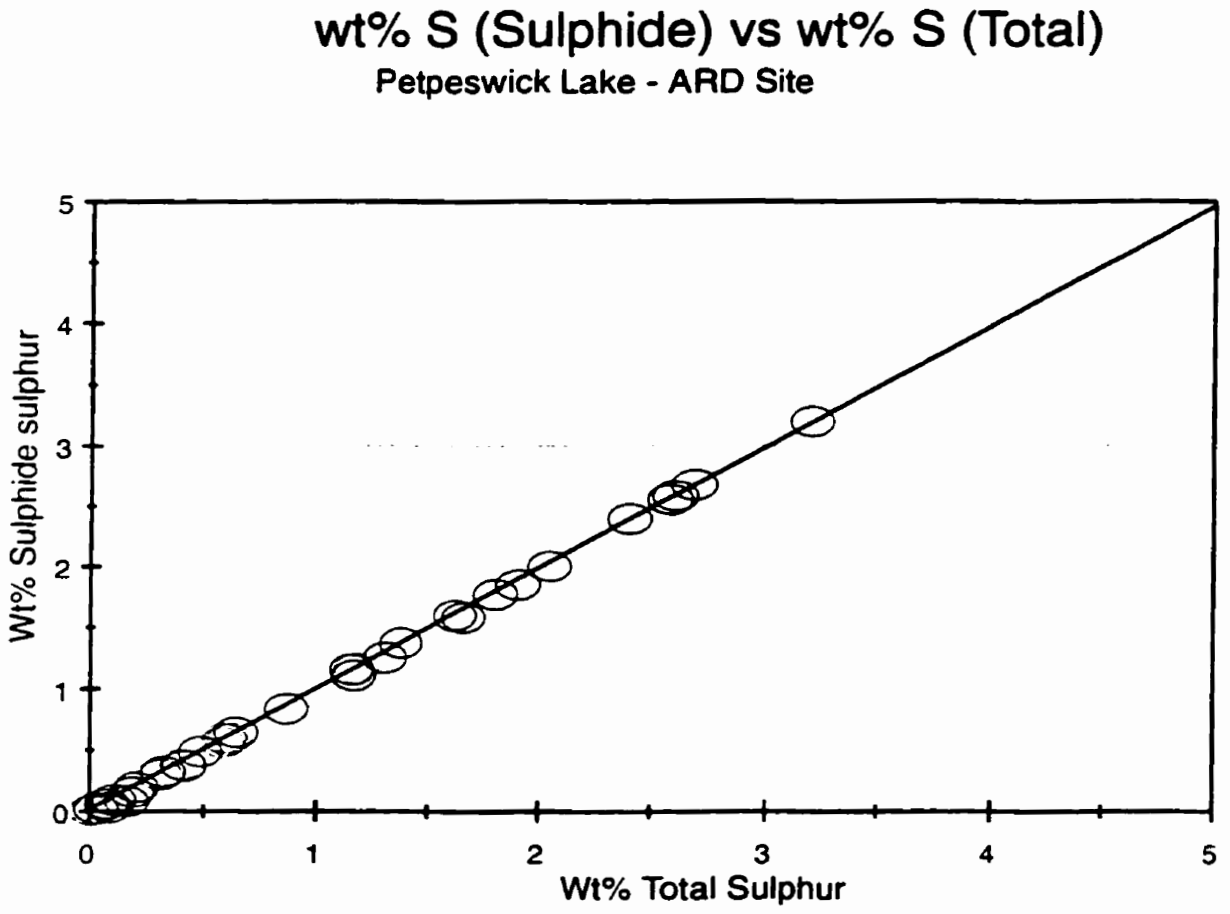

Figure 5.3 Plot of wt% total sulphur against wt% sulphide sulphur for samples taken at Petpeswick Lake ARD site (data taken from Jacques, Whitford and Associates, Limited, 1990)

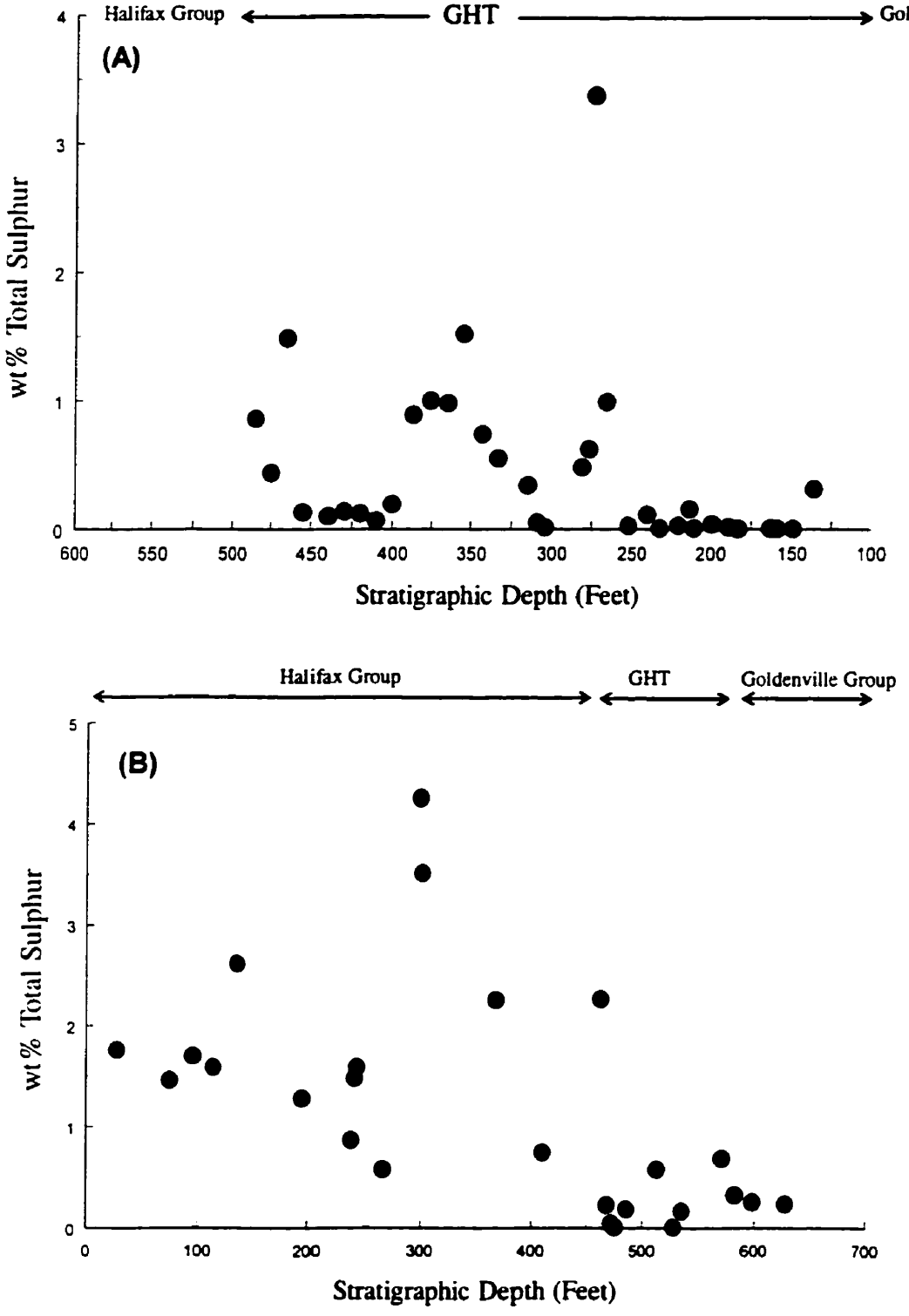

Figure 5.4 Plot of wt% total sulphur verses depth for the (A) Beaverbank Highway GHT samples (MF), and (B) Caribou drill hole samples (CB). (data for Beaverbank Highway samples taken from Feetham, 1996).

contents are in the lower part of the Halifax Group, and there is an overall decrease in sulphur with increasing depth from the Halifax to the Goldenville Groups. Sulphur content for the Beaverbank Highway GHT samples are generally in the range of 0 to 2 wt%.

5.4.2 Paste pH

Figure 5.5 shows a plot a paste pH against wt% total sulphur for 21 samples. Except for two samples, there is a decreasing trend of paste pH with increasing sulphur content. This may, in part, reflect the fact that samples with increased amounts of sulphide minerals generally contain little or no carbonate minerals. The two samples (CR-95-011 and CR-95-014) that have high wt% total sulphur and high paste pH contain calcite (see Appendix C). The lower paste pH of the samples with high wt% total sulphur may indicate that weathering has affected the samples and the crushed particles are coated with secondary minerals that are acidic. Price and Kwong (1997) suggest a similar process, and also show that particle size has an effect on paste pH with the finer particle size fraction having a lower paste pH.

It is evident that, even though the paste pH is a simple and quick laboratory test, it can be used as part of the assessment phase in a preliminary analysis of ARD prediction. Price and Kwong (1997) concluded that a paste pH measurement may indicate, to a certain extent, the degree of weathering in different particle sizes, as well as effects of residual alkalinity.

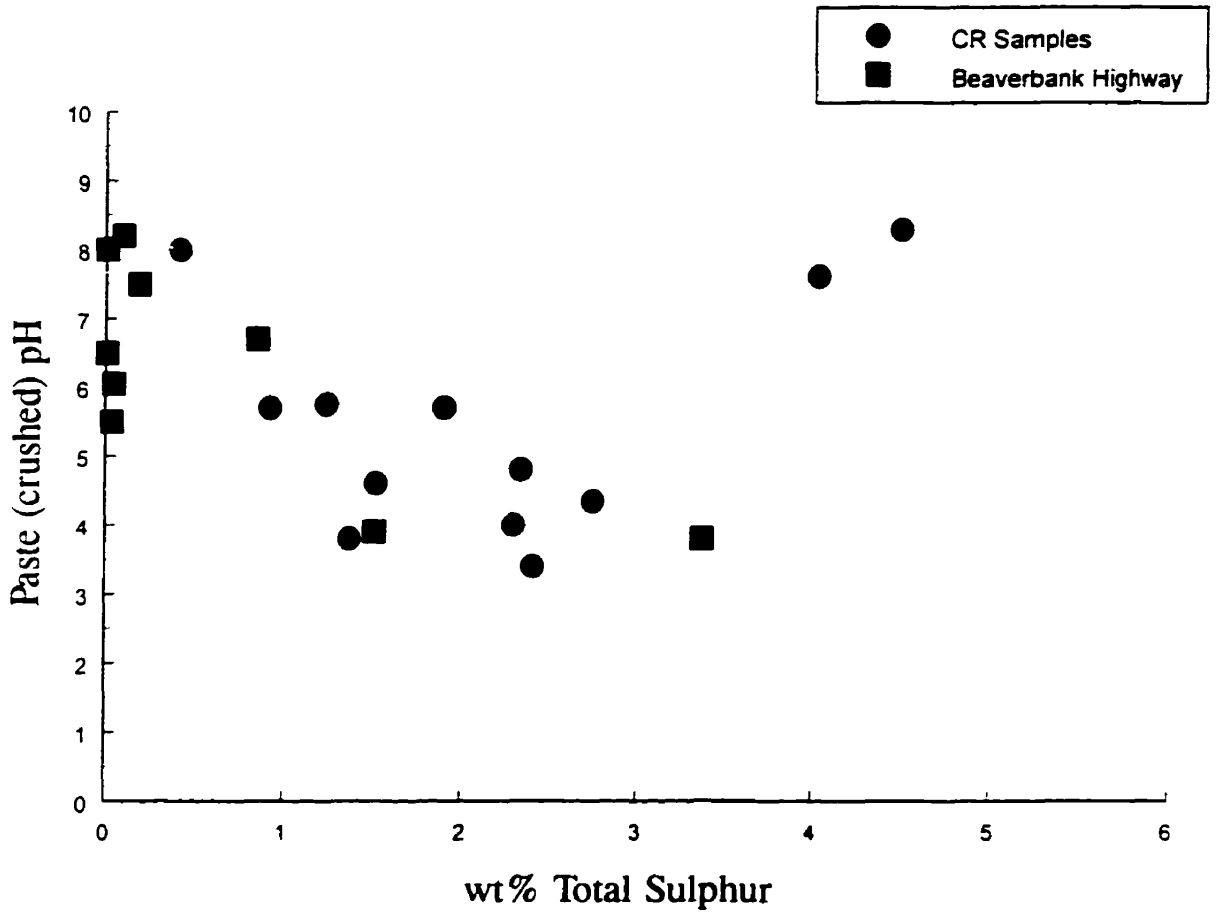

Figure 5.5 Plot of paste (crushed) pH against wt% total sulphur for Beaverbank Highway (MF) and CR samples (n = 21). The two samples with high sulphur and paste pH contain calcite.

5.4.3 Neutralization Potential

A total of 20 CR samples and Beaverbank Highway samples (MF) were analyzed for NP by both the Sobek and BCRIT methods. Figure 5.6 shows a plot of Sobek vs BCRIT NP values for the 20 samples. In general, the BCRIT method gives higher NP values, however, overall the values are considered to be in the low category for NP and the differences between the two tests are not significant. Since the samples have low NP in general, care must be taken in assessing the ARD potential, and further kinetic testing should be performed. One of the problems with low NP rocks is that low sulphur content, and small amounts of sulphide minerals become increasingly important. This is of particular concern when the sulphide minerals that are present, react quickly, and there is little chance of neutralizing the acidity produced.

5.4.4 Carbonate NP

An important consideration in calculating the carbonate NP value is to determine if the wt% total carbon can be used, or if considerable organic carbon is present, only the carbonate carbon content is appropriate. Figure 5.7 shows a plot of wt% total carbon (expressed as CO_2) vs wt% organic carbon (expressed as CO_2) for 51 samples including CR, Beaverbank Highway (MF), and the Caribou drill core (CB) (see Appendix C). The plots show there is considerable organic carbon present in many of the samples, and therefore only the carbonate carbon content should be used to calculate carbonate NP. Figure 5.8 shows calculated carbonate NP values plotted against total acid potential (TAP) for the 51 samples. In general, many of the samples contain very

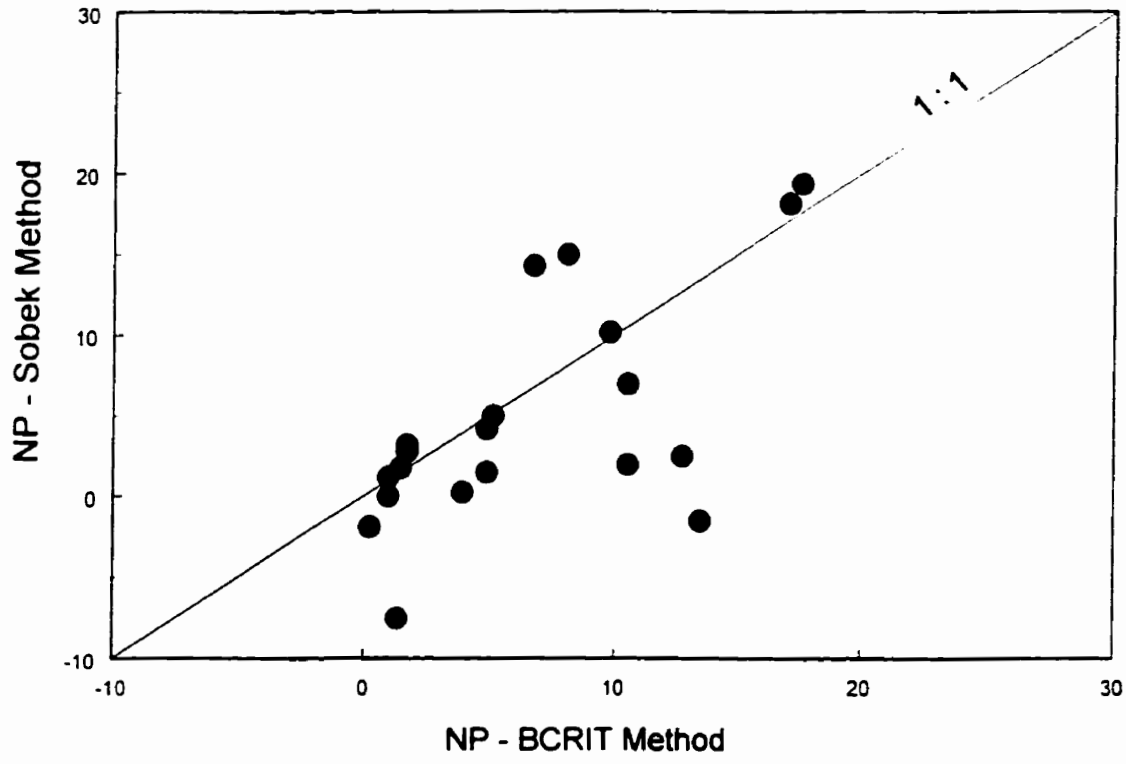

Figure 5.6 Plot of neutralization potential (NP) values determined by the Sobek method and the BCRIT method (units are tonnes CaCO3 / 1000 tonnes). Number of samples = 20 and include CR and Beaverbank Highway samples.

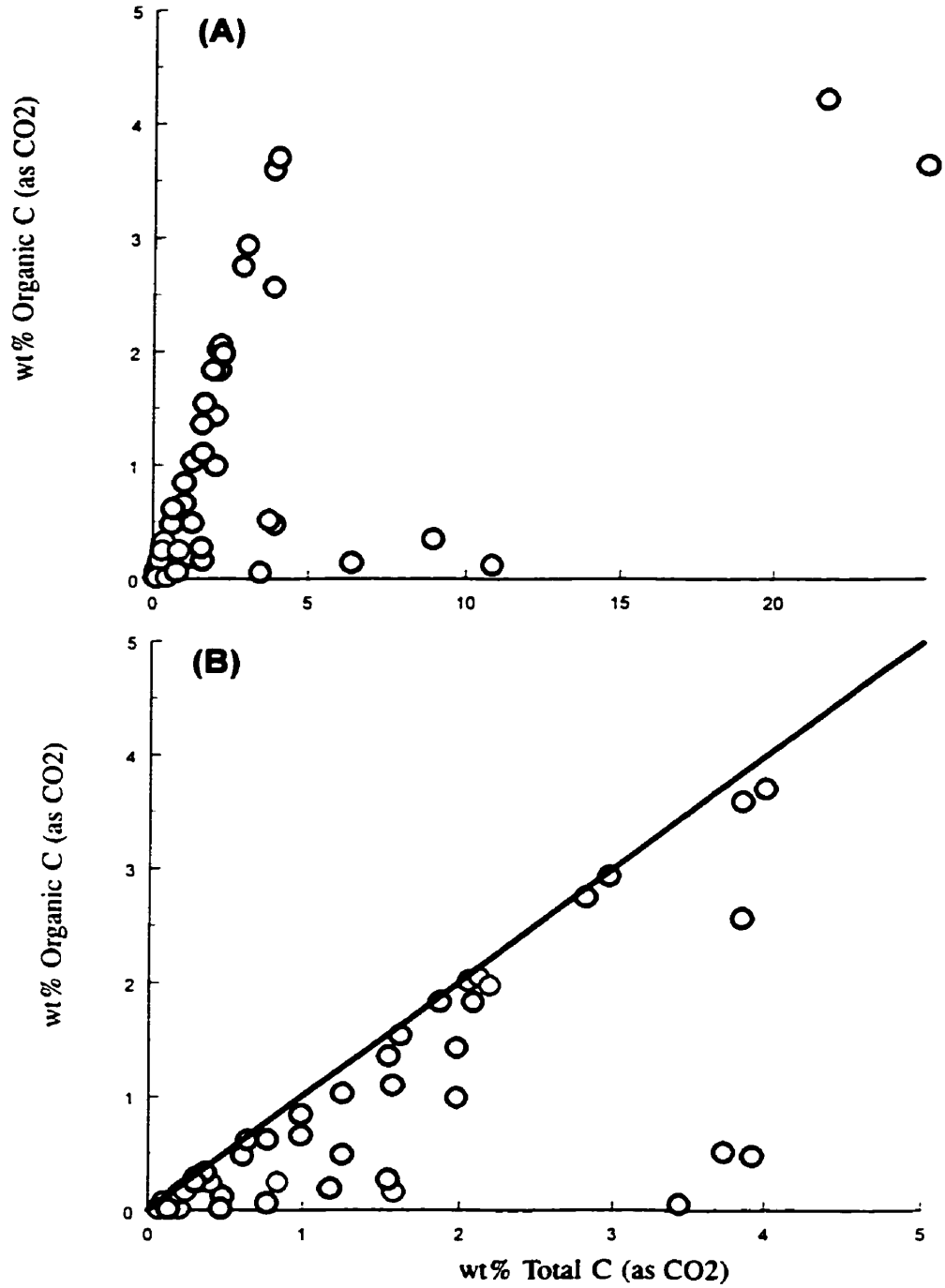

Figure 5.7 Plot of organic carbon against total carbon. Data show a significant portion of the carbon is organic. Note: wt% C recalculated as CO_2.
(A) Samples include some CR, MF, and CB samples.
(B) X-axis scale change to show more clearly the data trend of samples with lower total carbon content.

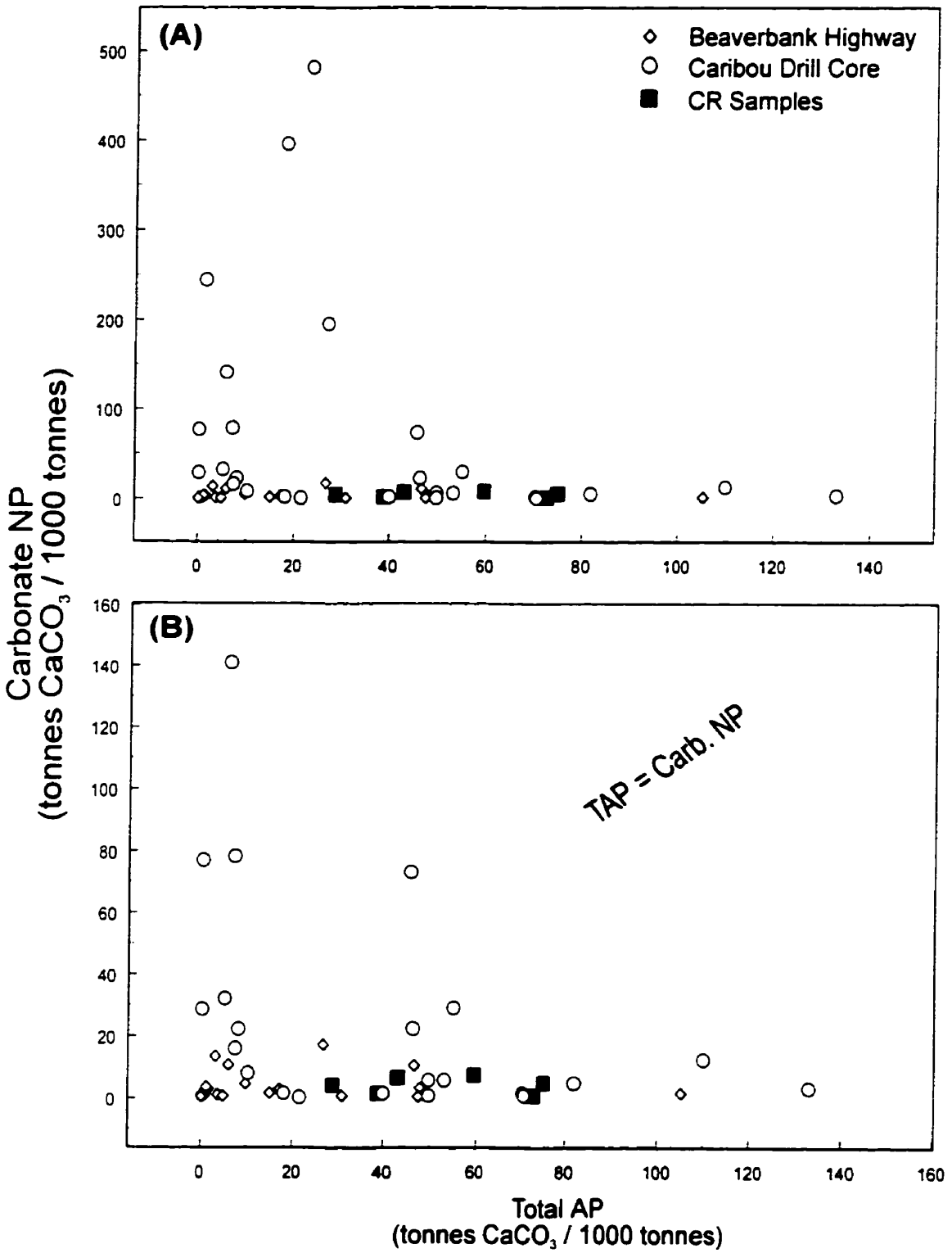

Figure 5.8 Plot of carbonate NP vs total acid potential (TAP). (A) shows all samples, (B) y-axis scale changed to show trends more clearly.

little carbonate NP. However, some samples do contain considerable amounts of carbonate NP, and these samples also contain very little TAP. Figure 5.9 shows a similar plot of over 200 samples collected mainly from the GHT throughout the Meguma Supergroup (data from Graves and Zentilli, 1988). There is a similar trend for these GHT samples. The samples with high carbonate NP values are known to contain carbonate minerals. However, care must be used when assessing these high carbonate NP values. Firstly, in addition to calcite, some of the carbonate minerals in the GHT are known to range in composition from kutnahorite - $CaMn(CO_3)_2$ to rhodochrosite - $MnCO_3$ (e.g., Hingston, 1985; MacInnis, 1986). As presented by Price (1997), when iron and manganese carbonates weather, subsequent hydrolysis of the iron and manganese creates acidity, and overall there is no net generation of alkalinity. Secondly, the amount of calcite, if present, is generally insignificant and typically occurs only in thin veinlets or small nodules. Therefore, the amount of calcite present in rocks of the Meguma Supergroup will not be significant enough for long term ARD neutralization. Thirdly, even where calcite is present, its reaction rate is so fast that it will only be effective for neutralization in the short term.

5.4.5 Net Neutralization Potential (NNP)

In order to assess the net neutralization potential of the samples, the simple method is to subtract AP from NP (NNP = NP - AP). If AP exceeds NP, the net neutralization potential is negative and, at least in theory, the sample is considered to be acid-generating. However, this is a simplistic approach and in practice, NNP numbers

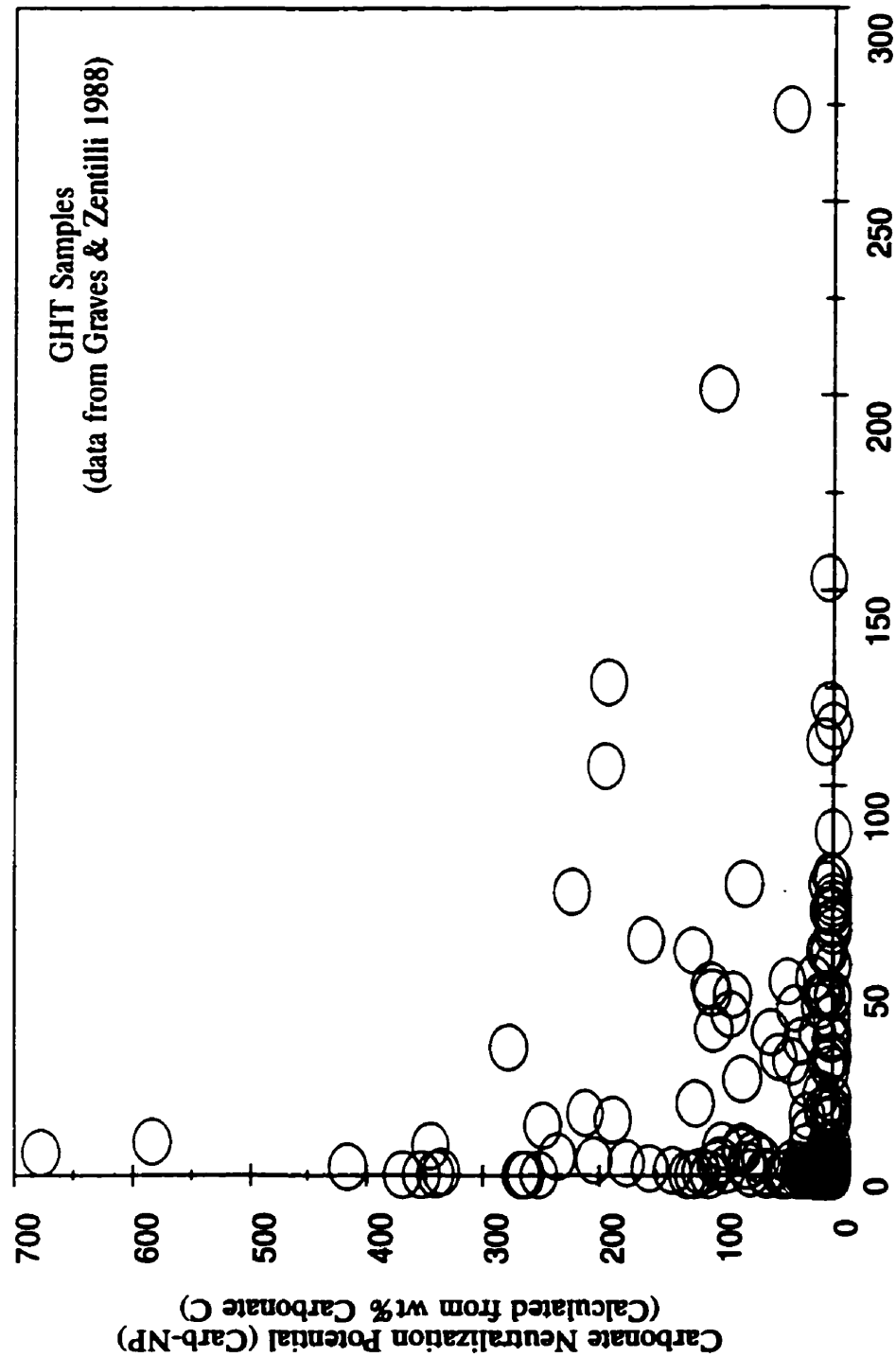

Figure 5.9 Plot of total acid potential (TAP) vs carbonate NP for over 200 samples of the GHT. Units are tonnes $CaCO_3$ / 1000 tonnes (data from Graves and Zentilli, 1988).

are rated according to specified criteria which are different in different jurisdictions. As presented by Jambor and Blowes (1998), it can generally be considered that NNP values >20 are low risk, NNP values of -20 or less are considered to be acid-producing, and values between +20 and -20 are uncertain.

An alternative way of presenting the NNP values is by using ratios. For example, various values of neutralization potential ratios (NPR = NP / AP) are used as screening criteria in British Columbia (Table 5.1). Figure 5.10 shows a log-log plot of wt% sulphide sulphur versus the NP/AP ratio and the screening criteria used in British Columbia. A <0.3 wt% sulphide sulphur cutoff value is used for rocks that are unlikely to be acid-generating and samples with >0.3 wt% are ranked according to the NP/AP ratios. Figure 5.11 shows log-log plots for the samples of this study. In the case of Nova Scotia, a 0.4 wt% sulphide sulphur is used as the cutoff (Environment Act, 1995). As discussed above, wt% total sulphur instead of sulphide sulphur is used in this study. In general, the majority of samples are acid-generating. Also, care should be taken when assessing samples containing between 0.1 and 0.4 wt% total sulphur considering the relatively low NP capacity as presented above. In all likelihood, a 0.4 wt% cutoff may be too high considering the overall low NP capacity of rocks in the Meguma Supergroup examined in this study. It is suggested that there is no need for a cutoff value in the Meguma Supergroup, especially for areas that are suspected to have high ARD potential based on factors such as geology, metamorphic grade, and magnetic signatures as presented in Chapter 7.

Table 5.1 Acid-base accounting screening criteria for the generation of ARD (data from ARD Guidlines for British Columbia - Price et al., 1997).

NP/AP	Potential for ARD	Comments
>4:1	none	no further ARD testing required unless materials are to be used as a source of alkalinity
2:1 to 4:1	low	not potentially ARD-generating unless significant preferential exposure of sulfides along fracture planes, or extremely reactive sulfides in combination with insufficiently reactive NP
2:1 to 1:1	possibly	possibly ARD-generating if NP is insufficiently reactive or is depleted at a faster rate than sulfides
<1:1	likely	likely ARD-generating

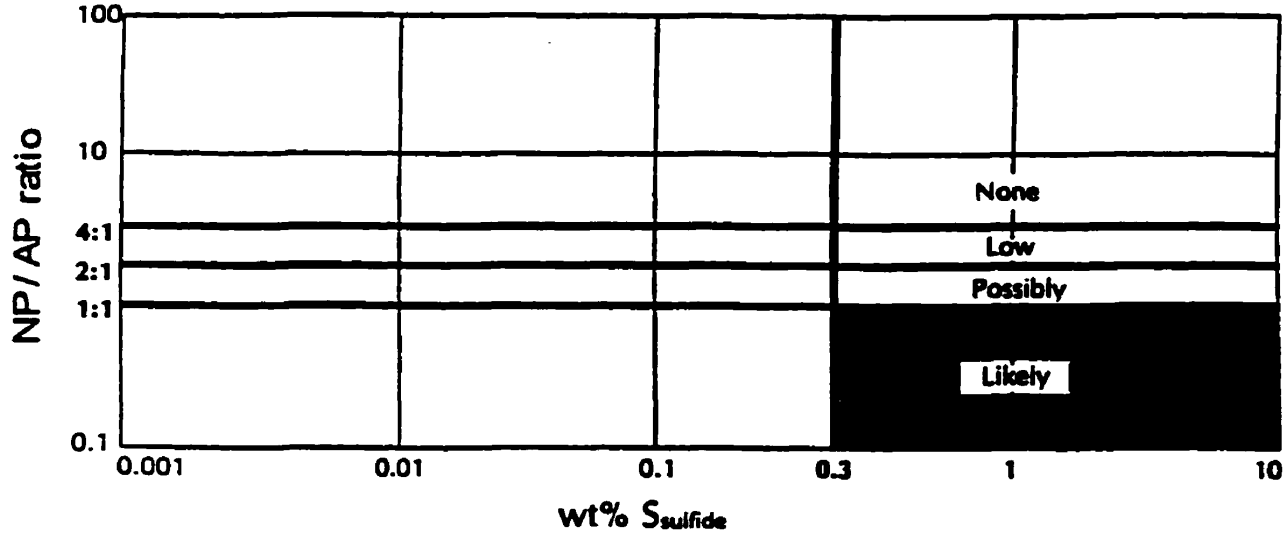

Figure 5.10 Example of a log-log plot of wt% sulphide sulphur verses NP / AP ratio. The plot shows guidelines for probable ARD generation (British Columbia - Price et al., 1997). Samples containing < 0.3 wt% sulphide sulphur are likely not to be acid-generating. For samples above the 0.3 wt% cutoff, ratings vary according to the NP /AP ratios.

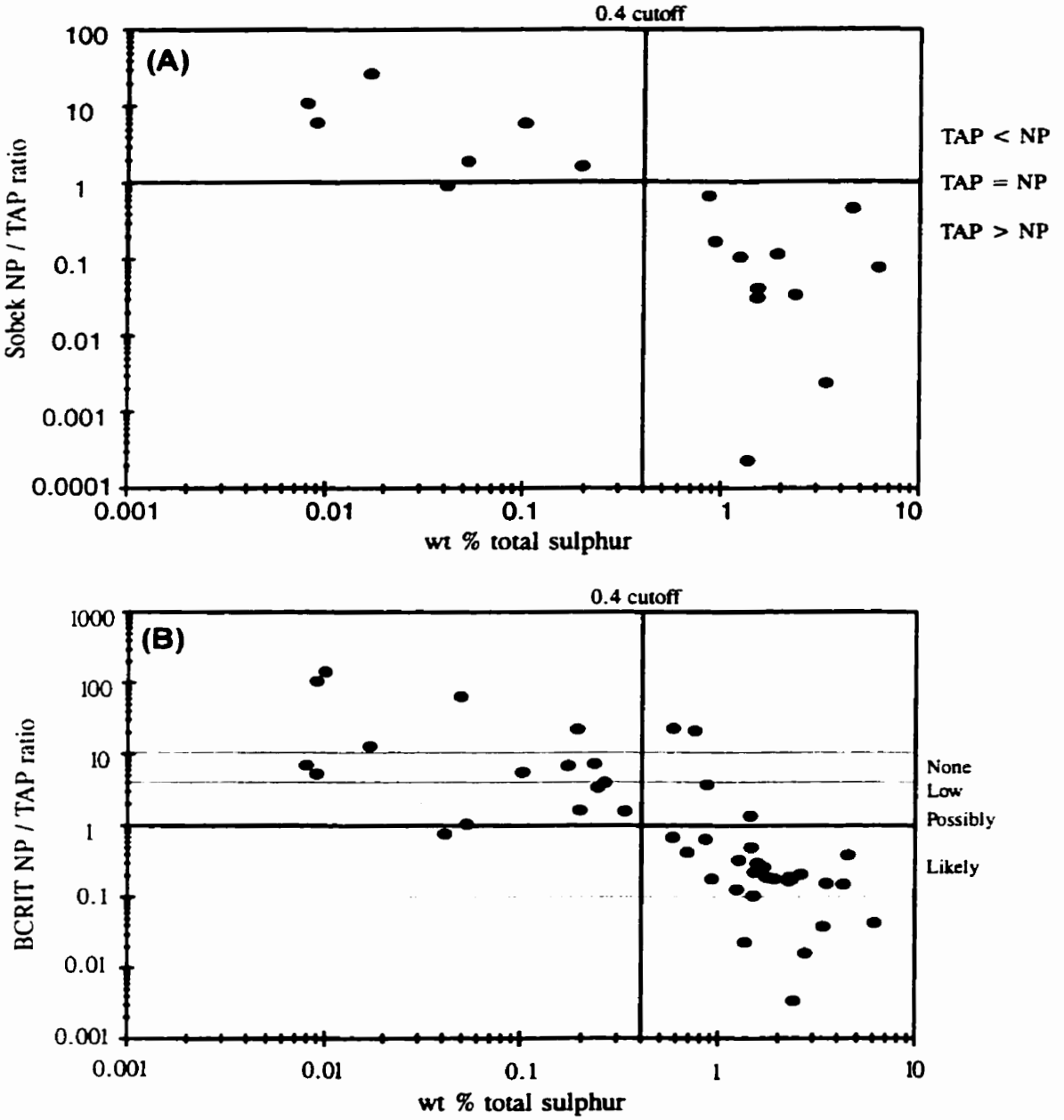

Figure 5.11 (A) plot of Sobek NP / TAP ratio vs wt% total sulphur, (B) plot of BCRIT NP / TAP ratio vs wt% total sulphur. Note half the total number of samples were analyzed by the Sobek method.

5.5 Using Magnetic Susceptibility To Determine Acid Potential

As presented in Chapter 2, considerable amounts of monoclinic pyrrhotite occur in the Halifax Group. Since monoclinic pyrrhotite is magnetic, it is reasonable to assume that magnetic susceptibility can be used to detect monoclinic pyrrhotite, and that the sulphide sulphur (total sulphur) content can be estimated by susceptibility measurements. In this study, magnetic susceptibility was measured with a hand-held, K-2 meter (Scintrex Limited) on 36 rock samples. The readings were taken on flat surfaces and the maximum value of five readings from different surfaces was recorded. A preliminary test was performed using only the first reading, as well as an average of five values, but these were found to be unsuitable. Depending on the location and distribution of pyrrhotite within the rock sample, the magnetic susceptibility values are highly variable and in many cases the surfaces gave a value of 0.00 (10^{-4} SI). As presented in Chapter 2, pyrrhotite occurs along cleavage planes and is not randomly distributed throughout the sample. This anisotropic distribution of pyrrhotite is reflected in the variability of the susceptibility readings with the highest values obtained where the face of the meter is the closest to mineralization.

Figure 5.12 shows a plot of susceptibility versus total acid potential (TAP) calculated from wt% total sulphur content. A least squares linear regression line through the data gives an equation of:

(5.5) $y = 97.44\ (\pm\ 11.96)\ (x) + 13.03\ (\pm\ 4.76)$

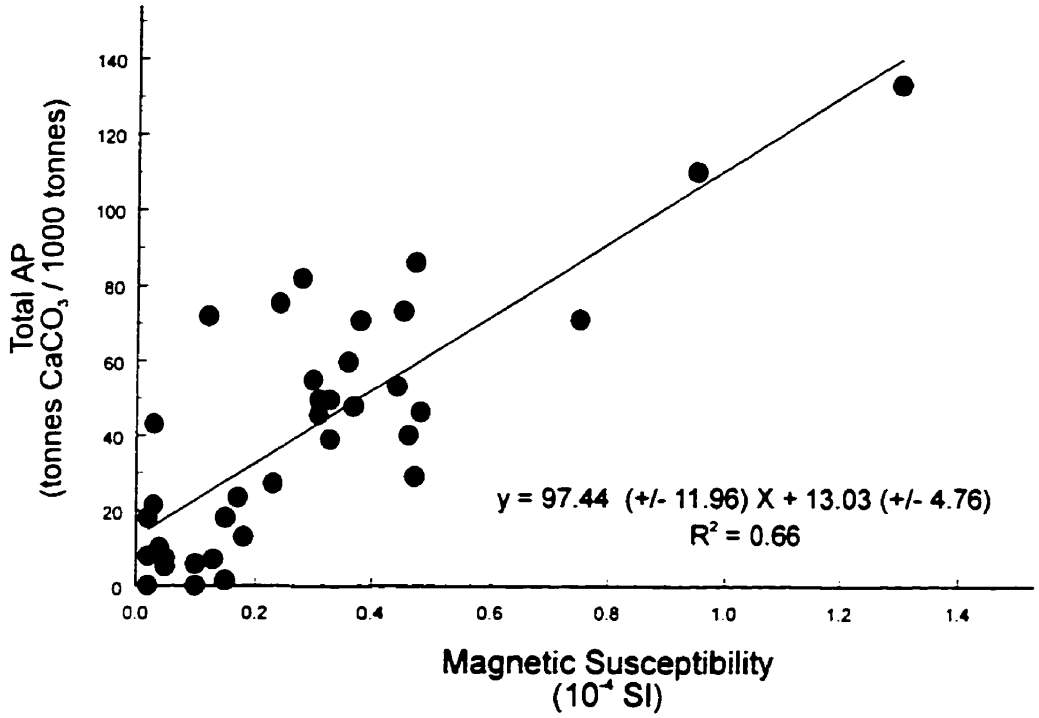

Figure 5.12 Plot of magnetic susceptibility vs total acid potential (TAP) for 36 samples. y = total acid potential, X = magnetic susceptibility.

where x = magnetic susceptibility (SI units of 10^{-4}) and y = TAP. This equation can be used to estimate the TAP provided some assumptions are made. It is assumed that all sulphur is in monoclinic pyrrhotite, however, other sulphide minerals may also be present. This simple test does not consider the intensity of magnetic susceptibility relative to mineral anisostropy. In other words, the same amount of pyrrhotite aligned along cleavage planes, may give higher magnetic susceptibility values than pyrrhotite that is randomly distributed throughout the sample. These factors lead to a medium R^2 value of 0.66 and account for some of the variation of the data points. Although the use of magnetic susceptibility to measure TAP may not be highly accurate, in the case of the Meguma Supergroup rocks, it is highly recommended because it is such an easy parameter to measure. Hundreds of measurements can be taken in several hours and it is a very useful tool, especially in preliminary ARD prediction investigations.

5.6 Discussion And Conclusions

In general, rocks in the Meguma Supergroup (lower Halifax Group) examined in this study contain little neutralizing potential. Differences between NP values determined by the Sobek method and the BCRIT method are interpreted to be of little significance, mainly because of the overall low NP values. In rocks where the neutralizing potential is significant, further mineralogical studies should be undertaken to access the type of carbonate minerals present. Iron and manganese carbonates are common, especially within the GHT (Mosher's Island Formation), and the overall presence of carbonate minerals should not be used as a "safe" indicator that the rocks

will not be net acid-generating.

Based on previous mineralogical studies (see Chapter 2), one of the common sulphide minerals present in the Halifax Group is monoclinic pyrrhotite. The reaction rate of this mineral is relatively fast compared to pyrite (Chapter 3) and, in the field, acidity can be produced quickly in the short term. Because of the low neutralizing potential, the rocks do not have significant capacity to neutralize the acid produced. This leads to surges of acidity which, as in the case of the Meguma Supergroup in Nova Scotia, can lead to fish kills and degradation of surrounding ecosystems.

It is not the intention here to disregard the usefulness of static ARD testing, but rather to draw attention to the fact that mineralogy must be considered an integral component of ARD prediction. As described by Price and Errington (1994):

"Where there is a potential for the generation of acid drainage or metal release through weathering or dissolution, the proponent should determine the range, variability, and central tendencies for the following properties: elemental composition; mineralogy; readily soluble constituents; sulphide types (amount, reactivity, and spatial distribution); carbonate types (amount, reactivity, and spatial distribution); and mineralogical and rock-fabric characteristics that will influence weathering."

Price et al. (1997), also discussed by Jambor and Blowes, (1998) expanded these requirements into the following information list:

1) identification of potential acidity and metal sources, with particular emphasis on sulphide mineralogy;

2) determination of potential contribution of barite to the sulfate-S measurement;

3) identification of the potential neutralization sources, with particular emphasis on carbonate mineralogy and ant potentially significant slow-release alkaline aluminosilicate sources;

4) identification of clay or carbonate (e.g., siderite and ankerite) minerals which contribute to the NP value measured in the lab, but may not provide similar

contributions in the field;

5) evaluation of the most reactive acid-generating and neutralization sources (sulphides and carbonates) and their potential to occur preferentially along fracture planes and in the fine-size fraction, where they are available to contribute to geochemical reactions;

6) identification of readily soluble constituents; and,

7) identification of any mineralogical or rock-fabric characteristic that will influence weathering.

Jambor and Blowes (1998) also discuss the routine use of XRD, SEM, and microprobe, among other techniques, for routine work in developing a mineralogical database needed in environmental studies. More details regarding the use of mineralogy in the assessment of ARD can be found in the two sources listed above.

Considering reactions 5.1 and 5.3 which are the basis for the BCRIT and Sobek methods respectively, it is important to note that some significant assumptions are made and that the reactions are somewhat hypothetical. Some of the assumptions include (Morin and Hutt, 1994):

1) all sulphur occurs in the solid phase only as S_2^{2-},
2) S_2^{2-} oxidizes completely to sulphate,
3) all S is included only in pyrite,
4) the only oxidants are molecular oxygen and water,
5) all iron oxidizes to the ferric (Fe^{3+}) state, and
6) all iron precipitates as $Fe(OH)_3$.

From a mineralogical point of view, assumption 3 is significant in terms of the Meguma Supergroup because not all sulphur is retained in pyrite. Pyrrhotite is also a significant phase but the static acid prediction tests do not distinguish between the two types of sulphide minerals. Table 5.2 shows a hypothetical situation that mineral assemblages would have on ARD prediction. Given similar acid potential (AP) and neutralization

potential (NP) values, the rates of both acid generation and acid neutralization will be substantially different (Jambor and Blowes, 1998). The differences in final results are related to the slower reactivity rate of pyrite relative to pyrrhotite, and the faster reactivity rate of calcite relative to siderite. A further consideration of the Fe and Mn carbonates is the relatively small (or zero) net acid consumption related to their dissolution. For example, siderite can consume acidity by the following reaction (Jambor and Blowes, 1998):

(5.6) $FeCO_3 + 2H^+ \text{---} > Fe^{2+} + CO_2 + H_2O$

or, at near-neutral conditions by the reaction (MEND, 1991):

(5.7) $FeCO_3 + 5/2\ H_2O + 1/4O_2 \text{---} > Fe(OH)_3 + HCO_3^- + H^+$

Therefore, siderite is not considered to be an effective acid neutralizing mineral.

Based on the discussions presented above it is clear that detailed mineralogical analyses should always be performed in conjunction with any static ARD prediction test program. The mineralogical databse can aid in the overall interpretation of acid-generating potential.

Chapter 6

Geophysical Methods For Detecting Shallow Sulphide Mineralization In The Halifax Group, Meguma Supergroup, Nova Scotia

6.1 Introduction

The presence of pyrrhotite and its magnetic properties at the scale of hand samples have been introduced above (Chapters 2 and 5). In this part of the study, the geophysical signature at the scale of outcrop or "construction depths" is investigated. In late 1984, Environment Canada approached the Geophysics Division of the former Nova Scotia Research Foundation Corporation (NSRFC) to investigate the use of geophysical methods for the detection of shallow sulphide mineralization in Meguma Supergroup metasedimentary rocks close to Halifax International Airport (Fig. 6.1). The "shallowness" of the mineralization specifically referred to construction depths (i.e., within a few meters of the surface) as it was known that the exposure and subsequent oxidation of the sulphide mineralization in the Halifax Group rocks caused acid rock drainage (ARD).

Reconnaissance geophysical test measurements were carried out over two grids (Fig. 6.1) in January, 1985 (NSRFC, 1985a). During April and May, 1985, test pits were excavated and rock samples collected at selected geophysical anomalies on both grids (NSRFC, 1985b). The previously unpublished NSRFC reports for this 1985 project documented one of the first, if not the first, environmental geophysics investigations of this type in Nova Scotia. The results of this part of the study indicate

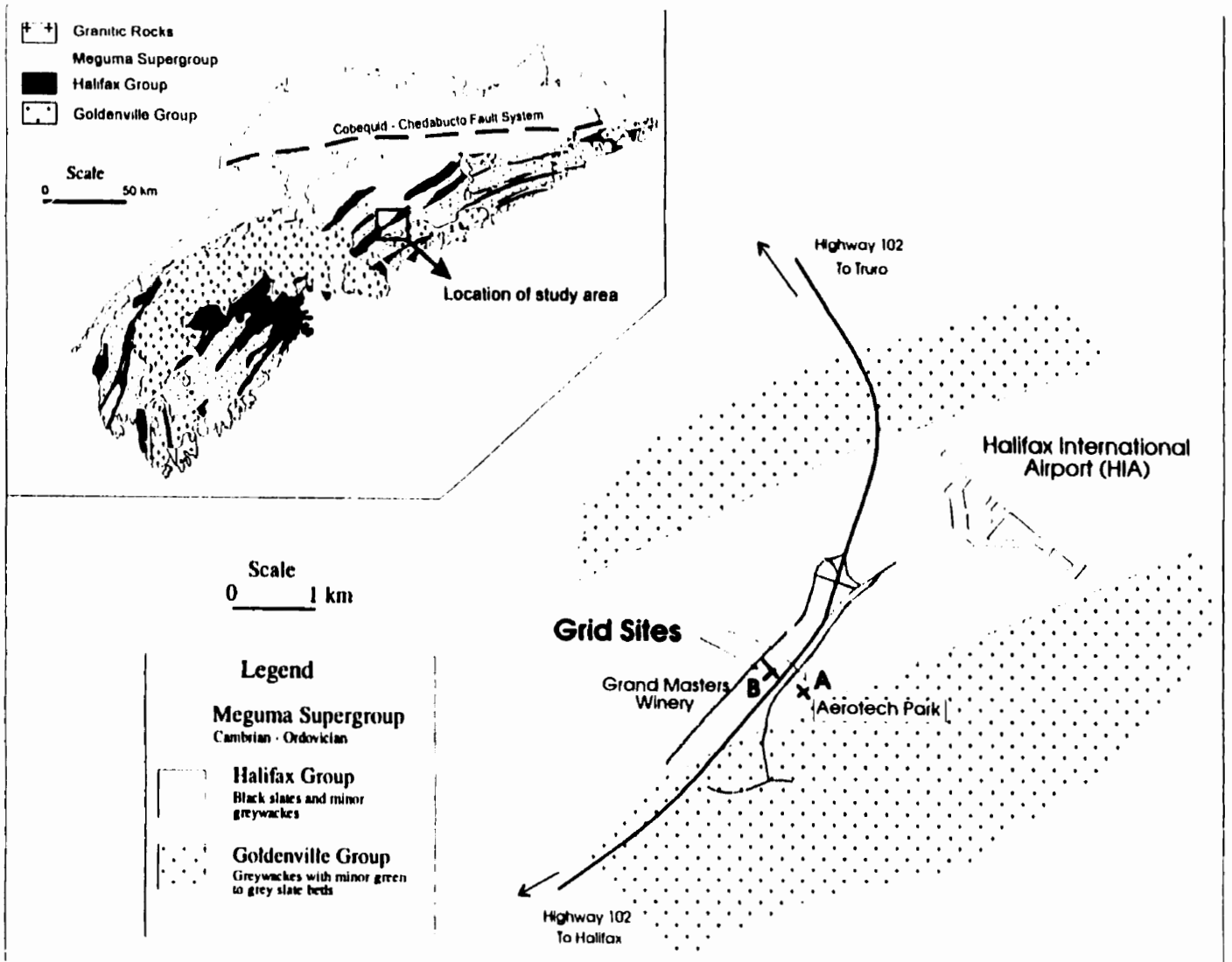

Figure 6.1. Simplified geological map and location of geophysical grids near Halifax International Airport. Inset map shows distribution of Meguma Supergroup in Nova Scotia.

that a combined terrain conductivity, magnetic and VLF EM survey appears to be a practicable method for detecting near surface sulphide mineralization in the Halifax Group rocks of Nova Scotia.

6.2 Acid Rock Drainage In The Meguma Supergroup Metasedimentary Rocks

The Meguma Supergroup in Nova Scotia (Fig. 6.1) consists of Late Cambrian-Early Ordovician greywackes interbedded with minor green to grey slates of the Goldenville Group and Early Ordovician black slates and minor greywackes of the Halifax Group. The Halifax Group rocks are known to contain substantial amounts (up to 10% by volume) of sulphide minerals. The major sulphide minerals are pyrrhotite and pyrite together with lesser amounts of chalcopyrite and arsenopyrite (McGrath, 1970; Schwarz and McGrath, 1974; Schwarz and Broome, 1994; King, 1997; Fox et al., 1997). The Goldenville Group is also known to contain sulphide minerals (e.g., pyrite, pyrrhotite and arsenopyrite) in thin slate beds in areas of gold occurrences (Sangster, 1990). However, the reconnaissance geophysical test grids are wholly situated on Halifax Group outcrop (Fig. 6.1).

For more than thirty years, ARD due to the oxidation of sulphide minerals in rocks of the Halifax Group has been recognized in various parts of Nova Scotia (Pettipas, 1979; Hennigar and Gibb, 1987; Lund et al., 1987; King and Hart, 1990; Pasava et al., 1995). ARD, characterized by a low pH (2 - 4) and a high dissolved metal content, arises from the exposure of the Halifax Group rocks due to construction activities such as highways and other development projects. The most publicized

example of ARD in Nova Scotia resulted from the construction of Halifax International Airport (Fig. 6.1), which commenced in the mid 1950's. Major amelioration efforts have been ongoing at the Airport from at least 1982 to the present (Worgan, 1987; S. Hicks, personal communication, 1998). Though ARD in the Goldenville Group, to our knowledge, has not been studied in detail, there is the potential for its taking place, particularly in areas of gold occurrences.

As a result of the ever present ARD problem, the Nova Scotia Department of the Environment (NSDOE), in association with Environment Canada, wrote "Guidelines for Development on Slates in Nova Scotia" in 1985. These were subsequently revised in 1991. Recently, NSDOE has passed the "Sulphide Bearing Material Disposal Regulations" of the Environment Act (Environment Act, 1994-95, c.1, s.1). These regulations require ARD predictive chemical tests be carried out prior to construction activities which will expose the rocks to oxidizing conditions. Examples of these tests include the British Columbia Research Initial Test (Bruynesteyn and Duncan, 1972) and the EPA-600 acid base accounting procedure (Sobek et al., 1978). However, these chemical tests are only useful if the rock can be sampled from outcrops or by drilling and trenching. Non destructive tests for the detection of sulphide minerals using geophysical methods are not included in the regulations.

6.3 Physical Properties Of Sulphide Minerals In Halifax Group Rocks

Pyrrhotite has a crystal structure that is deficient in iron, leading to the general formula $Fe_{1-X}S$, where X can range from 0 to 0.2. In order to maintain an electrically

neutral crystal structure, an ideal formula for pyrrhotite can be written as $(Fe^{2+}_{1-3x}Fe^{3+}_{2x})V_xS$, where V represents vacancies in the cation position (Klein and Hurlbut, 1993). The presence of Fe^{3+} has been confirmed spectroscopically by Pratt et al. (1994), who found approximately 30% Fe^{3+} in the pyrrhotites they studied from Mexico.

The iron deficiency and vacancy ordering in the pyrrhotite crystal structure gives the mineral its magnetic properties. One of the most iron-deficient end members is monoclinic pyrrhotite (Fe_7S_8), where $X=0.125$. Hence, the monoclinic pyrrhotite is ferrimagnetic while the other common hexagonal phases such as Fe_9S_{10} and $Fe_{11}S_{12}$ are antiferromagnetic (Dunlop and Ozdemir, 1997). Previous studies (Pasava et al., 1995; Fox et al., 1997) have shown that monoclinic pyrrhotite, with an approximate formula of Fe_7S_8, is present in the Halifax Group rocks near the Halifax International Airport. Pyrite, in the form of large (1-2 cm) pyrite crystals (or their outlines), also occurs in the slate exposures.

Although pyrrhotite was known to occur in the Halifax Group rocks in 1985, the prevalent view of personnel in Environment Canada at the time of the geophysical investigation described in this paper was that pyrite oxidation was the main cause of ARD. However, it is now known that pyrrhotite is a major contributor to ARD. The oxidation rate of pyrrhotite can be as much as 100 times faster than that of pyrite (e.g., Nicholson and Scharer, 1994). Therefore, "pulses" of ARD, which may cause adverse environmental effects (e.g., fish kills), can occur when Halifax Group rocks are exposed during construction activities.

Significant total field magnetic anomalies are known to be associated with the Halifax Group rocks (Geological Survey of Canada Aeromagnetic Series Maps 790G and 785G; 1960). Magnetic anomaly amplitudes vary between 300 and 600 nanotesla over the thick slate units of the Halifax Group. A dam site investigation (Howells and McKay, 1985) noted that the magnetic "fabric" of the Goldenville Group was delineated by detailed ground magnetic surveys due to the smaller magnetic anomalies associated with thin slate units within the greywackes. These smaller magnetic anomalies are, in comparison, tens of nanotesla in amplitude.

The magnetic anomalies over the slates of the Halifax Group are primarily caused by pyrrhotite whereas in the Goldenville Group greywackes they result from a single magnetic phase of magnetite (McGrath, 1970). These findings have since been confirmed by other workers (Schwarz and McGrath, 1974; Cameron and Hood, 1975; King, 1997). McGrath (1970) also concluded that magnetite was the dominant magnetic mineral in the highly metamorphosed contact aureoles surrounding the Devonian granites intruded into the Meguma Supergroup metasedimentary rocks.

The magnetic susceptibility ranges of pyrrhotite and magnetite ores are given as 1×10^{3} to 1×10^{-1} and 7×10^{-2} to 14 SI respectively (Parasnis, 1986). In contrast, pyrite ore has a magnetic susceptibility range of only 1×10^{-3} to 5×10^{-3} SI and is relatively non-magnetic. King (1997) reported mean susceptibilities ranging from a minimum of 0.11×10^{-3} (undivided Goldenville Group) to a maximum of 1.68×10^{-3} SI (upper beds, Goldenville-Halifax Transition zone) for rocks in the Meguma Supergroup of central Nova Scotia.

The electrical conductivity of slates may vary between 2.5×10^{-5} and 1.7 millimhos/metre (Telford et al., 1976). In contrast, sulphide minerals are relatively good (electronic) conductors. The electrical conductivities of pyrite, chalcopyrite and pyrrhotite are 102-107, 104-107, and 106-108 millimhos/metre respectively. We may conclude that significant sulphide mineralization in the Halifax Group will result in more conductive zones. Graphite, another good conductor (10-102 millimhos/metre; Telford et al., 1976), also occurs in the Halifax slates and will contribute to increased conductivities. However, graphite has a low (negative) magnetic susceptibility. Magnetite, if present, is also quite conductive (102-105 millimhos/metre; Telford et al., 1976) and will increase the overall rock conductivity.

These mineral properties were used to conclude that the detection of shallow sulphide mineralization in the Halifax Group would require geophysical methods capable of measuring conductivity (or resistivity) anomalies. It was also recognised that magnetometer surveys were needed to measure magnetic intensity or susceptibility variations. However, considering the more recent work on sulphide mineralization in the Meguma rocks it is apparent that the magnetic measurements will also measure the effect of the pyrrhotite content in the Halifax Group.

6.4 Selection Of The Geophysical Survey Methods

The following geophysical methods were selected for evaluation based on the discussion of conductivity/resistivity variations: Continuous Reading Ground Conductivity meter; Very Low Frequency (VLF) Electromagnetic (EM) meter; and an

Induced Polarization system.

Consideration of the magnetic susceptibility contrasts necessitated the inclusion of a magnetometer survey to provide a comparison with the conductivity (resistivity) measurements and the results of previous ground magnetometer measurements over Meguma Supergroup rocks (e.g., Golder Associates, 1983). NSRFC (1985b) commented that the magnetometer survey "would indicate any correlation or lack of correlation between anomalies due to variations in magnetic susceptibility and electrical conductivity (or resistivity)".

In addition, a spontaneous polarization survey was proposed to measure any natural or spontaneous potentials in the subsurface associated with the weathering of the sulphide-rich zones.

6.5 Geophysical Instrumentation

Geophysical equipment selection was constrained by the availability of local, or in house, instruments or rental equipment. The ground conductivity instrument selected was a Geonics EM31-D non-contacting terrain conductivity meter (McNeill, 1980). This horizontal twin loop system has an intercoil spacing of 3.7 meters and an operating frequency of 9.8 kHz. Its measurement accuracy is +/- 5% at 20 millimhos/m. It must be emphasised that this instrument was chosen to address the main purpose of the investigation (i.e., the detection of sulphide mineralization within construction depths below the ground surface). The effective exploration depth limit for the EM31-D is 3 meters when operated in the horizontal dipole configuration and 6

meters in the vertical dipole configuration.

A Very Low Frequency (VLF) Electromagnetic (EM) receiver measures in phase and out of phase (quadrature) components as percentages of the primary field. The Geonics VLF EM16 instrument utilizes 16-24 kHz signals broadcast by marine and air navigation systems. VLF EM surveys are an integral part of most mineral exploration programs and are particularly useful for delineating conductive fault and shear zones. Its effective exploration depth is several tens of meters.

Induced polarization (IP) effects were measured with a McPhar Dual Frequency System. This equipment measures both apparent resistivity (ohm-meters) and the induced polarization effect ("metal factor" in mhos/m). Disseminated sulphides with as little as 0.5% by volume "metallics" have been successfully identified as being the cause of IP anomalies.

The spontaneous potential equipment consisted of non-polarizing electrodes and a high impedance digital millivoltmeter. The non-polarizing electrodes were porous pots filled with copper sulphate solution. The high input impedance (more than 108 ohms) digital voltmeter was necessary so that negligible current was drawn from the ground during the measurements.

The total field magnetic measurements were made with a Scintrex MP-2 digital proton precession magnetometer which has a reading accuracy of +/- 1 nanotesla over its operating range.

6.6 Test Sites And Geophysical Survey Methods

6.6.1 Test Sites

The two test sites (Figs. 6.1, 6.2 and 6.3) were selected by Environment Canada personnel so as to sample different parts of the Halifax Group in the vicinity of Halifax International Airport. Site A (Fig. 6.2), which lies in Aerotech Park, to the east of Highway 102, had already been cleared and lay close to an area of previous geotechnical investigations. Site B (Fig. 6.3), which is situated near the former Grand Masters Winery building, to the west of Highway 102, had previously cut lines within its boundaries.

On both sites, Environment Canada personnel chained and staked two perpendicular lines of suitable length along the existing or newly cut lines. All ground measurements were in feet with station intervals at 25 foot (7.62 meters) spacing. Both test sites are located on relatively flat lying ground. The staked lines on each test site were configured so as to be, very approximately, either parallel or perpendicular to the bedding plane strike of the Halifax Group rocks.

6.6.2 Geophysical Survey Methods

Total field magnetic measurements were read at each station and magnetic diurnal variations removed by repeating measurements at base stations at short time intervals. The diurnal magnetic variations were found to be relatively subdued during the survey.

Due to time and weather limitations, and the reconnaissance nature of the

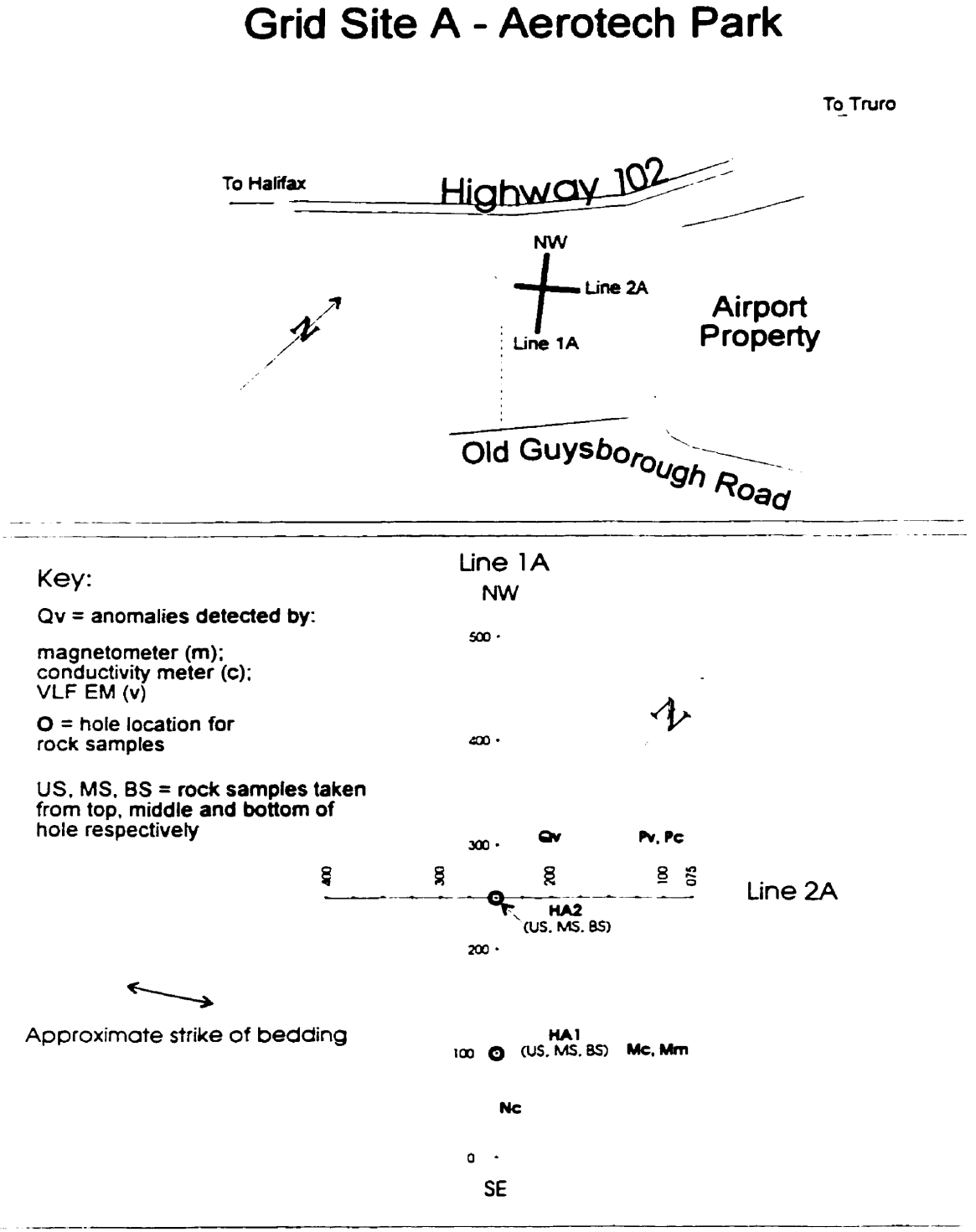

Figure 6.2 **Detailed map showing location of grid site A (Aerotech Park) with geophysical anomaly and rock sample locations.**

Grid Site B - Grand Masters Winery

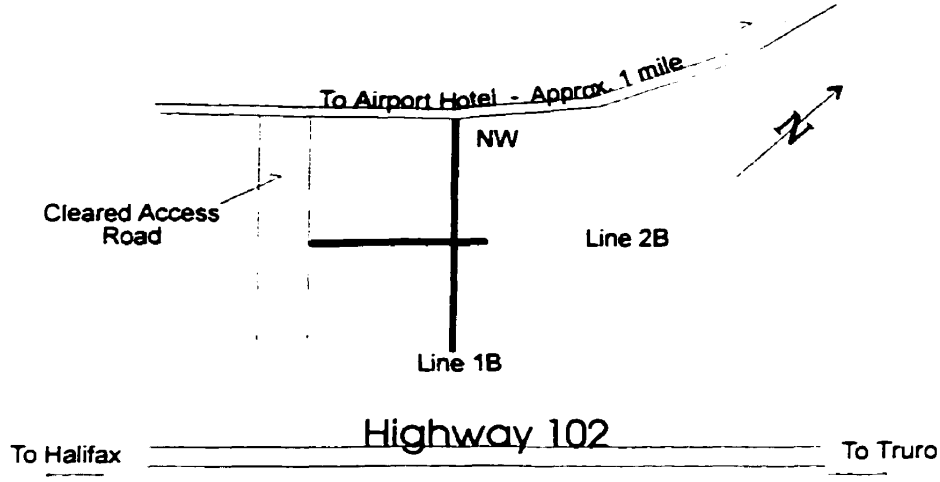

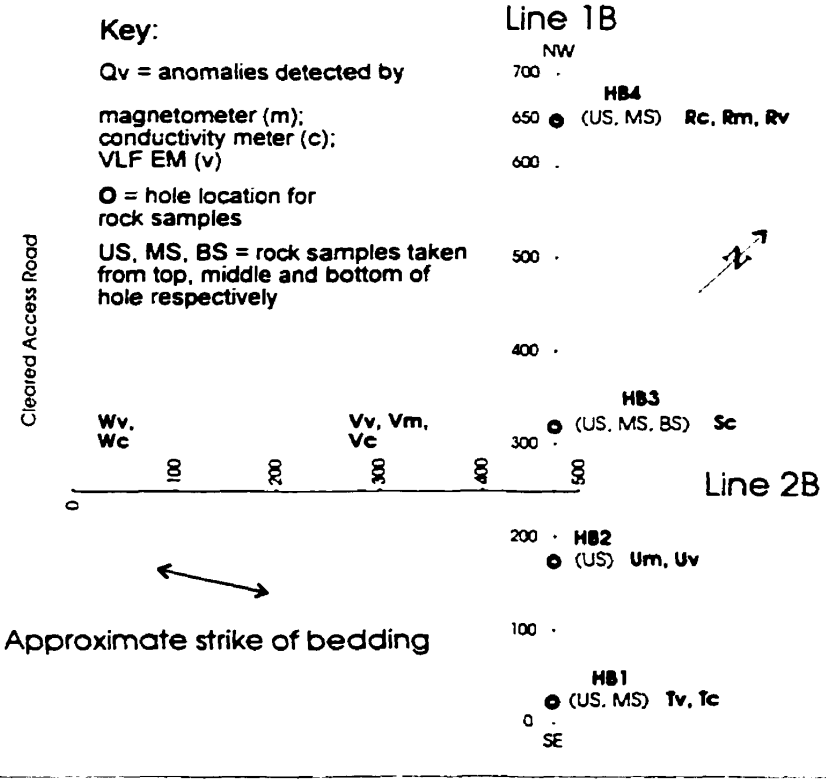

Figure 6.3 Detailed map showing location of grid site B (Grand Masters Winery) with geophysical anomaly and rock sample locations.

geophysical surveys, the terrain conductivity measurements were carried out at waist height in the vertical dipole configuration (6 meters effective penetration depth) at each station. Hence, conductivity layering beneath the surface was not measured. The VLF EM survey consisted of in-phase and out-of-phase (quadrature) measurements at each station.

The induced polarization equipment was employed in the dipole-dipole electrode configuration using steel electrodes. Some difficulties were encountered with this method which, at the time, were attributed to high surface resistivities and the winter ground conditions (i.e., frozen ground surface). Therefore, induced polarization measurements were only attempted on line 1A at both 12.5 (3.81 meters) and 25 (7.62 meters) feet dipole intervals.

The porous pots of the spontaneous potential system were buried a few inches (centimeters) in the ground and allowed to "sit" for a few minutes to obtain a good contact. Expanding spread measurements were acquired by keeping one electrode fixed at a base station while the second electrode was moved to successive locations along the survey line. Spontaneous potential gradients were measured by simultaneously moving both electrodes while maintaining a fixed horizontal distance between them. Expanding spread spontaneous potentials and gradients were successfully measured on line 1A.

6.7 Geology Of The Test Site Areas

The geology map (Faribault, 1909) of the area shows both test sites are located on the Halifax Group metasedimentary rocks. The slates have been folded into a

syncline with steeply dipping or vertical beds close to the syncline axis. The whole area is covered with a clayey-silt to silty-clay glacial till whose thickness varies from 0 to more than 4 meters.

Detailed geotechnical and other investigations were carried out within site A (Fig. 6.2) by Nolan, Davis and Associates (1983), Golder Associates (1983) and Jacques, Whitford and Associates (1981). These studies report near vertically dipping slate beds with the strike varying between 240° and 253°. A thin till, ranging from 0 - 3.42 meters in thickness, overlays the bedrock. However, its average thickness is less than 2 meters. Whilst carrying out magnetometer measurements, Golder Associates (1983) reported that "bedrock is exposed at the ground surface more frequently than was initially envisaged". A thin (0 - 0.53 meters) soil overlays both till and bedrock. Samples from test pits at site A show the pyrite is randomly distributed within the rocks and the mineralization is irregular both along strike and with depth (Nolan, Davis and Associates, 1983).

Prior to the geophysical tests described in this paper, there was little or no detailed geological information available for site B (Fig. 6.3). Extensive peat-like deposits were found to occur to the southwest of site B during land clearing operations.

6.8 Geophysical Survey Results

6.8.1 Site A, line 1A

This NW-SE line is approximately perpendicular to the bedding strike of the slates (Fig. 6.2). A relatively large (38 mmhos/m) conductivity anomaly (Mc on Fig.

6.4) occurs close to 100 feet (30.48 m) with a subsidiary anomaly, Nc, (26 mmhos/m) at 50 feet (15.24 m) directly to the south of Mc. The steep gradients indicate a shallow source for the conductivity anomaly. A coincident magnetic dipole anomaly is observed on the magnetometer profile (Mm on Fig. 6.4) which may be interpreted as being caused by a prism shaped body centred close to 125 feet (38.10 m).

Expanding spread and gradient spontaneous potential measurements were also carried out along line 1A. The expanding spread profile delineated a large (-300 millivolts) anomaly centred at 100 feet (30.48 m) shown as Mp on Fig. 6.4. Similarly, large spontaneous potential horizontal gradient fluctuations occur close to this location. We conclude that the causative body is both magnetic and conductive. Mineralized bodies almost always produce negative spontaneous potentials at their upper surfaces.

The VLF EM measurements show a coincident in-phase negative anomaly between 260 and 100 feet (79.25 and 30.48 m) indicative of a conductive body (Mv on Fig. 6.4). The in-phase profile has been filtered using a method described by Fraser (1969). The filter converts "crossovers" to positive anomalies and reverse "crossovers" to negative values while, at the same time, smoothing the data. The resulting filtered in-phase profile also gives a large positive anomaly at 112.5 feet (34.3 m.) which agrees with the conductivity anomaly, Mc.

Induced polarization measurements were carried out over that part of line 1A where magnetic or conductivity anomalies were not detected (approximately 225 to 285 feet or 68.58 to 86.87 m). A similar pattern occurs for both dipole spacings (12.5 and 25 feet or 3.81 and 7.62 m.). The relatively large, near surface apparent resistivities

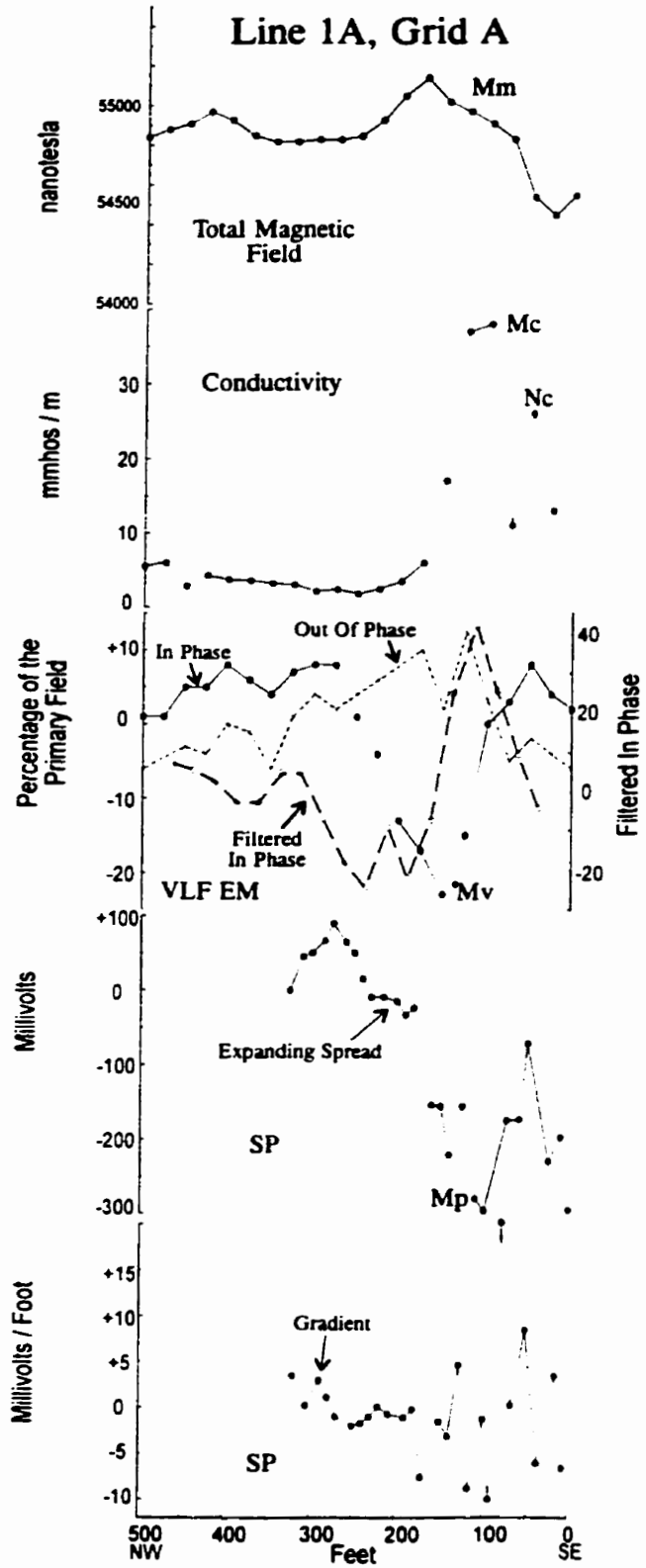

Figure 6.4 Magnetic, conductivity, VLF EM and SP profiles for line 1A, grid site A.

decrease rapidly with depth together with a near surface, relatively small, apparent induced polarization effect which increases slowly with depth.

6.8.2 Site A, line 2A

This line is almost parallel to the bedding strike (Fig. 6.2). As a result, not surprisingly, the magnetic profile shows low gradients and a relatively small increase (about 100 nanotesla) indicative of low susceptibility contrasts and/or causative bodies at depth (Fig. 6.5). The conductivity profile reveals an anomaly, approximately 5 mmhos/m in amplitude, centred at 100 feet (30.48 m). This anomaly is labelled Pc on Fig. 6.5.

The VLF EM profile suggests the presence of a conductor at about 212 feet (64.62 m) labelled as Qv on Fig. 6.5. Filtering of the in-phase profile suggests the conductor is at 162.5 feet (49.5 m).

6.8.3 Site B, line 1B

This line is approximately perpendicular to the strike of the bedding (Fig. 6.3). Three prominent magnetic anomalies are seen in Fig. 6.6. The largest, Rm, is a positive anomaly approximately 2400 nanotesla in amplitude with steep gradients suggesting a relatively shallow source. Anomaly Sm is of smaller amplitude (about +700 nanotesla) with less steep gradients. Anomaly Um is about +1000 nanotesla with gradients of intermediate slope. These three magnetic anomalies are sufficiently close that they interfere with each other.

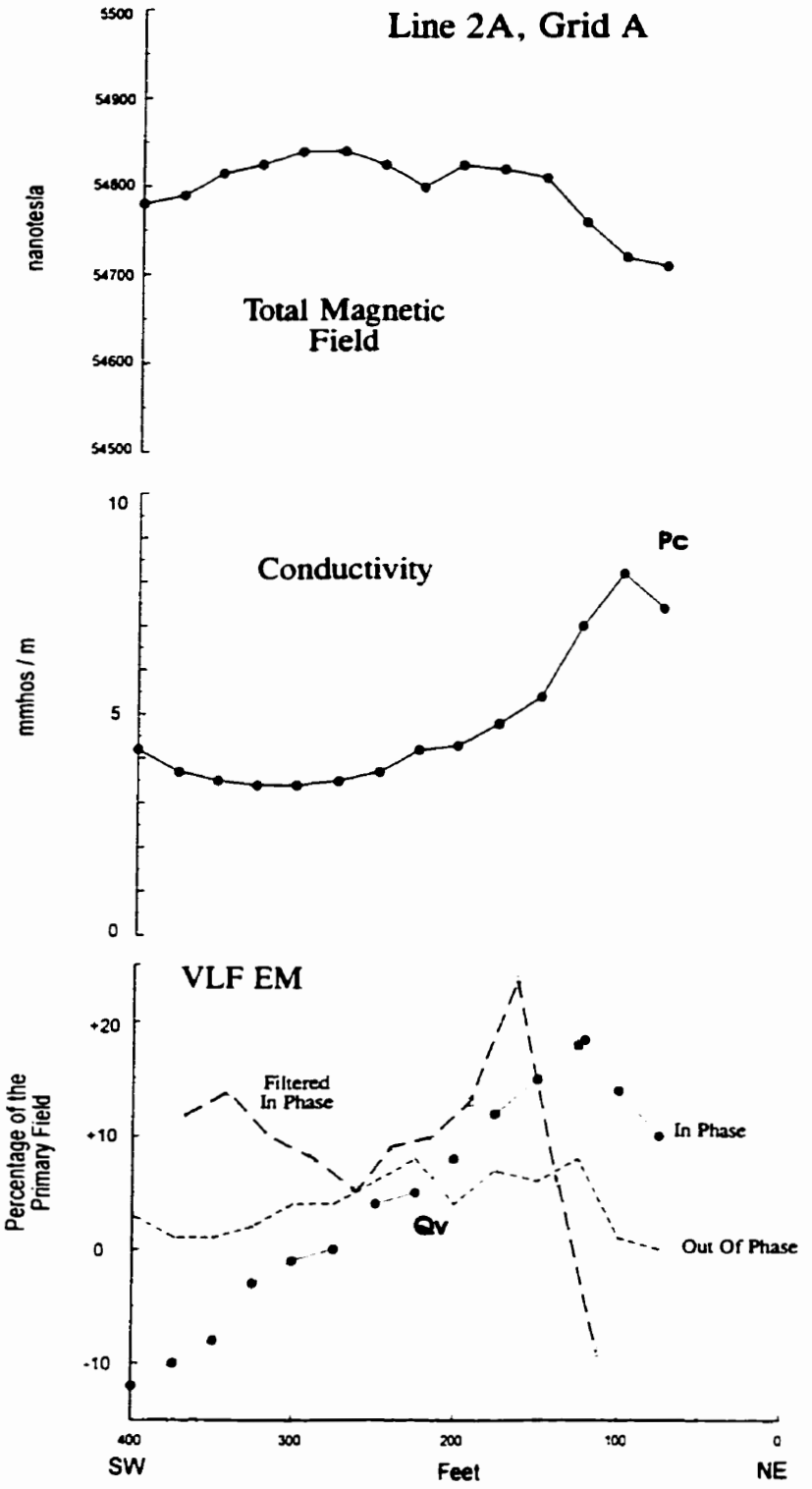

Figure 6.5 Magnetic, conductivity and VLF EM profiles for line 2A, grid site A.

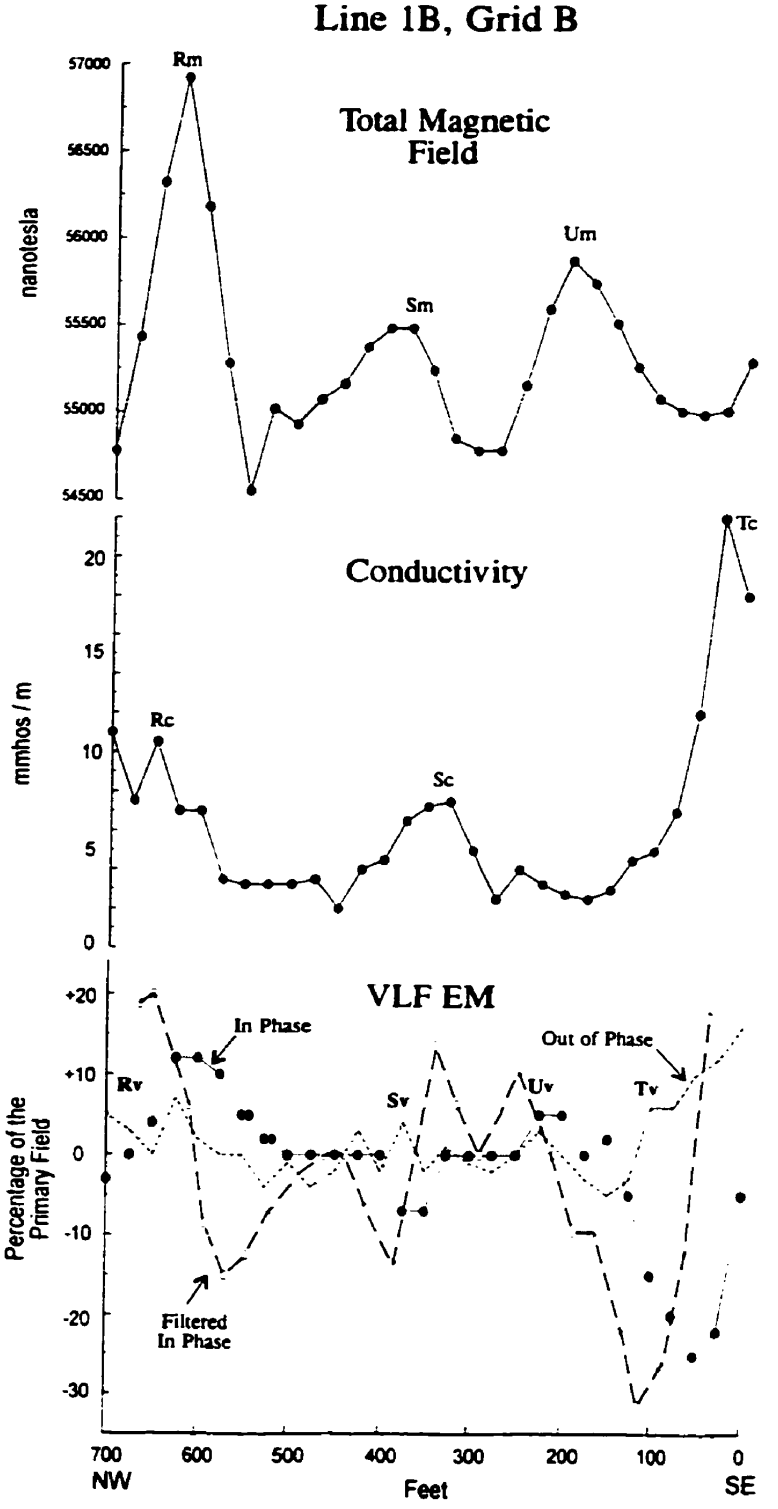

Figure 6.6 Magnetic, conductivity and VLF EM profiles for line 1B, grid site B.

On the conductivity profile (Fig. 6.6), a 7 mmhos/m conductivity anomaly, Rc, is directly correlated with the magnetic anomaly Rm. Though appearing to be offset horizontally by a short distance, the 5 mmhos/m conductivity anomaly, Sc, is sufficiently wide to be correlated with the magnetic anomaly Sm. However, the magnetic anomaly Um appears to have no corresponding conductivity anomaly whereas the conductivity anomaly Tc, at the southeast end of line 1B, has no corresponding magnetic anomaly.

The VLF EM profile (Fig. 6.6) has detected in-phase/out-of-phase conductor crossovers and anomalies corresponding to all the conductivity and magnetic anomalies (labelled Rv, Sv, Uv and Tv in Fig. 6.6). The filtered in-phase profile confirms this interpretation.

6.8.4 Site B, line 2B

Line 2B is approximately parallel to the bedding strike (Fig. 6.3). As would be expected, the magnetic profile (Fig. 6.7) is relatively featureless with the exception of the dipole anomaly, Vm, whose positive part is centred at 237 feet (72.24 m) and which has an amplitude of only 400 nanotesla. This anomaly is superimposed on a small increase in the total magnetic field from SW to NE.

The conductivity profile (Fig. 6.7) displays a very small (1 mmho/m) conductivity anomaly, Vc, offset by about 55 feet (16.6 m) to the northeast of the peak of Vm. From 200 feet (60.96 m) to the SW end of the profile, there is an increase of about 8 mmhos/m with the maximum at 0 feet (Wc). There is no corresponding

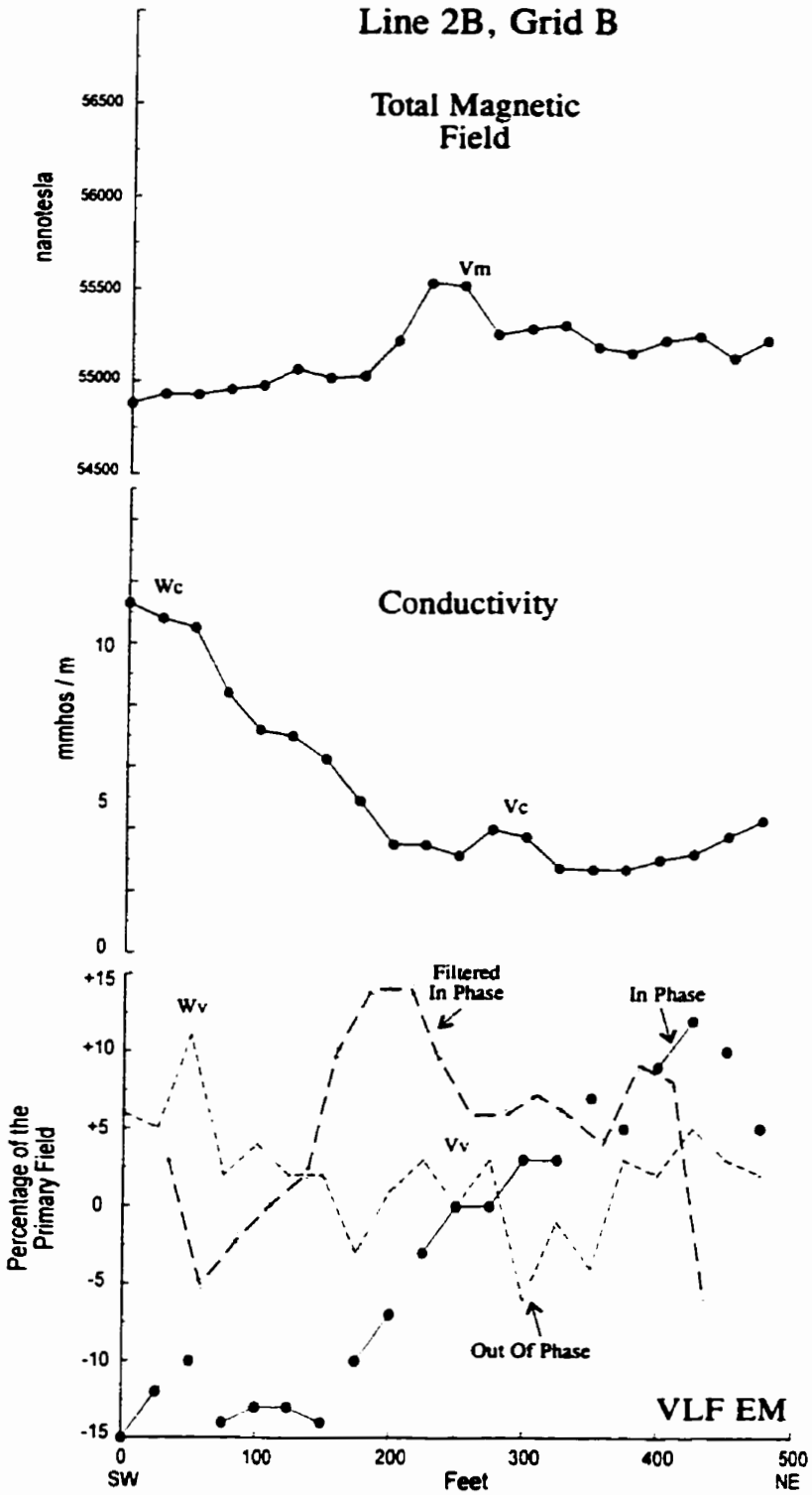

Figure 6.7 Magnetic, conductivity and VLF EM profiles for line 2B, grid site B.

magnetic anomaly.

The VLF EM profile (Fig. 6.7) displays a significant in-phase/out-of-phase cross over at approximately 250 feet, labelled Vv, to show its correspondence to the related magnetic and conductivity anomalies, Vm and Vc. Small in-phase and out-of-phase increases, labelled Wv on Fig. 6.7, may be the VLF EM anomaly expression of conductivity anomaly Wc. The filtered in-phase profile shows that its positive peak at 200 feet (61 m) is likely due to the same causative body as for Vm and Vc. Part of a filtered in phase positive anomaly is located close to Wv and Wc but is at the southwest limit of the data.

6.9 Rock Sampling On The Test Grids

Rock sampling was carried out, based on the results of the previously described geophysical measurements. The purpose of the rock sampling was to measure sulphide mineralization variation and to correlate the results with observed geophysical anomalies. This phase of the investigation used a backhoe to excavate rock samples at the locations shown in Figs. 6.2 (HA1 and HA2) and 6.3 (HB1 to HB4) which correspond to selected geophysical anomalies on lines 1A and 1B. These excavations were carried out in April, 1985.

Bedrock depths and overburden thickness varied over both lines (Fig. 6.8). At HB2, the bedrock surface was close to the 3 metre excavation limit of the backhoe. At each excavation, rock samples were obtained from bedrock. The intent was to obtain rock samples at different depths in each pit but this was not possible in pits HB1 and

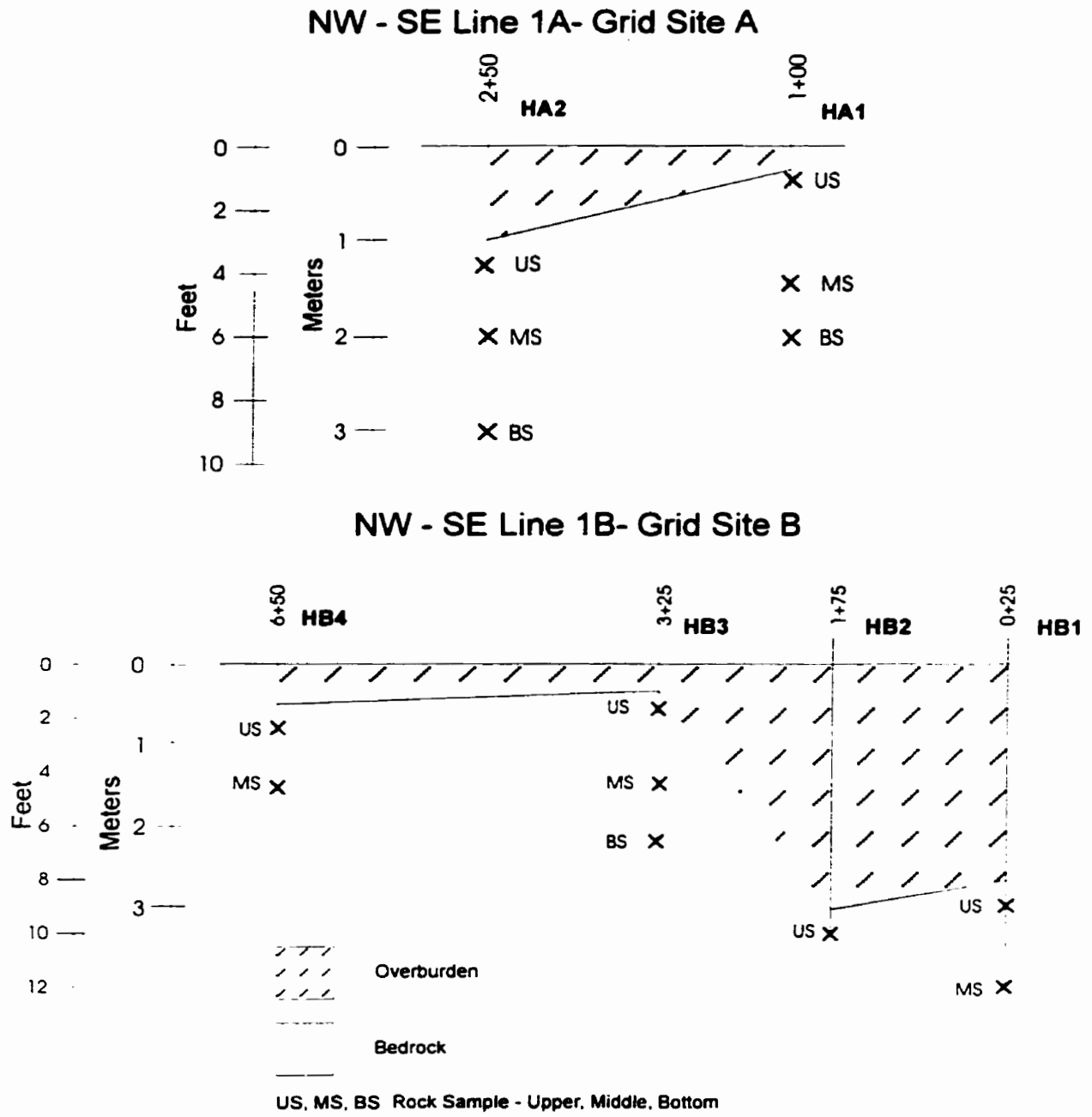

Figure 6.8 Overburden thicknesses, test pit and rock sample locations for lines 1A (grid site A) and 1B (grid site B).

HB2 due to large overburden thicknesses (Fig. 6.8). As a result of the overburden thickness variation, the rocks were sampled at widely varying depths below the ground surface in each pit.

6.10 Rock Sample Chemical Analyses

Environment Canada personnel specified the chemical analyses to be carried out for each rock sample. These were reported as follows: % weight for the total sulphur, pyritic sulphur, non-pyritic sulphide, magnetite and graphite content. The total sulphur content was measured using a Leco Automatic Sulphur Analyser. Pyritic sulphur content was determined using the ASTM D 2492 method which is the standard test for forms of sulphur in coal (American Society for Testing and Materials, 1990). Iron is measured from a dilute nitric acid extraction performed on the residue remaining after the sulphate extraction with dilute hydrochloric acid. The pyritic sulphur is calculated from the iron analysis assuming ideal FeS_2 and a stoichiometric ratio of sulphur to iron equal to 1.148. The non-pyritic sulphide content was determined by measuring acid evolution by back titration. "Magnetite" content was calculated from the Fe^{3+}, determined by wet chemical methods. Graphite content was determined by measuring the amount of carbon insoluble in hydrochloric acid. Total acid potential, in units of tonnes $CaCO_3$ / 1000 tonnes, is calculated by multiplying the total sulphur content by 31.25 (Price, 1997). The assumption made is that all of the total sulphur occurs in the form of pyrite and that all pyrite reacts by the following equation:

$$FeS_2 + 2CaCO_3 + 3.75O_2 + 1.5H_2O \text{ ---> } Fe(OH)_3 + 2SO_4^{2-} + 2Ca^{2+} + 2CO_2$$

In NSRFC (1985b), the total acid potential values were presented as "acid producing potential" and given in units of lbs/ton. Table 6.1 gives the results of the chemical analyses and the total acid potential has been recalculated in units of tonnes $CaCO_3$/1000 tonnes. In 1985, it was interpreted that the amounts of non-pyritic sulphides measured were insufficient to determine the identity and amount of individual non-pyritic sulphides as had been anticipated prior to the analyses.

6.11 Limitations Of The Rock Sample Chemical Analyses

The % weight total sulphur content is an accepted and valid measurement and can be used to calculate the total acid potential (Price, 1997). The analytical procedure (ASTM D 2492) used to determine the % weight "pyritic sulphur" content was designed to measure forms of sulphur in coal (American Society for Testing and Materials, 1990). The term "pyritic sulphur" is a simplification as, in the coal industry, it is usually not necessary to differentiate between and identify individual sulphide minerals. According to the test specifications, this procedure is a measure of the iron content after a nitric acid leach. It includes the iron content from other iron-bearing minerals in the rock samples. As previously described, considerable amounts of pyrrhotite and other sulphide minerals occur in the Halifax Group rocks (Fox et al., 1997). However, iron is also a constituent part of minerals such as biotite, chlorite, ilmenite, garnet and carbonates, all of which occur in the Halifax Group rocks

Table 6.1. Chemical Analyses of Rock Samples

Lab Number	Grid Sample Location	Description	% wt. Total Sulphur	Total Acid Potential (tonnes CaCO3) (per 1000 tonnes)	% wt. Pyritic Sulphur	% wt. Non Pyritic Sulphides	% wt. Graphitic Carbon	% wt. Fe2+
	Line 1A - Grid A							
1	250 (HA2)	Top	0.034	1.06	0.030	< 0.0005	0.18	1.98
2		Middle	0.170	5.31	0.030	0.0028	0.92	1.55
3		Bottom	0.070	2.19	0.013	< 0.0005	1.36	0.76
15	100 (HA1)	Top 1	2.000	62.50	1.860	0.0052	0.28	4.15
4		Top 2	0.850	26.56	0.690	0.0048	0.25	2.69
5		Middle	2.050	64.06	1.800	< 0.0005	1.27	1.40
6		Bottom	1.110	34.69	0.470	0.4260	0.60	2.45
	Line 1B - Grid B							
12	650 (HB4)	Top	1.000	31.25	0.500	0.0149	0.39	3.12
13		Middle	2.170	67.81	1.920	0.0308	0.18	5.82
9	325 (HB3)	Top	0.060	1.88	0.020	0.0012	0.42	4.06
10		Middle	2.190	68.44	1.660	0.0010	0.64	2.60
11		Bottom	2.790	87.19	1.690	0.0174	0.67	1.82
14	175 (HB2)	Top	0.230	7.19	0.130	0.0237	0.12	3.19
7	025 (HB1)	Top 1	0.570	17.81	0.430	< 0.0005	1.11	2.70
16		Top2	1.860	58.13	1.660	0.0040	0.30	2.96
8		Middle	1.600	50.00	0.800	0.2865	0.53	4.70

(Hingston, 1985; MacInnis, 1986; Feetham et al., 1997) . Hence, "pyritic sulphur" is a misnomer and a more appropriate term is "nitric acid leachable iron". For similar reasons, the "non-pyritic sulphide" values are inappropriate in that the terminology is not sufficiently specific to determine exactly what the "non-pyritic" content represents.

The analytical methods to determine the Fe^{2+} and Fe^{3+} content are valid. However, to calculate "total % weight magnetite content" using the Fe^{3+} values is probably incorrect again due to the substantial amounts of pyrrhotite and other iron-bearing minerals in the Halifax Group including chlorite, biotite, garnet, ilmenite and carbonate, all of which can contain Fe^{3+}.

The total % weight "graphitic carbon" in Table 6.1 should refer only to the % weight "non-carbonate carbon" present in the rock samples as other forms of carbonaceous material in addition to graphite are known to occur in the Halifax Group (MacInnis, 1986).

6.12 Rock Sample Resistivity Measurements

The electrical resistivities of some test site rock samples were measured using both tinfoil and copper electrodes. The rock samples were cut into rectangular blocks with their lengths at least four times greater than their widths and heights. Each specimen was water saturated for 12, 16 and 48 hours in water obtained from the grid sites. Saturation was achieved by placing the sample in a container of groundwater at room temperature and pressure and, in addition, at room temperature and in vacuo (for 12 hours).

Rock conductivities measured using the tinfoil electrodes have higher values at HA1 (1.5 - 7.7 mmhos/m) compared to HA2 (0.23 - 1.0 mmhos/m) on grid A (Fig. 6.8). The measured increase confirms the increase as measured by the ground conductivity meter (Fig. 6.4: Mc and Nc). The difference in amplitude between the laboratory and field conductivity values may be explained by the survey measurements being the result of the contribution from the entire conductive zone whereas the laboratory measurements are for individual rock specimens. Conductivity values for HB1, HB3 and HB4 on grid B (Fig. 6.8) are 0.5 - 2.3; 0.04 - 3.6; and 0.2 - 2.3 mmhos/m respectively. Each of these holes sampled locations at which elevated survey conductivity values were measured (Fig. 6.6). The copper electrodes gave higher but inconsistent conductivity values for the rock specimens.

6.13 Discussion

6.13.1 The Geophysical Measurements

The magnetic, terrain conductivity and VLF EM conductivity anomalies measured on grid sites A and B demonstrate three types of relationships:

6.13.1.1 Coincident magnetic and conductivity anomalies

Examples of coincident magnetic, terrain conductivity and VLF EM anomalies are Sm, Sc, Sv and Rm, Rc, Rv on line 1B (Fig. 6.6) and Mm, Mc, Mv on line 1A (Fig. 6.4). These anomalies, taken together, strongly suggest the presence of conductive and magnetic minerals close to the ground surface. In fact, the depth

detection limit of the terrain conductivity meter requires that the mineralization be within 6 meters of the ground surface. The large conductivity anomaly, Mc, on line 1A (Fig. 6.4) is coincident with a negative, spontaneous potential anomaly with steep gradients (Mp on Fig. 6.4) which confirms the presence of a shallow conductor. A crude depth estimate to the top of the conducting body, using the spontaneous potential anomaly, gives a value of 6 meters. Simple depth estimates of this type are usually overestimates. Pyrrhotite is both a conductive and magnetic and is the likely cause of these anomalies.

6.13.1.2 Conductivity anomalies for which there are no coincident magnetic anomalies

Conductivity anomalies Wc and Wv on line 2B (Fig. 6.7) and Pc on line 2A (Fig. 6.5) are examples of terrain and VLF EM conductivity anomalies for which there appear to be no corresponding magnetic anomalies. Unfortunately, both examples are towards the end of survey lines and are incomplete anomalies. The conductivity anomalies suggest the presence of non magnetic conductors. Pyrite and graphite are examples of minerals which satisfy these criteria.

6.13.1.3 Magnetic anomalies for which there are no coincident terrain conductivity anomalies.

Magnetic anomaly Vm, on line 2B (Fig. 6.7), has no corresponding terrain conductivity anomaly, though there is a small (1 mmho/m) terrain conductivity increase (Vc) about 50 feet (15 m) to the northeast. However, there is a coincident VLF EM

anomaly (in phase/out of phase crossover Vv). Similarly, magnetic anomaly Um (line 1B, Fig. 6.6) has no corresponding terrain conductivity anomaly but does have a coincident VLF EM anomaly. The small increase in magnetic values on line 2A (Fig. 6.5) are centered over the VLF EM crossover at Qv and may also be an example of this third relationship.

One of the conclusions of NSRFC (1985b) was that there was "little, or no, correlation between the magnetic anomalies and the conductivity anomalies". This conclusion was reported by Albright (1987) and was used by Samostie (1994) to state that "previous research indicated little correlation between magnetic anomalies and bedrock mineralization". However, the purpose of the geophysical investigation was to detect "shallow sulphide mineralization in the Meguma metasediments" (i.e., within construction depths of a few meters from the ground surface). The terrain conductivity meter, used in the vertical dipole configuration, has an effective penetration depth of 6 meters. Hence, in the case of coincident magnetic and VLF EM anomalies with no accompanying terrain conductivity anomaly, we are detecting magnetic and conductive bodies which lie below the maximum 6 m exploration depth of the terrain conductivity meter. For instance, simple infinite line pole depth estimates for Um and Vm give depths to the causative body of 31-43 m and 15-28 m respectively. These bodies are probably not of significance to any construction activities.

In light of the above, we must correct the NSRFC (1985b) report conclusion to state that there is some correlation between the magnetic and conductivity anomalies. Any lack of correlation may either be due to the depth of the causative bodies and the

maximum exploration depth of the terrain conductivity meter (chosen to investigate down to construction depths only) or may be the result of bodies which are conductive but not magnetic. It is incorrect to state that there is little correlation between magnetic anomalies and bedrock mineralization (Samostie, 1994) considering the known abundance of pyrrhotite in the Halifax Group.

6.13.2 Correlation of the Geophysical Anomalies and the Rock Sample Analyses

The % weight total sulphur and carbon alone have been used for the geophysical and geochemical correlations given the previous discussion on the limitations of the chemical analyses.

On line 1A (Fig. 6.2), bedrock samples from HA1 were collected at three depths (approximately 0.2, 1.2 and 1.8 m below the ground surface: Fig. 6.8). Bedrock was covered by a very thin (0.1 m) overburden layer at this pit. HA1 is located at the centre of the 36 mmhos/m terrain conductivity anomaly Mc, and at one of the crossover points of the VLF EM anomaly, Mv (Fig. 6.4). The filtered in-phase peak also coincides with these anomalies. The rock analyses (Fig. 6.9) show relatively large amounts of total sulphur and corresponding total acid potential, for samples at all three depths. The magnetic dipole anomaly (Mm), the conductivity anomalies (Mc and Nc) and the chemical analyses for HA1 (Figs. 6.4 and 6.9) suggest the presence of minerals which are both conductive and magnetic. The most likely candidate is pyrrhotite.

Test pit HA2 was selected so as to sample an area of extremely low terrain conductivity readings (approximately 2 mmhos/m) directly NW of anomalies Mc, Mv

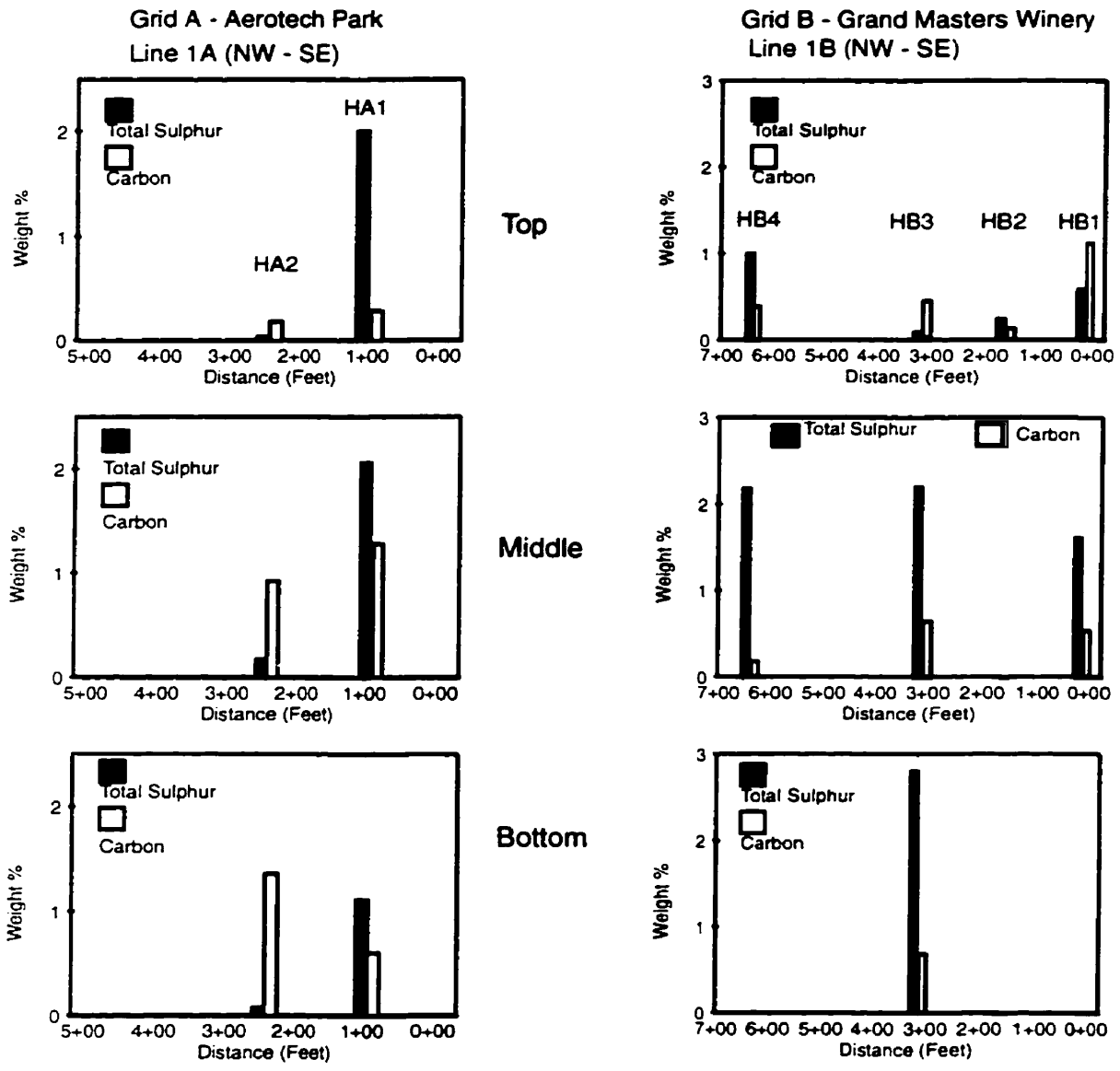

Figure 6.9 Bar graphs showing amounts of total sulphur and carbon in rock samples taken from 1A (grid site A) and 1B (grid site B).

and Mm (Fig. 6.4). As might be expected, the total sulphur content and, hence, total acid potentials are extremely low (Fig. 6.9). The samples from this test pit were taken at greater depths (1.1, 1.8 and 2.7 m in Fig. 6.8) than for HA1 due to the increase in overburden thickness (0.9 m in Fig. 6.8).

As a comparison with the field measurements, multi-layer theoretical response calculations (McNeill, 1980) were carried out for the terrain conductivity meter in the vertical dipole configuration at a height of 1 metre above the ground surface for line 1A at pits HA1 and HA2. For HA2, a conductivity of 1 mmho/m was obtained for the rocks with minor mineralization which lay beneath 1 metre of overburden (with an assumed conductivity of 5.5 mmhos/m). For HA1, the model gave a mineralized slate conductivity of 40 mmhos/m using the same overburden conductivity and an overburden thickness of 0.15 m. These theoretical calculations also gave apparent conductivities at the surface of 2.1 and 37.5 mmhos/m for the non-mineralized and mineralized slates respectively.

On line 1B, grid B (Fig. 6.3) overburden thickness is quite variable, ranging from a minimum of 0.3 m at HB3 to a maximum of 2.9 m at HB2 (Fig. 6.8). Hence, rock samples were collected at considerably different depths in test pits HB1 to HB4. The locations of these test pits were chosen to sample rocks at which conductivity and magnetic anomalies were measured (HB1: Tc and Tv; HB2: Um and Uv; HB3: Sm, Sc and Sv; HB4: Rm, Rc and Rv in Figs. 6.3 and 6.8). For pits HB3 and HB4, where the overburden is thinner and samples taken from shallower depths compared with HB1 and HB2, elevated levels of total sulphur and total acid potential were measured (Fig. 6.9)

with the exception of the shallowest (0.8 m) sample from HB3. This is in good agreement with the conductivity and magnetic anomalies measured over both pits. The lower gradients of the anomalies at HB3 compared with HB4 may reflect the lack of mineralization in the topmost metre of bedrock at HB3. HB1, coincident with the large terrain conductivity anomaly, Tc, also displays elevated total sulphur content (Table 6.1). However, rock samples from HB2, where there is no terrain conductivity anomaly, give low total sulphur values (though only the top of the rock surface was sampled due to the deeper overburden at this location).

At HB2, the rock sample Fe^{3+} content may be used to estimate magnetic susceptibility as approximately 500 x 10^{-6} cgs units if the Fe^{3+} content is equated with an assumed magnetite content of 4%, (Heiland, 1963). Assuming the magnetic anomaly, Um, is caused by a vertically polarized, infinite, horizontal cylinder (Nettleton, 1940) of radius 12.2 m and depth to centre 15.2 m and that the earth's magnetic field is 50,000 nanotesla, we arrive at a magnetic anomaly amplitude of about 100 nanotesla neglecting remanent magnetization. The magnetic anomaly, Um (Fig. 6.6), is approximately 1000 nanotesla. Therefore, the major contribution to this magnetic anomaly must be explained by a mineral which is both conductive (VLF EM anomaly Uv, Fig. 6.6) and magnetic and which attains a significant percentage by weight below the 6 m effective exploration depth of the terrain conductivity meter. We may conclude that it is likely that pyrrhotite mineralization is present in significant quantities at a depth of greater than 6 m in order to explain the large magnetic and VLF EM anomalies at HB2.

We have suggested that the horizontal and vertical distribution of magnetic and conductive sulphides in the Halifax Group are the cause of the apparent conductivity and magnetic anomalies. However, some conductivity variations may also be due to other factors such as graphite content, changes in bedrock depth (overburden thickness), moisture content, rock and overburden porosity, concentration of dissolved electrolytes in the contained moisture, temperature and phase state of the pore water, amount and composition of colloids and subsurface layer thickness and conductivity contrasts (McNeill, 1980). An example is conductivity anomaly Wc at the southwest end of line 2B (Fig. 6.7). This anomaly is shown as a gradual conductivity increase towards the end of the line. As there is no sample control (test pits) on this line, an alternative interpretation is that this conductivity increase is the result of increasing overburden conductivity, decreasing overburden thickness or a combination of both effects.

6.14 Conclusions

Reconnaissance geophysical surveys on two grids near Halifax International Airport have demonstrated that conductivity and magnetic anomalies have defined zones of sulphide mineralization within construction depths from the ground surface in the Halifax Group bedrock. This has been proved by chemical analyses of rock samples excavated from test pits located on selected geophysical anomalies. Increased levels of total sulphur were measured at all test pits where terrain conductivity anomalies are present. Two test pits, one on each grid, deliberately chosen to sample areas where no

terrain conductivity anomaly occurred, gave extremely low levels of total sulphur.

A combination of terrain conductivity meter, magnetometer and VLF EM meter is the most effective instrument package to carry out this type of environmentally oriented survey. Readings can be recorded rapidly by one person using automated data recording systems. The effective exploration depth limit of the terrain conductivity meter ensures that any terrain conductivity anomalies recorded are within construction depths in the surveyed area. Though the spontaneous potential equipment also defined conductivity anomalies, it, and the induced polarization equipment required longer equipment deployment times and additional personnel for effective operation.

Three types of relationships were observed from combinations of terrain conductivity, magnetic and VLF EM anomalies. The first consists of coincidental terrain conductivity, magnetic and VLF EM anomalies which defines conductive and magnetic mineralization within 6 m of the ground surface as defined by the terrain conductivity meter. We suggest the main mineral responsible for this combination of anomalies is pyrrhotite with or without pyrite. The second comprises terrain conductivity anomalies with no coincident magnetic anomalies (though VLF EM anomalies may also occur). Pyrite and/or graphite mineralization within 6 m of the ground surface may cause this combination of anomaly types. The third consists of magnetic and VLF EM anomalies with no coincident terrain conductivity anomalies. These result from magnetic and conductive mineralization, probably pyrrhotite with or without pyrite, at depths greater than 6 m.

As with all remote sensing methods, ground truthing is essential for the

interpretation of the geophysical data. Chemical and mineralogical analyses of rock samples obtained from outcrop, test pits and boreholes ensure the validity of any conclusions drawn from the geophysical interpretation. Geophysical surveys will rapidly define trends, amplitudes and widths of sulphide mineralization in the Meguma rocks of Nova Scotia in advance of construction projects. Hence, there is a strong case for including these types of geophysical surveys for construction activities in the Environment Act. Geophysical surveys would point the site investigation to critical areas where the exposure of sulphide mineralization may generate ARD. This should reduce the costs of subsequent treatment.

It is acknowledged that in built up areas, electromagnetic and magnetic surveys may not be practicable due to interference from power lines, buildings and other electromagnetic and magnetic sources. Also, the presence of sulphide mineralization does not necessarily imply that ARD will occur. The overall assessment of ARD must also include consideration of such factors as oxidizing conditions, temperature effects, rainfall amounts, and the presence or absence of bacteria. In other words, the development ARD is site specific.

It is important to note the reconaissance nature of this work and that the number of bedrock samples collected, and extent of the geophysical grids are limited. Although this limitation does not invalidate the results of the study, we recognize more work would be helpful to more rigorously define the correlation between sulphide mineralization and geophysical anomalies. Future considerations should include expanded grid size and more bedrock sampling for mineralogy and geochemistry. As

discussed in Chapters 2 and 5, detailed mineralogical studies combined with geochemical analyses are essential in the assessment of ARD and such studies would considerably improve the ability to interpret geophysical surveys more precisely.

Chapter 7

GIS-Based Knowledge-Driven And Data Driven Modelling For The Prediction Of Acid Rock Drainage In The Meguma Supergroup, Nova Scotia

7.1 Introduction

In previous chapters, several methods of assessing ARD potential in the Meguma Supergroup have been outlined. For example, total acid potential (TAP) of a rock sample can be calculated from a total sulphur analysis (Chapter 5). Also, arguments have been presented for the use of magnetic susceptibility of rock samples to detect the location of monoclinic pyrrhotite which is an important acid producing mineral (Chapter 5). However, these methods are useful mainly for a detailed assessment of ARD potential, on the scale of individual rock samples, collected from exposed bedrock or from drill core. A database containing magnetic susceptibility measurements or total sulphur analyses over large areas within the Meguma Supergroup is not available, and much of the area does not have exposed bedrock, so the direct measurement of ARD potential is not possible in many areas.

The best solution to the ARD problem is avoidance. Once ARD begins, it is difficult to stop and remediation is expensive. Considering large scale construction activities, such as the building of highways or the construction of a pipeline, it is important to locate in a regional sense, the areas with high ARD potential so they can be avoided. In cases where avoidance is impossible, plans can be prepared for more detailed evaluation, but it is still important to know in the first phase of planning,

"where?" and "how many?" areas may require such detailed work.

The objective of this chapter is to define broad areas in the southeastern part of the Meguma Supergroup (Fig. 7.1) that have high ARD potential. The concepts used in mineral exploration, and the development of "mineral potential" or "favourability" maps, are used to predict areas that may cause ARD, "if the rocks are disrupted and exposed to oxidizing conditions". An important underlying assumption used for predicting ARD, is that the mere presence of sulphide mineralization will lead to ARD generation. In the field, this may or may not be the case depending on a variety of factors such as abundance and type of sulphide minerals, presence or absence of bacteria, and access to oxidizing fluids. The ARD conditions referred to here, are those that develop from exposed bedrock, waste rock piles, open quarries, or any similar conditions that expose bedrock to oxidizing conditions. This does not include mine site tailings impoundments where rocks are processed to fine-grained material. In such areas, mineral textures, associations, and grain size all are changed substantially from their original state, and under these conditions, the potential for ARD generation must be assessed at each site.

In order to predict ARD potential on a regional scale within the Meguma Supergroup, a number of factors come into play. For example, monoclinic pyrrhotite can be located using airborne vertical gradient magnetic data, but only within the Halifax Group. Magnetite is known to exist in the Goldenville Group (Chapter 6). Therefore, data from various sources (in this example, geology and magnetic data) must be integrated, and there is no one single database that can be used. For this study, six

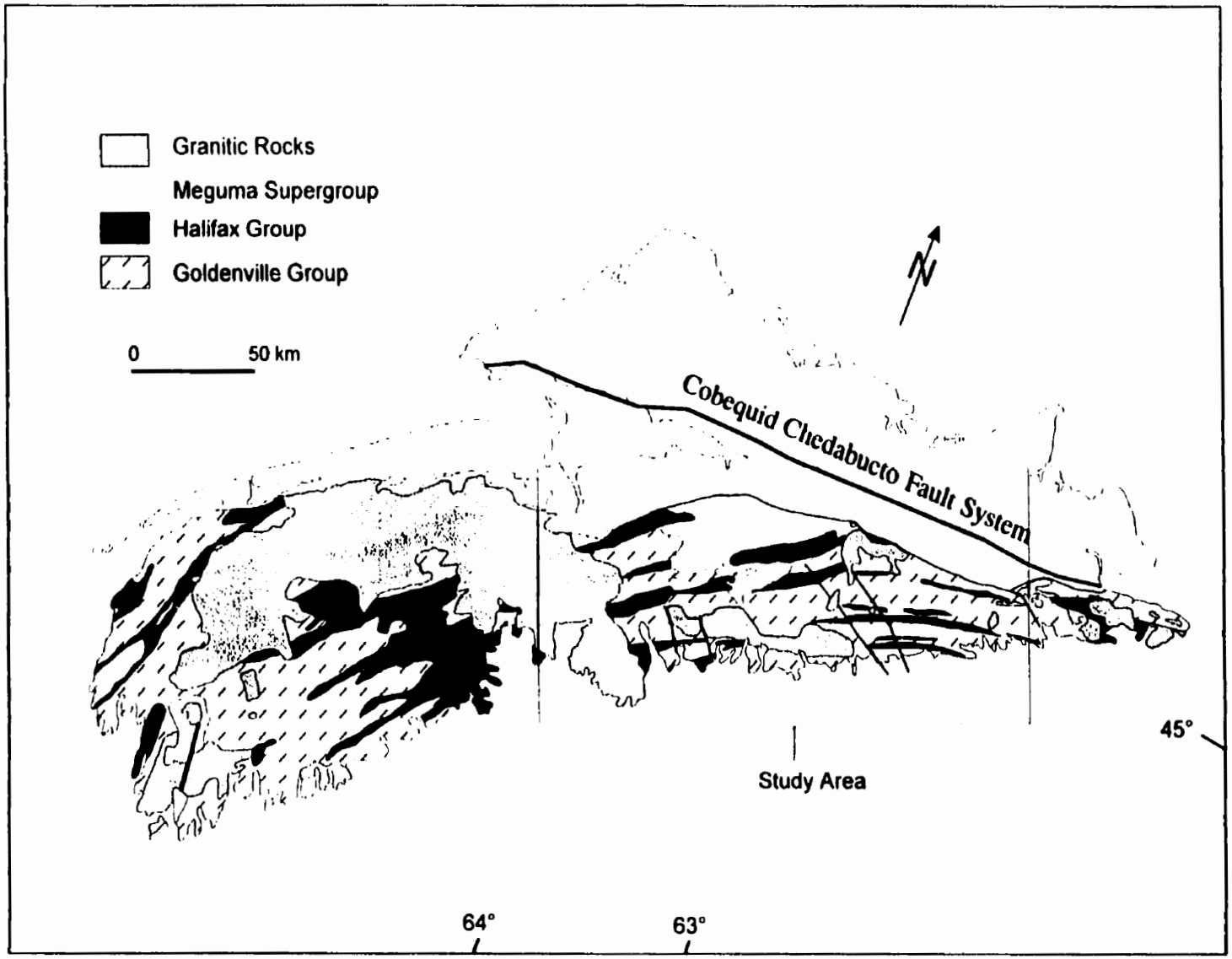

Figure 7.1. Simplified geological map of Nova Scotia showing the distribution of the Meguma Supergroup and the location of the study area (modified from Keppie, 1979a).

regional-scale, digital maps including geology, regional metamorphism, contact metamorphism, location of anticlines, location of Goldenville-Halifax Transition zone (GHT), and vertical gradient magnetics have been used. All of these geological factors are interpreted to have, at least some, influence on the potential for the bedrock to produce ARD. The rationale for choosing these particular data layers is explained in more detail in the next sections.

The data are integrated using Boolean and fuzzy logic (knowledge-driven) and weights of evidence (data-driven) map modelling techniques. Each of these techniques have their own strengths and weaknesses. The Boolean method is simple and easy to apply, but lacks the ability to weight different input map layers or map classes. The output map shows only those areas that do have ARD potential or do not have ARD potential, based on the input criteria. The fuzzy logic technique has the ability to weight individual maps, as well as the classes of each map. Both the Boolean and fuzzy logic map integration techniques are expert-driven, and are subjective in that the output maps reflect the criteria chosen by the expert. On the other hand, the weights of evidence method is a data-driven technique and is a more objective approach in that it uses the location of known mineral occurrences, in combination with evidence maps, to statistically estimate weights (W^+ and W^-) for each map. The weights are then used to calculate a posterior probability of ARD potential.

7.2 Previous Work

There has been little work performed on the regional-scale prediction of ARD in

the Meguma Supergroup with the exception of two studies. The first study was carried out by Porter-Dillon Limited (1987), in the Mahone Bay area of southwestern Nova Scotia. In that study, geological factors including lithology, metamorphic grade, and mineral occurrences were combined with anthropogenic activities (quarries and potential land use) to produce an ARD risk map. The influencing factors were laid out in flowchart format, and manually combined to produce a map showing low, medium, and high ARD risk areas.

In the second study, Samostie (1994) used a GIS to produce ARD risk maps for the entire province of Nova Scotia. That study included ARD risk from mining areas, in addition to disturbance of bedrock of the Meguma Supergroup. Samostie's work differed from the first study in several important aspects. Firstly, the input criteria consisted of less geological data (mainly bedrock geology), and included location of mining areas, roads, land use, stream and lake sediment geochemistry, and surface water chemistry. Secondly, the risk maps were produced within a GIS and interaction matrices and classification algorithms were used to combine the data.

The present study differs from these two studies in two important aspects. The first lies in the definition of "risk" assessment. The previous studies placed an emphasis on land use and bedrock disturbance in assigning high risk areas. For example, Samostie removed all sulphide mineral occurrences from his database that were not mined or exploited, on the assumption that if left undisturbed, there is no ARD risk. In the present study, the emphasis is on predicting where ARD "may occur if the bedrock is exposed to oxidizing conditions". In this sense, it is not an environmental risk

assessment that is being performed, but rather answering the question "What is the potential for ARD to develop?". Local effects and the risk to the environment from existing ARD areas are not considered in this study.

The second aspect where this study differs, is in the use of GIS and the map modelling techniques used to combine layers of evidence. Samostie used a knowledge-driven approach where specific areas were rated as high, medium or low risk, and the input maps were combined to create a final composite map. Different methods of combining data layers were not explored.

In terms of using GIS to produce favourability maps for mineral exploration, details on concepts and methodology, as well as examples for gold potential in the Meguma Supergroup in Nova Scotia, are presented in Bonham-Carter et al. (1988), Bonham-Carter (1989), Bonham-Carter et al. (1990), and Bonham-Carter (1994). Much of the background information presented in this chapter is from those sources. According to Wright and Bonham-Carter (1996), the overall process of producing favourability maps using GIS can be outlined in four main steps:

1) establish a conceptual model,
2) build a spatial database,
3) process that data, and
4) generate the favourability maps through integration modelling.

Each of these steps is discussed in more detail in the following sections.

7.3 Conceptual Model

A single model for all sulphide mineralization in the Meguma Supergroup does

not exist, and the type of mineralization that may be responsible for ARD generation comes from a variety of sources, each with its own possible model of formation. For example, sulphide mineralization is known to be associated with gold mineralization in gold districts, mainly in the Goldenville Group (e.g., Graves, 1976; Malcolm, 1976; Kontak et al., 1990); lead-zinc mineralization is associated with pyrite and pyrrhotite within the GHT (e.g., Binney et al., 1986; MacInnis, 1986); and stratigraphically controlled pyrrhotite and pyrite mineralization occurs mainly in the Halifax Group and GHT (see Chapter 2). For this study, it is intended that only major, regional-scale features be used to predict ARD areas; not the local features that may be developed at single mineral deposits. For example, the entire GHT is used as a possible source for sulphide minerals, and no attempt is made to determine variations within the GHT that may lead to local differences in abundance or type of mineralization. The data used, and the rationale for choosing the data, are discussed in more detail in the following section.

7.4 Data Sets

In order to predict where ARD generation is possible within the Meguma Supergroup, it is necessary to find the areas that contain sulphide mineralization. In addition to the presence or absence of mineralization, mineral texture and type of sulphide minerals are also important considerations (see Chapter 2). The bedrock geology map is useful in that the Halifax Group is known to contain abundant pyrrhotite and pyrite (Chapter 2), and the Goldenville Group contains sulphide mineralization in

gold districts.

In the Halifax Group, pyrrhotite typically occurs along cleavage planes (Chapter 2). The location of granitic intrusions is important in this respect because the rocks in contact metamorphic aureoles do not contain a well-developed cleavage. In these areas, movement of oxidizing fluids to pyrrhotite mineral surfaces is more restricted compared to well-cleaved rocks that have developed fractures or joints parallel to the cleavage. This is especially important, for example, where freeze/thaw cycles can easily break the bedrock along cleavage or parallel joints/fractures, exposing pyrrhotite to oxidizing conditions. The regional metamorphic grade is important for similar reasons. Low grade, greenschist facies rocks have a well-developed cleavage which provides much easier access of oxidizing fluids to pyrrhotite.

The location of the GHT is important because it contains significant sulphide mineralization, and is a control for elevated trace element content (Graves and Zentilli, 1988).

In terms of structure, it has been suggested that pyrrhotite/pyrite mineralization in the Halifax Group increases in abundance towards the centers of major structural features (Cameron and Hood, 1975). Also, in the Goldenville Group, gold districts are spatially related to major anticlines.

For the magnetic data, the pyrrhotite within the Halifax Group and GHT is the monoclinic variety which is the most magnetic of all pyrrhotite types (Chapter 2). Therefore, high magnetic zones indicate the presence of this mineral (Chapters 2, 5, and 6). Based on these generalized observations, the following datasets have been used:

Bedrock Geology - geological map of Nova Scotia compiled by Keppie (1979). Scale 1: 500 000 (E00 format).

Regional Metamorphism - metamorphic map of Nova Scotia compiled by Keppie and Muecke (1979). Scale 1:1 000 000 (E00 format).

Contact Metamorphism - distribution of granitic polygons taken from the geological map.

Anticline Axial Traces - structural map of Nova Scotia compiled by Keppie (1979). Scale 1:1 000 000 (E00 format).

GHT - linears extracted from the geological map.

Vertical Gradient Airborne Magnetic Survey - Geological Survey of Canada, airborne survey. Data subsequently processed by D.A. Raymond (at the College of Geographic Sciences - COGS), converted to PIX format and scaled to 8 bit.

The "raw" GIS data layers were supplied on CD-ROM to the Center of Geographic Sciences (Tim Webster) by the Nova Scotia Department of Natural Resources in Arc/Info EOO format.

7.5 Data Processing

One of the problems of using the regional scale digital data in this study is that it is not precisely known how accurate the data is in terms of spacial location and "inferred" geology. For example, the geological map (Keppie, 1979) was compiled from a variety of sources, and the geological boundaries are likely to be inferred in many cases, and where the boundaries are shown, the possible locational error is unknown. As another example, the GHT is inferred to be located between the Halifax and Goldenville Groups but it has not been mapped in detail throughout the study area.

However, it is known from studies in southwestern Nova Scotia, to have a maximum thickness of about 2 km (O'Brien, 1986). The necessary approach taken to deal with unknown accuracy and inferred geology, is to simplify the data. This takes the form of reclassification to simplify some of the data (geology, regional metamorphism, magnetics) and to create buffer zones or proximity maps for the line data (GHT, anticlines, and contact metamorphism).

Lookup tables were used to reclassify and simplify the geological map into the following classes: 1) water, 2) other, 3) Goldenville, 4) Halifax, and 5) granites. The lookup tables are shown in Table 7.1. The map of regional metamorphic grade was reclassified interactively, and simplified to show classes of: 1) greenschist facies - chlorite grade, 2) greenschist facies - biotite grade, 3) amphibolite facies, 4) granite, and 5) water. The vertical gradient magnetic map was reclassified into three equal interval classes of low, medium, and high magnetic response.

Three proximity maps were created including: 1) proximity to granitic intrusions (to outline contact metamorphic aureoles), 2) proximity to GHT, and 3) proximity to anticlines. All the reclassified and proximity maps are shown in Figure 7.2 and the classes defined for each map are shown in the map legends. Further details about how each of the classes are used and the justification of weighting the classes to define ARD potential are presented below for each of the modelling techniques used.

7.6 Data Integration And Map Modelling

The final step in producing the ARD prediction maps involves integration of the

Table 7.1 Attribute tables used to create simplified geological map used in the modelling.

Digital Map Code	Simplified Code
Wat	Water
?DC	Other
CC	Other
DCNM	Other
ECCNSM	Other
EDK	Other
EJM	Other
g	Other
gd	Other
H-C	Other
LCPB	Other
LT	Other
SA	Other
EK	Clay/Silica Sand
LTBNM	Fundy Gp
LTWNM	Fundy Gp
LTWSM	Fundy Gp
TJNM	Fundy Gp
LCSV	Pictou Gp
CWB	Canso Gp
ECW	Windsor Gp
ECWaSM	Windsor Gp
ECWbSM	Windsor Gp
ECWcSM	Windsor Gp
ECC	Horton Gp
ECH	Horton Gp
ECHB	Horton Gp
ECS	Horton Gp
COG	Goldenville Fm
COGg	Goldenville Fm
COGm	Goldenville Fm
COH	Halifax Fm
COHm	Halifax Fm
Ca	Granitoid
Dcg	Granitoid
Dcgd	Granitoid
Dcgt	Granitoid
Dcmg	Granitoid
Dgd	Granitoid

Simplified Code (Keyfield) For intermediate step	Simplified Code Intermediate step
Water	0
Other	1
Clay/Silica Sand	1
Fundy Gp	1
Pictou Gp	1
Canso Gp	1
Windsor Gp	1
Horton Gp	1
Goldenville Fm	2
Halifax Fm	3
Granitoid	4

Simplified Code Final Legend	Simplifed Digital Map Legend For Modelling
0	"0:Water"
1	"1:Other"
2	"2:Goldenville Fm"
3	"3:Halifax Fm"
4	"4:Granitoid"

Figure 7.2 Input maps used as evidence for map modelling. A) simplified geology, B) regional metamorphism, C) buffered anticlines, D) buffered GHT, E) contact metamorphism (buffered granitoids), F) vertical gradient magnetics.

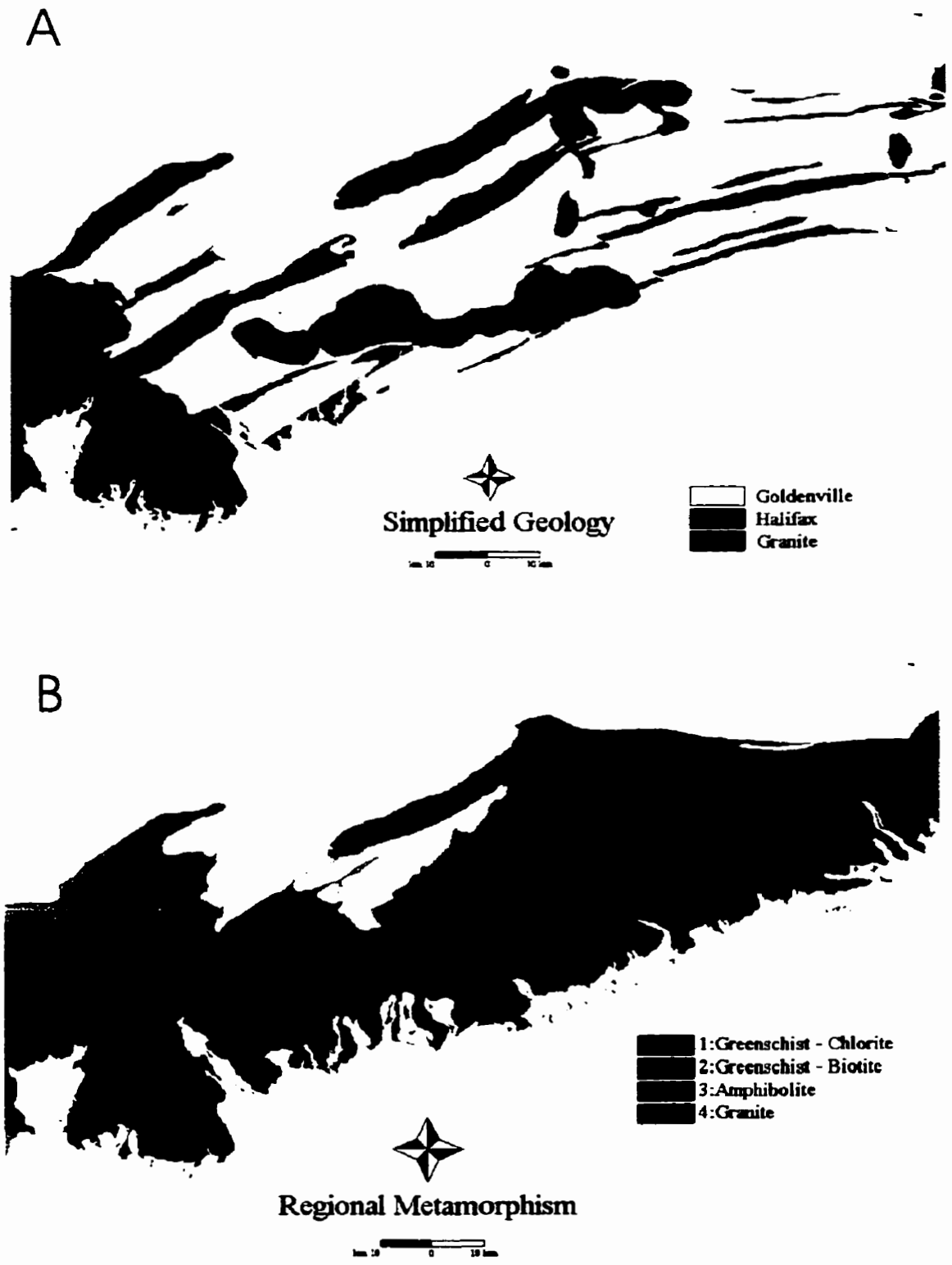

Figure 7.2 (Continued)

C

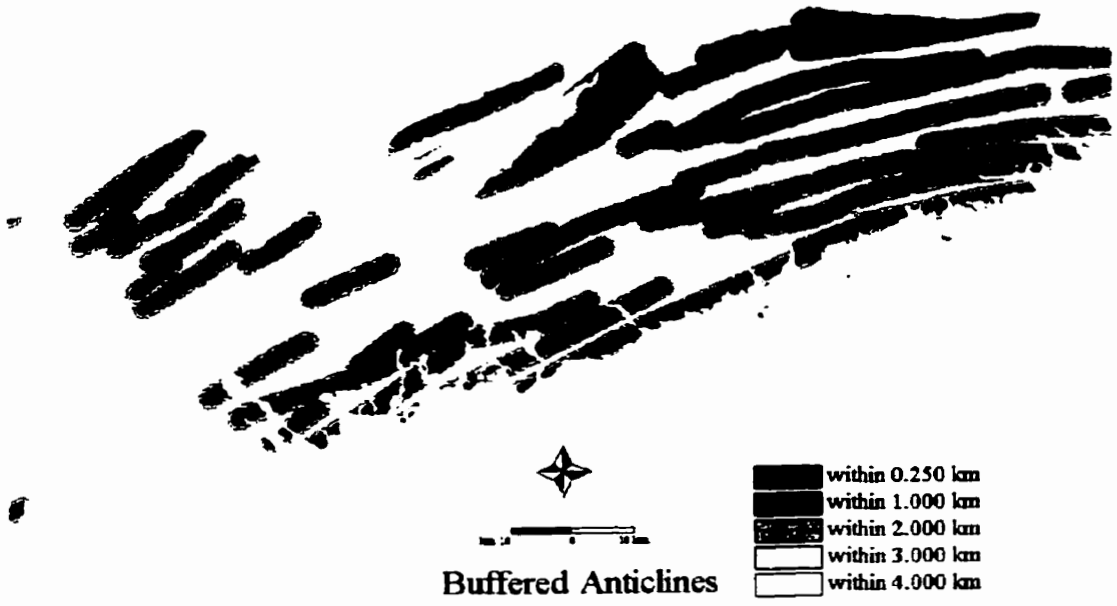

D

Figure 7.2 (Continued)

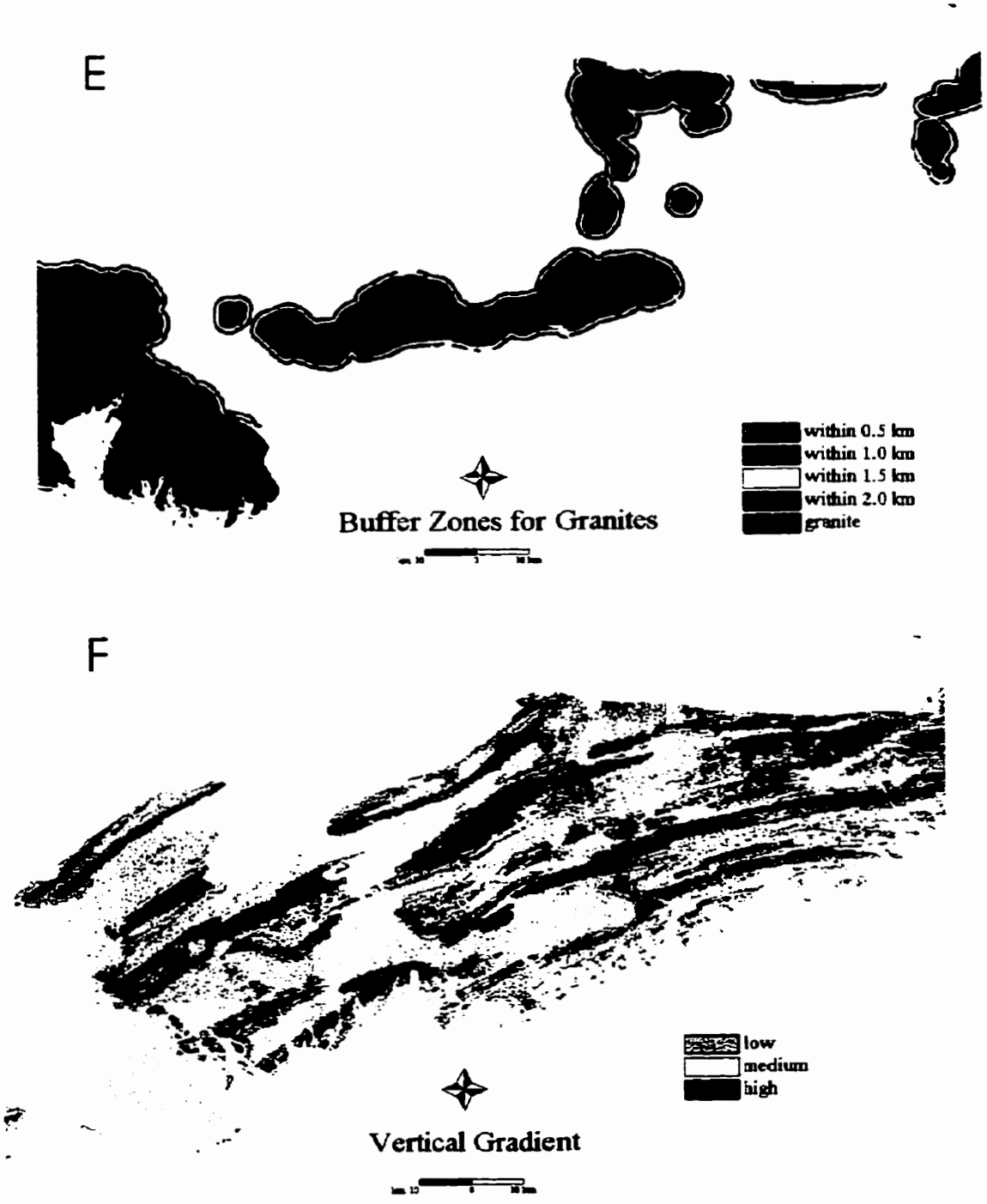

Figure 7.2 (Continued)

input maps (layers of evidence). For this study, the modelling techniques used are Boolean, fuzzy logic, and weights of evidence. The final input maps are geology, regional metamorphism, buffered granites, buffered anticlines, buffered GHT, and vertical gradient magnetics. The modelling techniques were performed through the use of model equations (Appendix D). Attribute tables containing three columns of class, Boolean, and fuzzy membership (fm) values were created for use with the model equations. The values were chosen based on geological experience and field observations of rocks in the Meguma Supergroup. There are no set criteria or standards for ARD prediction, and the criteria presented here are essentially based on subjective judgement.

7.6.1 Boolean Logic Modelling

Boolean logic involves sets where each object of the set has membership values of 1(TRUE) or 0 (FALSE). Boolean logic map modelling involves combining a set of input maps to produce a single binary output map, where class 1 represents areas that satisfy all the criteria (in this case, high ARD potential), and class 0 represents all the remaining areas. The methods of combining the sets are defined by Boolean algebra that has three operations (Bonham-Carter, 1994): AND (logical intersection), OR (logical union), and NOT (complementation).

In this study, Boolean values for each class in the input maps are set to either 0 (no ARD potential), or 1 (ARD potential is present) as shown in Table 7.2. The values were chosen to be conservative, and to include as much of the criteria as possible but

Table 7.2 Boolean values used for the Boolean model. Class numbers correspond to the legends in the input maps shown in Figure 7.2

Input Maps	Class	Boolean Value	Name
Simplified Geology	1	0	Water
	2	0	Other
	3	0	Goldenville
	4	1	Halifax
	5	0	Granitoid
Regional Metamorphism	1	1	Chlorite Facies
	2	1	Biotite Facies
	3	0	Amphibolite Facies
	4	0	Granite
Magnetics	1	0	Low
	2	0	Medium
	3	1	High
Contact Metamorphism	1	1	0.5 km
	2	1	1.0 km
	3	1	1.5 km
	4	1	2.0 km
	5	0	Granite
	0	1	> 2.0 km
Anticlines	1	1	0.25 km
	2	0	1.0 km
	3	0	2.0 km
	4	0	3.0 km
	5	0	4.0 km
	0	0	> 4.0 km
GHT	1	1	0.5 km
	2	0	1.0 km
	3	0	1.5 km
	4	0	2.0 km
	0	0	> 2.0 km

also to remain within scientific reason.

The Halifax Group, chlorite and biotite zones (greenschist facies), high magnetic areas, within 0.25 km of anticlines, and within 0.5 km of the GHT were all given values of 1, indicating a potential for ARD development. For the contact metamorphic map, all areas except granites were given a value of 1 indicating that contact metamorphism does not influence the potential for ARD. Sulphide mineralization and ARD does occur within contact metamorphic zones (see Chapter 2). In this case the map could be omitted, however it is used in the fuzzy logic modelling discussed below (Section 7.6.2) and is included here for comparison.

The Boolean AND operator is used to combine the geology, magnetic, regional metamorphic, and contact metamorphic maps. Considering the Boolean values assigned to each map class, this combination scheme essentially shows all areas where there is high magnetic signatures in the Halifax Group, in the lowest regional metamorphic grade areas. Based on the data presented in previous Chapters, this will define areas containing pyrrhotite and associated sulphide minerals including pyrite, marcasite, and chalcopyrite as presented in Chapter 2. The results of this operation are then combined with the anticline and GHT maps using the Boolean OR operator. It is known that the GHT contains sulphide minerals and an elevated metal content (Graves and Zentilli, 1988), and the anticline map is used to define the areas that have the potential to contain sulphide mineralization through the association with gold deposits. The final output is a binary map with a value of 1 where the criteria are met (ARD potential) and 0 otherwise (no ARD potential). The Boolean program used to produce the final binary

map is presented in Appendix D. The output map for the Boolean model is shown in Figure 7.3.

One of the benefits of the Boolean approach is its simplicity and it is relatively practical and easily applied. However, a drawback to the approach is that the criteria used cannot be given weights that depend on their relative significance. In other words, there is no possibility of "may-be" areas of ARD generation. For example, it may be argued that areas classified as "medium" on the magnetic map, or areas within 1.5 km (instead of 0.25 km) of anticlines could contain sulphide mineralization. A zone of pyrite within the Goldenville Group and not near a major anticline, would not be defined by the criteria used here. This is a limitation of the method and it should be emphasized that the output map is not guaranteed to define all areas with ARD potential. However, if used in the broad sense, the map certainly defines areas that would warrant further detailed investigation. To refine the criteria, and to model areas based on a ranking scale from high to low ARD potential, the fuzzy logic method can be used.

7.6.2 Fuzzy Logic Modelling

Fuzzy logic modelling is an expert-driven approach in that the weighting of input evidence is controlled by the expert. In classical set theory, a set is a collection of objects, and objects are either a member of a set (membership value = 1), or not a member of a set (membership value = 0). The fuzzy logic approach uses fuzzy set theory, which allows for each object of a set to have continuous membership values

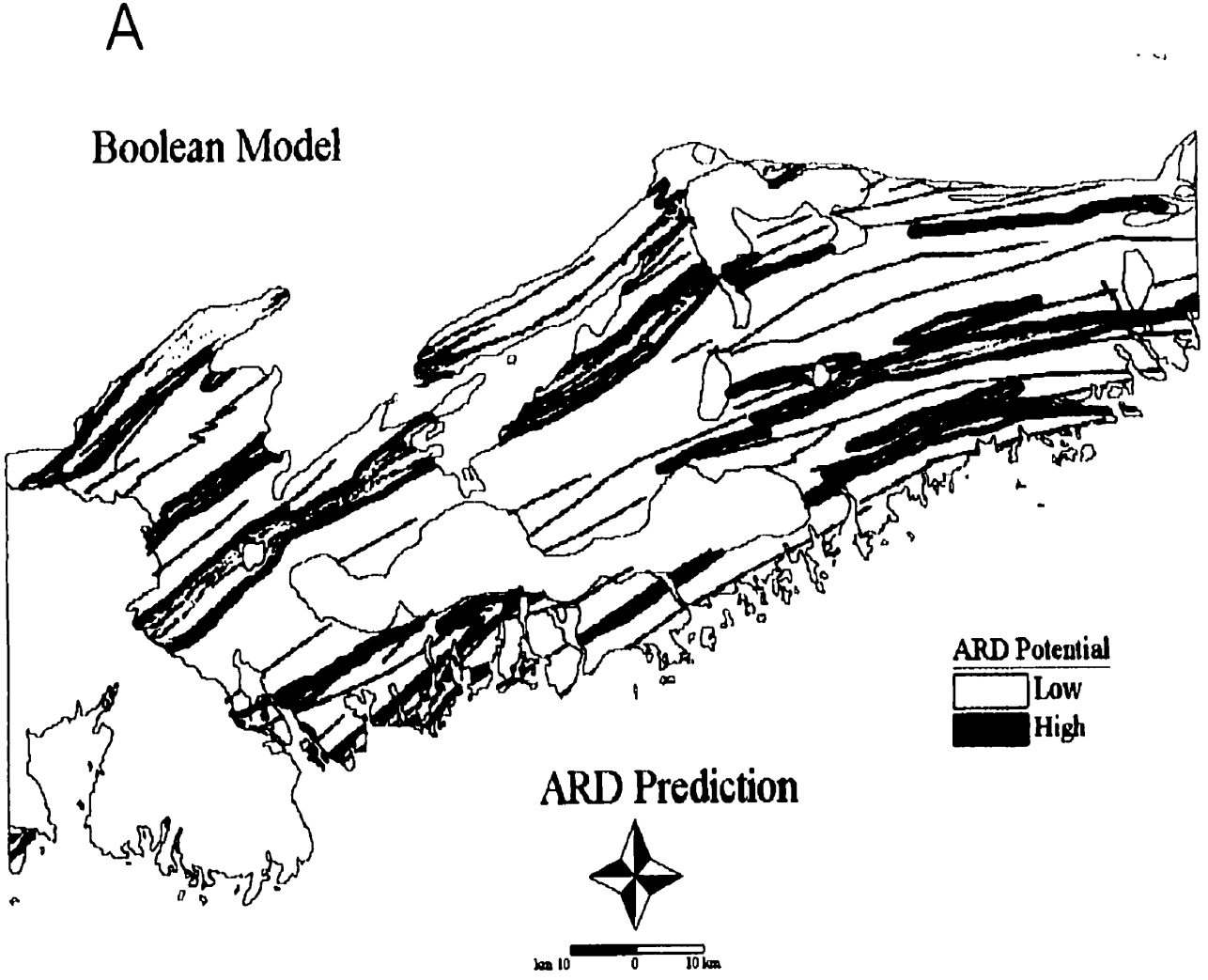

Figure 7.3 ARD prediction maps. A) Boolean model, B) fuzzy logic model, and C) weights of evidence model

B

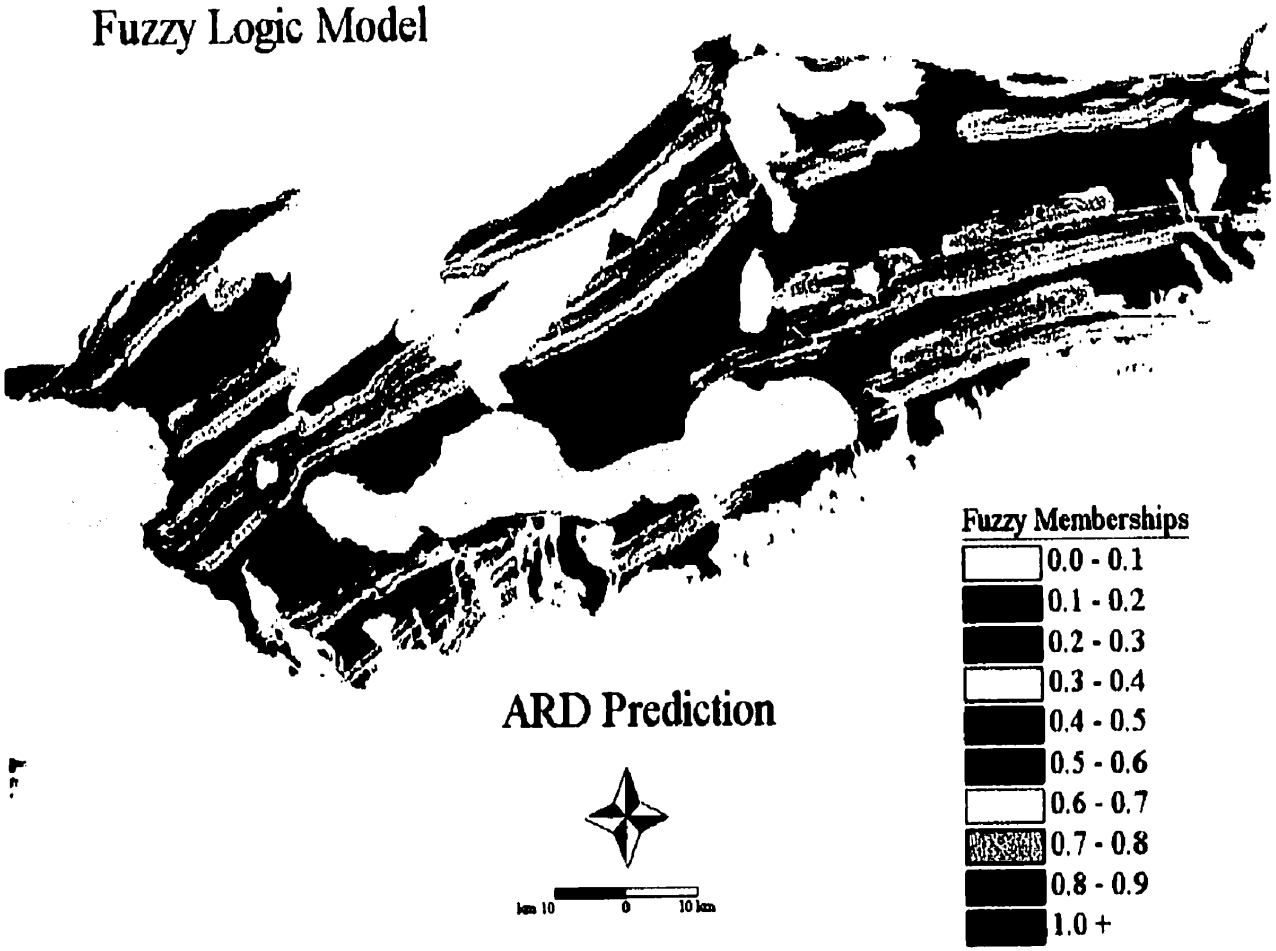

Figure 7.3 (Continued)

C

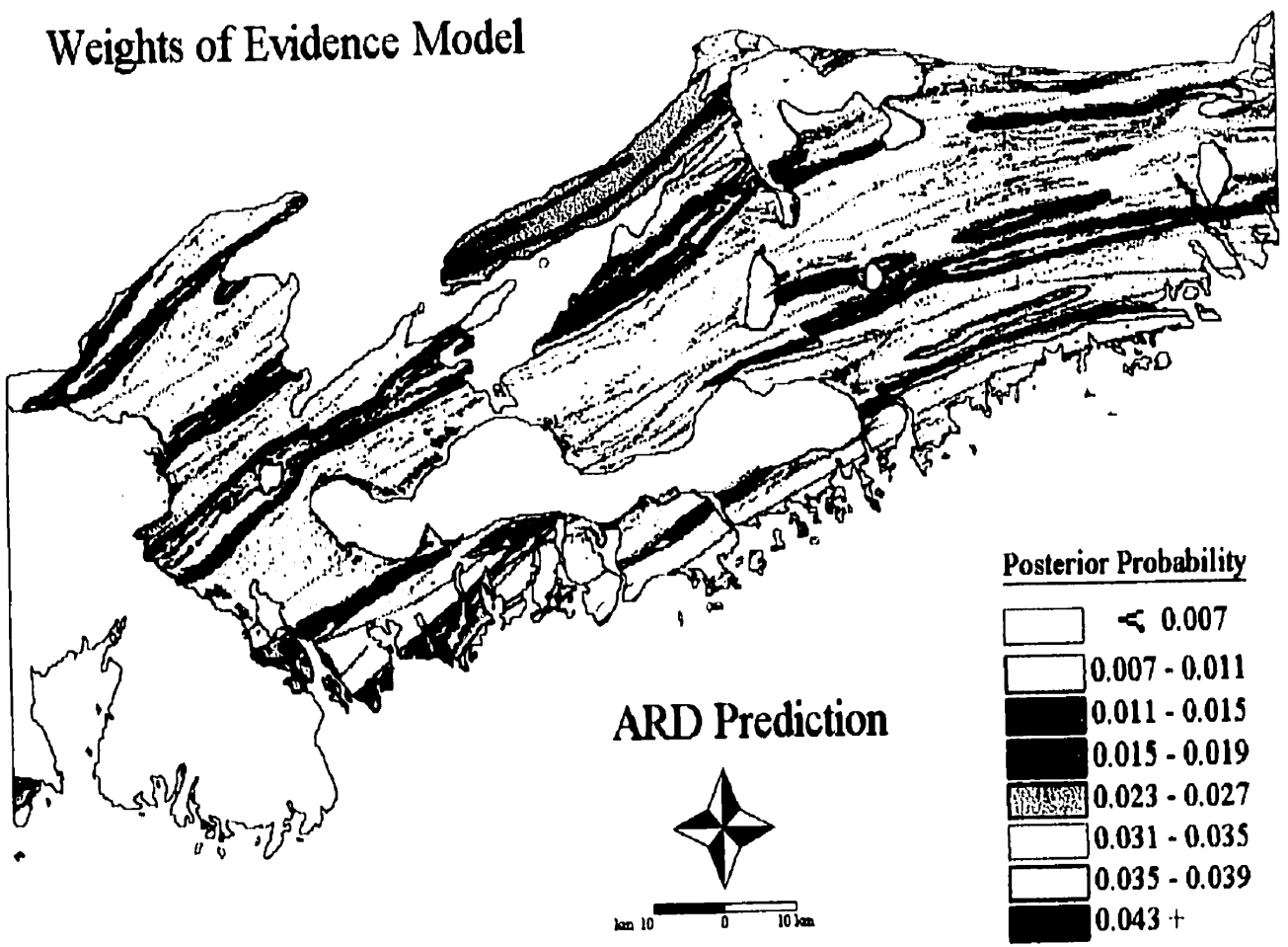

Figure 7.3 (Continued)

between 0 and 1 (0 = full non-membership and 1 = full membership), depending on the "degree of membership". Simply, a fuzzy set is a set of paired values, the first value representing the object of the set, the second value representing the grade or degree of membership (Zadeh, 1965). A fuzzy set can be defined in the following way. If X = {x} defines a space of objects, then A is the fuzzy set in X and is defined as the set of ordered pairs in the following equation:

$$A = \{x, \mu(x)\} \tag{7.1}$$

where $x \in X$ and $\mu_A(x)$ is the membership function (An et al., 1991; Wright and Bonham-Carter, 1996). Using an example from this study, let A represent the pixels of a map containing sulphide mineralization, and X = {x} is the space of objects reflecting vertical gradient magnetic values. The membership function for A could be represented as shown in Table 7.3.

Table 7.3 Fuzzy membership values for vertical gradient magnetics used in this study.

Magnetic Intensity	Class	Fuzzy Membership ($\mu_A(x)$)
low	1	0.1
medium	2	0.6
high	3	1.0

The flexibility of fuzzy logic modelling lies in the different methods of combining the fuzzy membership values. Five of the main combination functions are

fuzzy AND, fuzzy OR, fuzzy algebraic product (FAP), fuzzy algebraic sum (FAS), and the gamma operation. The fuzzy AND and OR functions are basically the minimum and maximum of the membership values of each of the input maps respectively. The FAP is the product of all membership values of the input maps and the result tends to be small (decreasive), due to multiplying values less than 1 together. The output value is always smaller than, or equal to, the smallest contributing input membership value. The FAS has a complementary effect to the FAP function, and the output is always greater than, or equal to, the largest contributing membership value (increasive). The following equation shows how to calculate the FAS:

(7.2) $[1 - (1-a) * (1-b) * .....]$

where a and b are membership values for two maps a and b.

The gamma operation is defined in terms of the FAP and the FAS by the following equation:

(7.3) $$\mu_{Combination} = (FAS)^{\gamma} * (FAP)^{1-\gamma}$$

where $^{\gamma}$ is the gamma operator and has a value between 0 and 1. Choosing a low value for gamma, the function is decreasive and FAP predominates, whereas for a high value of gamma, the operation is increasive and the FAS predominates. If gamma equals 1, the output is the same as the FAS, whereas if gamma equals 0, the output is the same as

the FAP (Fig. 7.4).

For this study, the fuzzy membership values chosen for each input map are shown in Table 7.4. The choice of values for each map class is entirely subjective and is based partly on new data presented in previous chapters of this thesis, as well as geological knowledge about the Meguma Supergroup obtained from the literature. The rationale for the value choices is similar in some respects to that of the Boolean model. The factors that are considered to be most important for defining ARD potential are given values of 1 (full membership). The rest of the classes are scaled to values less than 1 depending on how much of an influence the input map is considered to have. For example, in terms of geology and magnetics, the Halifax Group with a high magnetic signature has high ARD potential based on the abundance of monoclinic pyrrhotite (Chapter 2). Therefore, both the Halifax Group and the "High" class on the magnetic map are given fuzzy membership values of 1 (full membership). The zones within 0.5 km of the GHT are also given values of 1 with the rest of the classes of the GHT map scaled below 1. The values assigned to each class on the anticline map is based on the interpretation that it is less likely to encounter sulphide mineralization near anticlines in the Goldenville Group than it is to encounter pyrrhotite in the Halifax Group. Therefore, the highest membership value given on the anticline map is 0.5 (within a distance of 0.25 km of major anticlines). Arguably, the actual values chosen for any of the input maps in this study may differ depending on the expert assigning the values. However, the most important point about assigning fuzzy membership values is the relative ranking of classes rather than if a certain class is assigned a 0.5 or 0.6.

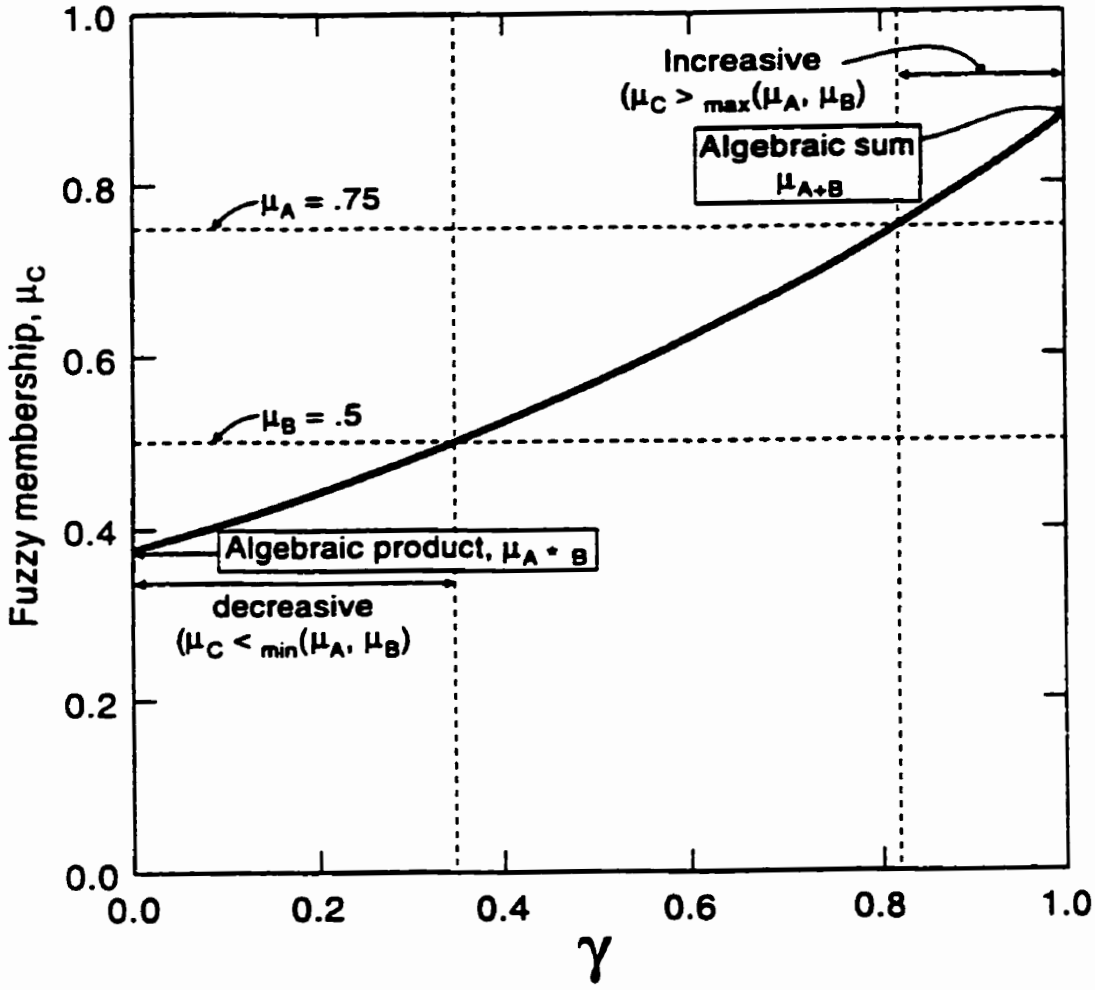

Figure 7.4 Graph of fuzzy membership, μ_c, obtained by combining two fuzzy memberships, μ_A and μ_B, versus γ. The graph shows the effect of variations in γ for the case of combining two values, $\mu_A = 0.75$ and $\mu_B = 0.5$. In the case where $\gamma = 0$, the combination equals the fuzzy algebraic product. In the case where $\gamma = 1$, the combination equals the fuzzy algebraic sum. (From Bonham-Carter, 1994).

Table 7.4 Fuzzy membership values used for the fuzzy model. Class numbers correspond to the legends in the input maps shown in Figure 7.2

Input Maps	Class	Fuzzy Memberships	Name
Simplified Geology	1	0.0	Water
	2	0.0	Other
	3	0.6	Goldenville
	4	1.0	Halifax
	5	0.0	Granitoid
Regional Metamorphism	1	1.0	Chlorite Facies
	2	1.0	Biotite Facies
	3	0.5	Amphibolite Facies
	4	0.0	Granite
Magnetics	1	0.1	Low
	2	0.6	Medium
	3	1.0	High
Contact Metamorphism	1	0.6	0.5 km
	2	0.7	1.0 km
	3	0.7	1.5 km
	4	0.8	2.0 km
	5	0.0	Granite
	0	1.0	> 2.0 km
Anticlines	1	0.5	0.25 km
	2	0.4	1.0 km
	3	0.4	2.0 km
	4	0.3	3.0 km
	5	0.2	4.0 km
	0	0.1	> 4.0 km
GHT	1	1.0	0.5 km
	2	0.8	1.0 km
	3	0.6	1.5 km
	4	0.5	2.0 km
	0	0.4	> 2.0 km

The inference network to combine the input maps used in this study is shown in Figure 7.5. Geology and magnetics are combined using the fuzzy AND operator. Considering the membership values in Table 7.4, the results of this operation (Map A) are that the highest ranking is assigned to the Halifax Group where it contains a high magnetic signature. The rest of the areas are ranked below the highest value, according to the membership values of each class. The GHT and anticline maps are combined using the fuzzy OR operator. This has the effect of selecting both the GHT and the anticline areas separately, based on their fuzzy membership values (Map B). Map A and Map B are then combined with the regional metamorphic and contact metamorphic maps using the gamma operation with a gamma value of 0.5. This essentially averages the four input maps to create the final ARD prediction map. The program used to run the fuzzy logic modelling is presented in Appendix D. The program was written such that a gamma value could be entered interactively. The output map is presented in Figure 7.3.

7.6.3 Weights of Evidence Modelling

The weights of evidence method is a data-driven technique that uses the location of known mineral occurrences to estimate weights that are based on a measured association between predictor map patterns and the location of the mineral occurrences. Detailed discussions of weights of evidence modelling are presented in Bonham-Carter et al. (1988, 1989), Bonham-Carter (1994), and Wright and Bonham-Carter (1996). The following introduction is taken from these sources.

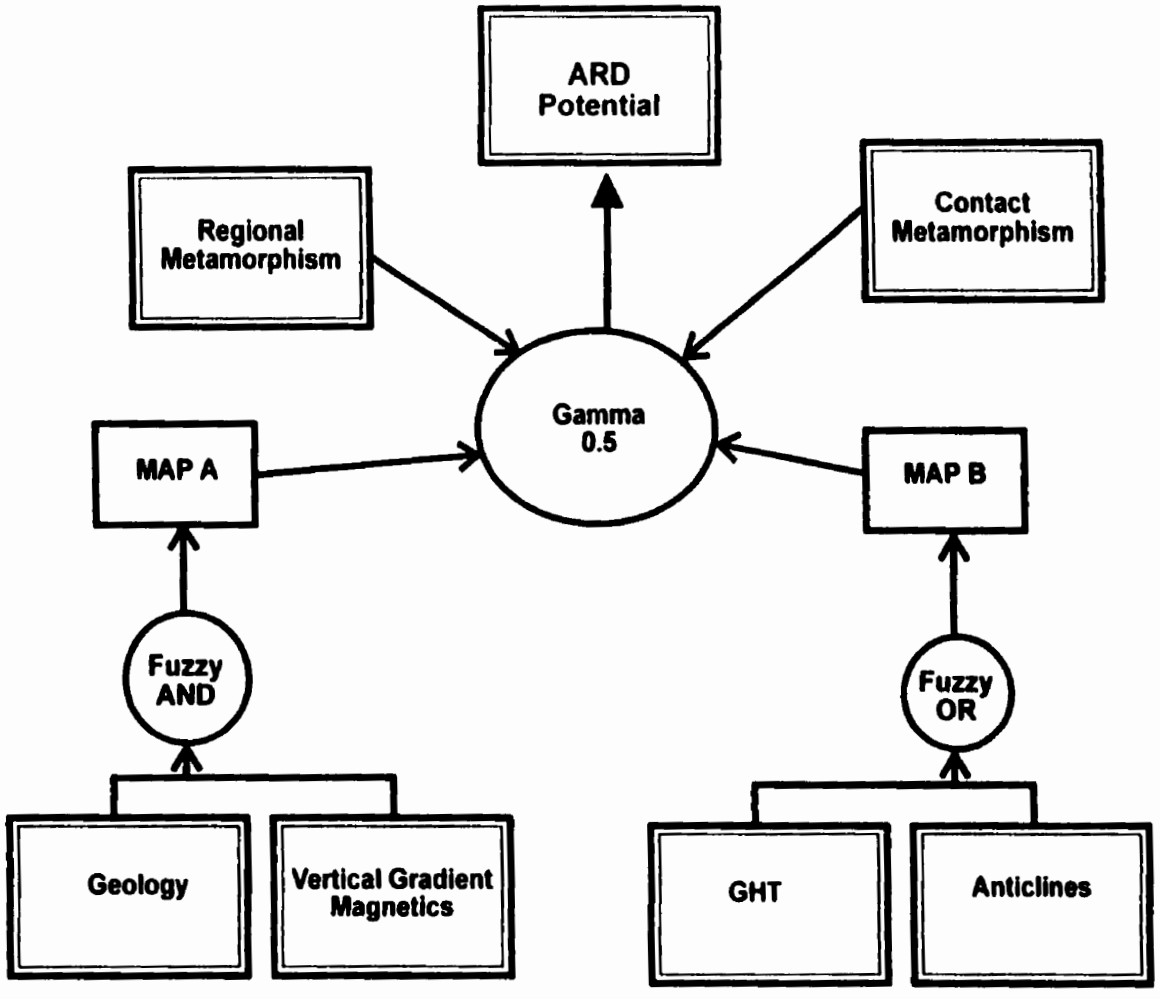

Figure 7.5 A simply inference network for predicting acid rock drainage using fuzzy logic as the inference engine. The knowledge base is contained within map attribute tables containing fuzzy membership functions. Modified from Bonham-Carter (1994).

In the selected study area, each sulphide mineral occurrence is assigned to a unit cell of area u km^2 and the total study area represented by t km^2. The number of unit cells containing an occurrence is given by N(D), where N( ) is the count of cells and D is the presence of deposits. The total area of the region is represented by N(T) = t/u unit cells. The prior probability of a cell containing an occurrence is P(D) and can be taken as the ratio N(D)/N(T). Posterior probability is equal to the prior probability times a factor that is estimated from evidence. Evidence may be present or absent depending on the favourability of the evidence. Therefore, posterior probability may be larger or smaller than the prior probability, depending on "how favourable" the evidence is.

Evidence in this case comes from predictor maps that are commonly reduced to binary form resulting in an area that is more favourable for sulphide mineral occurrences (pattern present) and an area that is less favourable for sulphide mineral occurrences (pattern absent). Considering a binary predictor map B_j, the "pattern present" area is $N(B_j)$ unit cells, and the "pattern absent" area is $N(\overline{B_j}) = N(T) - N(B_j)$.

Given the **presence** of the j-th binary pattern, the posterior probability that a cell contains an occurrence is:

$$P(D|B_j) = \frac{P(B_j|D)\ P(D)}{P(B_j|D)\ P(D) + P(B_j|\overline{D})\ P(\overline{D})} \tag{7.4}$$

where $\overline{D}$ = *absence of deposits*. Given the **absence** of the j-th binary pattern, the

posterior probability that a cell contains an occurrence is:

$$P(D|\overline{B}_j) = \frac{P(\overline{B}_j|D)\ P(D)}{P(\overline{B}_j|D)\ P(D) + P(\overline{B}_j|\overline{D})\ P(\overline{D})} \tag{7.5}$$

The posterior log odds of a cell containing a deposit, given the **presence** of the j-th binary pattern is:

$$\textit{posterior}\ \log\ \textit{odds}\ (D|B_j) = \textit{prior}\ \log\ \textit{odds}\ (D) + W_j^+ \tag{7.6}$$

and given the **absence** of the j-th binary pattern is:

$$\textit{posterior}\ \log\ \textit{odds}\ (D|\overline{B}_j) = \textit{prior}\ \log\ \textit{odds}\ (D) + W_j^- \tag{7.7}$$

The positive and negative weights of evidence are defined as:

$$W_j^+ = \ln \frac{P(B_j|D)}{P(B_j|\overline{D})} \tag{7.8}$$

and

$$W_j^- = \ln \frac{P(\overline{B}_j|D)}{P(\overline{B}_j|\overline{D})} \tag{7.9}$$

respectively. The overall measure of spatial association between mineral occurrences and the binary pattern is the contrast, C, that is defined as:

$$C_j = |\ W_j^+ - W_j^-\ | \tag{7.10}$$

In the case where n binary predictor maps are used as evidence, the posterior log odds

can be expressed as:

$$(7.11) \qquad \textit{posterior} \log \textit{odds}\ (D) = \textit{prior} \log \textit{odds}\ (D) + \sum_{j=1}^{n} W_j^{k(j)}$$

where $W_j^{k(j)}$ is positive for the presence of the j-th binary pattern, and negative for the absence of the j-th binary pattern. The posterior probability used to create the final ARD potential map can then be calculated from the posterior log odds. An important assumption made in this study is that the binary input maps used as evidence are conditionally independent. Conditional independence is necessary to satisfy Bayesian probability theory when combining two or more maps by this data-driven technique.

For this study, a total of 121 sulphide mineral occurrences, and five input maps were used as evidence including geology, regional metamorphism, buffered anticlines, buffered GHT, and vertical gradient magnetics. The contact metamorphic map, used in the fuzzy logic approach, was not used in the weights of evidence modelling because it is known that sulphide mineralization does occur in contact metamorphic areas (Chapter 2). The location of approximately half of the mineral occurrences were extracted from the Nova Scotia Department of Natural Resources Mineral Occurrence Database, most of which are gold occurrences. It is important to note here that although these are defined as gold occurrences in the database, there is a known association of gold with sulphide mineralization. Therefore, for this study, these locations are considered to be sulphide mineral occurrences and the presence or absence of gold is not important in this context. The remaining sulphide mineral occurrences were either selected from a

variety of sources including Hingston (1985) and King (1994), or were areas visited during the course of study (Chapter 2). The underlying assumption for all the mineral occurrences used here is that all sulphide minerals are treated the same (i.e., there is no attempt to distinguish between pyrrhotite, pyrite, or chalcopyrite).

Evidence maps used in weights of evidence modelling are usually reduced to binary form through a process of pattern optimization. For the five input maps used as evidence for this study, three (proximity to anticlines, proximity to GHT, and vertical gradient magnetics) were optimized in order to maximize the spatial association between the sulphide mineral occurrences and the predictor pattern of the evidence map. The optimization process involves calculating weights for each successive class, using cumulative areas and the number of sulphide mineral occurrences in each class. For each class, the contrast, C, is then calculated which represents the measure of association between the pattern and mineral occurrences. Table 7.5 shows the results using an example for the proximity to anticline map. The table shows the cumulative area, number of occurrences, positive (w+) and negative (w-) weights, and contrast for each class. The total land area is 8121.37 km^2 for the study area. Figure 7.6 shows a plot of contrast against distance showing that the maximum contrast value occurs at a distance of 0.25 km (class 1) from the center of anticlines. This indicates that the highest spatial association occurs within 0.25 km of anticlines and a binary map is produced using this 0.25 value as the optimum threshold value between pattern present and pattern absent.

For the two categorical maps (geology and regional metamorphism), the class

Table 7.5 Summary of weights for cumulative distances from the center of major anticline structures using a unit cell of 1 km^2. The contrast (C) has a maximum value at a distance of 0.25 km from the center (at class 1).

Class	Distance	Cumulative Area (km^2)	Cumulative Sulphide Occurrences	w+	w-	C
1	**0.25 km**	**506.19**	**18**	**0.89**	**-0.10**	**0.99**
2	1.0 km	2031.46	51	0.53	-0.26	0.80
3	2.0 km	3808.57	73	0.26	-0.30	0.55
4	3.0 km	5045.05	88	0.16	-0.33	0.49
5	4.0 km	5749.78	99	0.15	-0.48	0.63
	>4.0	Total = 8121.37	121			

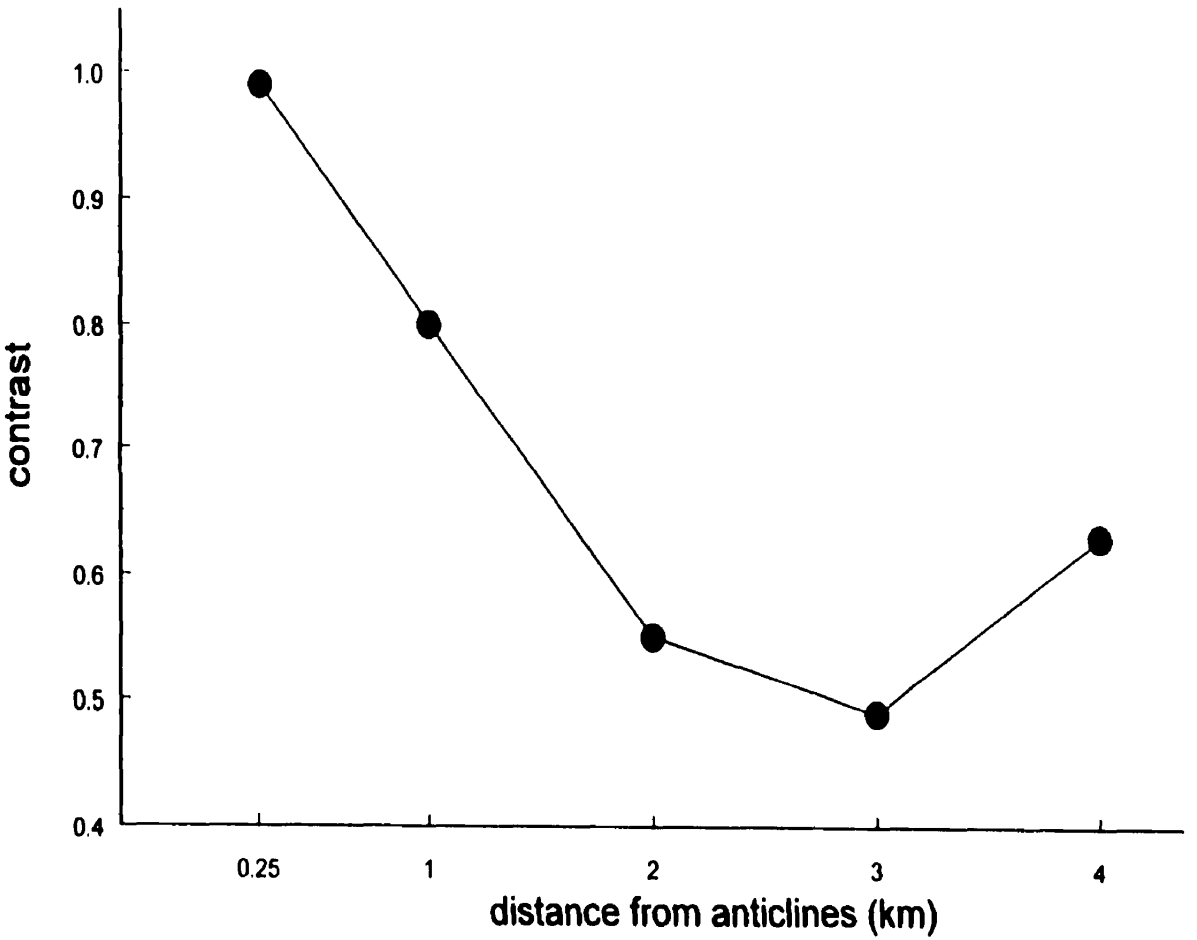

Figure 7.6. Graph of contrast versus distance from anticlines. The maximum contrast occurs at 0.25 km, which is taken as the cutoff between binary classes for this evidence map.

corresponding to the highest contrast value was chosen to represent 1, and all other classes within each map were taken as 0, in order to produce the binary maps. A summary of the calculations showing class, positive and negative weights, and contrast values for all five evidence maps are shown in Table 7.6. The calculations were performed in spreadsheet format following the computer program presented in Appendix 2 of Bonham-Carter (1994). Several published examples were used to check the spreadsheet calculations.

The weights of evidence model equation used to calculate posterior probabilities is presented in Appendix D. The final posterior probability map (or ARD potential map) showing areas that are favourable for the generation of ARD is presented in Figure 7.3.

7.7 Comparison Of Favourability Maps

The results of the three modelling techniques, Boolean logic, fuzzy logic, and weights of evidence, show some broad similarities. Figure 7.7 shows four areas (numbered 1 to 4) that have been visited during the course of this study and are known to have ongoing ARD problems. All four areas have been outlined by all the modelling methods used in this study, and show either moderate to high ARD potential. All four areas are associated with rocks belonging to the Halifax Group and/or the GHT, and as well, are in high magnetic areas. Conversely, within the study area, there are no areas that are known to have ARD, that have been defined as having low ARD potential by any of the methods. However, it is important to note that this should not be taken as the

Table 7.6 Summary of weights of evidence calculations determined for each input evidence map. The positive and negative weights are used in the model equation (Appendix D) to generate a posterior probability map showing ARD potential. Using geology as an example, the positive weight 0.92 is used for pattern present, and the negative weight -0.37 is used for pattern absent in the binary map.

Class	Class Description	Positive Weight (w+)	Negative Weight (w-)	Contrast (C)	Evidence Map
4	Halifax Group	0.92	-0.37	1.29	geology
1	within 0.25 km	0.89	-0.10	0.99	anticlines
3	high	0.55	-0.12	0.67	magnetics
2	biotite facies	0.18	-0.16	0.34	regional metamorphism
1	within 0.5 km	0.22	-0.03	0.25	GHT

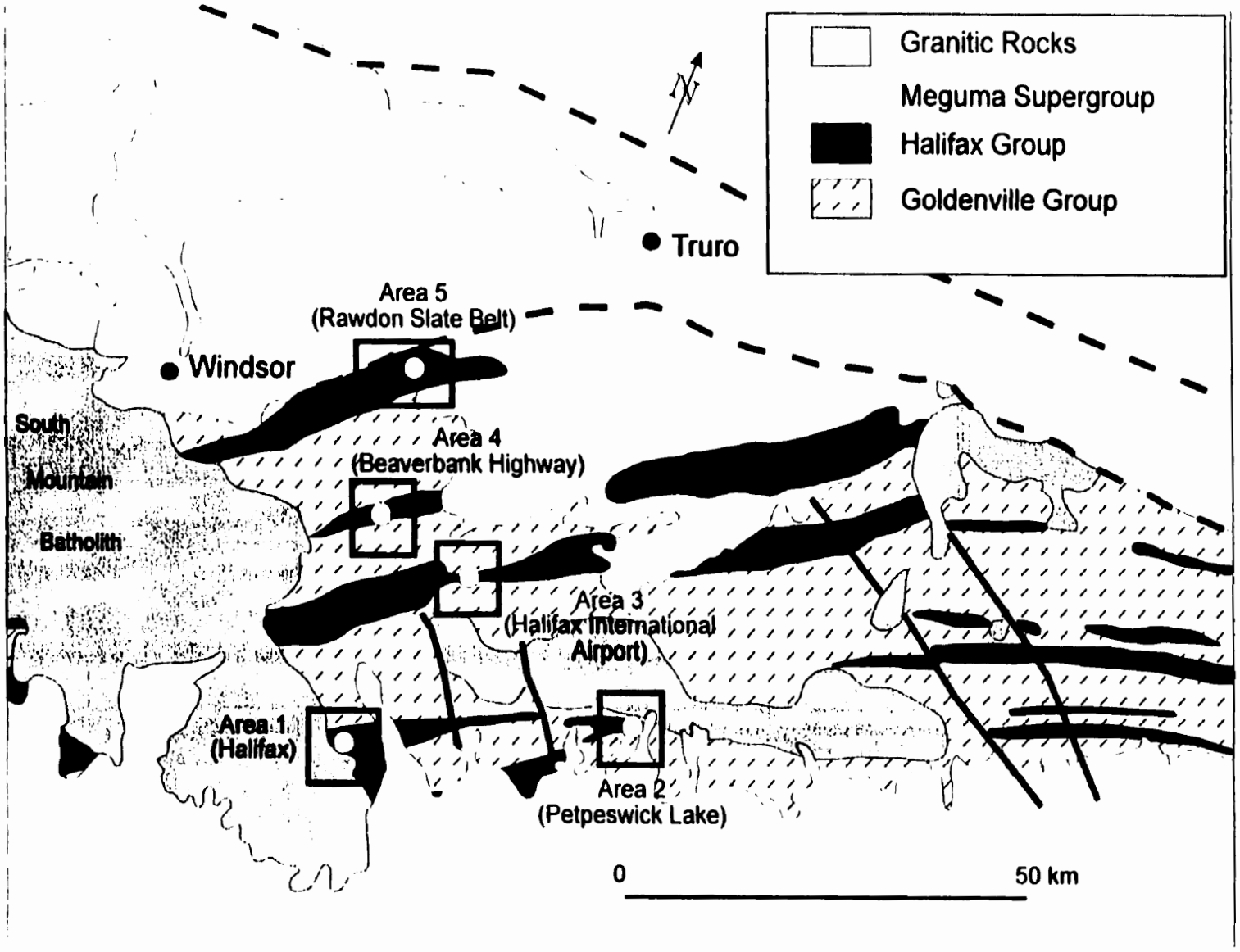

Figure 7.7. Geological map showing location of four ARD sites (numbered 1 to 4). Location 5 discussed in text (geology modified from Keppie, 1979a).

final analysis. For example, in theory, ARD could develop in the Goldenville Group where there is extensive pyrite mineralization that is not associated with either a gold occurrence or anticlines. In such a case, based on the evidence used in this study, the area could be defined as having low ARD potential. Similarly, pyrite or marcasite mineralization in the Halifax Group, that is not associated with magnetic pyrrhotite, and not close to the GHT, could be defined as having low ARD potential.

Comparing the results of the three modelling methods also reveals some major differences. This is especially important in comparing the results of the Boolean logic method with the results of either the fuzzy logic or weights of evidence methods. For the Boolean logic method, evidence is assigned either a "yes" or "no" value, and the resulting map shows either ARD potential or no ARD potential. However, for the fuzzy logic and weights of evidence methods, ARD potential is ranked (or scaled) from low to high. The result of these differences means that some areas on the Boolean map are defined as having no ARD potential, whereas for the fuzzy logic or weights of evidence maps, the areas are defined as having at least some ARD potential. An example of this occurs at the center of area 5 on Figure 7.7, which shows no ARD potential in the Boolean logic model (Fig. 7.3 A) but is defined as having at least moderate ARD potential in the fuzzy logic and weights of evidence models (Figs. 7.3 B and C). The rocks in this area belong to the Halifax Group, are not highly magnetic, and there are no major anticlines at this location (Fig. 7.2 C). Such areas should be interpreted with caution and more detailed work is necessary. This is a clear example showing that it is important to use all available data to assess ARD potential, and that no single method is

the best. The Boolean method should not be used by itself without comparing the results to the fuzzy logic and weights of evidence methods.

This leads to the final question as to how the ARD potential maps should be used. The intention is that they be used in a broad, regional sense, as a "first pass" indication of possible ARD areas. For example, this could be important in the initial planning stages of major construction activities such as the building of a pipeline or highway. Areas that show high ARD potential should be viewed as requiring further detailed work, and it is likely that such areas would eventually require drilling and detailed sampling for chemical analyses. It is also likely that plans would be required for ARD remediation and/or prevention. Areas defined as having medium to low ARD potential are not guaranteed to be "safe" and may still require more detailed analysis. One of the most important aspects of determining if a specific area has the potential to produce ARD is geological mapping. This can be done on any scale from reconnaissance to detailed, and should always be performed in any ARD study.

7.8 Summary And Conclusions

Each of the map modelling techniques, Boolean logic, fuzzy logic, and weights of evidence, used in this study have advantages and disadvantages. The Boolean logic method is simple and easy to apply, but it is not flexible in its ability to assign weights for different classes. The output map shows only those areas that have ARD potential or do not have ARD potential . There is no flexibility in assigning "possible" or "maybe" areas. This approach would be the best method if every factor concerning

ARD potential was known. However, it is important to note that there are still many uncertainties with respect to the generation of ARD and there is plenty of scope for further work in defining what factors affect ARD potential in the Meguma Supergroup.

The fuzzy logic technique is more flexible in its ability to assign weights to individual evidence maps and map classes. This knowledge-driven technique is better than the Boolean method in its ability to handle uncertain or imprecise data. Through the use of the fuzzy membership function, each of the evidence layers can be assigned values so that the importance of each layer is ranked. The fuzzy logic method is also relatively simple to use and easy to implement, but is also robust. Complex inference engines can be implemented depending on the complexity of the problem to be solved.

The weights of evidence method is the only technique used in this study that is entirely driven by the data used, and offers a good comparison to the expert-driven, Boolean and fuzzy logic methods. The posterior probability map showing ARD potential, defines similar "high-risk" areas compared to the expert-driven techniques. However, the method relies on the known location of sulphide mineral occurrences to calculate weights for each evidence layer, and may not be appropriate in situations where there is a limited number of known occurrences. The method also requires that the evidence layers be conditionally independent which is assumed in this study. This is a limitation in this study and generally should be checked for as one of the steps in the weights of evidence modelling procedure.

In all maps produced by the techniques presented in this thesis, in general the areas showing the highest potential to develop ARD are associated with the Halifax

Group and/or the GHT, and are areas having the highest magnetic signatures. This results from the presence of monoclinic pyrrhotite that is well-known to be problematic for producing ARD. However, as a final caution, there are no guarantees that all possible ARD producing areas have been outlined, and in the final analysis the prediction of ARD potential should always include the decisions of experts.

Chapter 8

Conclusions And Future Work

1) By far, the predominant sulphide mineral in the samples of sulphidic slates from the lower Halifax Group examined in this study is pyrrhotite. Also present, in lesser amounts are: pyrite, marcasite, chalcopyrite, arsenopyrite and sphalerite. Microprobe data indicate that the pyrrhotite is mainly the monoclinic variety (Fe_7S_8). The compositions of all pyrrhotite crystals probed are between 45.5 and 47.5 atomic % Fe, in the ideal monoclinic pyrrhotite range. Data from pyrrhotite in drill core samples from the Halifax International Airport also suggest the pyrrhotite is predominantly monoclinic Fe_7S_8. Common impurities in the pyrrhotite, detected with the microprobe, are Ni, Co, and As.

XRD analyses of pyrrhotite from five samples show typical, almost equal intensity double peaks, indicative of monoclinic pyrrhotite. These data confirm the results of the microprobe work. Comparisons of pyrrhotite compositions among samples taken from different geological settings (i.e., within and outside the contact metamorphic aureoles of granitic intrusions) suggest there is little to no regional variation in pyrrhotite composition.

2) Detailed image analyses of pyrite, monoclinic and hexagonal pyrrhotite, arsenopyrite, galena, and sphalerite, at various stages of oxidation over a six week period, has led to important information about the controls of reactivity rates. Galvanic

interactions play a significant role, especially in the galvanic protection of chalcopyrite within pyrrhotite. Pyrite and arsenopyrite, when in contact with pyrrhotite, may also be galvanically protected, although these occurrences are much rarer than that of chalcopyrite within pyrrhotite.

Crystal lattice affects (e.g., intergrowth textures, crystal orientations, subgrain boundaries) are also significant. Lamellar intergrowth textures have been observed within pyrrhotite and possibly marcasite, and both minerals react significantly faster relative to pyrite, arsenopyrite, chalcopyrite, and sphalerite, all of which have smooth surfaces. The intergrowth texture is crystallographically controlled and differential oxidation occurs between lamellae and host. Subgrain formation is well developed in all pyrrhotite aggregates, and in some arsenopyrite observed in this study. Different subgrains oxidize at different rates, and subgrain boundaries appear to be more highly oxidized then the subgrain centers.

The presence of bacteria has the overall affect of increasing the reaction rates for most sulphide minerals studied. In general, the order of reactivity between sterile and microbial treatments did not change with the exception of monoclinic and hexagonal pyrrhotite. Hexagonal pyrrhotite, containing more iron than the monoclinic type, oxidized faster in the presence of bacteria, possibly reflecting an enhanced oxidation of ferrous to ferric iron.

3) The secondary minerals resulting from sulphide oxidation can be properly identified, and due to their different solubilities, an effort should always be made in this

direction. The seasonal variations in iron and sulphate in any given system will depend on the abundance and type of secondary minerals. Any attempt at geochemical modelling of ARD must include the formation of these unstable secondary minerals. Trace element distributions can also be affected by secondary mineral precipitation, oxidation, and dissolution.

4) In general, rocks in the Meguma Supergroup contain little neutralizing potential. In places where the neutralizing potential is significant, further mineralogical studies should be undertaken to access the type of carbonate minerals present. Iron and manganese carbonates are common, especially within the GHT, and the overall presence of carbonate minerals should not be used as a "safe" indicator that the rocks will not be net acid-generating. The most common sulphide mineral present in the Halifax Group is monoclinic pyrrhotite. The reaction rate of this mineral is relatively fast and, in the field, acidity can be produced quickly in the short term. Because of the low neutralizing potential, the rocks do not have significant capacity to neutralize the acid produced. This leads to surges of acidity which can lead to fish kills and degradation of surrounding ecosystems.

In the rocks examined in this study, differences between NP values determined by the Sobek method and the BCRIT method are interpreted to be of little significance, mainly because of the overall low NP values. Detailed mineralogical analyses should always be performed in conjunction with any static test program, and can aid in the overall interpretation of the potential for rocks to be net acid-generating.

5) Reconnaissance geophysical surveys on two grids near Halifax International Airport have demonstrated that conductivity and magnetic surveys can define zones of sulphide mineralization within bedrock of the lower Halifax Group. This has been demonstrated by chemical analyses of rock samples excavated from test pits located on selected geophysical anomalies. Increased levels of total sulphur were measured at nearly all test pits where terrain conductivity and magnetic anomalies (derived from magnetic pyrrhotite) are present.

6) GIS map modelling has proven to be an effective method of outlining areas within the Meguma Supergroup that may cause acid rock drainage in the future. Boolean modelling is simple and easy to apply, but is not flexible in its ability to assign weights for different classes. The output map shows only those areas that have the highest possibility of producing ARD, however, this approach is still very useful for land use planning purposes. It can give an indication as to where the "worst-case" areas within the Meguma Supergroup exist, and would be an important step in a preliminary analysis for ARD prediction.

The fuzzy logic technique is much more flexible in its ability to assign weights to individual maps and map classes. This knowledge-driven technique is better than the Boolean method in its ability to handle uncertain or imprecise data. Through the use of the fuzzy membership function, each of the evidence layers can be assigned values so that the importance of each layer is ranked. The fuzzy logic method is also relatively simple to use and easy to implement, but is also robust. Complex inference engines can

be implemented depending on the complexity of the problem to be solved.

The posterior probability map produced by the data-driven, weights of evidence method appears to give good results based on what is known about existing ARD areas studied in this thesis. The weights of evidence map also shows similar "high-risk" areas compared to the expert-driven techniques.

In all maps produced by the techniques presented in this thesis, in general the areas showing the highest potential to develop ARD are associated with the Halifax Group and/or the GHT, and are areas having the highest magnetic signatures. This results from the presence of monoclinic pyrrhotite that is well-known to be problematic for producing ARD.

7) It is clear that an accurate prediction of the intensity and duration of acid rock drainage must involve a detailed study of the minerals involved, because many of the controls are mineralogically related and site-specific. Whether or not ARD actually occurs in any given area depends on numerous factors and can only be assessed on a site-specific basis. Thorough sampling and accurate testing to predict ARD potential, including detailed mineralogical studies, are an essential step in land use planning throughout the Meguma Supergroup, and any other regions that contain sulphide-bearing bedrock.

Future considerations should include the following:

1) detailed sulphide mineral paragenesis correlated with individual formations

throughout the Meguma Supergroup. This would allow for better prediction capabilities based on geology and stratigraphy. Also, a detailed account of mineral textures, including exsolution intergrowth textures should be performed. This aids in the interpretation of the metamorphic history of the rocks, and also helps predict where certain types of sulphide minerals may occur (e.g., in cleavage planes).

2) For reactivity rate experiments it would be useful to measure iron and sulphate release into solution in order to better understand the mechanism of dissolution. Such measurements could also include any trace elements that may be present.

3) An expanded database of secondary mineralogy is essential to understand the sources and sinks of both major and trace elements in the field. First, more samples for basic mineral identification is required. Second, trace element distributions in the secondary minerals should be measured. A sample collection program should be based on seasonal variation in order to understand the precipitation and dissolutions reactions involved in wetting and drying periods.

4) An expanded geophysical survey combined with adequate bedrock sampling for mineralogy and geochemistry is required to confirm the correlation between geophysical anomalies and bedrock sulphide mineralization.

Appendix A

Methodologies for the BC Research Initial Test (BCRIT) and the Sobek Method (EPA - 600 Method) for acid-base accounting

BC Research Initial Test (BCRIT) Procedure

(Bruynesteyn and Duncan, 1979)

1. Initial Test

(a) Sample - The sample selected must be taken in such a manner that it is truly representative of the type of mineralization being examined. A composite made up of split drill core or of randomly selected grab samples should be satisfactory. The number of samples to be examined will depend on the variability of the mineralization and must be left to the discretion of the geologist taking the samples. The bulk sample is crushed to a size which can be conveniently handled, (i.e., -2 inch) and then thoroughly mixed and approximately a 2 lb portion split out, using the usual coning and quartering technique. This sample is then pulverized to pass a 100 mesh screen and used for assay, the titration test, and the confirmation test if necessary.

(b) Assay - The pulverized sample is assayed in duplicate for total sulphur. The use of a Leco furnace is recommended, although a chemical oxidation technique followed by barium sulphate precipitation is satisfactory. The total sulphur assay value is expressed as pounds of sulphuric acid per ton of sample, assuming a 1:1 conversion factor, which is the acid-producing potential of the sample.

(c) Titration Test - Duplicate 10 gram portions of the pulverized sample are suspended in 100 ml of distilled or de-ionized water and stirred for approximately fifteen minutes. The natural pH of the sample is then recorded and the sample titrated to pH 3.5 with 1.0 Normal sulphuric acid and left stirring. If an automatic titrator is used the test is continued until less than 0.1 ml of acid is added over a 4 hour period. If manual titration is used, the addition of acid is repeated every half-hour (approximately) until the pH change

over a 4 hour period is 0.1 pH unit or less. The total volume of acid added is recorded and converted to lbs per ton of sample. This is the acid consuming ability of the sample, ie:

For a 10 gram sample:
acid consuming ability (or NP) (kg / tonne) = mL 1.0N H_2SO_4 * 4.9

(d) Interpretation - If the acid consuming value (in kg of acid per tonne of sample) exceeds the acid-producing potential (kg per tonne) then the sample will not be a source of acid mine drainage and no additional work is necessary. If the acid consumption is less than the acid-producing potential, the possibility of acid mine water production exists and the confirmation test should be conducted.

Sobek Method (EPA - 600 Method)

(Sobek et al., 1978; taken from Price, 1997)

During digestion, do not boil samples. If boiling occurs, discard sample and rerun. Before titrating with acid, fill buret with acid and drain completely. Before titrating with base, fill buret with base and drain completely to assure that free titrant is being added to the sample.

Chemicals

1) Carbon dioxide-free water: Heat distilled water just to boiling in the beaker. Allow to cool slightly and pour into a container equipped with ascarite tube. Cool to room temperature before using.

2) Hydrochloric acid (HCl) solution, 0.1 N certified grade.

3) Sodium hydroxide (NaOH), approximately 0.5 N: Dissolve 20.0 g of NaOH pellets in carbon dioxide-free water and dilute to 1 liter. Protect from CO_2 in the air with ascarite tube. Standardize solution by placing 50 mL of certified 0.1 N HCl in a beaker and titrating with the prepared 0.5 N NaOH until a pH of 7.00 is obtained. Calculate the normality of the NaOH using the following equation:

   N2 = (N1V1)/V2, where:
   V1 = Volume of HCl used.
   N1 = Normality of HCl used.
   V2 = Volume of NaOH used.
   N2 = Calculated normality of NaOH.

Note: Other methods of standardizing prepared NaOH solution, such as the use of triplicate accurately weighed samples of potassium acid phthalate, can be employed and should be consistent with a laboratory's QA/QC procedures.

4) Sodium hydroxide (NaOH) approximately 0.1 N: Dilute 200 mL of 0.5 N NaOH with carbon dioxide-free water to a volume of 1 liter. Protect from CO_2 in air with ascarite tube. Standardize solution by placing 20 mL of certified 0.1 N HCl in a beaker and titrating with the prepared 0.1 N NaOH until a pH of 7.00 is obtained. Calculate the normality of the NaOH using the equation in No. 3 above.

Note: Other methods of standardizing prepared NaOH solution, such as the use of triplicate accurately weighed samples of potassium acid phthalate, can be employed and should be consistent with a laboratory's QA/QC procedures.

5) Hydrochloric acid (HCl,) approximately 0.5 N: Dilute 42 mL of concentrated HCl to a volume of 1 liter with distilled water. Standardize solution by placing 20 mL of the known normality NaOH prepared in No. 3 above in a beaker and titrating with the prepared HCl until a pH of 7.00 is obtained. Calculate the normality of the HCl using the following equation:

N1 = (N2V2)/V1, where:
V2 = Volume of NaOH used.
N2 = Normality of NaOH used.
V1 = Volume of HCl used.
N2 = Calculated normality of HCl.

6) Hydrochloric acid (HCl), approximately 0.1 N: Dilute 200 mL of 0.5 HCl to a volume of 1 liter with distilled water. Standardize solution as in step 5 above, but use 20 mL of the known normality NaOH prepared in No. 4 above.

7) Hydrochloric acid (HCl), 1 part acid to 3 parts water: Dilute 250 mL of concentrated HCl with 750 mL of distilled water.

Materials

1) Flasks, Erlenmeyer, 250 mL.

2) Buret, 100 mL (one required for each acid and one for each base).

3) Hot plate, steam bath can be substituted.

4) pH meter equipped with combination electrode.

5) Balance, can be read to 0.01 g.

Procedure

1) Place approximately 0.5 g of sample (less than 60 mesh) on a piece of aluminum foil.

2) Add one or two drops of 1:3 HCl to the sample. The presence of $CaCO_3$ is indicated by a bubbling or audible "fizz".

3) Rate the bubbling or "fizz" in step 2 as indicated in Table 1.

Table 1: Volumes and Normalities of Acid Addition for NP Determination Based on Fizz Rating

Fizz Rating	Add mL of HCl	Normality of Added HCl
None	20	0.1
Slight	40	0.1
Moderate	40	0.5
Strong	80	0.5

4) Weigh 2.00 g of sample (less than 60 mesh) into a 250 mL Erlenmeyer flask.

5) Carefully add HCl indicated by Table 1 into the flask containing sample.

6) Heat nearly to boiling, swirling flask every 5 minutes, until reaction is complete. Note: Reaction is complete when no gas evolution is visible and particles settle evenly over the bottom of the flask.

7) Add distilled water to make a total volume of 125 mL.

8) Boil contents of flask for one minute and cool to slightly above room temperature. Cover tightly and cool to room temperature. CAUTION: Do not place rubber stopper in hot flask as it may implode upon cooling.

9) Titrate using 0.1 N NaOH or 0.5 N NaOH (concentration exactly known) to pH 7.0 using a pH meter and buret. The concentration of NaOH used in the titration should correspond to the concentration of the HCl used in No. 5 above. NOTE: Titrate with NaOH until a constant reading of pH 7.0 remains for at least 30 seconds.

10) If less than 3 mL of the NaOH is required to obtain a pH of 7.0, it is likely that the HCl added was not sufficient to neutralize all of the base present in the 2.00 g sample. A duplicate sample should be run using the next higher volume or concentration of acid as indicated in Table 1.

11) Run a blank for each volume or normality of acid using steps 5, 7, 8, and 9 above.

Calculations

1) Constant (C) = (mL acid in blank) / (mL base in blank).

2) mL acid consumed = (mL acid added) - (mL base added multiplied by C).

3) Neutralization Potential (as t $CaCO_3$ equivalent/1000 t material) = (mL of acid consumed) * (25.0) * (N of acid).

Interpretation of Results

Effective Field-NP is a site-specific value, estimated through static and kinetic tests as explained above and in Chapter 8 and 10 of Price (1997). Nevertheless, some general interpretation guidelines are available.

1) All Lab-NP procedures underestimate Field-NP where aluminosilicate minerals are sufficiently reactive and alone provide effective neutralization (Morin and Hutt, 1994 and 1997). In these cases, NP should be calculated from whole-rock, multi-element and mineralogical data.

2) For carbonate systems, studies in British Columbia have shown that the NP method of Sobek et al. (1978) may slightly overestimate Field-NP (e.g., Minesite Drainage Assessment Group, 1996).

Appendix B

Location map and stratigraphic descriptions for MF samples (Beaverbank Highway samples) and CB samples (Caribou drill core).

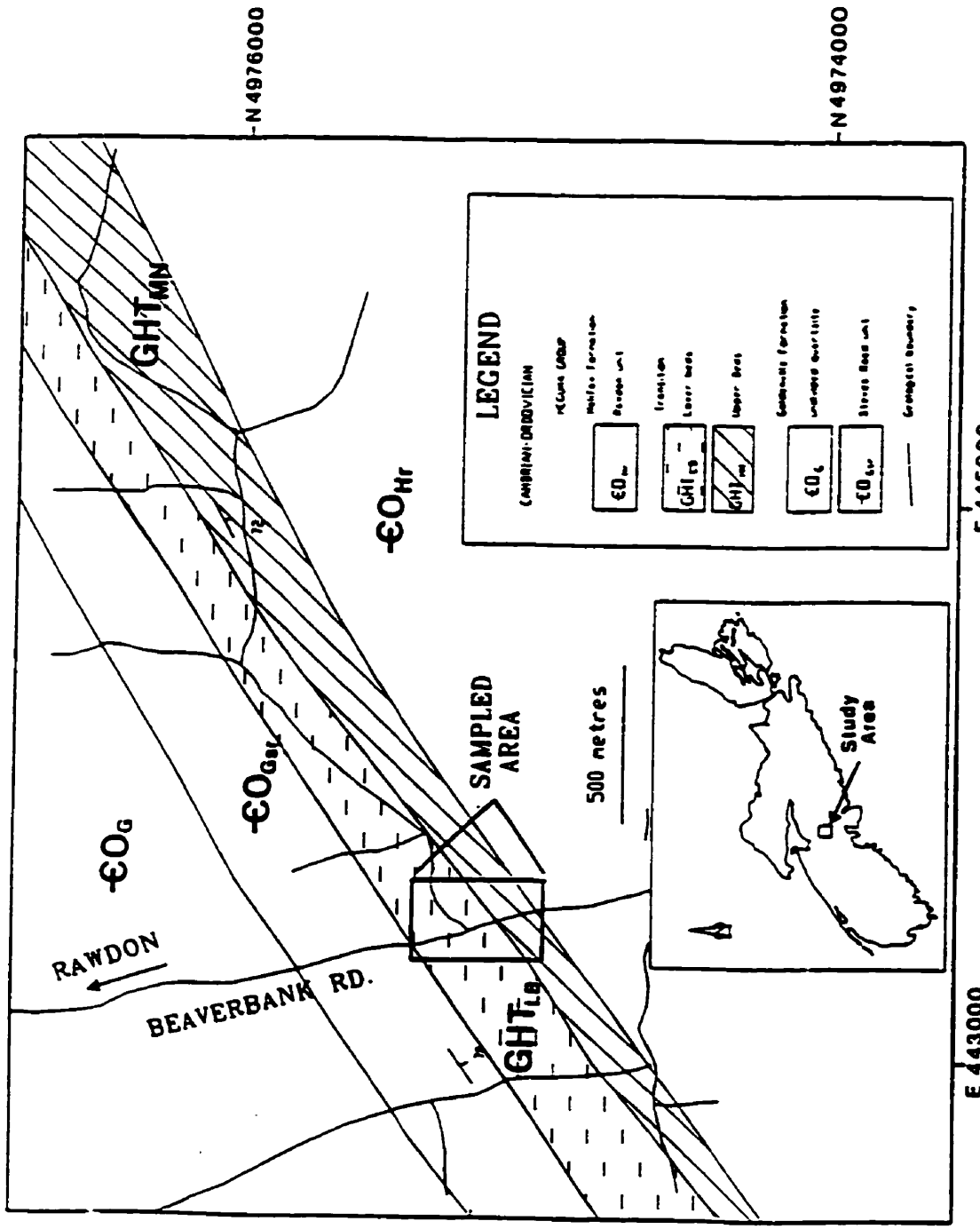

Location map for geochemical rock samples (MF samples), Beaverbank Highway section (taken from Feetham, 1996).

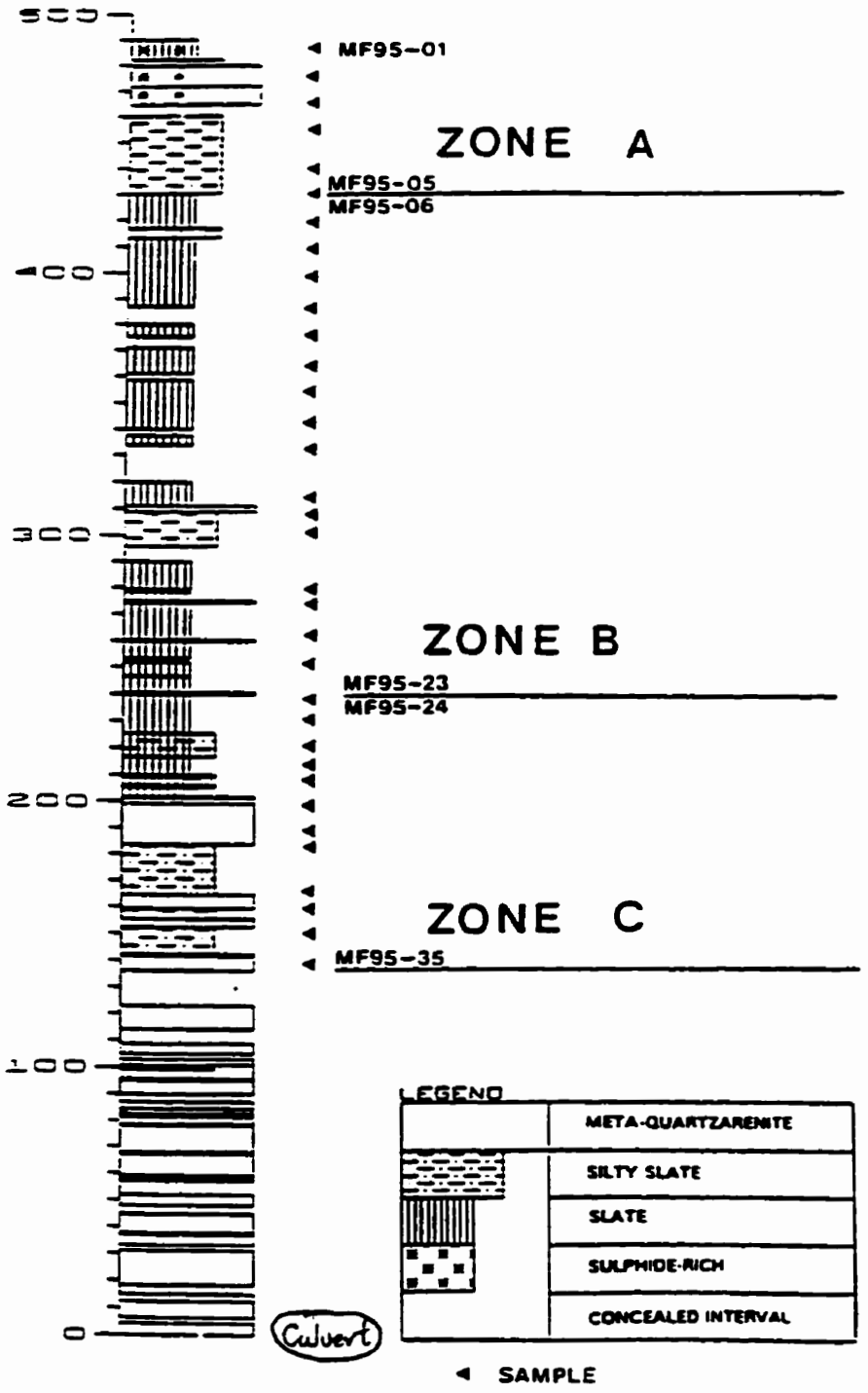

Stratigraphic section of Beaverbank Highway site showing location of MF samples to lithostratigraphic zones (taken from Feetham, 1996).

Drillhole Details for LL81-5A

Property: Lake Mine	Latitude: 8+00 S	Angle: -75°
Claim: 57-B	Longitude: 6+00 W	Core Diameter: NQ
Reference Map: 11E/2B	Bearing: 350° from magnetic north	Total Depth: 628.80 m

Units Present in LL81-5A

Unit	Drilling Depth (m)	Stratigraphic Thickness (m)		Description
overburden	0.00-3.40			
C	3.40-465.50 (top absent)	351		fining upward sequences of pyrrhotitic, in-part carbonate-rich metasiltstones and carbonaceous slate
B	465.50-589.18	113	32	coticule- and nodule-rich lithologies, similar to those noted directly below
			56	interbedded chloritic, pyrrhotitic meta-argillites and very fine- to fine-grained metawacke
			25	monotonously interbedded chloritic, pyrrhotitic silty slates
A	589.18-628.80 (bottom absent)	36		fining upward sequences of metawackes and silty slates

Drillhole details for Caribou drill core (CB samples) showing stratigraphic description and thicknesses (taken from Burns, 1997).

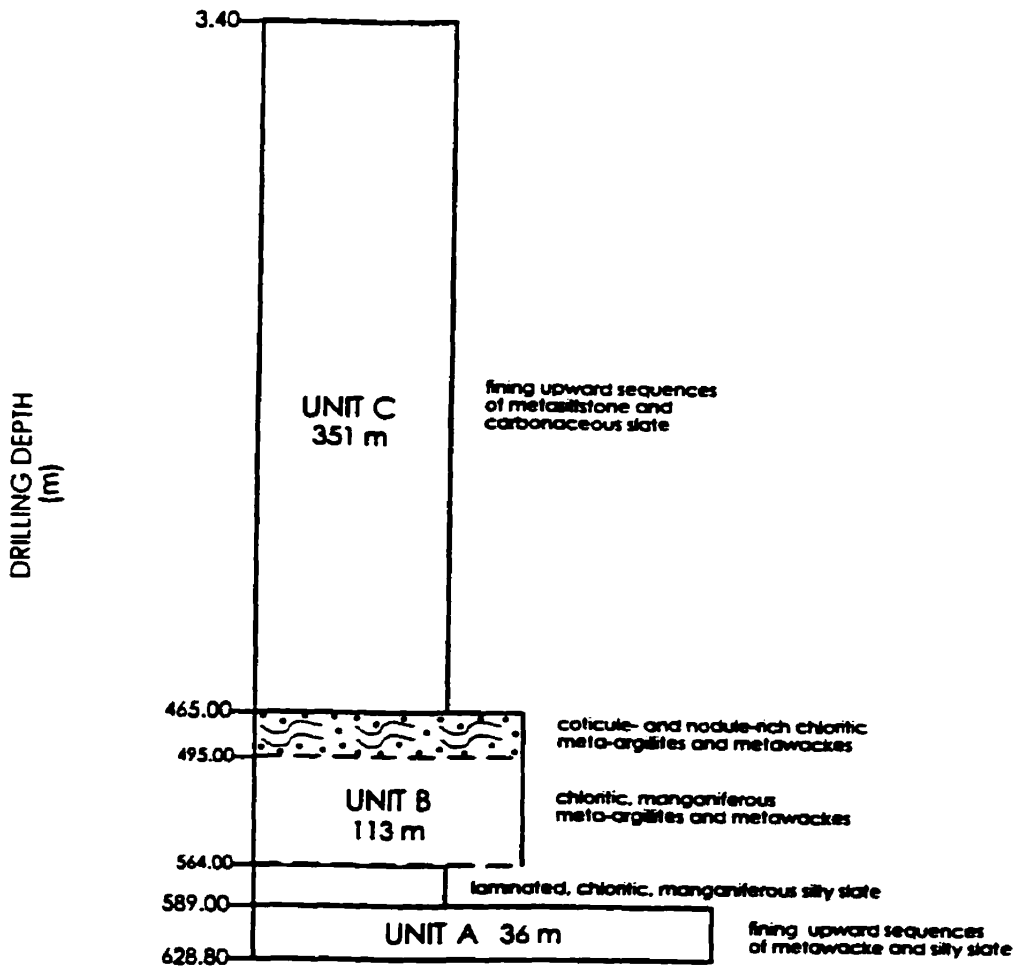

Stratigraphic section for the Caribou drill core (taken from Burns, 1997).

Sample	Depth (m)	Description	Thin Section Produced	Microprobed	Unit
LL81-5A-005-01	029.10-028.96	carbonaceous slate with a large quantity of cleavage-parallel pyrrhotite blebs	Yes	Yes	C
LL81-5A-013-01	075.75-075.50	highly folded, laminated, pyrrhoutic, medium-grained metasiltstone	Yes	No	C
LL81-5A-017-01	095.42-095.27	thin-bedded, fining upward sequences, consisting of convoluted parallel- and ripple cross laminated, pyrrhotitic metasiltstone overlain by muddy, parallel-laminated meta-argillite and capped by carbonaceous slate	No	No	C
LL81-5A-020-01	113.81-113.70	pyrrhotitic, carbonaceous silty slate with an interbed of pyrrhotitic, very fine-grained metasiltstone.	Yes	Yes	C
LL81-5A-034-01	195.56-195.43	folded, silty, carbonaceous slate and very fine-grained metasiltstone, with pyrrhoutic, fine-grained metawacke ball and pillow structures	Yes	No	C
LL81-5A-042-03	237.96-237.84	alternating pyrrhotitic parallel-laminations of carbonate-rich, very fine-grained metawacke and carbonaceous slate, grading into an interval of pyrrhotitic, carbonate-rich metawacke, showing rusty staining in hand sample	Yes	No	C
LL81-5A-042-02	241.01-240.92	parallel-laminated, medium-grained metasiltstone with a crosscutting carbonate-pyrrhotite vein showing normal offset	Yes	No	C
LL81-5A-043-02	242.83-242.68	typical carbonaceous, grey silty slate with pyrrhotitic, fine-grained metasiltstone and fine-grained metasiltstone ball structures	Yes	No	C
LL81-5A-047-01	266.46-266.34	carbonaceous, arsenopyrite- and pyrrhoutite-rich slate with minor cone-in-cone-type structures	Yes	Yes	C
LL81-5A-053-02	301.37-301.25	carbonaceous slate interbedded with pyrrhotitic metasiltstone	No	No	C
LL81-5A-053-01	299.72-299.62	convoluted parallel- and ripple cross-laminated, pyrrhotitic, medium-grained metasiltstone	Yes	No	C
LL81-5A-065-01	368.65-368.51	carbonaceous slate with pyrrhotitic, fine-grained metasiltstone interbeds	Yes	No	C
LL81-5A-072-01	410.14-409.95	pyrrhotitic, extremely carbonate-rich, carbonaceous slate with cone-in-cone-type structures	Yes	Yes	C
LL81-5A-081-02	461.88-461.72	carbonaceous slate with pyrrhotitic medium-grained metasiltstone interbed	Yes	Yes	C
LL81-5A-082-02	467.76-467.60	chloritic silty slate with coticules	Yes	Yes	B
LL81-5A-082-01	471.73-471.58	coticule- and nodule-rich, chloritic silty slate,	No	No	B
LL81-5A-084-01	475.10-474.96	chloritic silty slate with coticules and nodules	Yes	No	B
LL81-5A-086-02	485.61-485.42	contorted coticule within chloritic silty slate	No	No	B

Sample descriptions (CB samples) for the Caribou drill core (taken from Burns, 1997).

Sample	Depth (m)	Description	Thin Section Produced	Microprobed	Unit
LL81-5A-091-01	513.20-513.07	parallel-laminated, chloritic, pyrrhotitic, fine-grained metasiltstone overlain by chloritic, pyrrhotitic, medium-grained metasiltstone	Yes	No	B
LL81-5A-093-01	528.64-528.57	chloritic silty slate overlain by convoluted ripple cross- and parallel-laminated metasiltstone	No	No	B
LL81-5A-095-01	536.48-536.34	chloritic silty slate with poorly-developed cotcules	Yes	Yes	B
LL81-5A-101-01	571.95-571.82	chloritic, pyrrhotitic silty slate	Yes	No	B
LL81-5A-105-01	598.71-598.55	carbonate-rich, medium-grained metawacke overlain by silty slate	No	No	A
LL81-5A-107-01	607.04-606.91	carbonate-rich, fine-grained metawacke with a silty slate interbed	Yes	Yes	A
LL81-5A-110-02	627.80-627.70	chloritic silty slate with carbonate- and muscovite- filled fractures throughout, similar to chloritic silty slate seen in Unit B	Yes	No	A

Sample descriptions (CB samples) for the Caribou drill core (taken from Burns, 1997).

Appendix C

Methods for determining the parameters in the following table (terminology mainly from Price, 1997).

G) fizz = method in Appendix A
H) crushed (paste) pH = pH measurement of paste made by adding distilled water to powdered sample

I) total S = LECO titration (Daltech - C. Cole)
J) sulphide S = total S after HCl treatment minus total S after HNO_3 treatment
K) sulphate S = total S minus total S after HCl treatment
L) $BaSO_4$ S = insoluble sulphate S = barium as %Ba from metal analyses • (32.06/137.34)
M) organic S = total S after HNO3 treatment minus $BaSO_4$ S
N) del S (sulphur discrepancy) = total S - (sulphate S + $BaSO_4$ S + sulphide S + organic S)

O) AP (acid potential) = calculated by (sulphide S + del S • 31.25)
P) TAP (total acid potential) = calculated by (Total S * 31.25)

Q) Sobek NP = method in Appendix A (Daltech - C. Cole)
R) BC Research = method in Appendix A (Daltech - C. Cole)

S) total C (as % C) = LECO titration (Daltech - C. Cole)
T) total C (as % CO_2) = total C (as C) • 3.6642
U) organic C (as % C) = LECO titration after acid leach (Daltech - C. Cole)
V) organic C (as %CO_2) = organic C (as C) • 3.6642
W) carbonate C (as CO_2) = total C (as CO_2) - organic C (as CO_2)

X) Carb NP = carbonate C • (100.09/44.01) • 10
Y) NNP (net neutralization potential) = Sobek NP - AP
Z) TNNP (total net neutralization potential) = Sobek NP - TAP
AA) CNNP (carbonate net neutralization potential) = Carb NP - AP
AB) CTNNP (carbonate total net neutralization potential)= Carb NP - TAP
AC) NPR (neutralization potential ratio) = Sobek NP / AP
AD) TNPR (total neutralization potential ratio) = Sobek NP / TAP
AE) CNPR (carbonate neutralization potential ratio) = Carb NP / AP
AF) CTNPR (carbonate total neutralization ratio) = Carb NP / TAP

A	B	C	D	E	F	G	H	I	J	K
4	Sample	Hole No.	From	To	Location	Fizz	Crushed	Total -S	Sulphide-S	Sulphate-S
5							(Paste)	(%)	(%)	(%)
6							pH			
7	CR-95-001				Bayers Lake	none	5.75	1.25		
8	CR-95-002				Bayers Lake	none	4.80	2.34		
9	CR-95-003				Bayers Lake	none	5.70	0.93		
10	CR-95-004				Mount Uniacke	none	3.40	2.41		
11	CR-95-005				Mount Uniacke	none	3.80	1.38		
12	CR-95-006				Mount Uniacke	none	5.70	1.91		
13	CR-95-007				Beaverbank	none	4.60	1.53		
14	CR-95-008				Beaverbank	none	4.00	2.30		
15	CR-95-009				Beaverbank		7.99	0.42		
16	CR-95-010				Beaverbank	none	4.34	2.75		
17	CR-95-011	13			Eastvilie		7.60	4.04		
18	CR-95-012	13			Eastville	slight		6.12		
19	CR-95-013	13			Eastville			0.01		
20	CR-95-014	12			Eastville	moderate	8.27	4.50		
21	CR-95-015	6			Eastville	slight		0.02		
22	CR-95-016	18			Eastville			2.54		
23	CR-95-017	24			Eastville			2.52		
24	MF95-01				Beaverbank Highway	slight	6.70	0.86		
25	MF95-02				Beaverbank Highway			0.44		
26	MF95-03				Beaverbank Highway			1.49		
27	MF95-04				Beaverbank Highway			0.13		
28	MF95-05				Beaverbank Highway	slight	8.20	0.10		
29	MF95-06				Beaverbank Highway			0.14		
30	MF95-07				Beaverbank Highway			0.12		
31	MF95-08				Beaverbank Highway			0.07		

A	B	C	D	E	F	G	H	I	J	K
4	Sample	Hole No.	From	To	Location	Fizz	Crushed	Total -S	Sulphide-S	Sulphate-S
5							(Paste)	(%)	(%)	(%)
6							pH			
32	MF95-09				Beaverbank Highway	slight	7.50	0.20		
33	MF95-10				Beaverbank Highway			0.89		
34	MF95-11				Beaverbank Highway			1.00		
35	MF95-12				Beaverbank Highway			0.98		
36	MF95-13				Beaverbank Highway	none	3.90	1.52		
37	MF95-14				Beaverbank Highway			0.74		
38	MF95-15				Beaverbank Highway			0.55		
39	MF95-16				Beaverbank Highway			0.34		
40	MF95-17				Beaverbank Highway	none	6.05	0.05		
41	MF95-18				Beaverbank Highway			0.02		
42	MF95-19				Beaverbank Highway			0.48		
43	MF95-20				Beaverbank Highway			0.62		
44	MF95-21				Beaverbank Highway	none	3.80	3.37		
45	MF95-22				Beaverbank Highway			0.99		
46	MF95-23				Beaverbank Highway			0.03		
47	MF95-24				Beaverbank Highway			0.12		
48	MF95-25				Beaverbank Highway	none	6.50	0.01		
49	MF95-26				Beaverbank Highway			0.03		
50	MF95-27				Beaverbank Highway			0.16		
51	MF95-28				Beaverbank Highway			0.01		
52	MF95-29				Beaverbank Highway	none	5.50	0.04		
53	MF95-30				Beaverbank Highway			0.02		
54	MF95-31				Beaverbank Highway			0.01		
55	MF95-32				Beaverbank Highway	none	8.00	0.01		
56	MF95-33				Beaverbank Highway			0.01		

A	B	C	D	E	F	G	H	I	J	K
4	Sample	Hole No.	From	To	Location	Fizz	Crushed	Total -S	Sulphide-S	Sulphate-S
5							(Paste)	(%)	(%)	(%)
6							pH			
57	MF95-34				Beaverbank Highway			0.01		
58	MF95-35				Beaverbank Highway			0.31		
59	CB-1				Caribou			1.76		
60	CB-2				Caribou			1.46		
61	CB-3				Caribou			1.70		
62	CB-4				Caribou			1.59		
63	CB-5				Caribou			2.62		
64	CB-6				Caribou			1.28		
65	CB-7				Caribou			0.87		
66	CB-8				Caribou			1.48		
67	CB-9				Caribou			1.59		
68	CB-10				Caribou			0.58		
69	CB-11				Caribou			4.26		
70	CB-12				Caribou			3.52		
71	CB-13				Caribou			2.26		
72	CB-14				Caribou			0.75		
73	CB-15				Caribou			2.27		
74	CB-16				Caribou			0.23		
75	CB-17				Caribou			0.05		
76	CB-18				Caribou			0.01		
77	CB-19				Caribou			0.19		
78	CB-20				Caribou			0.58		
79	CB-21				Caribou			0.01		
80	CB-22				Caribou			0.17		
81	CB-23				Caribou			0.69		

A	B	C	D	E	F	G	H	I	J	K
4	Sample	Hole No.	From	To	Location	Fizz	Crushed	Total -S	Sulphide-S	Sulphate-S
5							(Paste)	(%)	(%)	(%)
6							pH			
82	CB-24				Caribou			0.33		
83	CB-25				Caribou			0.26		
84	CB-26				Caribou			0.24		

A	B	L	M	N	O	P	Q	R	S	T
4	Sample	BaSO4-S	Organic-S	del-S	AP	TAP	Sobek-NP	TAP	BC-Research	Total C
5		(%)	(%)	(%)	(t CaCO3/)	(t CaCO3/)	(t CaCO3/)	kgH2SO4/tonne	kg H2SO4/tonne	% C
6					1000 t)	1000 t)	1000 t)			
7	CR-95-001					39.06	4.20	38.25	4.90	0.44
8	CR-95-002					73.13	2.50	71.60	12.74	0.51
9	CR-95-003					29.06	4.99	28.46	5.15	0.42
10	CR-95-004					75.31	-1.87	73.75	0.25	0.60
11	CR-95-005					43.13	0.01	42.23	0.98	1.09
12	CR-95-006					59.69	6.99	58.45	10.54	0.27
13	CR-95-007					47.81	1.99	46.82	10.54	0.21
14	CR-95-008					71.88	-1.50	70.38	13.48	0.08
15	CR-95-009					13.13		12.85		
16	CR-95-010					85.94	-7.50	84.15	1.35	
17	CR-95-011					126.25		123.62		
18	CR-95-012					191.25	15.00	187.27	8.10	
19	CR-95-013					0.34		0.34		
20	CR-95-014					140.63	65.00	137.70	54.00	
21	CR-95-015					0.53	14.30	0.52	6.75	
22	CR-95-016					79.38		77.72		
23	CR-95-017					78.75		77.11		
24	MF95-01					26.88	18.15	26.32	17.15	0.34
25	MF95-02					13.75		13.46		
26	MF95-03					46.56		45.59		0.43
27	MF95-04					4.19		4.10		
28	MF95-05					3.19	19.38	3.12	17.64	0.23
29	MF95-06					4.31		4.22		
30	MF95-07					3.81		3.73		0.08
31	MF95-08					2.16		2.11		

A	B	L	M	N	O	P	Q	R	S	T
4	Sample	BaSO4-S	Organic-S	del-S	AP	TAP	Sobek-NP	TAP	BC-Research	Total C
5		(%)	(%)	(%)	(t CaCO3/)	(t CaCO3/)	(t CaCO3/)	kgH2SO4/tonne	kg H2SO4/tonne	% C
6					1000 t)	1000 t)	1000 t)			
32	MF95-09					6.09	10.19	5.97	9.80	0.13
33	MF95-10					27.81		27.23		
34	MF95-11					31.25		30.60		0.10
35	MF95-12					30.63		29.99		
36	MF95-13					47.50	1.50	46.51	4.90	0.17
37	MF95-14					23.13		22.64		
38	MF95-15					17.19		16.83		0.17
39	MF95-16					10.63		10.40		
40	MF95-17					1.66	3.19	1.62	1.72	0.04
41	MF95-18					0.53		0.52		
42	MF95-19					15.00		14.69		0.07
43	MF95-20					19.38		18.97		
44	MF95-21					105.31	0.25	103.12	3.92	0.02
45	MF95-22					30.94		30.29		
46	MF95-23					0.88		0.86		0.06
47	MF95-24					3.59		3.52		
48	MF95-25					0.28	1.75	0.28	1.47	0.06
49	MF95-26					1.00		0.98		
50	MF95-27					4.97		4.87		0.03
51	MF95-28					0.34		0.34		
52	MF95-29					1.28	1.19	1.25	0.98	0.11
53	MF95-30					0.59		0.58		
54	MF95-31					0.19		0.18		0.03
55	MF95-32					0.25	2.78	0.24	1.72	
56	MF95-33					0.19		0.18		0.03

A	B	L	M	N	O	P	Q	R	S	T
4	Sample	BaSO4-S	Organic-S	del-S	AP	TAP	Sobek-NP	TAP	BC-Research	Total C
5		(%)	(%)	(%)	(t CaCO3/)	(t CaCO3/)	(t CaCO3/)	kgH2SO4/tonne	kg H2SO4/tonne	% C
6					1000 t)	1000 t)	1000 t)			
57	MF95-34					0.19		0.18		
58	MF95-35					9.78		9.58		0.06
59	CB-1					55.00		53.86	10.29	1.05
60	CB-2					45.63		44.68	61.25	1.02
61	CB-3					53.13		52.02	13.72	0.57
62	CB-4					49.69		48.65	11.03	1.05
63	CB-5					81.88		80.17	16.90	0.34
64	CB-6					40.00		39.17	12.99	0.58
65	CB-7					27.19		26.62	100.90	2.44
66	CB-8					46.25		45.29	22.79	0.54
67	CB-9					49.69		48.65	14.46	0.56
68	CB-10					18.13		17.75	414.30	5.90
69	CB-11					133.13		130.36	19.85	0.27
70	CB-12					110.00		107.71	16.66	0.54
71	CB-13					70.63		69.16	12.01	0.77
72	CB-14					23.44		22.95	494.40	6.77
73	CB-15					70.94		69.46	11.76	0.81
74	CB-16					7.19		7.04	51.70	1.07
75	CB-17					1.53		1.50	97.02	2.97
76	CB-18					0.31		0.31	44.10	0.94
77	CB-19					5.94		5.81	130.34	1.73
78	CB-20					18.13		17.75	12.25	0.09
79	CB-21					0.28		0.28	29.40	0.42
80	CB-22					5.31		5.20	36.02	0.43
81	CB-23					21.56		21.11	9.07	0.08

A	B	L	M	N	O	P	Q	R	S	T
4	Sample	BaSO4-S	Organic-S	del-S	AP	TAP	Sobek-NP	TAP	BC-Research	Total C
5		(%)	(%)	(%)	(t CaCO3/)	(t CaCO3/)	(t CaCO3/)	kgH2SO4/tonne	kg H2SO4/tonne	% C
6					1000 t)	1000 t)	1000 t)			
82	CB-24					10.31		10.10	16.17	0.13
83	CB-25					8.13		7.96	32.10	0.32
84	CB-26					7.50		7.34	25.24	0.21

A	B	U	V	W	X	Y	Z	AA	AB
4	Sample	Total C	Organic C	Organic C	Carbonate C	Carb-NP	NNP	TNNP	CNNP
5		%CO2	% C	% CO2	% CO2	(t CaCO3/)	(t CaCO3/)	(t CaCO3/)	(t CaCO3/)
6						1000 t)	1000 t)	1000 t)	1000 t)
7	CR-95-001	1.61	0.42	1.54	0.07	1.67		-34.86	
8	CR-95-002	1.87	0.50	1.83	0.04	0.83		-70.63	
9	CR-95-003	1.54	0.37	1.36	0.18	4.17		-24.07	
10	CR-95-004	2.20	0.54	1.98	0.22	5.00		-77.18	
11	CR-95-005	3.99	1.01	3.70	0.29	6.67		-43.12	
12	CR-95-006	0.99	0.18	0.66	0.33	7.50		-52.70	
13	CR-95-007	0.77	0.17	0.62	0.15	3.33		-45.82	
14	CR-95-008	0.28	0.06	0.23	0.05	1.08		-73.38	
15	CR-95-009								
16	CR-95-010							-93.44	
17	CR-95-011								
18	CR-95-012							-176.25	
19	CR-95-013								
20	CR-95-014							-75.63	
21	CR-95-015							13.77	
22	CR-95-016								
23	CR-95-017								
24	MF95-01	1.25	0.13	0.49	0.76	17.25		-8.73	
25	MF95-02								
26	MF95-03	1.56	0.30	1.10	0.47	10.58			
27	MF95-04								
28	MF95-05	0.84	0.07	0.25	0.59	13.42		16.19	
29	MF95-06								
30	MF95-07	0.30	0.07	0.25	0.05	1.17			
31	MF95-08								

A	B	U	V	W	X	Y	Z	AA	AB
4	Sample	Total C	Organic C	Organic C	Carbonate C	Carb-NP	NNP	TNNP	CNNP
5		%CO2	% C	% CO2	% CO2	(t CaCO3/)	(t CaCO3/)	(t CaCO3/)	(t CaCO3/)
6						1000 t)	1000 t)	1000 t)	1000 t)
32	MF95-09	0.47	0.00	0.01	0.45	10.25		4.10	
33	MF95-10								
34	MF95-11	0.36	0.09	0.33	0.03	0.75			
35	MF95-12								
36	MF95-13	0.64	0.17	0.62	0.02	0.50		-46.00	
37	MF95-14								
38	MF95-15	0.60	0.13	0.48	0.12	2.83			
39	MF95-16								
40	MF95-17	0.13	0.00	0.01	0.12	2.67		1.53	
41	MF95-18								
42	MF95-19	0.24	0.05	0.16	0.07	1.67			
43	MF95-20								
44	MF95-21	0.07	0.00	0.01	0.05	1.25		-105.06	
45	MF95-22								
46	MF95-23	0.23	0.05	0.18	0.05	1.08			
47	MF95-24								
48	MF95-25	0.20	0.04	0.15	0.05	1.25		1.47	
49	MF95-26								
50	MF95-27	0.10	0.02	0.07	0.03	0.58			
51	MF95-28								
52	MF95-29	0.40	0.07	0.24	0.16	3.58		-0.09	
53	MF95-30								
54	MF95-31	0.10	0.02	0.08	0.03	0.58			
55	MF95-32							2.53	
56	MF95-33	0.10	0.02	0.08	0.02	0.50			

A	B	U	V	W	X	Y	Z	AA	AB
4	Sample	Total C	Organic C	Organic C	Carbonate C	Carb-NP	NNP	TNNP	CNNP
5		%CO2	% C	% CO2	% CO2	(t CaCO3/)	(t CaCO3/)	(t CaCO3/)	(t CaCO3/)
6						1000 t)	1000 t)	1000 t)	1000 t)
57	MF95-34								
58	MF95-35	0.20	0.00	0.01	0.19	4.25			
59	CB-1	3.85	0.70	2.56	1.28	29.17			
60	CB-2	3.74	0.14	0.51	3.22	73.33			
61	CB-3	2.09	0.50	1.83	0.26	5.83			
62	CB-4	3.85	0.98	3.59	0.26	5.83			
63	CB-5	1.25	0.28	1.03	0.22	5.00			
64	CB-6	2.13	0.56	2.05	0.07	1.67			
65	CB-7	8.94	0.09	0.34	8.60	195.50			
66	CB-8	1.98	0.27	0.99	0.99	22.50			
67	CB-9	2.05	0.55	2.02	0.04	0.83			
68	CB-10	21.62	1.15	4.21	17.40	395.83			
69	CB-11	0.99	0.23	0.84	0.15	3.33			
70	CB-12	1.98	0.39	1.43	0.55	12.50			
71	CB-13	2.82	0.75	2.75	0.07	1.67			
72	CB-14	24.81	0.99	3.63	21.18	481.67			
73	CB-15	2.97	0.80	2.93	0.04	0.83			
74	CB-16	3.92	0.13	0.48	3.44	78.33			
75	CB-17	10.88	0.03	0.12	10.76	244.75			
76	CB-18	3.44	0.02	0.05	3.39	77.08			
77	CB-19	6.34	0.04	0.14	6.20	141.00			
78	CB-20	0.33	0.07	0.25	0.07	1.67			
79	CB-21	1.54	0.07	0.27	1.27	28.83			
80	CB-22	1.58	0.04	0.16	1.41	32.17			
81	CB-23	0.30	0.08	0.29	0.01	0.33			

A	B	U	V	W	X	Y	Z	AA	AB
4	Sample	Total C	Organic C	Organic C	Carbonate C	Carb-NP	NNP	TNNP	CNNP
5		%CO2	% C	% CO2	% CO2	(t CaCO3/)	(t CaCO3/)	(t CaCO3/)	(t CaCO3/)
6						1000 t)	1000 t)	1000 t)	1000 t)
82	CB-24	0.48	0.03	0.12	0.36	8.08			
83	CB-25	1.17	0.05	0.19	0.98	22.33			
84	CB-26	0.77	0.02	0.07	0.70	16.00			

A	B	AC	AD	AE	AF	AG	AH	AI
4	Sample	CTNNP	NPR	TNPR	BCR-TNPR	CNPR	CTNPR	
5		(t CaCO3/)						
6		1000 t)						
7	CR-95-001			0.11	0.13		0.04	
8	CR-95-002			0.03	0.18		0.01	
9	CR-95-003			0.17	0.18		0.14	
10	CR-95-004				0.00		0.07	
11	CR-95-005			0.00	0.02		0.15	
12	CR-95-006			0.12	0.18		0.13	
13	CR-95-007			0.04	0.23		0.07	
14	CR-95-008				0.19		0.02	
15	CR-95-009							
16	CR-95-010				0.02			
17	CR-95-011							
18	CR-95-012			0.08	0.04			
19	CR-95-013							
20	CR-95-014			0.46	0.39			
21	CR-95-015			26.92	12.98			
22	CR-95-016							
23	CR-95-017							
24	MF95-01			0.68	0.65		0.64	
25	MF95-02							
26	MF95-03						0.23	
27	MF95-04							
28	MF95-05			6.08	5.65		4.21	
29	MF95-06							
30	MF95-07						0.31	
31	MF95-08							

A	B	AC	AD	AE	AF	AG	AH	AI
4	Sample	CTNNP	NPR	TNPR	BCR-TNPR	CNPR	CTNPR	
5		(t CaCO3/)						
6		1000 t)						
32	MF95-09			1.67	1.64		1.68	
33	MF95-10							
34	MF95-11						0.02	
35	MF95-12							
36	MF95-13			0.03	0.11		0.01	
37	MF95-14							
38	MF95-15							
39	MF95-16							
40	MF95-17			1.93	1.06		1.61	
41	MF95-18							
42	MF95-19						0.11	
43	MF95-20							
44	MF95-21			0.00	0.04		0.01	
45	MF95-22							
46	MF95-23						1.24	
47	MF95-24							
48	MF95-25			6.22	5.34		4.44	
49	MF95-26							
50	MF95-27						0.12	
51	MF95-28							
52	MF95-29			0.93	0.78		2.80	
53	MF95-30							
54	MF95-31						3.11	
55	MF95-32			11.12	7.03			
56	MF95-33						2.67	

A	B	AC	AD	AE	AF	AG	AH	AI
4	Sample	CTNNP	NPR	TNPR	BCR-TNPR	CNPR	CTNPR	
5		(t CaCO3/)						
6		1000 t)						
57	MF95-34							
58	MF95-35						0.43	
59	CB-1				0.19		0.53	
60	CB-2				1.37		1.61	
61	CB-3				0.26		0.11	
62	CB-4				0.23		0.12	
63	CB-5				0.21		0.06	
64	CB-6				0.33		0.04	
65	CB-7				3.79		7.19	
66	CB-8				0.50		0.49	
67	CB-9				0.30		0.02	
68	CB-10				23.34		21.84	
69	CB-11				0.15		0.03	
70	CB-12				0.15		0.11	
71	CB-13				0.17		0.02	
72	CB-14				21.54		20.55	
73	CB-15				0.17		0.01	
74	CB-16				7.35		10.90	
75	CB-17				64.71		159.84	
76	CB-18				144.12		246.67	
77	CB-19				22.42		23.75	
78	CB-20				0.69		0.09	
79	CB-21				106.75		102.52	
80	CB-22				6.92		6.05	
81	CB-23				0.43		0.02	

A	B	AC	AD	AE	AF	AG	AH	AI
4	Sample	CTNNP	NPR	TNPR	BCR-TNPR	CNPR	CTNPR	
5		(t CaCO3/)						
6		1000 t)						
82	CB-24				1.60		0.78	
83	CB-25				4.03		2.75	
84	CB-26				3.44		2.13	

Appendix D

SPANS modelling programs for Boolean logic, fuzzy logic, and weights of evidence methods.

Boolean Logic Model

```
local int a,b,c,d,e,f,g,i,j,k,l,m,booland,final

a = class ("geoquad2")
b = class ("metaquad")
c = class ("vg_class")
d = class ("buf_gra4")
e = class ("buf_ght1")
f = class ("bufantil")

g = keyedtable ("geoquad2", "class", a, "boolean")
i = keyedtable ("metaquad", "class", b, "boolean")
j = keyedtable ("vg_class", "class", c, "boolean")
k = keyedtable ("buf_gra4", "class", d, "boolean")
l = keyedtable ("buf_ght1", "class", e, "boolean")
m = keyedtable ("bufantil", "class", f, "boolean")

booland = (g*i*j*k)

if (booland =1 or l=1 or m=1) then
final = 1
else
final = 0
endif

call result (final)
```

Fuzzy Logic Model

```
local int a,b,c,d,e,f
local float g,i,j,k,l,m,fzand, fzor, gam, fprod, fsum, fgam

a = class("buf_ght1")
b = class("buf_gra4")
c = class("bufanti1")
d = class("geoquad2")
e = class("metaquad")
f = class("vg_class")

g = keyedtable ("buf_ght1", "class", a, "fm")
i = keyedtable ("buf_gra4", "class", b, "fm")
j = keyedtable ("bufanti1", "class", c, "fm")
k = keyedtable ("geoquad2", "class", d, "fm")
l = keyedtable ("metaquad", "class", e, "fm")
m = keyedtable ("vg_class", "class", f, "fm")

fzand = min (k,m)
fzor = max (g,j)

input "Value of Gamma?" gam

fprod = i*l*fzand*fzor
fsum = 1 - ((1 - fzand) * (1 - i)*(1 - fzor)*(1 - l))
fgam = pow(fsum,gam)*pow(fprod, 1-gam)

call result (fgam)
```

Weights of Evidence Model

(Note: positive and negative weights calculated in spreadsheet as discussed in text).

```
local float priop, postp, f1,f2,f3,f4,f5, sumw, prioro, lprioro, posto,
lposto

priop = 121.0/8121.37
prioro = priop/(1-priop)
lprioro = ln(prioro)

if (class("buf_ght1")=1) then
f1=0.22
else
f1= -0.03
endif

if (class("bufanti1")=1) then
f2=0.89
else
f2= -0.10
endif

if (class("metaquad")=2) then
f3=0.18
else
f3= -0.16
endif

if (class("geoquad2")=4) then
f4=0.92
else
f4= -0.37
endif

if (class("vg_class") =3) then
f5=0.55
else
f5 = -0.12
endif

sumw = f1 + f2 + f3 + f4 + f5
lposto = sumw + lprioro
posto = exp(lposto)
postp = posto / (1 + posto)
call result (postp)
```

References

Ahonen, L. and Tuovinen, O.H. 1992. Alterations in surfaces and textures of minerals during the bacterial leaching of a complex sulfide ore. Geomicrobiology Journal, 10, pp. 207-217.

Albright, R. 1987. Prediction of acid drainage in Meguma slates. In Proceedings, Acid Mine Drainage Seminar/Workshop, Halifax, Nova Scotia, March 23-26, 1987. Environment Canada, pp. 245-261.

Alpers, C. N. and Nordstrom, D.K. 1991. Geochemical evolution of extremely acid mine waters at Iron Mountain, California: Are there any lower limits to pH? In: Second International Conference on the Abatement of Acidic Drainage, Sept. 16-18, 1991, Montreal, Canada, v. 2, pp. 321-342.

Alpers, C.N., Blowes, D.W., Nordstrom, D.K. and Jambor, J.L. 1994a. Chapter 9: Secondary minerals and acid mine-water chemistry. In: short course handbook on environmental geochemistry of sulfide mine-wastes. J.L. Jambor and D.W. Blowes (eds.). Mineralogical Association of Canada, Waterloo, Ontario, pp. 247-270.

Alpers, C.N., Nordstrom, D.K. and Thompson, J.M. 1994b. Chapter 22: Seasonal variations of Zn/Cu ratios in acid mine water from Iron Mountain, California. In: Environmental Geochemistry of Sulphide Oxidation. Charles N. Alpers and David W. Blowes (eds.). American Chemical Society, Washington D.C., pp. 324-344.

American Society for Testing and Materials 1990. D2492 standard test method for forms of sulphur in coal. Annual Book of ASTM Standards, Volume 05.05, pp. 251-256.

An, P., Moon, W.M. and Rencz, A. 1991. Application of fuzzy set theory to integrated mineral exploration. Canadian Journal of Exploration Geophysics, 27, 1, pp. 1-11.

Arnold, R.G. 1966. Mixtures of hexagonal and monoclinic pyrrhotite and the measurement of the metal content of pyrrhotite by X-ray diffraction. American Mineralogist, 51, pp. 1221-1227.

Arnold, R.G. 1967. Range in composition and structure of 82 natural terrestrial pyrrhotites. Canadian Mineralogist, 9, pp. 31-50.

Arnold, R.G. 1969. Pyrrhotite phase relations below 304 $\pm$ 6° C at $<$ 1 atm total pressure. Economic Geology, 64, pp. 405-419.

Bacon, J.R. and Maas, R.P. 1979. Contamination of Great Smoky Mountains trout streams by exposed Anakeesta Formation. Journal of Environmental Quality, 8, 4, pp. 538-542.

Banfield, J.F. and Nealson, K.H. (eds.) 1997. Geomicrobiology: Interactions Between Microbes and Minerals. Mineralogical Society of America, Reviews in Mineralogy, Volume 35, 448p.

Bechard, G. 1993. Microbial process for the treatment of acid mine drainage using cellulosic substrates. Unpublished PhD thesis, Carleton University, Ottawa, Ontario.

Bechard, G., McCready, R.G.L., Koren, D.W. and Rajan, S. 1995. Microbial treatment of acid mine drainage at Halifax International Airport. In Proceedings, Conference on Mining and the Environment, Sudbury, Ontario, Canada, May 28-June 1, 1995. T.P. Hynes and M.C. Blanchette (eds.). CANMET, Ottawa, Vol. 2, pp. 545-554.

Bhatti, T.M., Bigham, J.M., Carlson, L. and Tuovinen, O.H. 1993. Mineral products of pyrrhotite oxidation by *Thiobacillus ferrooxidans*. Applied and Environmental Microbiology, 59(6), pp. 1984-1990.

Bigham, J.M. 1994. Mineralogy of ochre deposits formed by sulfide oxidation. In The environmental geochemistry of sulfide mine-wastes: short course handbook, Volume 22, pp. 103-132.

Bigham, J.M., Carlson, L. and Murad, E. 1994. Schwertmannite, a new iron oxyhydroxysulfate from Pyhasalmi, Finland, and other localities. Mineralogical Magazine, 58, pp. 641-648.

Bigham, J.M., Schwertmann, U., Traina, S.J., Winland, R.L. and Wolf, M. 1996. Schwertmannite and the chemical modeling of iron in acid sulfate waters. Geochimica et Cosmochimica Acta, 60, 12, pp. 2111-2121.

Binney, W.R., Jenner, K.A., Sangster, A.L. and Zentilli, M. 1986. A stratabound zinc-lead deposit in Meguma Group metasediments at Eastville, Nova Scotia. Maritime Sediments and Atlantic Geology, 22, pp. 65-88.

Bonham-Carter, G.F., Agterberg, F.P. and Wright, D.F. 1988. Integration of geological datasets for gold exploration in Nova Scotia. Photogrammetry and Remote Sensing, 54, 11, pp. 1585-1592.

Bonham-Carter, G.F., Reddy, R.K.T. and Galley, A.G. 1994. Knowledge-driven modelling of volcanogenic massive sulphide potential with a geographic information system. In: Mineral Deposit Modeling. R.V. Kirkham, W.D. Sinclair, R.I. Thorpe, and J.M. Duke (eds.). Geological Association of Canada, Special Paper 40, pp. 735-749.

Bonham-Carter, G.F., 1994. Geographic information systems for geoscientists: modelling with GIS. Pergamon Press, Oxford, 398p.

Bottaro, C.S. 1994. A study of problematic acid production from iron sulphides using atomic absorption spectrophotometry. Unpublished BSc Honours thesis, Department of Chemistry, St. Mary's University, Halifax, Nova Scotia, 61p.

Brown, J.C.S. 1997. Interpreting and implementing the precautionary principle: the management of sulphide bearing materials in Nova Scotia. Unpublished MES thesis. Dalhousie University, Halifax, Nova Scotia.

Bruynesteyn, A. and Duncan, D.W. 1979. Determination of acid production potential of waste materials. Met. Soc. AIME, Paper A-79-29, 10p.

Burns, C.G. 1997. Stratigraphy of the Goldenville Group - Halifax Group Transition (GHT) of the Meguma Supergroup at Caribou Gold District (drillcore LL81-5A), Nova Scotia. Unpublished BSc thesis, Dalhousie University, Halifax, Nova Scotia.

Callister, W.D. Jr. 1993. Materials science and engineering: an introduction, 3rd ed. John Wiley & Sons, Inc. New York, NY. pp. 68-87.

Calow, R.W., Hevenor, D. and Masson-Stogran, D. 1995. Comparison of the BC Research and the EPA acid mine drainage predictive static tests. Sudbury '95 Conference Proceedings, Mining and the Environment, 2, pp. 605-612.

Cameron, G.W. and Hood, P.J. 1975. Residual aeromagnetic anomalies associated with the Meguma Group of Nova Scotia and their relationship to gold mineralization. Geological Survey of Canada, Paper 75-1C, pp. 197-211.

Carpenter, R.H. and Desborough, B.A. 1964. Range in solid solution and structure of naturally occurring troilite and pyrrhotite. American Mineralogist, 49, pp. 1350-1365.

Chen, T.T., Dutrizac, J.E., Owens, D.R. and LaFlamme, J.H.G. 1980. Accelerated tarnishing of some chalcopyrite and tennantite specimens. Canadian Mineralogist, 18, pp. 173-180.

Clark, A.H. 1966. Stability field of monoclinic pyrrhotite. Transactions of the Institution of Mining and Metallurgy, Section B, 75, pp. 232-235.

Craig, J.R. and Scott, S.D. 1974. Sulphide phase equilibria (Chapter 5). In Reviews in mineralogy, Volume 1, Sulphide Mineralogy. P.H. Ribbe (ed.). Mineralogical Society of America, pp. CS-1 - CS-110.

Environment Act S.N.S. 1994-95, c. 1, section 66. Order in Council 95-296 (April 11, 1995), N.S. Reg. 57/95, 7 pp.

Environmental Protection Service (EPS), Atlantic Region, 1976. A report on the causes of fish kills in the Shubenacadie River at Enfield, Nova Scotia. Environmental Services Branch.

Fairbairn, H.W., Hurley, P.M., Pinson, W.H. and Cormier, R.F. 1960. Age of granitic rocks of Nova Scotia. Bulletin of the Geological Society of America, 71, pp. 399-414.

Faribault, E.R. 1909. Waverley Sheet, Geological Survey of Canada, Map 67.

Feetham, M. 1996. Lithogeochemistry of the Goldenville-Halifax transition zone (GHT) at North Beaverbank, Nova Scotia. Unpublished BSc thesis, St. Mary's University, Halifax, Nova Scotia.

Feetham, M., Ryan, R.J., Pe-Piper, G. and O'Beirne-Ryan, A.M. 1997. Lithogeochemical characterization of the Beaverbank unit of the Halifax Formation, Meguma Group, and acid drainage implications. Atlantic Geology, 33, 2, pp. 133-141.

Fleet, M.E. 1971. The crystal structure of a pyrrhotite (Fe_7S_8). Acta Crystallography, B27, pp. 1864-1867.

Fox, D., Robinson, C. and Zentilli, M. 1997. Pyrrhotite and associated sulphides and their relationship to acid rock drainage in the Halifax Formation, Meguma Group, Nova Scotia. Atlantic Geology, 33, pp. 87-103.

Fraser, D.C. 1969. Contouring of VLF-EM data. Geophysics, 34, pp. 958-967.

Geological Survey of Canada, Aeromagnetic Series Maps 790G and 785G, 1960.

Garrels, R.M. and Christ, C.L. 1965. Solutions, Minerals, and Equilibria. Harper, New York, NY.

Golder Associates, 1983. Subsurface investigation definition of slate/quartzite contact, Part of Phase 1, Aerotech Business Park, Halifax County, Nova Scotia. Unpublished Consultant Report.

Graves, M.C. and Zentilli, M. 1988. The lithochemistry of metal-enriched coticules in the Goldenville-Halifax transition zone of the Meguma Group, Nova Scotia. In Current Research, part B. Geological Survey of Canada, Paper 88-1B, pp. 251-261.

Haysom, S.J., Horne, R. and Pe-Piper G. 1997. The opaque mineralogy of metasedimentary rocks of the Meguma Group, Beaverbank-Rawdon area, Nova Scotia. Atlantic Geology, 33, 2, pp. 105-120.

Heiland, C.A. 1963. Geophysical Exploration. Hafner Publishing Company, New York and London, 1013p.

Henderson, J.R., Wright, T.O. and Henderson, M.N. 1986. A history of cleavage and folding: An example from the Goldenville Formation, Nova Scotia. Geological Society of America Bulletin, 97, pp. 1354-1366.

Hennigar T.W. and Gibb, J.E. 1987. Surface and groundwater impacts of acid mine drainage from the Meguma slates of Nova Scotia. In Proceedings, Acid Mine Drainage Seminar/Workshop, Halifax, Nova Scotia, March 23-26, 1987. Environment Canada, pp. 165-187.

Howells, K. and McKay, A.G. 1985. A total magnetic field and seismic survey over a possible dam site at Bennery Lake, Halifax County, Nova Scotia. Nova Scotia Research Foundation Corporation Report for Nolan, Davis and Associates.

Jacques, Whitford and Associates 1981. Soil investigation - proposd airport industrial park, Halifax County, Nova Scotia. Unpublished Consultant Report.

Jacques, Whitford and Associates Ltd. 1990. Acidic slate assessment, Highway 107 construction, Petpeswick Lake, Halifax County. Unpublished Consultant Report for Nova Scotia Department of Environment, March, 1990, 63p.

Jambor, J.L. 1994. Mineralogy of sulfide-rich tailings and their oxidation products. In The Environmental Geochemistry of Sulphide Mine-wastes. Short Course Handbook, Mineralogical Association of Canada, 22, pp. 59-102.

Jambor, J.L. and Blowes, D.W. 1998. Chapter 12: Theory and application of mineralogy in environmental studies of sulphide-bearing mine waste. In: modern approaches to ore and environmental mineralogy. L.J. Cabri and D.J. Vaughan (eds.). Mineralogical Association of Canada, Short Course Volume 27, Ottawa, Ontario. pp. 367-401.

Janzen, M.P., Nicholson, R.V. and Scharer, J.M. 1997. The role of enhanced particle surface area, crystal structure and trace metal content on pyrrhotite oxidation rates in tailings. In: Fourth International Conference on Acid Rock Drainage, Volume 1, pp. 401-415.

Jenner, K. 1982. A study of sulphide mineralization in Gold Brook, Colchester County, Nova Scotia. B.Sc. Honours thesis, Dalhousie University, Halifax, Nova Scotia.

Jones, C.F., LeCount, S., Smart, R. S.C. and White, T.J. 1992. Compositional and structural alteration of pyrrhotite surfaces in solution: XPS and XRD studies. Applied Surface Science, 55, pp. 65-85.

Jones, R.A. 1997. Relative chemical and biological oxidation of sulphides in the Meguma Supergroup, Nova Scotia: the role of mineralogy, texture and composition. B.Sc. Honours thesis, Dalhousie University, Halifax, N.S., March, 1997.

Jones, R.A and Fox, D. 1997. Relative chemical and biological oxidation of sulphides in the Meguma Supergroup, Nova Scotia: the role of mineralogy, texture and composition. Atlantic Geology, 33, p. 64.

Keppie, J.D. and Muecke, G.M. 1979. Metamorphic map of Nova Scotia. Nova Scotia Department of Mines and Energy.

Keppie, J.D. 1979a. Geological Map of Nova Scotia. Nova Scotia Department of Mines and Energy.

Keppie, J.D. 1979b. Structural Map of Nova Scotia. Nova Scotia Department of Mines and Energy.

Kerekes, J., Freedman, B., Howell, G. and Clifford, P. 1984. Comparison of the characteristics of an acidic eutrophic, and an acidic oligotrophic lake near Halifax, Nova Scotia. Water Pollution Research Journal of Canada, 15, 4, pp. 1-9.

King, M.S. 1997. Magnetic susceptibility mapping: applications for the Meguma Group, central Nova Scotia. Atlantic Geology, 33, pp. 121-131.

King, M. 1985. Acid drainage and the acidification of Nova Scotia waters. Environment Canada Report, 38p.

King, M. 1987. Contribution of acidity and heavy metals to surface and groundwater by pyritiferous slates in the vicinity of the Halifax Airport. Unpublished MASc thesis, Technical University of Nova Scotia, Halifax, Nova Scotia.

King, M. and Hart, W. 1987. Contribution of acidity and heavy metals to surface and groundwater by pyritiferous slates in the vicinity of the Halifax Airport. Contract report for Environment Canada.

King, M. and Hart, W. 1990. Groundwater contribution to acid drainage from the Halifax Formation in Nova Scotia. Canadian Water Resources Journal, 15, pp. 357-365.

Klein, C. and Hurlbut, C.S. 1985. Manual of Mineralogy. John Wiley & Sons, Inc., 596p.

Knee, K. 1995. Magnetic susceptibility of Halifax Formation Slates at the Halifax International Airport: correlation with potential for acid drainage. B.Sc. Honours thesis, Dalhousie University, Halifax, N.S., 45p.

Kwong, Y.T.J. and Lawrence, J.R. 1994. Mineralogical controls of sulfide oxidation. National Hydrology Research Institute, Contribution No. 94010, 87p.

Kwong, Y.T.J., Lawrence, J.R. and Swerhone, D.W. 1994. Interplay of geochemical, electrochemical and microbial controls in the oxidation of common sulphide minerals (abstract). In: Third International Conference On The Abatement Of Acidic Drainage, Volume 2, Pittsburgh, PA, April 24-29, p. 419.

Kwong, Y.T.J. 1995. Influence of galvanic sulfide oxidation on mine water chemistry. In Proceedings, Conference on Mining and the Environment, Sudbury, Ontario, Canada, May 28-June 1, 1995. Edited by T.P. Hynes and M.C. Blanchette. CANMET, Ottawa, Vol. 2, pp. 477-483.

Kwong, E.C.M., Scharer, J.M., Byerley, J.J. and Nicholson, R.V. 1995. Prediction and control of bacterial activity in acid mine drainage. *In* Proceedings, Conference on Mining and the Environment, Sudbury, Ontario, Canada, May 28-June 1, 1995. *Edited by* T.P. Hynes and M.C. Blanchette. CANMET, Ottawa, Vol. 1, pp. 211-216.

Lianxing, G. and Vokes F.M. 1996. Intergrowths of hexagonal and monoclinic pyrrhotites in some sulphide ores from Norway. Mineralogical Magazine, 60, pp. 303-316.

Loukola-Ruskeeniemi, K. 1990. Metalliferous black shales - a probable source of mercury in pike in Lake Kolmisoppi, Sotkamo, Finland. Bulletin of the Geological Society of Finland, 62, pp. 167-175.

Loukola-Ruskeeniemi, K. 1992. Geochemistry of Proterozoic metamorphosed black shales in eastern Finland, with implications for exploration and environmental studies. PhD thesis, University of Helsinki, Finland.

Lund, O.P., Vaughan, J. and Thirumurthi, D. 1987. Impact of acid drainage pollution from mineralized slate at Halifax airport. Water Pollution Resources Journal of Canada, 2, pp. 308-325.

Lund, O.P. 1987. Acid drainage from mineralized slate at the Halifax International Airport. In Proceedings, Acid Mine Drainage Seminar/Workshop, Halifax, Nova Scotia, March 23-26, 1987. Environment Canada, pp. 137-165.

MacInnis, I.N., Silver, S.R., Pasava, J., Graves, M.C. and Zentilli, M. 1994. Experimental evaluation of the relative acid drainage potential of pyrite and pyrrhotite. Atlantic Geology, 30, 1, p. 75.

MacInnis, I.N. 1986. Lithogeochemistry of the Goldenville-Halifax transition (GHT) of the Meguma Group in the manganiferous zinc-lead deposit at Eastville, Nova Scotia. B.Sc. Honours thesis, Dalhousie University, Halifax, Nova Scotia, 138p.

Manchester, K. 1986. Survey of quarry pits in the Halifax Formation rocks of southwestern Nova Scotia. Environment Canada Report, 5p.

McCready, R.G.L. 1987. A review of the physical, chemical and biological measures to prevent acid mine drainage: an application to the pyritic Halifax shales. *In* Proceedings, Acid Mine Drainage Seminar/Workshop, Halifax, Nova Scotia, March 23-26, 1987. Minister of Supply and Services Canada, Ottawa, Ontario. pp. 333-355.

McGrath, P.H. 1970. Aeromagnetic interpretation Appalachia, New Brunswick and Nova Scotia (11D, E, F, K; 20O, P; 21 A, G, H, J). Geological Survey of Canada, Paper 70-1A, pp. 79-82.

McIntosh, J.M. and Groat, L.A. (eds.) 1997. Biological-Mineralogical Interactions. Mineralogical Association of Canada, Short Course Volume 25, Ottawa, Ontario. 239p.

McIntosh, J.M., Silver, M. and Groat, L.A. 1997. Chapter 4: Bacteria and the breakdown of sulphide minerals. In: Biological-Mineralogical Interactions. Mineralogical Association of Canada, Short Course Volume 25, Ottawa, Ontario, pp. 63-92.

McNeill, J.D. 1980. Electromagnetic terrain conductivity measurement at low induction numbers. Technical Note TN-6, Geonics Ltd., 15p.

MEND (Mine Environment Neutral Drainage Program) 1991. New methods for determination of key mineral species in acid generation prediction by acid-base accounting. Department of Energy, Mines and Resources Canada, Canada Centre for Mineral and Energy Technology, MEND Project 1.16.1c.

Minesite Drainage Assessment Group 1996. Static and kinetic testwork for prediction of acidic drainage and metal leaching at the Red Mountain Project, British Columbia, Canada. Report submitted to the Government of British Columbia, April, 1996.

Morimoto, N., Gyobu, A., Mukaiyama, H. and Izawa, E. 1975. Crystallography and stability of pyrrhotites. Economic Geology, 70, pp. 824-833.

Morin, K.A. and Hutt, N.M. 1994. Observed preferential depletion of neutralization potential over sulphide minerals in kinetic tests: site-specific criteria for safe NP/AP ratios. In: Proceedings of the Third International Conference on the Abatement of Acidic Drainage, April 24-29, Pittsburgh, PA. pp. 148-156.

Morin, K.A. and Hutt, N.M. 1997. Environmental Geochemistry of Minesite Drainage: Practical Theory and Case Studies. MDAG Publishing, Vancouver, British Columbia, Canada.

Murad, E., Schwertmann, U., Bigham, J.M. and Carlson, L. 1994. Chapter 14: Mineralogical characteristics of poorly crystallized precipitates formed by oxidation of Fe^{2+} in acid sulfate waters. In: Environmental Geochemistry of Sulfide Oxidation. American Chemical Society Symposium Series 550, pp. 190-200.

Murray, E.W., Goudey, S.P., McCready, R.G.L. and Salley, J. 1988. Laboratory and field testing of a salt-supplemented clay cap as an impermeable seal over pyritic slates. Mine drainage and surface mine reclamation conference. April 17-22, Pittsburg, PA., pp. 52-58.

Mycroft, J.R., Nesbitt, H.W. and Pratt, A.R. 1995. X-ray photoelectron and Auger electron spectroscopy of air oxidized pyrrhotite: distribution of oxidized species with depth. Geochim. Cosmochim. Acta., 59, pp. 721-733.

Natarajan, K.A. 1990. Electrochemical aspects of bioleaching of base-metal sulphides. In Microbial mineral recovery. Edited by H.L. Ehrlich and C.L. Brierley. McGraw-Hill Publishing Co., New York, NY, pp. 79-106.

Nettleton, L.L. 1940. Geophysical Prospecting for Oil. McGraw-Hill Book Company, Inc., 444 p.

Nicholson, R.V. and Scharer, J.M. 1994. Laboratory studies of pyrrhotite oxidation kinetics. In Environmental Geochemistry of Sulphide Oxidation. Edited by Charles N. Alpers and David W. Blowes. American Chemical Society, Washington D.C., pp. 14-30.

Nicholson, R.V. 1994. Iron-sulphide oxidation mechanisms: laboratory studies. In The Environmental Geochemistry of Sulphide Mine-wastes. Short Course Handbook, Mineralogical Association of Canada, 22, pp. 163-183.

Nolan, Davis and Associates 1983. Acidic drainage study for the Aerotech Business Park. Unpublished Consultant Report.

Nordstrom, D.K. 1982. Aqueous pyrite oxidation and the consequent formation of secondary iron minerals. *In* Acid sulfate weathering, SSSA Special Publication Number 10, Proceedings of a symposium sponsored by Divisions S-9, S-2, S-5, and S-6 of the Soil Science Society of America, August 5-10, 1982. Edited by J.A. Kittrick, D.S. Fanning and L.R. Hossner. Soil Science Society of America, Madison, Wisconsin, pp. 37-56.

Nordstrom, D.K. and Southam, G. 1997. Chapter 11: Geomicrobiology of sulphide mineral oxidation. In Geomicrobiology: Interactions Between Microbes and Minerals J.F. Banfield and K.H. Nealson (eds.). Mineralogical Society of America, Reviews in Mineralogy, Volume 35, pp. 361-390.

Nova Scotia Department of Environment, 1995. Sulphide bearing material disposal regulations. *In* Environment Act S.N.S. 1994-95, c. 1, section 66. Order in Council 95-296 (April 11, 1995), N.S. Reg. 57/95.

NSRFC, 1985a. Test geophysical methods to detect shallow sulphide mineralization in Cambro-Ordovician slates near Halifax International Airport, Nova Scotia. Nova Scotia Research Foundation Corporation, Report 1-85, 23p.

NSRFC, 1985b. The evaluation of some geophysical methods for the detection of shallow sulphide mineralization. Nova Scotia Research Foundation Corporation, Final Report 5-85, 51p.

O'Brien, B.H. 1986. Preliminary report on the geology of the Mahone Bay area, Nova Scotia. In Current Research, Part A, Geological Survey of Canada, Paper 86-1A, pp. 439-444.

O'Brien, B.H. 1988. A study of the Meguma Terrane in Lunenburg County, Nova Scotia. Geological Survey of Canada, Open File Report, 1823, 128p.

Parasnis, D.S. 1986. Principles of Applied Geophysics. Chapman and Hall, New York, NY, 402p.

Pasava, J., Graves, M.C., MacInnis, I.N. and Zentilli, M. 1995. Black slates - A source of acid drainage at the Halifax International Airport, Nova Scotia, Canada. In Mineral Deposits: From their origin to their environmental impacts. Proceedings of the Third Biennial SGA Meeting, Prague, Czech Republic, August 28-31, 1995, pp. 785-788.

Pettipas, B. 1979. A statistical evaluation of the effect of acid leachate on water quality, in Union Square, Lunenburg County. Nova Scotia Department of the Environment Report, June, 1979, 56p.

Philips, 1993. X'PERT Installation and user manuals, 7 volumes.

Porter Dillon Limited 1985. Environmental study of the Salmon River watershed in the vicinity of the Halifax International Airport, Halifax, Nova Scotia. Unpublished Consultant Report for Transport Canada, Final Report, April, 1985, pp. 1.1-12.1.

Pratt, A.R., Nesbitt, H.W. and Mycroft, J.R. 1996. The increased reactivity of pyrrhotite and magnetite phases in sulphide mine tailings. Journal of Geochemical Exploration, 56, pp. 1-11.

Pratt, A.R., Muir, I.J. and Nesbitt, H.W. 1994. X-ray photoelectron and Auger electron spectroscopic studies of pyrrhotite and mechanism of air oxidation. Geochimica et Cosmochimica Acta, 58, 2, pp. 827-841.

Price, W.A. 1997. Guidelines and recommended methods for the prediction of metal leaching and acid rock drainage at minesites in British Columbia (Draft #1 - April, 1997). Reclamation Section, Energy and Minerals Division. Ministry of Employment and Investment, BC. 143p.

Price, W.A. and Errington, J.C. 1994. ARD policy for mine sites in British Columbia. U.S. Bureau of Mines Special Publication SP06A-94, 4, pp. 285-293.

Price, W.A., Morin, K. and Hutt, N. 1997. Guidelines for the prediction of acid rock drainage and metal leaching for mines in British Columbia: part II. Recommended procedures for static and kinetic testing. In: Proceedings Fourth International Conference on Acid Rock Drainage, Volume 1, pp. 15-30.

Ramdohr, P. 1969. The ore minerals and their intergrowths. Pergamon Press, Oxford.

Roberts, J.D. 1986. The viability of peat as a treatment medium for acid mine drainage. Masters of Environmental Studies (MES) thesis, Dalhousie University, Halifax, NS, 137p.

Robinson, C. 1996. Pyrrhotite composition and its relationship to acid drainage potential in the Halifax Formation, Meguma Group, Nova Scotia. B.Sc. Honours thesis, Dalhousie University, Halifax, Nova Scotia, 72p.

Ryan, R.J. 1994. Preliminary investigations of Meguma Group stratigraphy in the Beaverbank area, Nova Scotia. In Mines and Minerals Branch, Report of Activities, 1993; Nova Scotia Department of Natural Resources, Mines and Energy Branches Report 94-1, pp. 137-140.

Ryan, R.J., Fox, D., Horne, R., Corey, M.C. and Smith, P.K. 1996. Preliminary stratigraphy of the Meguma Group in central Nova Scotia. In Minerals and Energy Branch, Report of Activities 1995, Nova Scotia Department of Natural Resources, Mines and Mineral Branch Report 96-1, pp. 27-34.

Samostie, A. 1994. Assessment of Acid Mine Drainage Risk in Nova Scotia: An Application of Geographic Information Systems (GIS). Master of Environmental Studies thesis, Dalhousie University, Halifax, Nova Scotia, 180p.

Sangster, A.L. 1990. Metallogeny of the Meguma Terrane, Nova Scotia. In Mineral Deposit Studies in Nova Scotia, Volume 1. Edited by A.L. Sangster. Geological Survey of Canada, Paper 90-8, pp. 115-162.

Schaeffer, M.F. and Clawson, P.A. 1996. Identification and treatment of potential acid-producing rocks and water quality monitoring along a transmission line in the Blue Ridge Province, southwestern North Carolina. Environmental and Engineering Geoscience, II, 1, pp. 35-48.

Schenk, P.E. 1970. Regional variation of the flysh-like Meguma Group (Lower Paleozoic) of Nova Scotia compared to Recent sedimentation off the Scotian Shelf. Geological Association of Canada, Special Paper 7, pp. 127-153.

Schenk, P.E. 1983. The Meguma Terrane of Nova Scotia - an aid to trans-Atlantic correlation. In Regional trends in the geology of the Appalachian-Caledonian-Hercynian-Mauritanide orogeny. P.E. Shenk (ed). NATO ASI Series C, 116, pp. 121-130.

Schenk, P.E. 1995. Meguma Zone (Chapter 3). In Geology of the Appalachian-Caledonian Orogen in Canada and Greenland. Edited by H. Williams. Geological Survey of Canada, Geology of Canada, no. 6, pp. 261-277.

Schwarz, E.J. and Broome, J. 1994. Magnetic Anomalies due to pyrrhotite in Paleozoic metasediments in Nova Scotia, Eastern Canada. Journal of Applied Geophysics, 32, pp. 1-10.

Schwarz, E.J. and McGrath, P.H. 1974. Aeromagnetic anomalies related to pyrrhotite occurrences in the Canadian Appalachian region. Geological Survey of Canada, Paper 74-1, Current Research, Part B, pp. 107-108.

Schwertmann, U., Bigham, J.M. and Murad, E. 1995. The first occurrence of schwertmannite in a natural stream environment. European Journal of Mineralogy, 7, pp. 547-552.

Silver, M. 1988. Construction of a wetland vegetated system designed to decrease acid and toxic metal loadings from quarry effluents. Marvin Silver Scientific Ltd., July, 1988, 16p.

Singer, P.C. and Stumm, W. 1970. Acidic mine drainage: the rate-determining step. Science, 167, pp. 1121-1123.

Sobek, A.A., Schuller, W.A., Freeman, J.R. and Smith, R.M. 1978. Field and laboratory methods applicable to overburdens and minesoils. EPA 600/2-78-054, pp. 47-55.

Steger, H.F. 1982. Oxidation of sulfide minerals VII. Effect of temperature and relative humidity on the oxidation of pyrrhotite. Chemical Geology, 35, pp. 281-295.

Taylor, L.A. 1971. Oxidation of pyrrhotites and the formation of anomalous pyrrhotite. Carnegie Institution of Washington. Year Book 70, pp. 287-289.

Taylor, F.C. and Schiller, E.A. 1966. Metamorphism of the Meguma Group of Nova Scotia. Canadian Journal of Earth Sciences, 3, pp. 959-973.

Telford, W.M., Geldart, L.P., Sheriff, R.E. and Keys, D.A. 1976. Applied Geophysics. Cambridge University Press, 860p.

Thompson, B.D. 1978. An investigation of Meguma bedrock leaching in the Shubenacadie-Stewiacke river basin, Technical Report #8. Prepared for the Shubenacadie-Stewiacke River Basin Board, 48p.

Vaughan, D.J. and Craig, J.R. 1978. Mineral Chemistry of Metal Sulphides. Cambridge University Press, Cambridge.

Waldron, J.W.F. 1992. The Goldenville-Halifax transition, Mahone Bay, Nova Scotia: relative sea-level rise in the Meguma source terrane. Canadian Journal of Earth Sciences, 29, pp. 1091-1105.

Worgan, J. 1987. Acid mine drainage in reactive slates, "The Halifax International Airport Case" Transport Canada perspective. In Proceedings, Acid Mine Drainage Seminar/Workshop, Halifax, Nova Scotia, March 23-26, 1987. Environment Canada, pp. 127-135.

Wright, D.F. and Bonham-Carter, G.F., 1996. VHMS favourability mapping with GIS-based integration models, Chisel Lake-Anderson Lake area. In Extech I: A multidisciplinary approach to massive sulphide research in the Rusty Lake-Snow Lake Greenstone Belts, Manitoba. G.F. Bonham-Carter, A.G. Galley, and G.E.M. Hall (eds.). Geological Survey of Canada, Bulletin 426, pp. 339-376.

Wuensch, B.J. 1974. Sulphide crystal chemistry. In Sulfide Mineralogy, Mineralogical Society of America, Short Course Notes, Volume 1, P.H. Ribbe (ed.), pp. w21-w43.

Zadeh, L.A. 1965. Fuzzy Sets. Information and Control, 8, pp. 338.353.

Zentilli, M., Graves, M.C., Mulja, T. and MacInnis, I. 1986. Geochemical characterization of the Goldenville-Halifax transition of the Meguma Group of Nova Scotia: preliminary report. Current Research, Part A, Geological Survey of Canada, Paper 86-1A, pp. 423-428.